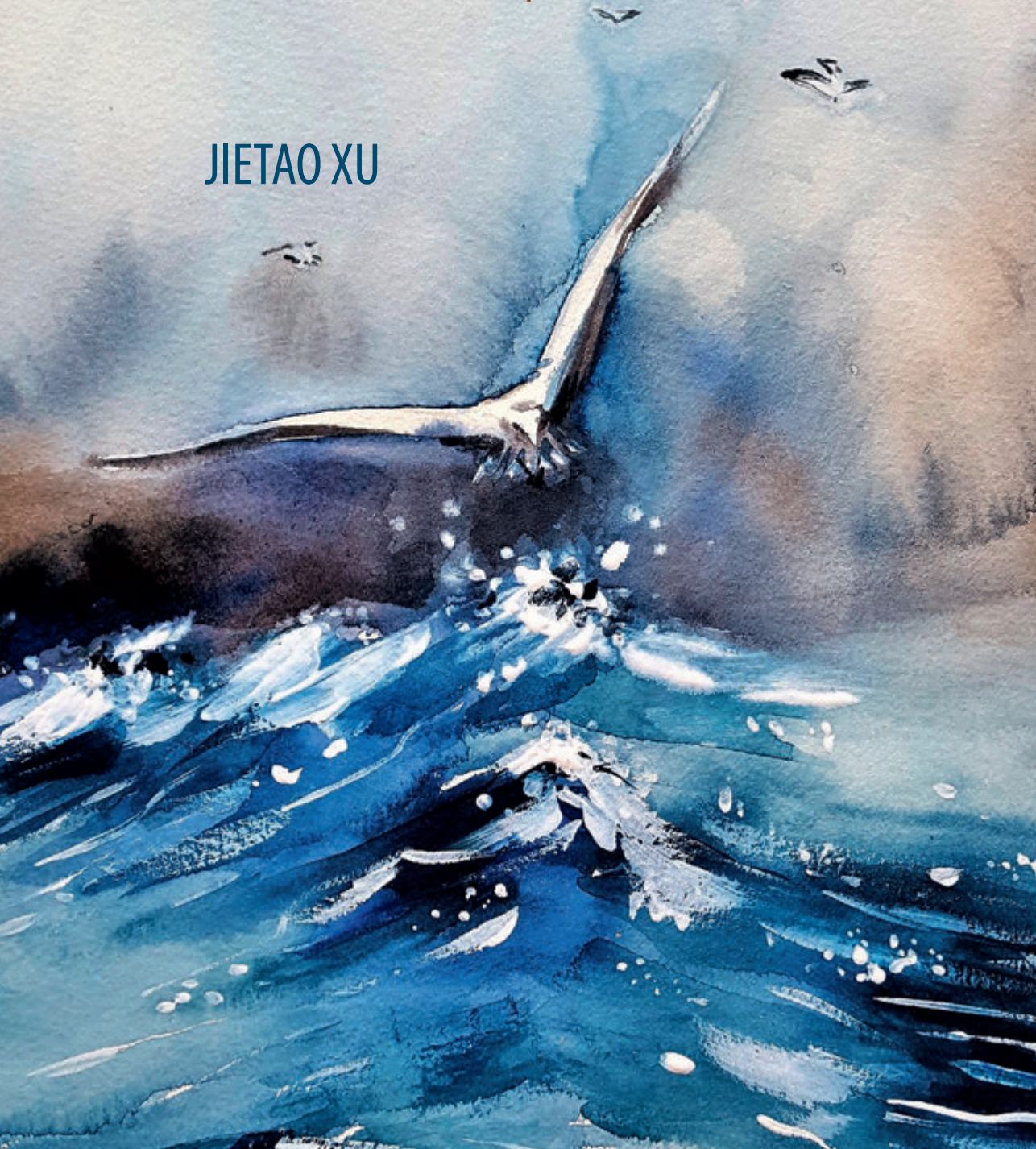


REGENERATION OF THE OSTEOCHONDRAL UNIT

Understanding biomaterial-driven endogenous repair using
in vitro, *ex vivo* and preclinical models

JIETAO XU



Regeneration of the Osteochondral Unit

Understanding biomaterial-driven endogenous repair using *in vitro*, *ex vivo* and preclinical models

J. Xu

ISBN: 978-94-6506-280-8

Cover design: Ridderprint, the Netherlands

Printing: Ridderprint, the Netherlands

© Copyright J. Xu, Rotterdam, the Netherlands, 2024

All rights reserved. No part of this thesis may be reproduced, stored in a retrieval system or transmitted in any of form or by any means without prior written permission of the author or, when appropriate, of the scientific journal in which parts of this thesis have been published.

The printing of this thesis was financially supported by:

- The department of Orthopaedics and Sports Medicine, Erasmus MC University Medical Center, Rotterdam
- Erasmus University Rotterdam, Rotterdam
- Medical Delta



Regeneration of the Osteochondral Unit

Understanding biomaterial-driven endogenous repair using *in vitro*, *ex vivo* and preclinical models

Regeneratie van de Osteochondrale Eenheid

Inzicht in biomateriaal gedreven endogeen herstel met behulp van *in vitro*, *ex vivo* en preklinische modellen

Thesis

to obtain the degree of Doctor from the
Erasmus University Rotterdam
by command of the
rector magnificus

Prof. dr. ir. A.J. Schuit

and in accordance with the decision of the Doctorate Board.
The public defence shall be held on

Thursday 14 November 2024 at 13.00 hrs
by

Jietao Xu
born in Zhejiang, China.

Doctoral Committee:

Promotors:

Prof. dr. G.J.V.M. van Osch
Prof. dr. P.A.J. Brama
Prof. dr. E.J. Farrell

Other members:

Prof. dr. H. Brommer
Dr. N. Bravenboer
Dr. B.C.J. van der Eerden

CONTENTS

Chapter 1	Introduction	7
Chapter 2	Engineered biochemical cues of regenerative biomaterials to enhance endogenous stem/progenitor cells (ESPCs)-mediated articular cartilage repair	29
Chapter 3	Modulating design parameters to drive cell invasion into hydrogels for osteochondral tissue formation	79
Chapter 4	Incorporating strontium enriched amorphous calcium phosphate granules in collagen/collagen-magnesium-hydroxyapatite osteochondral scaffolds improves subchondral bone repair	111
Chapter 5	Effectiveness of BMP-2 and PDGF-BB adsorption onto a collagen/collagen-magnesium-hydroxyapatite scaffold in weight-bearing and non-weight-bearing osteochondral defect bone repair: <i>in vitro</i> , <i>ex vivo</i> and <i>in vivo</i> evaluation	155
Chapter 6	Effect of sex on scaffold-enhanced subchondral bone repair in experimentally induced osteochondral defects in female and castrated male goats	191
Chapter 7	An articular cartilage culture model to study mechanisms of cartilage calcification <i>ex vivo</i> : the role of different zones	213
Chapter 8	Discussion	239
Chapter 9	Summary	255
Appendices	List of publications	271
	PhD portfolio	275
	Acknowledgements	279
	Curriculum Vitae	283

1

Introduction

INTRODUCTION

Osteochondral defects: a clinical challenge

Osteochondral defects are characterised by damage to the osteochondral unit within a joint that involves the articular cartilage, the cartilage-bone interface, and the underlying subchondral bone (Figure 1). According to Outerbridge classification, (osteo)chondral defects can be scored as grade I (softening and swelling of articular cartilage), grade II (fragmentation and fissuring affecting less than 1.5 cm), III (fragmentation and fissuring affecting greater than 1.5 cm), and grade IV (cartilage erosion to subchondral bone) [1]. (Osteo)chondral lesions were detected in over 60% of patients who underwent knee arthroscopies [2, 3], in which 12-19.2% of patients were scored as grade IV lesions [2, 3]. In the knee, ankle, and hip joints, these (osteo)chondral defects present as disruptions in the articular surface, often causing clinical symptoms such as pain, swelling, and reduced joint function.

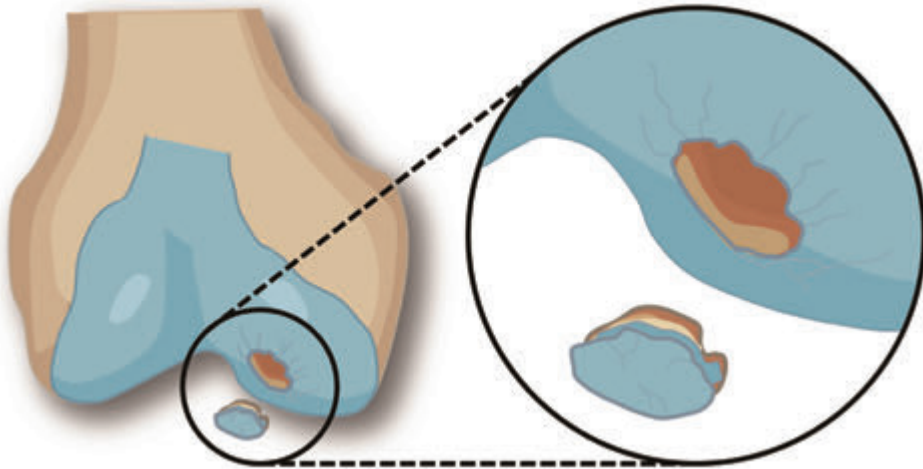


Figure 1: A schematic of an osteochondral defect.

The causes of osteochondral defects differ in various joints. Repetitive overloading leads to the natural wear of cartilaginous tissue in the weight-bearing joints [4]. This is one of the major causes of osteochondral defects in knee and hip joints in an ageing population. Osteochondral defects occur in 6.5 out of 100 ankle sprains, while up to 50% of patients with acute ankle sprains and fractures present osteochondral lesions [5]. Congenital conditions like developmental dysplasia of the hip can also contribute to the development of osteochondral defects. Other possible causes have been proposed, such as ischemia and genetic effects [6]. Of all these proposed aetiologies, trauma-related injuries and natural degradation are the most common causes of osteochondral defects.

The pathophysiology of osteochondral lesions is significantly associated with the physiological functions of the osteochondral unit. Osteochondral tissue plays a vital role in the transfer and distribution of the mechanical loading in the skeletal system during its

movements. Given the vital role of surface articular cartilage in smooth joint movement and proper load distribution, its integrity ensures the functioning of the joint. However, the avascular nature of cartilage hampers its inherent self-repair capacity when damaged. Damage of surface cartilage down to bone represents the most severe scenario for cartilage lesions [1], as the damaged subchondral bone disrupts the mechanical and biochemical environment of the unit. Mechanical instability potentially influences the progression of cartilage degradation. Therefore, osteochondral repair requires the complete restoration of the articular cartilage, the underlying subchondral bone, and the cartilage-bone interface for its physiological functions, which poses a significant challenge in orthopaedic surgery [7].

The osteochondral unit: hierarchical characteristics

Articular cartilage, calcified cartilage and subchondral bone layers possess different mechanical and physiological properties. With different compositions and structures, the different layers of osteochondral units synergise to enable joint movements, provide mechanical support, and distribute forces efficiently. However, this hierarchical and organisational unit complicates the repair process further.

Articular cartilage

Articular cartilage covers the surface of the subchondral bone in joints (Figure 2). It functions to provide a load-bearing surface to enable smooth joint movements. The functional characteristics of articular cartilage are intrinsically associated with its composition and structure. Articular cartilage consists of chondrocytes and extracellular matrix. Mature articular cartilage exhibits a zonal structure in the superficial, transitional, and deep zone with various chondrocyte maturity/shape/density [8]. Chondrocytes in the superficial zone are flattened and oriented parallel to one another. In the middle, randomly distributed round chondrocytes are present in the transitional zone. The deep zone is characterised by spherical chondrocytes. The balance between anabolic and catabolic processes, mediated by chondrocytes residing within the cartilage, is crucial for maintaining tissue homeostasis and integrity.

The extracellular matrix in articular cartilage primarily contains water (70-80%, wet weight), type II collagen fibres (15-25%, wet weight), and proteoglycans (5-10%, wet weight) [9]. Besides, small quantities of collagen type VI, IX, and XI are present in articular cartilage. The abundance of negative charge derived from these proteoglycans results in water retention. The high-water content within the cartilage matrix imbues it with resilience and lubrication, essential for absorbing compressive forces and reducing friction during joint articulation. The zonal architecture of mature articular cartilage also displays variations in type II collagen fibre orientation [8]. The superficial zone presents the highest concentration of type II collagen that is primarily oriented parallel to the surface of the cartilage for smooth movement of joints. In the middle, more randomly distributed type II collagen fibres are present in the transitional zone, providing resistance to compression. The type II collagen fibres in the deep zone are characterised by being oriented perpendicular to the cartilage surface, penetrating deep into the underlying subchondral bone. This perpendicular alignment provides crucial anchorage and structural support, enhancing resistance to shear forces [8]. Overall, this zonal structure provides tensile strength and structural integrity, allowing the cartilage to maintain its shape and resist

deformation under loading. Thus, the intricate relationship between its biochemical components and function underscores the importance of preserving its composition and structural integrity for optimal joint function.

Calcified cartilage

Mature articular non-calcified cartilage is integrated with the underlying subchondral bone plate through a calcified cartilage layer (Figure 2) with an approximate 20-250 μm thickness. This calcified cartilage layer consists of chondrocytes embedded in the calcified matrix, which is mainly composed of sodium hyaluronate, collagen, and hydroxyapatite [10]. The amount of type II collagen in the calcified matrix is around three times lower than that of the hyaline cartilage layer, and the amount of hydroxyapatite is around 25% less than that of subchondral bone as well in healthy human knee joints [11], indicating the transitional role of calcified cartilage. The cell density in calcified cartilage is half less than that in hyaline cartilage [12]. Two junctional interfaces of calcified cartilage, the upper interface connecting non-calcified cartilage and the lower interface connecting the subchondral bone plate, indicate the structural integration of the cartilage [12].

Without calcified cartilage, the mechanical transition from non-calcified articular cartilage to the underlying subchondral bone plate might undergo a mechanically discontinuous transition. Calcified cartilage, as a transitional layer, can minimise the shear stress it is exposed to [13-15]. In addition to the biomechanical role, calcified cartilage also plays a vital role in biochemical communication. With a lower diffusion coefficient than the non-calcified cartilage, calcified cartilage functions as a barrier that limits diffusion and prevents vascular invasion from the subchondral bone to non-calcified cartilage [16].

Subchondral bone

The subchondral bone is the bony layer beneath the cartilage (Figure 2). The subchondral bone consists of organic and inorganic biomaterials. The inorganic component primarily consists of hydroxyapatite crystals for rigidity, and the organic part is largely comprised of type I collagen fibres, proteoglycan, and water, providing elasticity and flexibility [17]. Anatomically, it consists of two parts: the subchondral bone plate and the subchondral trabecular bone. The subchondral bone plate is connected to the upper calcified cartilage layer. This is a more compact layer providing firm support [17]. Subchondral trabecular bone is a highly porous cancellous bony structure, offering elasticity for absorbing shock during joint loading [17]. The interspaces are usually filled with vessels and bone marrow.

The subchondral bone is crucial in absorbing and distributing the forces produced during locomotion, providing excellent deformability [18]. The forces exerted on the articular cartilage are transferred to the subchondral bone during locomotion. Compliance with the subchondral trabecular bone is crucial for enabling the joint to deform under loading. Overall, subchondral bone serves to provide both nourishment and mechanical support for cartilage [19]. Therefore, changes in the subchondral bone will influence metabolism of articular cartilage and the osteochondral microenvironment, chemically and mechanically [19].

Cross-talk between articular cartilage, calcified cartilage and subchondral bone

The close physical association among articular cartilage, calcified cartilage and subchondral bone leads to the concept of biophysical and biochemical crosstalk across the

osteocondral unit. Calcified cartilage functions as a transitional layer biophysically and biochemically. Mechanically, with the network of branching collagen fibrils, calcified cartilage can transmit force from articular cartilage to the subchondral bone and minimise shear stress [20, 21]. Biochemically, due to its lower diffusion coefficient compared to the uncalcified region, calcified cartilage acts as a barrier that prevents vascular invasion from the subchondral bone and restricts diffusion [22]. Despite this, several growth factors and cytokines secreted by both articular cartilage and subchondral bone can traverse between zones, influencing the homeostasis of osteochondral tissue [19, 23-25]. This interplay might be facilitated by intercellular communication through gap junction channels between cells [26]. This communication carries potential implications for understanding the mechanisms that regulate cell interactions in both physiological and pathological states [26].

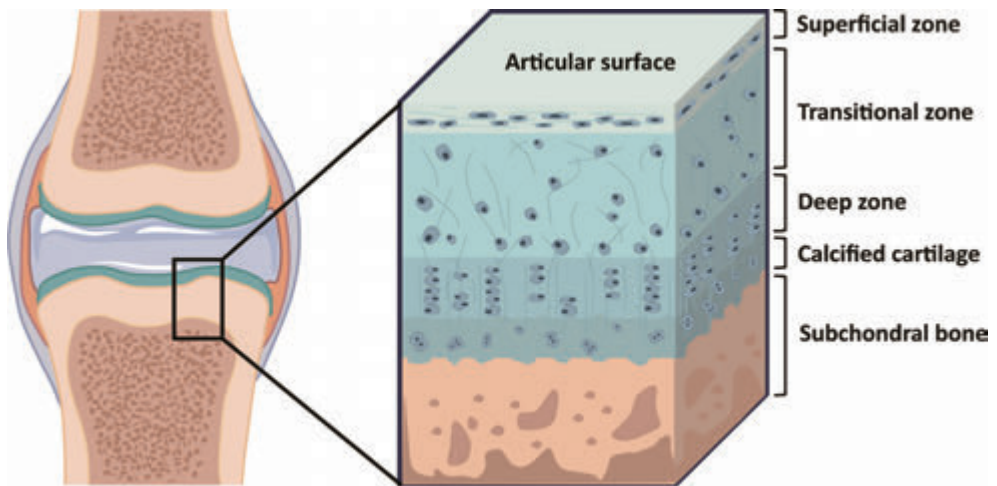


Figure 2: An overview of the hierarchical osteochondral unit.

(Osteo)Chondral defects: current surgical treatment options

In case of an (osteo)chondral defect, treatment selection in clinics is based on defect type, size and location. Non-surgical management aims to diminish debilitating symptoms and improve function. Specifically, conservation strategies include restricting physical activities, reducing weight-bearing, immobilisation, muscle-strengthening exercises, physical instrumental therapy, and non-steroidal anti-inflammatory drugs (NSAIDs). Such conservative strategies are effective in only 50-60% of cases [27, 28]. However, according to a retrospective study, 30% of patients treated with conservative strategies would develop osteoarthritis within 35 years [29]. The size of the osteochondral lesion, lesion stability and age are recognised as prognostic factors [30-33]. Patients with a large defect (> 12 mm²) or clinical presentation with swelling or locking, should be considered for surgical management [33].

Due to the hierarchical and organisational architecture, reconstructing the natural structure of the osteochondral unit is the ideal restorative treatment. According to a meta-analysis, 19% (39 out of 205) of the patients treated with surgical approaches developed

osteoarthritis within 10 years [34], which is lower than conservative strategies. Based on the size, depth, location, type and age, there are numerous surgical techniques such as fixation, microfracture, and restorative procedures, including osteochondral autograft or allograft transplantation, autologous matrix-induced chondrogenesis (AMIC), autologous chondrocyte implantation (ACI), and matrix induced autologous chondrocyte implantation (MACI).

Fixation of large (osteo)chondral fragments (>1 cm²) resulting from traumatic injuries or diseases such as osteochondritis dissecans, into the osteochondral defect via arthroscopy or open surgery can be attempted. This can be the first surgical option in certain cases since it has the potential to reattach and heal the native osteochondral defects [35]. The clinical outcomes of fixation can be significantly impacted by the quality of cartilage, age of the patients, mechanical environments, stability and size of the fragments [36]. However, in degradation-derived osteochondral lesions, osteochondral fragments are usually not present. Microfracture, whether performed alone or in combination with other surgeries such as fragment fixation, is intended to induce the migration of progenitor cells from the bone marrow to the defects. The released marrow elements, such as growth factors and stem cells from the bone marrow provide an enriched environment and repair materials for osteochondral repair [37]. As a result, fibrocartilage will fill the defect [38, 39]. Unfortunately, although it achieves good short-term to medium-term results, the poor mechanical properties of fibrocartilage usually lead to deterioration of clinical outcomes in long-term follow-ups [40]. Nanofracture with less trabecular fragmentation and compaction is being developed for better restoration of osteochondral quality [41, 42]. To prevent the regression seen in microfracture, AMIC aims to capture the progenitor cells released from the underlying bone by microfracture and provide a supporting network for tissue regeneration using the application of a cell-free microstructural scaffold [43]. When a primary repair is not feasible, osteochondral autograft transplantation is intended to fill the defect with autografts that are harvested from less critical locations (e.g., margins of the femoral condyles) [35]. Donor-site morbidity is a major concern in osteochondral autograft strategy, especially for large defects. For such cases, osteochondral allograft transplantation with cryopreserved cadaveric, fresh frozen or fresh samples can be used to fill the defects. However, storage techniques, the short life, and the higher cost restrict their availability [44]. As another way to minimise donor-site morbidity, ACI aims to harvest chondrocytes (200-300 mg cartilage only) from the patient. Chondrocytes are isolated, and proliferated *in vitro*, and then implanted in the defects. The first-generation ACI utilised periosteum autografts to contain chondrocytes. Periosteum autograft was replaced by porcine collagen membranes in the second generation, while chondrocytes were impregnated into the collagen matrix *in vitro* before implantation in the third-generation (matrix-induced autologous chondrocyte implantation MACI) [35].

To investigate the outcomes of these surgical options for (osteo)chondral lesions, a meta-analysis compiled results from 21 randomised controlled trials involving microfracture, osteochondral autograft transplantation, and ACIs. With a similar rate of re-operation, re-intervention and adverse events, microfracture indeed results in poor long-term outcomes [45]. ACI was recommended based on surgical efficacy and safety [45]. So far, variable clinical outcomes have been reported in limited randomised controlled trials. Long-lasting

and durable osteochondral repair cannot be achieved via current surgical management options [46].

Future tissue engineering approaches for osteochondral defect repair: regenerative biomaterials

Tissue engineering has emerged as one of the promising alternatives for tissue repair, offering potential management for complete osteochondral repair, which involves the regeneration of articular cartilage, subchondral bone, and cartilage-bone interface (calcified cartilage). Despite the significant progress in the fields of cartilage and bone engineering over the past decades, successful osteochondral regeneration remains a formidable challenge. Biomaterial-based scaffolds, tissue-forming cells, and biochemical and biophysical factors are the principal components of tissue engineering. This endeavour requires a deep understanding of osteochondral biology, particularly the intricate interplay between cell behaviours and physico-chemical cues of biomaterials. However, integrating these components into effective and enduring solutions for osteochondral repair poses ongoing challenges.

Biomaterials

Biomaterials provide structural support, biophysical and biochemical stimuli for tissue-forming cells. These biophysico-chemical cues profoundly influence cell-cell and cell-matrix interactions, thus significantly impacting tissue repair. Cells, crucial players in tissue regeneration, express various receptors of bioactive factors, enabling them to respond to signals that regulate essential processes such as migration, adhesion, proliferation, differentiation, inflammation and matrix production. Therefore, the capacity of biomaterials to contain and deliver bioactive factors is crucial for manipulating cell behaviours. In addition, mechanical strength, degradation rate, and micro-structure of biomaterials will significantly impact tissue homeostasis and remodelling. An ideal biomaterial for osteochondral repair should possess non-toxic, non-immunogenic, biocompatible, suitable biodegradable and mechanical properties and chondrogenic and/or osteogenic properties [46].

Though there is currently no perfect biomaterial that possesses all these necessary properties for osteochondral repair, several promising natural or synthetic biomaterials have been developed (Figure 3A). Natural biomaterials, such as collagen, chitosan, alginate, gelatin, and hyaluronic acid, are characterised by excellent biocompatibility, non-toxic features and non-immunogenic properties. These natural polymers are present in native tissues and are thus beneficial for cell migration, proliferation, and differentiation [47]. Unfortunately, the similarity to native tissues leads to a relatively fast degradation [47]. Moreover, their low mechanical properties are not suitable for sufficient mechanical support. Conversely, synthetic materials, such as polylactic acid (PLA), can provide flexibly tunable mechanical, physical, and chemical properties, albeit synthetic polymers lack biocompatibility [47, 48]. Hybrid biomaterials can combine the advantages of different natural and/or synthetic materials, aiming to maximise the comprehensive performance and avoid the shortcomings of each single material. For instance, as a natural hydrophilic polymer, gelatin is characterised by good biocompatibility, solubility, and degradability [49]. Nevertheless, when the temperature is above 37 °C, the gelatin will transfer to a solution due to the poor thermostability of gelatin. And some chemical crosslinking

reagents for gelatin hydrogels are poisonous [49]. Gelatin methacryloyl (GelMA) is produced by replacing amino groups of gelatin with methacryloyl groups in methacrylic anhydride. In this way, gelatin obtains the feature of photocrosslinking while still capable of supporting cell behaviours as the aspartic acid (RGD) peptide, which provides options for cell adhesion, and matrix metalloproteinase (MMP), which provides the possibility to degrade the matrix, are maintained [50]. Furthermore, the chemical and physical properties of GelMA can be flexibly modulated [51, 52].

For bone tissue engineering, ceramics, bioglass, and metallic materials are three commonly applied biomaterials, and are usually combined with natural and/or synthetic polymers. For instance, a clinically used osteochondral scaffold utilises collagen as the cartilage layer and combines natural collagen and hydroxyapatite as the bony layer. This scaffold has regenerated the articular cartilage and the subchondral bone pre-clinically and clinically [53-58]. Ti6Al4V, with a similar Young's modulus to natural bone, is an outstanding representative of metallic material. To improve the osteogenic property, the Ti6Al4V can be coated by osteogenic biomaterials such as polydopamine-assisted hydroxyapatite [59]. However, the non-biodegradable nature of metallic materials limits the application as an ideal material for bone tissue engineering. Progress has been made on the development of iron- or magnesium-based biodegradable metal scaffolds for bone tissue engineering, although extensive investigations on the design criteria, toxicity, osteogenesis, biodegradation rate etc. *in vitro* and *in vivo* are required [60-62]. Overall, the biomaterials for subchondral bone should possess excellent biomechanical strength, osteogenic properties, biocompatibility and a suitable degradation rate.

Biomaterial forms: hydrogels and scaffolds

To fill the osteochondral defect, biomaterials are commonly in the form of injectable hydrogels or solid scaffolds (Figure 3B). Hydrogels can be tailored to be injectable for minimally invasive administration to the defect site. Their significant water content facilitates effective nutrient and waste exchange. Injectable hydrogels have been widely applied for cartilage regeneration due to their structural and mechanical similarity to the cartilage extracellular matrix. Moreover, the injection of precursor solutions followed by *in vivo* gelation of hydrogels enables the filling of irregularly shaped osteochondral defects. Although the mechanical properties of hydrogels are tunable to suit various biomedical applications, hydrogels, with significant water content, typically lack the mechanical strength for subchondral bone repair compared to solid scaffolds.

Solid scaffolds are typically pre-designed and manufactured. Various fabrication techniques yield different features in scaffold architecture, such as pore size, pore shape and interconnectivity [63]. For instance, electrospinning develops polymers with high tensile strength, but the organic solvents used are toxic, and the pore size/shape is less controllable [64]. Similarly, freeze drying uses cytotoxic solvents, although it has an excellent control of pore size [65]. However, the pre-designed shape poses challenges in perfectly fitting in the irregular osteochondral defects. Additive manufacturing enables direct forms of materials using computer-aided design models. Highly complex, repeatable, topologically precise and controllable structures can be achieved [63]. Various additive manufacturing techniques, such as fused deposition modelling, stereolithography, bioprinting (when living cells are incorporated) etc. enable the production of patient-

specific or customised scaffolds for tissue engineering [63]. These features enable complex designs like multiple layers and gradient structures of scaffolds.

Structure designs: hierarchical or gradient substitution

Considering the multiple-layer structure of the osteochondral unit, a biomaterial-based scaffold designed with bilayers or multiple layers can more effectively emulate the biophysical and biochemical environment (Figure 3B). These dissimilar layers can be made of two or more biomaterials or simply have different structures like porosity or pore size. Bilayered scaffolds comprise two layers designed to facilitate the regeneration of articular cartilage and subchondral bone simultaneously. For instance, a clinically used bilayered collagen/collagen-hydroxyapatite-magnesium (Col/Col-HAp-Mg) scaffold utilises collagen as the cartilage layer, and combines natural collagen, hydroxyapatite and magnesium as the bony layer [53-58]. Trilayered scaffolds aim for simultaneous regeneration of articular cartilage, calcified cartilage, and subchondral bone. For instance, a novel tri-layered scaffold utilises type II collagen and chondroitin sulphate as the cartilage layer, type II collagen and hydroxyapatite for calcified cartilage formation, and type I collagen and hydroxyapatite as the bone layer [66].

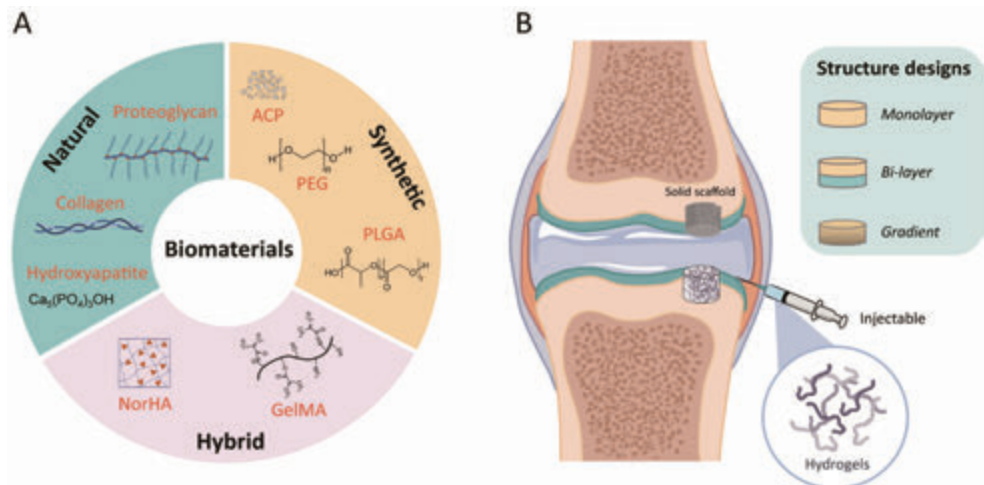


Figure 3. Schematic diagrams of engineering regenerative biomaterials for osteochondral repair. (A) examples of natural, synthetic and hybrid biomaterials. (B) graphical illustration of injectable hydrogels and solid scaffolds, and the structure designs of scaffolds for osteochondral repair.

Given the gradient structure of the osteochondral unit with a smooth transition from the cartilage to the subchondral bone, and different cell responses to diverse biophysical and biochemical cues such as stiffness, pore size, geometry and growth factors, gradient scaffolds that are optimised for zonal cell types and structure of the osteochondral unit seems to be promising. Generally, gradient hydrogel possesses at least one gradual and continuous spatiotemporal biophysical or biochemical property [67]. Pore-size or pore-shape gradient scaffolds for tissue regeneration were investigated. Large pore size causes tissue-forming cells to flow through after attachment, while medium or small ones allow cell infiltration [68]. 3D printing technology offers a unique opportunity to fabricate gradient scaffolds with specific stiffness, pore size or porosity [69]. Sultan et al. engineered

water-based cellulose nanocrystal hydrogels using 3D printing with controlled pore sizes and gradient pore structure [70]. 3D printing gradually became a definite part of osteochondral regeneration due to its flexibility in customised size, shape, structure and performance.

Tissue engineering approaches: cells seeding and acellular strategies

In some osteochondral tissue engineering strategies, scaffolds are initially seeded with exogenous tissue-forming cells to promote tissue repair (Figure 4A). Chondrocytes and mesenchymal stromal cells (MSCs) are two commonly proposed cell types for osteochondral repair. The use of differentiated cells, however, encounters several limitations throughout the successive processes of harvesting, isolating, expanding, culturing, seeding, and implantation. For instance, chondrocytes are limited in their availability and are at risk of dedifferentiation during expansion. In contrast, MSCs have received widespread attention due to their multipotency, sufficient sources and rapid proliferation. However, directing their differentiation towards chondrocytes remains challenging. MSCs are able to form cartilage-like tissue *in vitro*, but the proportion of the constituents, such as type II collagen, is dissimilar with native hyaline articular cartilage [71]. Despite the wide application and promising results, the cell seeding strategy is still facing challenges in the choice of cell source (e.g. as bone marrow, adipose tissue, synovium, periosteum), *in vitro* expansion, differentiation, and phenotype maintenance.

Unlike cell-seeded scaffolds, acellular strategies aim to recruit endogenous cells to induce tissue repair. In the natural state, there are various niches of stem/progenitor cells in articular cartilage, subchondral bone marrow, and intra- or peri-articular tissues, such as synovium, synovial fluid, fat pad, ranvier groove, periosteum and meniscus (Figure 4A). Many types of endogenous stem/progenitor cells, such as bone marrow-derived and synovium-derived stem cells, in specific niches of knee joints, have been identified [72]. These native endogenous stem/progenitor cells are involved in the complicated endogenous osteochondral repair process. To repair osteochondral defects, the infiltration of these surrounding endogenous stem/progenitor cells into the osteochondral lesions is a crucial stage. Then, after repopulating, endogenous cells are directed to chondrogenic and osteogenic differentiation. However, despite the fact that our body possesses inherent mechanisms to recruit a number of endogenous stem/progenitor cells, these are normally not sufficient for complete tissue repair due to limited recruited cells and limited released growth factors. Moreover, these endogenous stem/progenitor cells possess various differentiation capacities for adipogenesis, osteogenesis, and chondrogenesis. For instance, microfracture aims to induce the migration of MSCs from the underlying bone marrow to the defects [37]. However, bone marrow stem cells possess a high tendency towards chondrocyte hypertrophy and bone formation limits further application. As a result, bone and fibrocartilage will fill the defect instead of hyaline cartilage [73].

To favour particular endogenous stem/progenitor cells migration, proliferation, and differentiation, acellular strategies need to provide a biomimetic and biodegradable three-dimensional structure, and suitable biophysical and biochemical cues. With acellular strategies, cell-free scaffolds can be easily scaled up for large-scale tissue engineering applications, as they do not require large quantities of cells for seeding. Several acellular commercial products, such as MaioRegen®, have been approved by regulatory bodies, and

have achieved satisfactory clinical results, indicating the promising application of acellular strategies [74-76].

Acellular strategy: tunable biophysico-chemical cues to facilitate osteochondral repair

Cells can distinguish the geometry, stiffness, orientation, and elasticity of the extracellular matrix (Figure 4B), and adapt their behaviours according to these biomechanical cues of the extracellular matrix [77-81]. Given the intricate topographies and 3D architecture present within the native extracellular matrix, many studies aiming to test cellular interactions within controlled microenvironments at a cellular level have been reported. For instance, appropriate pore size and interconnectivity can facilitate cell migration, metabolic substances and nutrient diffusion. Previous studies have demonstrated that cell functions and tissue regeneration efficiency rely heavily on pore size [82, 83]. In a gelatin scaffold with various pore sizes ranging from 50 to 500 μm , chondrocytes prefer the pore size between 250 to 500 μm for better proliferation and extracellular matrix production, probably because of the space for cell metabolism [82]. Conversely, the chondrocytes differentiated to an osteogenic pathway with the larger pore size (300-500 μm) [83]. A role of substrate stiffness on cell behaviour such as migration, adhesion and proliferation has also been demonstrated. Focal adhesions are structures that connect cells to the ECM and transmit mechanical cues from the ECM to the cytoskeleton. In turn, the cytoskeleton reinforces the focal adhesion dynamics, leading to changes in cell shape and migration. Vainieri et al. tested MSCs migration in hyaluronic acid-tyramine hydrogels with different crosslinking densities. They demonstrated that cell migration was inhibited in stiffer hyaluronic acid-tyramine hydrogels, indicating cell migration limitation in highly crosslinked materials due to physical impediment or lower mesh size [79]. These attempts highlight the promise of acellular strategies with controllable biophysical cues for osteochondral repair.

Many exogenous biochemical cues, such as bioactive factors, additional components or metallic ions, can be integrated into biomaterials to modulate the physiological activities of endogenous stem/progenitor cells (Figure 4) [53-58, 79, 84, 85]. Numerous bioactive factors, such as platelet-derived growth factor and bone morphogenetic protein, play crucial roles in recruiting endogenous stem/progenitor cells, facilitating cell adhesion, proliferation, differentiation, and the generation and sustenance of cartilaginous extracellular matrix. However, the elevation of bioactive factor concentrations in tissues following injury is typically confined to a brief timeframe. Actually, one of the major aims of microfracture is to introduce growth factors from the underlying bone marrow (by stimulating bleeding and subsequent release of factors from platelets and immune cells), although this does not recruit particular and sufficient growth factors [37]. The engineering of biomaterials as delivery vehicles has emerged as a promising strategy to enhance the cartilage repair process. By encapsulating and releasing adequate bioactive factors into local defect areas, these biomaterials can stimulate the recruitment of more endogenous stem/progenitor cells from their niches, thus guiding further tissue repair [86]. Detailed information on favourable biochemical cues to enhance osteochondral repair will be discussed in Chapter 2.

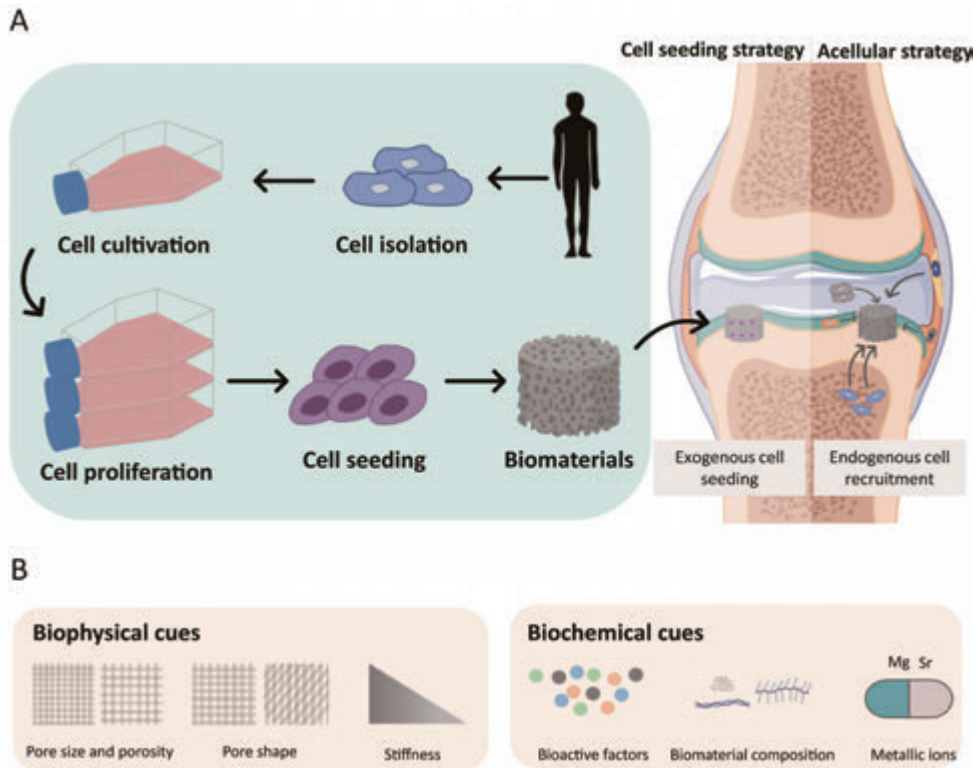


Figure 4. Overview of cell seeding and acellular strategies. (A) Scaffolds are initially seeded with exogenous tissue-forming cells to promote tissue repair in cell seeding strategies. Acellular strategies aim at promoting endogenous stem/progenitor cells migration, proliferation, differentiation, and matrix production. (B) Suitable biophysical and biochemical cues are favourable for both cell seeding and acellular strategies.

Cellular strategy: current challenges in endogenous osteochondral repair

The endogenous repair strategy is a promising alternative method for *in situ* osteochondral repair via cell recruitment into the injury site. The scaffolds/hydrogels with specific biophysical and biochemical cues placed at the injury site provide support for cell migration, adhesion, proliferation and differentiation. In the past decades, although many preclinical endogenous regenerative strategies have been proposed, only a scarce number of studies have advanced to the clinical stage due to some difficulties and challenges. First of all, the mechanism of endogenous repair remains unclear, including (1) the cell migration routes from the niches to the injury site; (2) the effects of migrated cells (not only the progenitor cells but also immune cells etc.) in the repair process; (3) the interaction between the migrated cells and extracellular matrix in endogenous repair. Then, the hierarchical and organisational osteochondral unit complicates the repair process further. Regenerating hyaline cartilage, calcified cartilage and subchondral bone separately and simultaneously poses a challenge for an acellular strategy. Differentiation towards (non)hypertrophic chondrocytes and osteoblasts requires various growth factors

and cell sources increasing the challenge. Meanwhile, the complex mechanical environments of the osteochondral defects can greatly affect cartilage/bone regeneration. Although many natural and synthetic biomaterials have been fabricated and investigated in osteochondral repair, none of these encompasses all the properties for an ideal scaffold. Novel biomaterials with high biocompatibility and bioactivity, but also excellent mechanical properties, bio-functionality and tunable degradation, are needed for better cell migration, adhesion and differentiation. Another challenge limiting the application of these strategies is the insufficient and nonspecific recruitment of endogenous stem/progenitor cells. Ideally, a well-designed biomaterial-based scaffold with specific biophysical and biochemical cues should be able to accurately recruit particular endogenous stem/progenitor cells, promote adhesion, proliferation and differentiation to target phenotypes, and thus complete tissue repair.

Aims and outline of this thesis

This thesis aims at improving osteochondral defect repair utilising endogenous cells via manipulating biochemical and biophysical cues of acellular biomaterials, including modulating crosslinking density or degradation kinetics, incorporating bioactive molecules or novel components into biomaterials.

Articular cartilage possesses very limited self-repair capacity. In **Chapter 2**, we review the challenges for acellular biomaterials-based endogenous articular cartilage repair, and summary novel design and application with favourable biochemical cues to guide the endogenous stem/progenitor cells for cartilage repair. In **Chapter 3**, we investigate the effect of biochemical and biophysical modifications, including the degree of functionalisation, degradability, and addition of a fibrillar component, on cell migration and tissue formation *in vitro*, *ex vivo* and *in vivo*.

Subchondral bone provides both nutritional and mechanical support for articular cartilage. Unrepaired subchondral bone impacts the long-term survival of overlying newly-regenerated cartilage in the osteochondral defect. There is a higher requirement in mechanical properties for bone tissue engineering compared to cartilage. To improve subchondral bone repair, we investigate the effect of biochemical modifications on the osteogenic capacity of a clinically used bi-layered collagen/collagen-magnesium-hydroxyapatite osteochondral scaffold. In **Chapter 4**, we modify the synthesis technology of amorphous calcium phosphate for incorporation of strontium, and incorporate strontium-enriched amorphous calcium phosphate granules into this collagen/collagen-magnesium-hydroxyapatite scaffold. In **Chapter 5**, we add bone morphogenetic protein 2 and/or platelet-derived growth factor-BB into this scaffold. We use a range of *in vitro*, *ex vivo* and *in vivo* mouse and goat models to assess cell behaviour and tissue repair. In addition, we examine the effect of sex on scaffold-enhanced subchondral bone repair in experimentally induced osteochondral defects in **Chapter 6**. To this aim, we pool and re-use control data (collagen/collagen-magnesium-hydroxyapatite scaffold only) from **Chapter 4** and **Chapter 5** on the subchondral bone repair capacity in both weight-bearing and non-weight-bearing locations of the stifle joint in castrated male and female goats.

The regeneration of the interface between cartilage and bone, i.e. the layer of calcified cartilage, is considered critical for functional regeneration of the osteochondral unit. This interface is important for force transmission, structural stabilisation and material diffusion.

Because regeneration of the layer of calcified cartilage is a challenge, we develop an *ex vivo* model to study the formation of the layer of calcified cartilage in **Chapter 7**. This model can be used to increase the understanding of the process of formation of a mature cartilage/bone interface as well as to *ex vivo* screen candidate factors that affect calcified cartilage formation in articular cartilage repair procedures.

This thesis concludes with **Chapter 8**, which generally discusses the broader implications of our findings, followed by conclusions and future perspectives aimed at improving osteochondral defect repair through the control of biochemical and biophysical cues of biomaterials. **Chapter 9** contains a summary in English, Dutch and Chinese.

REFERENCES

- [1] Outerbridge RE. The etiology of chondromalacia patellae. *The Journal of Bone and Joint Surgery. British Volume*. 1961;43(4):752-757.
- [2] Curl WW, Krome J, Gordon ES, Rushing J, Smith BP, Poehling GG. Cartilage injuries: A review of 31,516 knee arthroscopies. *Arthroscopy: The Journal of Arthroscopic & Related Surgery*. 1997;13(4):456-460.
- [3] Widuchowski W, Widuchowski J, Trzaska T. Articular cartilage defects: Study of 25,124 knee arthroscopies. *The Knee*. 2007;14(3):177-182.
- [4] Grimm NL, Weiss JM, Kessler JI, Aoki SK. Osteochondritis dissecans of the knee: pathoanatomy, epidemiology, and diagnosis. *Clin Sports Med*. 2014;33(2):181-188.
- [5] Saxena A, Eakin C. Articular Talar Injuries in Athletes: Results of Microfracture and Autogenous Bone Graft. *The American Journal of Sports Medicine*. 2007;35(10):1680-1687.
- [6] Durur-Subasi I, Durur-Karakaya A, Yildirim OS. Osteochondral Lesions of Major Joints. *Eurasian J Med*. 2015;47(2):138-144.
- [7] Deng C, Chang J, Wu C. Bioactive scaffolds for osteochondral regeneration. *Journal of Orthopaedic Translation*. 2019;17:15-25.
- [8] Buckwalter JA, Mow VC, Ratcliffe A. Restoration of injured or degenerated articular cartilage. *JAAOS-Journal of the American Academy of Orthopaedic Surgeons*. 1994;2(4):192-201.
- [9] Cohen NP, Foster RJ, Mow VC. Composition and dynamics of articular cartilage: structure, function, and maintaining healthy state. *Journal of Orthopaedic & Sports Physical Therapy*. 1998;28(4):203-215.
- [10] Zhou H, Yuan L, Xu Z, Yi X, Wu X, Mu C, Ge L, Li D. Mimicking the composition and structure of the osteochondral tissue to fabricate a heterogeneous three-layer scaffold for the repair of osteochondral defects. *ACS Applied Bio Materials*. 2022;5(2):734-746.
- [11] Zhang Y, Wang F, Tan H, Chen G, Guo L, Yang L. Analysis of the mineral composition of the human calcified cartilage zone. *Int J Med Sci*. 2012;9(5):353-360.
- [12] Wang F, Ying Z, Duan X, Tan H, Yang B, Guo L, Chen G, Dai G, Ma Z, Yang L. Histomorphometric analysis of adult articular calcified cartilage zone. *Journal of Structural Biology*. 2009;168(3):359-365.
- [13] Broom ND, Poole CA. A functional-morphological study of the tidemark region of articular cartilage maintained in a non-viable physiological condition. *J Anat*. 1982;135(Pt 1):65-82.
- [14] Radin EL, Rose RM. Role of Subchondral Bone in the Initiation and Progression of Cartilage Damage. *Clin Orthop Relat Res*. 1986;213 :34-40.
- [15] Mente PL, Lewis JL. Elastic modulus of calcified cartilage is an order of magnitude less than that of subchondral bone. *Journal of Orthopaedic Research*. 1994;12(5):637-647.
- [16] Wang W, Ye R, Xie W, Zhang Y, An S, Li Y, Zhou Y. Roles of the calcified cartilage layer and its tissue engineering reconstruction in osteoarthritis treatment. *Front Bioeng Biotechnol*. 2022;10:911281.
- [17] McIlwraith CW, Frisbie DD, Kawcak CE, Van Weeren R. Joint disease in the horse. *Elsevier Health Sciences*. 2015.
- [18] McCarty DJ, Koopman WJ. Arthritis and allied conditions: a textbook of rheumatology. *Arthritis and allied conditions: a textbook of rheumatology*. 1993;pp. 2 v. 2100-2102.

- [19] Sharma AR, Jagga S, Lee SS, Nam JS. Interplay between cartilage and subchondral bone contributing to pathogenesis of osteoarthritis. *Int J Mol Sci.* 2013;14(10):19805-19830.
- [20] Radin EL, Rose RM. Role of subchondral bone in the initiation and progression of cartilage damage. *Clin Orthop Relat Res.* 1986;213:34-40.
- [21] Hargrave-Thomas E, van Sloun F, Dickinson M, Broom N, Thambyah A. Multi-scalar mechanical testing of the calcified cartilage and subchondral bone comparing healthy vs early degenerative states. *Osteoarthritis and Cartilage.* 2015;23(10):1755-1762.
- [22] Boushell MK, Hung CT, Hunziker EB, Strauss EJ, Lu HH. Current strategies for integrative cartilage repair. *Connective Tissue Research.* 2017;58(5):393-406.
- [23] Malinin T, Ouellette EA. Articular cartilage nutrition is mediated by subchondral bone: a long-term autograft study in baboons. *Osteoarthritis Cartilage.* 2000;8(6):483-491.
- [24] Burr DB, Radin EL. Microfractures and microcracks in subchondral bone: are they relevant to osteoarthrosis? *Rheum Dis Clin North Am.* 2003;29(4):675-685.
- [25] Lajeunesse D, Reboul P. Subchondral bone in osteoarthritis: a biologic link with articular cartilage leading to abnormal remodeling. *Curr Opin Rheumatol.* 2003;15(5):628-633.
- [26] Carpintero-Fernandez P, Gago-Fuentes R, Wang HZ, Fonseca E, Caeiro JR, Valiunas V, Brink PR, Mayan MD. Intercellular communication via gap junction channels between chondrocytes and bone cells. *Biochimica et Biophysica Acta (BBA)-Biomembranes.* 2018;1860(12):2499-2505.
- [27] Zengerink M, Struijs PA, Tol JL, van Dijk CN. Treatment of osteochondral lesions of the talus: a systematic review. *Knee Surg Sports Traumatol Arthrosc.* 2010;18(2):238-246.
- [28] Howell M, Liao Q, Gee CW. Surgical Management of Osteochondral Defects of the Knee: An Educational Review. *Current Reviews in Musculoskeletal Medicine.* 2021;14(1):60-66.
- [29] Sanders TL, Pareek A, Johnson NR, Carey JL, Maak TG, Stuart MJ, Krych AJ. Nonoperative Management of Osteochondritis Dissecans of the Knee: Progression to Osteoarthritis and Arthroplasty at Mean 13-Year Follow-up. *Orthopaedic Journal of Sports Medicine.* 2017;5(7):2325967117704644.
- [30] Cahill BR, Phillips MR, Navarro R. The results of conservative management of juvenile osteochondritis dissecans using joint scintigraphy. A prospective study. *Am J Sports Med.* 1989;17(5):601-605; discussion 605-606.
- [31] Krause M, Hapfelmeier A, Möller M, Amling M, Bohndorf K, Meenen NM. Healing predictors of stable juvenile osteochondritis dissecans knee lesions after 6 and 12 months of nonoperative treatment. *Am J Sports Med.* 2013;41(10):2384-2391.
- [32] Nakayama H, Iseki T, Kambara S, Yoshiya S. Analysis of risk factors for poor prognosis in conservatively managed juvenile osteochondritis dissecans of the lateral femoral condyle. *Knee.* 2016;23(6):950-954.
- [33] Andriolo L, Candrian C, Papiro T, Cavicchioli A, Perdisa F, Filardo G. Osteochondritis Dissecans of the Knee - Conservative Treatment Strategies: A Systematic Review. *Cartilage.* 2019;10(3):267-277.
- [34] Han QX, Tong Y, Zhang L, Sun J, Ma J, Liu X, Zhang S, Jiang B, Li Y. Comparative efficacy of osteochondral autologous transplantation and microfracture in the knee: an updated meta-analysis of randomized controlled trials. *Arch Orthop Trauma Surg.* 2023;143(1):317-328.

- [35] Howell M, Liao Q, Gee CW. Surgical Management of Osteochondral Defects of the Knee: An Educational Review. *Curr Rev Musculoskelet Med*. 2021;14(1):60-66.
- [36] Robert H, Elise S, Dubois H, French Arthroscopic S. Osteochondritis dissecans of the knee, results of 43 refixations. *Arthroscopie*. 1998;11(4):177-181.
- [37] Steadman JR, Rodkey WG, Briggs KK, Rodrigo JJ. The microfracture technic in the management of complete cartilage defects in the knee joint. *Orthopade*. 1999;28(1):26-32.
- [38] Gill TJ, Asnis PD, Berkson EM. The treatment of articular cartilage defects using the microfracture technique. *J Orthop Sports Phys Ther*. 2006;36(10):728-738.
- [39] Schizas N, Savvidou O, Triantafyllopoulos I, Papadakis S, Dontas I, Papagelopoulos P. Adjuvant therapies for the enhancement of microfracture technique in cartilage repair. *Orthop Rev (Pavia)*. 2019;11(3):7950.
- [40] Kowalczyk M, Musahl V, Fu FH. Cochrane in CORR®: Surgical Interventions (Microfracture, Drilling, Mosaicplasty, and Allograft Transplantation) for Treating Isolated Cartilage Defects of the Knee in Adults. *Clin Orthop Relat Res*. 2018;476(1):16-18.
- [41] Zedde P, Cudoni S, Giachetti G, Manunta ML, Masala G, Brunetti A, Manunta AF. Subchondral bone remodeling: comparing nanofracture with microfracture. An ovine *in vivo* study. *Joints*. 2016;4(2):87-93.
- [42] Tahta M, Akkaya M, Gursoy S, Isik C, Bozkurt M. Arthroscopic treatment of osteochondral lesions of the talus: Nanofracture versus hyaluronic acid-based cell-free scaffold with concentration of autologous bone marrow aspirate. *J Orthop Surg (Hong Kong)*. 2017;25(2):2309499017717870.
- [43] Volz M, Schaumburger J, Frick H, Grifka J, Anders S. A randomized controlled trial demonstrating sustained benefit of Autologous Matrix-Induced Chondrogenesis over microfracture at five years. *Int Orthop*. 2017;41(4):797-804.
- [44] Chahal J, Gross AE, Gross C, Mall N, Dwyer T, Chahal A, Whelan DB, Cole BJ. Outcomes of osteochondral allograft transplantation in the knee. *Arthroscopy*. 2013;29(3):575-588.
- [45] Zamborsky R, Danisovic L. Surgical Techniques for Knee Cartilage Repair: An Updated Large-Scale Systematic Review and Network Meta-analysis of Randomized Controlled Trials. *Arthroscopy*. 2020;36(3):845-858.
- [46] Zhou L, Malda VO, Stoddart MJ, Lai Y, Richards RG, Ho KW, Qin L. Innovative Tissue-Engineered Strategies for Osteochondral Defect Repair and Regeneration: Current Progress and Challenges. *Advanced Healthcare Materials*. 2020;9(23):2001008.
- [47] Asghari F, Samiei M, Adibkia K, Akbarzadeh A, Davaran S. Biodegradable and biocompatible polymers for tissue engineering application: a review. *Artif Cells Nanomed Biotechnol*. 2017;45(2):185-192.
- [48] Jeuken RM, Roth AK, Peters RJRW, Van Donkelaar CC, Thies JC, Van Rhijn LW, Emans PJ. Polymers in cartilage defect repair of the knee: current status and future prospects. *Polymers*. 2016;8(6):219.
- [49] Young S, Wong M, Tabata Y, Mikos AG. Gelatin as a delivery vehicle for the controlled release of bioactive molecules. *J Control Release*. 2005;109(1-3):256-274.
- [50] Van Den Bulcke AI, Bogdanov B, De Rooze N, Schacht EH, Cornelissen M, Berghmans H. Structural and rheological properties of methacrylamide modified gelatin hydrogels. *Biomacromolecules*. 2000;1(1):31-38.

- [51] Sun M, Sun X, Wang Z, Guo S, Yu G, Yang H. Synthesis and Properties of Gelatin Methacryloyl (GelMA) Hydrogels and Their Recent Applications in Load-Bearing Tissue. *Polymers (Basel)*. 2018;10(11):1290.
- [52] Schwab A, Wesdorp MA, Xu J, Abinzano F, Loebel C, Falandt M, Levato R, Eglin D, Narcisi R, Stoddart MJ, Malda J, Burdick JA, D'Este M, van Osch G. Modulating design parameters to drive cell invasion into hydrogels for osteochondral tissue formation. *J Orthop Translat*. 2023;41:42-53.
- [53] Tampieri A, Sandri M, Landi E, Pressato D, Francioli S, Quarto R, Martin I. Design of graded biomimetic osteochondral composite scaffolds. *Biomaterials*. 2008;29(26):3539-3546.
- [54] Sosio C, Di Giancamillo A, Deponti D, Gervaso F, Scalera F, Melato M, Campagnol M, Boschetti F, Nonis A, Domeneghini C, Sannino A, Peretti GM. Osteochondral repair by a novel interconnecting collagen-hydroxyapatite substitute: a large-animal study. *Tissue Eng Part A*. 2015;21(3-4):704-715.
- [55] Levingstone TJ, Thompson E, Matsiko A, Schepens A, Gleeson JP, O'Brien FJ. Multi-layered collagen-based scaffolds for osteochondral defect repair in rabbits. *Acta Biomater*. 2016;32:149-160.
- [56] Kon E, Delcogliano M, Filardo G, Pressato D, Busacca M, Grigolo B, Desando G, Marcacci M. A novel nano-composite multi-layered biomaterial for treatment of osteochondral lesions: technique note and an early stability pilot clinical trial. *Injury*. 2010;41(7):693-701.
- [57] Perdisa F, Filardo G, Sessa A, Busacca M, Zaffagnini S, Marcacci M, Kon E. One-Step Treatment for Patellar Cartilage Defects With a Cell-Free Osteochondral Scaffold: A Prospective Clinical and MRI Evaluation. *Am J Sports Med*. 2017;45(7):1581-1588.
- [58] Di Martino A, Perdisa F, Filardo G, Busacca M, Kon E, Marcacci M, Zaffagnini S. Cell-Free Biomimetic Osteochondral Scaffold for the Treatment of Knee Lesions: Clinical and Imaging Results at 10-Year Follow-up. *Am J Sports Med*. 2021;49(10):2645-2650.
- [59] Li Y, Yang W, Li X, Zhang X, Wang C, Meng X, Pei Y, Fan X, Lan P, Wang C, Li X, Guo Z. Improving Osteointegration and Osteogenesis of Three-Dimensional Porous Ti6Al4V Scaffolds by Polydopamine-Assisted Biomimetic Hydroxyapatite Coating. *ACS Applied Materials & Interfaces*. 2015;7(10):5715-5724.
- [60] Chen Y, Xu Z, Smith C, Sankar J. Recent advances on the development of magnesium alloys for biodegradable implants. *Acta Biomaterialia*. 2014;10(11):4561-4573.
- [61] Putra NE, Leeftang MA, Taheri P, Fratila-Apachitei LE, Mol JMC, Zhou J, Zadpoor AA. Extrusion-based 3D printing of *ex situ*-alloyed highly biodegradable MRI-friendly porous iron-manganese scaffolds. *Acta Biomaterialia*. 2021;134:774-790.
- [62] Dong J, Tümer N, Leeftang MA, Taheri P, Fratila-Apachitei LE, Mol JMC, Zadpoor AA, Zhou J. Extrusion-based additive manufacturing of Mg-Zn alloy scaffolds. *Journal of Magnesium and Alloys*. 2022;10(9):2491-2509.
- [63] Suamte L, Tirkey A, Barman J, Jayasekhar Babu P. Various manufacturing methods and ideal properties of scaffolds for tissue engineering applications. *Smart Materials in Manufacturing*. 2023;1:100011.
- [64] Roseti L, Parisi V, Petretta M, Cavallo C, Desando G, Bartolotti I, Grigolo B. Scaffolds for bone tissue engineering: state of the art and new perspectives. *Materials Science and Engineering: C*. 2017;78:1246-1262.

- [65] Eltom A, Zhong G, Muhammad A. Scaffold techniques and designs in tissue engineering functions and purposes: a review. *Advances in Materials Science and Engineering*. 2019;2019.
- [66] Cao R, Xu Y, Xu Y, Brand DD, Zhou G, Xiao K, Xia H, Czernuszka JT. Development of Tri-Layered Biomimetic Atelocollagen Scaffolds with Interfaces for Osteochondral Tissue Engineering. *Adv Healthc Mater*. 2022;11(11): e2101643.
- [67] Genzer J, Bhat RR. Surface-bound soft matter gradients. *Langmuir*. 2008;24(6):2294-2317.
- [68] Qazi TH, Tytgat L, Dubruel P, Duda GN, Van Vlierberghe S, Geissler S. Extrusion Printed Scaffolds with Varying Pore Size As Modulators of MSC Angiogenic Paracrine Effects. *ACS Biomater Sci Eng*. 2019;5(10):5348-5358.
- [69] Qazi TH, Tytgat L, Dubruel P, Duda GN, Van Vlierberghe S, Geissler S. Extrusion Printed Scaffolds with Varying Pore Size As Modulators of MSC Angiogenic Paracrine Effects. *ACS Biomaterials Science & Engineering*. 2019;5(10):5348-5358.
- [70] Sultan S, Mathew AP. 3D printed scaffolds with gradient porosity based on a cellulose nanocrystal hydrogel. *Nanoscale*. 2018;10(9):4421-4431.
- [71] Somoza RA, Welter JF, Correa D, Caplan AI. Chondrogenic differentiation of mesenchymal stem cells: challenges and unfulfilled expectations. *Tissue Eng Part B Rev*. 2014;20(6):596-608.
- [72] Yang Z, Li H, Yuan Z, Fu L, Jiang S, Gao C, Wang F, Zha K, Tian G, Sun Z, Huang B, Wei F, Cao F, Sui X, Peng J, Lu S, Guo W, Liu S, Guo Q. Endogenous cell recruitment strategy for articular cartilage regeneration. *Acta Biomaterialia*. 2020;114:31-52.
- [73] Madry H, Kon E, Condello V, Peretti GM, Steinwachs M, Seil R, Berruto M, Engebretsen L, Filardo G, Angele P. Early osteoarthritis of the knee. *Knee Surg Sports Traumatol Arthrosc*. 2016;24(6):1753-1762.
- [74] Drobnič M, Kolar M, Verdonk P, Vannini F, Robinson D, Altschuler N, Shabshin N, Kon E. Complex osteochondral lesions of the talus treated with a novel bi-phasic aragonite-based implant. *The Journal of Foot and Ankle Surgery*. 2021;60(2):391-395.
- [75] Albano D, Martinelli N, Bianchi A, Messina C, Malerba F, Sconfienza LM. Clinical and imaging outcome of osteochondral lesions of the talus treated using autologous matrix-induced chondrogenesis technique with a biomimetic scaffold. *BMC Musculoskeletal Disorders*. 2017;18:1-7.
- [76] Kaipel M, Schreiner M, Kellner R, Klikovits J, Apprich S, Brix M, Boszotta H, Domayer S, Trattnig S. Beneficial clinical effects but limited tissue quality following osteochondral repair with a cell-free multilayered nano-composite scaffold in the talus. *Foot and Ankle Surgery*. 2017;23(4):302-306.
- [77] Friedl P, Wolf K. Plasticity of cell migration: a multiscale tuning model. *J Cell Biol*. 2010;188(1):11-19.
- [78] Lo CM, Wang HB, Dembo M, Wang YL. Cell movement is guided by the rigidity of the substrate. *Biophys J*. 2000;79(1):144-152.
- [79] Vainieri ML, Lolli A, Kops N, D'Atri D, Eglin D, Yayon A, Alini M, Grad S, Sivasubramanian K, van Osch G. Evaluation of biomimetic hyaluronic-based hydrogels with enhanced endogenous cell recruitment and cartilage matrix formation. *Acta Biomater*. 2020;101:293-303.
- [80] Abagnale G, Sechi A, Steger M, Zhou Q, Kuo CC, Aydin G, Schalla C, Müller-Newen G, Zenke M, Costa IG, van Rijn P, Gillner A, Wagner W. Surface Topography Guides

Morphology and Spatial Patterning of Induced Pluripotent Stem Cell Colonies. *Stem Cell Reports*. 2017;9(2):654-666.

[81] Schwartz Z, Martin JY, Dean DD, Simpson J, Cochran DL, Boyan BD. Effect of titanium surface roughness on chondrocyte proliferation, matrix production, and differentiation depends on the state of cell maturation. 1996;30(2):145-155.

[82] Lien SM, Ko LY, Huang TJ. Effect of pore size on ECM secretion and cell growth in gelatin scaffold for articular cartilage tissue engineering. *Acta Biomaterialia*. 2009;5(2):670-679.

[83] Stenhamre H, Nannmark U, Lindahl A, Gatenholm P, Brittberg M. Influence of pore size on the redifferentiation potential of human articular chondrocytes in poly(urethane urea) scaffolds. *Journal of Tissue Engineering and Regenerative Medicine*. 2011;5(7):578-588.

[84] Zhang N, Lock J, Sallee A, Liu H. Magnetic Nanocomposite Hydrogel for Potential Cartilage Tissue Engineering: Synthesis, Characterization, and Cytocompatibility with Bone Marrow Derived Mesenchymal Stem Cells. *ACS Appl Mater Interfaces*. 2015;7(37):20987-20998.

[85] Li CJ, Park JH, Jin GS, Mandakbayar N, Yeo D, Lee JH, Lee JH, Kim HS, Kim HW. Strontium/Silicon/Calcium-Releasing Hierarchically Structured 3D-Printed Scaffolds Accelerate Osteochondral Defect Repair. *Adv Healthc Mater*. 2024;e2400154.

[86] Yang Z, Li H, Yuan Z, Fu L, Jiang S, Gao C, Wang F, Zha K, Tian G, Sun Z, Huang B, Wei F, Cao F, Sui X, Peng J, Lu S, Guo W, Liu S, Guo Q. Endogenous cell recruitment strategy for articular cartilage regeneration. *Acta Biomater*. 2020;114:31-52.

2

Engineered biochemical cues of regenerative biomaterials to enhance endogenous stem/progenitor cells (ESPCs)-mediated articular cartilage repair

Liangbin Zhou[#], Jietao Xu[#], Andrea Schwab, Wenxue Tong, Jiankun Xu, Lizhen Zheng, Ye Li, Zhuo Li, Shunxiang Xu, Ziyi Chen, Li Zou, Xin Zhao, Gerjo J.V.M. van Osch, Chunyi Wen, Ling Qin

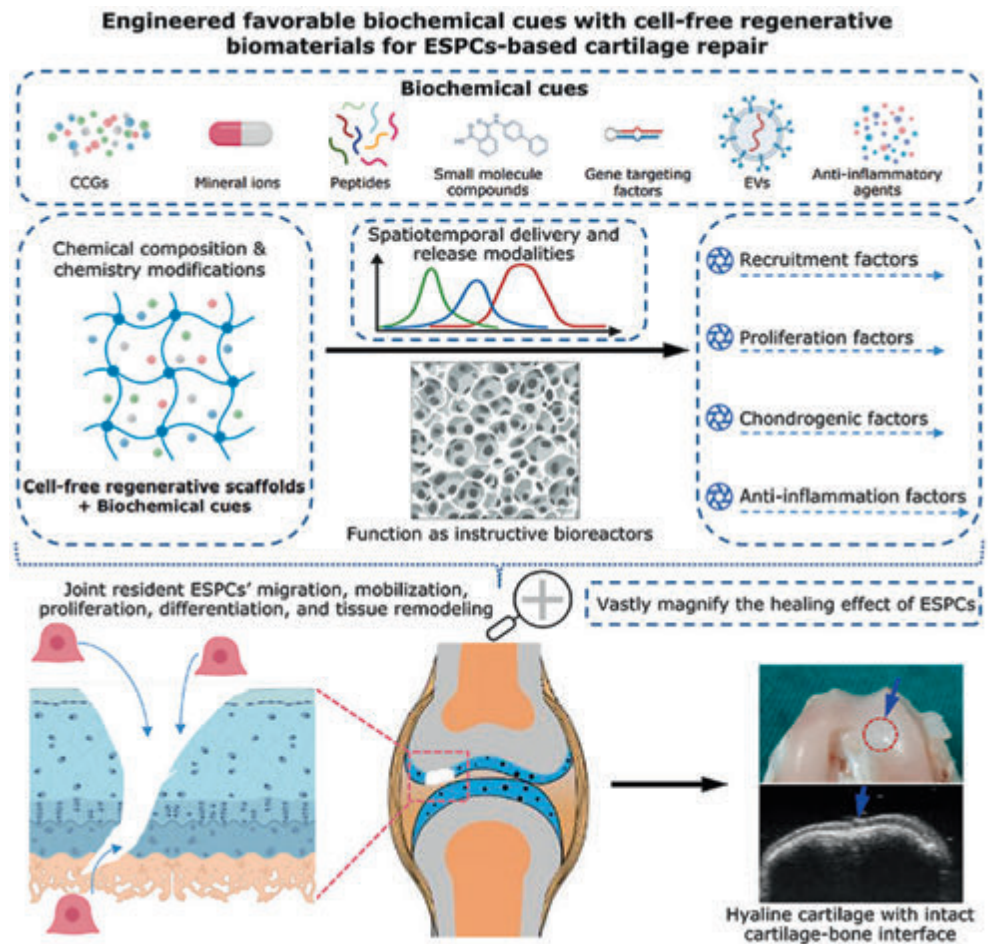
[#]Authors contributed equally to this work

Bioact Mater. 2023 May 2;26:490-512.

ABSTRACT

As a highly specialized shock-absorbing connective tissue, articular cartilage (AC) has very limited self-repair capacity after traumatic injuries, posing a heavy socioeconomic burden. Common clinical therapies for small- to medium-size focal AC defects are well-developed endogenous repair and cell-based strategies, including microfracture, mosaicplasty, autologous chondrocyte implantation (ACI), and matrix-induced ACI (MACI). However, these treatments frequently result in mechanically inferior fibrocartilage, low cost-effectiveness, donor site morbidity, and short-term durability. It prompts an urgent need for innovative approaches to pattern a pro-regenerative microenvironment and yield hyaline-like cartilage with similar biomechanical and biochemical properties as healthy native AC. Acellular regenerative biomaterials can create a favorable local environment for AC repair without causing relevant regulatory and scientific concerns from cell-based treatments. A deeper understanding of the mechanism of endogenous cartilage healing is furthering the (bio)design and application of these scaffolds. Currently, the utilization of regenerative biomaterials to magnify the repairing effect of joint-resident endogenous stem/progenitor cells (ESPCs) presents an evolving improvement for cartilage repair. This review starts by briefly summarizing the current understanding of endogenous AC repair and the vital roles of ESPCs and chemoattractants for cartilage regeneration. Then several intrinsic hurdles for regenerative biomaterials-based AC repair are discussed. The recent advances in novel (bio)design and application regarding regenerative biomaterials with favorable biochemical cues to provide an instructive extracellular microenvironment and to guide the ESPCs (e.g. adhesion, migration, proliferation, differentiation, matrix production, and remodeling) for cartilage repair are summarized. Finally, this review outlines the future directions of engineering the next-generation regenerative biomaterials toward ultimate clinical translation.

Keywords: regenerative biomaterials; endogenous stem/progenitor cells (ESPCs); articular cartilage (AC) repair; biochemical cues



1. INTRODUCTION

Articular cartilage (AC) is a smooth, avascular, and aneural connective tissue with unique composition and structure [1,2]. Its structure and function are mainly dependent on chondrocytes that control the turnover of extracellular matrix (ECM) and maintain homeostasis. It is located at the bone surface to provide a wear-resistant and load-bearing interface within synovial joints [2]. The poor intrinsic healing potential of AC usually leads to permanent functional impairment and osteoarthritis (OA) in the absence of adequate treatment [1,2]. There will be a growing number of young patients suffering from cartilage injuries caused by trauma in the coming decades. Nonsurgical treatments such as intra-articular hyaluronic acid (HA) injections and oral nonsteroidal anti-inflammatory drugs mainly focus on reducing clinical symptoms and preventing the progression of AC damage [3]. To regenerate neocartilage tissues in the lesion site, surgical interventions, such as microfracture, mosaicplasty, ACI, and MACI are proposed and extensively applied [4]. Through drilling small holes in the bone to a depth of around 2-4 mm at the injury site, arthroscopic microfracture is used, in part, to access the endogenous multipotent mesenchymal stem cells from the underlying bony region and promote their migration, proliferation, and chondrogenic differentiation; while ACI and MACI implant cultured chondrocytes-formed microtissues into the defect area under a natural or synthetic membrane via surgical procedures [4]. The above-mentioned surgical treatments (i.e. endogenous cartilage repair and cell-based therapies) have achieved varying degrees of success. On the other side, these approaches face several drawbacks, such as limited chondrocytes or cartilage sources, incapability to repair large-size AC defects, and the reconstructed tissue consisting of mechanically inferior fibrocartilage and integrates with surrounding cartilage incompletely, leading to poor resistance to shear forces and deterioration in a longer follow-up [5].

In recent decades, numerous studies have shown native ESPCs are involved in the complicated endogenous cartilage repair process, which is mainly dependent on the infiltration of these surrounding ESPCs into the cartilage lesions and subsequent cell behavior [6]. Without any exogenous interventions (e.g. allogeneic or xenogeneic cells transplantation, scaffolds implantation, and bioactive factors presentation and delivery), despite our body can rely on the inherent mechanism to recruit a few ESPCs, the capability of endogenous regeneration and repair is usually insufficient and incomplete, particularly in the longer term. For example, the clinical results of debridement and microfracture are inconsistent. The repaired tissue is predominantly fibrocartilage, which cannot be comparable to hyaline cartilage in terms of durability [7]. During neocartilage formation, aberrant collagen expression can be observed as a consequence of two different pathways, leading to the emergence of fibrocartilage (collagen I/II) or hypertrophic cartilage (collagen X). To regenerate hyaline cartilage (collagen II) both *in vivo* or/and *in vitro*, we should consider the strategies to provide low oxygen tension and suitable differentiation cocktails to induce chondrogenesis with less or no expression of collagen II and X [8]. In fact, the increased concentrations of chemokines, growth factors (GFs), and cytokines in tissues after AC injury is limited and last for a short period. Only a low number of ESPCs are recruited and able to function properly [9]. Meanwhile, with an in-depth understanding of the mechanism behind endogenous cartilage repair, various innovative cell-free regenerative biomaterial strategies have emerged as promising solutions for ESPCs-

mediated cartilage regeneration [10,11] (Figure 1). Acellular regenerative biomaterials-based ESPCs-mediated AC repair might be superior to exogenous cell-based therapeutic approaches in terms of handling procedures, accessibility of cell sources, donor-site morbidities, risk of disease transmission, costs, some regulatory issues, and translational barriers [12] (Figure 1). In the scenario of ESPCs-mediated AC repair, regenerative biomaterials are defined as the scaffolds used to coax the body into recreating a pro-regenerative environment, influencing the immune system, and restoring the structure and function of damaged cartilage [13-15]. Despite more mechanistic studies being required, they are already poised to gain an immediate patient impact, representing an alternative paradigm for AC regeneration. Meta-analysis of *in vivo* animal studies indicated that implanting acellular regenerative biomaterials substantially enhanced AC repair by 15.6% compared with non-treated blank controls, i.e. endogenous cartilage repair [16]. Biologics supplementation could considerably improve AC regeneration by 7.6% in contrast to control scaffolds [16]. These results suggested cell-free engineered regenerative biomaterials with favorable biochemical cues could enhance ESPCs-mediated AC repair. Regenerative biomaterials usually act as instructive scaffolds to provide structural support for cell infiltration, matrix deposition, and tissue remodeling and regeneration (Figure 1). Encouragingly, in March 2022 the FDA approved Agili-C™, a cell-free, off-the-shelf implant for repairing cartilage and osteochondral defects (OCD) [17], providing us with more confidence in our proposed strategy. From the scope of sources, three main types of regenerative scaffolds that are typically used for AC restoration, including natural biomaterials (e.g. cellulose, alginate, chitosan, gelatin, collagen, fibrin, chondroitin sulfate (CS), agarose, and HA), synthetic biomaterials (e.g. polyethylene glycol (PEG), polyvinyl alcohol (PVA), polycaprolactone (PCL), poly (lactic-co-glycolic acid) (PLGA), poly (propylene fumarates) (PPF), poly (NiPAAm), and polyurethane (PU)) and composite constructs [10]. Through different engineering methodologies of (bio)design and (bio)fabrication, these three-dimensional (3D) porous regenerative scaffolds can be functionalized with some tailored favorable biochemical cues, tunable chondro-immunomodulation, and various spatiotemporal delivery/release modalities [18-26] (Figure 1). The injectable or implantable regenerative biomaterials (by themselves or combined with biomolecules) can kick-start and vastly magnify the body's intrinsic cartilage healing potential [9,27,28]. These biomaterials can bring a pro-regenerative microenvironment and take advantage of this friendly microenvironment as a natural bioreactor. Within this bioreactor, multiple stimuli derived from the regenerative scaffolds are capable of activating and recruiting a large population of joint-resident ESPCs toward the lesion site, guiding their migration, mobilization, proliferation, and chondrogenesis to generate natural hyaline-like AC eventually [9,27,28] (Figure 1). With huge translational potential, this strategy has attracted widespread attention and might represent one of the most promising therapies for chondral defects [29].

Unfortunately, most current proposed strategies for AC defects merely emphasize the regulation of a single healing period (i.e. cellular colonization), overlooking the integrity and continuity of distinct stages, which cannot provide an optimal solution for ESPCs-mediated AC repair. In this review, we emphasize all repair procedures rather than merely ESPCs migration. The ability to precisely control the regenerative scaffold-based *in vivo* microenvironment is still nascent. However, we feel that given the rapid progress in understanding the mechanism of endogenous AC healing and regenerative scaffolds, it is

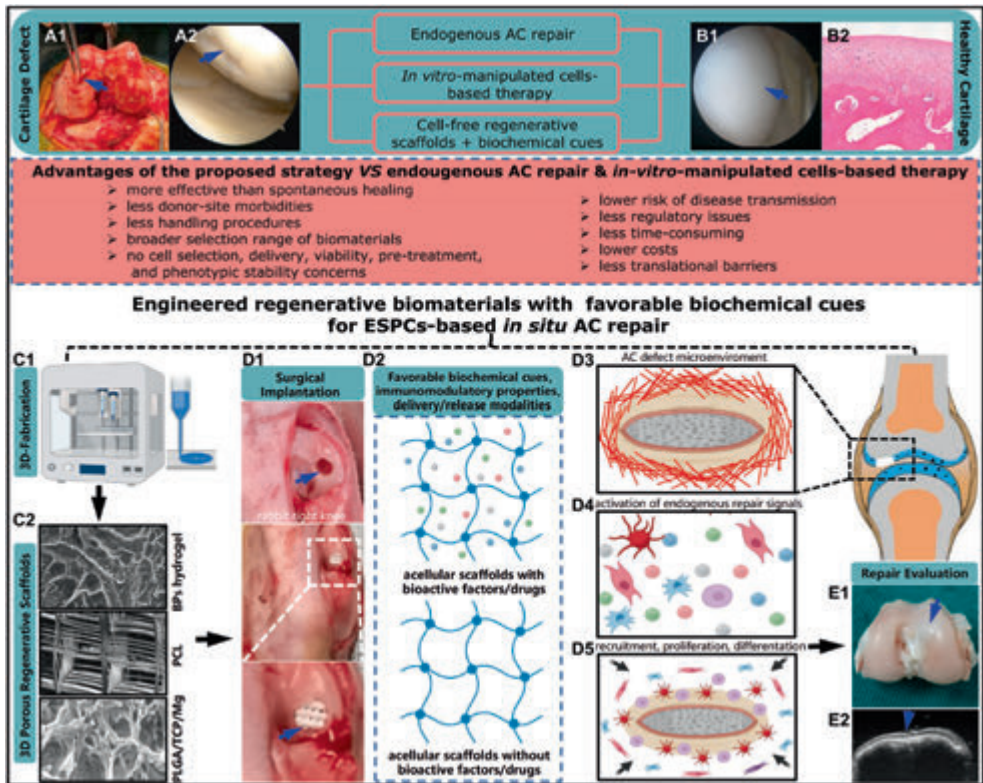


Figure 1. Schematic diagram of the ESPCs-mediated cartilage repair strategies through 3D macro/microporous acellular engineered regenerative biomaterials. (A1) Clinical photograph of an AC defect of the distal femoral condyle from the right knee of a 21-year-old male patient. (A2) Knee arthroscopic imaging of an advanced stage of AC defect of a 65-year-old female patient. (B1) An arthroscopy shows the smooth surface of healthy hyaline cartilage. (B2) The hematoxylin and eosin (HE) staining image indicates the unique hierarchical structure of the osteochondral unit including the upper AC. (C1) The fabrication of regenerative biomaterials by novel 3D-(bio)printing technologies. (C2) The scanning electron microscope (SEM) images demonstrate the porous architecture and desirable connectivity of the regenerative scaffolds (e.g. Bisphosphonates (BPs)-based hydrogel, PCL, and PLGA/TCP/Mg scaffolds). (D1) The surgical implantation of engineered regenerative biomaterials into the osteochondral lesion site (3 mm × 3 mm) in a rabbit model. (D2) The implanted acellular regenerative scaffolds (loaded with or without biomolecules, i.e., chemoattractants) which possess favorable biochemical cues, immunomodulation properties, and drug delivery/release profiles represent promising options for AC repair. (D3) Schematic illustration of the microenvironment around the cartilage defect. (D4) The activation of endogenous repairing signals. (D5) Possible illustration of the improved recruitment of numerous joint-resident ESPCs toward the lesion site by engineered regenerative scaffolds and enhanced proliferation and chondrogenesis of ESPCs, matrix production, and remodeling. (E1) One example of the engineered regenerative scaffolds for ESPCs-based AC repair: 12 weeks post-implantation into rabbits, the 3D-printed magnesium (Mg)-based acellular composite scaffold treatment improves to form smooth-surfaced cartilage, which has a similar hyaline-like appearance compared with adjacent AC tissue. (E2) The high-frequency ultrasound image shows the newly regenerated cartilage layer and cartilage-bone interface in the previous defect location. (A1, A2, and B1 images courtesy of Dr. Kevin Ki-Wai Ho and Dr. Yang Liu; C1, and D2-D5 were created by BioRender; Others are from the ongoing research project in our lab).

now the right time to discuss these issues and opportunities. This review mainly focuses on the engineered regenerative biomaterials-based approaches for guiding ESPCs for AC repair. In the first part, the potential mechanism of endogenous cartilage repair and the significance of ESPCs, chemokines, cytokines, and GFs (CCGs) will be discussed and summarized. Followed by a number of currently existing crucial challenges, various recent multidisciplinary achievements and advances in ESPCs-mediated strategies by manipulating the various amenable biochemical cues (e.g. chemical composition, biochemical modification, chemokines, cytokines and GFs, mineral ions, functional peptides, small molecule compounds, gene targeting factors, extracellular vesicles (EVs), immunomodulatory agents, and delivery/release profiles) of engineered regenerative biomaterials will be highlighted and discussed. The last part comprises conclusions and perspectives, accompanied by several critical open questions that still need to be addressed.

2. THE VITAL ROLES OF ESPCS, CHEMOKINES, CYTOKINES, AND GROWTH FACTORS (CCGS) FOR ESPCS-MEDIATED AC REPAIR

2.1. Endogenous cartilage healing and its possible mechanism

Intrinsic tissue regeneration capabilities are distinct among different species. Comparing with non-mammalian vertebrates, mammals and humankind possess limited inherent tissue self-healing capability due to genetic, developmental, immunologic, and tissue complexity differences [27,30]. For instance, the axolotl salamander (*Ambystoma mexicanum*) can heal large chondral defects and regenerate normal hyaline AC and joint structure even if limb amputation, whereas our human beings cannot [31]. Particularly noteworthy is that the endogenous cartilage repair potential decreases with aging, phylogeny, and ontogeny due to ESPCs exhaustion [32,33]. It implies that young and juvenile patients hold greater potential for endogenous cartilage healing than the elderly [34]. Unlike exogenous regenerative approaches, endogenous cartilage regeneration does not depend on exogenous cells, scaffolds, and biomolecules and only depends on the innate self-healing potential [35].

The typical repair process of AC defects is extremely complicated. It consists of a sequence of dynamic biological responses following a similar pattern, including hemostasis, inflammation, and remodeling stages (ESPCs recruitment from surrounding niches, proliferation, chondrogenesis, matrix deposition, and maturation) [36]. Under ideal conditions, these stages function coordinately with each other to assure the best repairing outcome. The presence of specific cells (e.g. immune cells, stem cells, and chondrocytes etc.) and vascular supply are the two prominent essential elements. After hemostasis, immune cells (e.g. neutrophils, macrophages, etc.) are recruited and activated by cytokines and chemoattractants secreted by the platelets [36,37]. Then immune cells can secrete some anti-inflammation factors and chondrogenic cytokines. This can further suppress inflammation and give rise to cellular exudation into the damaged area for fibrous network formation, which is invaded by ESPCs and chondrocytes during the remodeling phase, aiming to restore the original structure and function [37]. Therefore, some immune cells (i.e. macrophages) can act as a potential target for AC repair [38]. The inflammation and remodeling phases rely on the vascular supply. Thus, compared to

partial-thickness AC defects, the endogenous repair of full-thickness AC defects and OCD follow a different approach because of the participation of the vascular system from the lower subchondral bone [10,39]. The articular surface of full-thickness AC defects and OCD can self-repair without cell transplantation probably by recruiting endogenous cells from adjacent tissues and activating the autotherapy process [40]. This process is accompanied by inflammation and remodeling phases. However, the endogenous repair of partial-thickness AC defects is different due to the absence of a vascular system, limited inflammation, and insufficient chemokines and GFs. Moreover, the chondrocytes are imprisoned in glycosaminoglycans (GAGs) and collagens and are limited to migrate to the injured area from the surrounding cartilage. Thus, endogenous intra- and peri-articular ESPCs are even more vital in this context [40]. Therefore, joint-resident ESPCs from local or adjacent cell niches post-traumatically play a central role in endogenous cartilage healing. Maintaining homeostasis is finely tuned by a complicated network of signaling molecules and pathways (e.g. TGF- β , BMP, MAPK, Wnt/ β -catenin, NF- κ B, Ihh, HIF-1 α , HIF-2 α , IGF-1, and FGF) (Figure 2). Studying endogenous cartilage repair and its underlying mechanism will help us understand how the human AC heals and repairs itself spontaneously. Additionally, it could assist researchers in developing innovative regenerative biomaterials as instructive bioreactors for guiding ESPCs to heal the AC more.

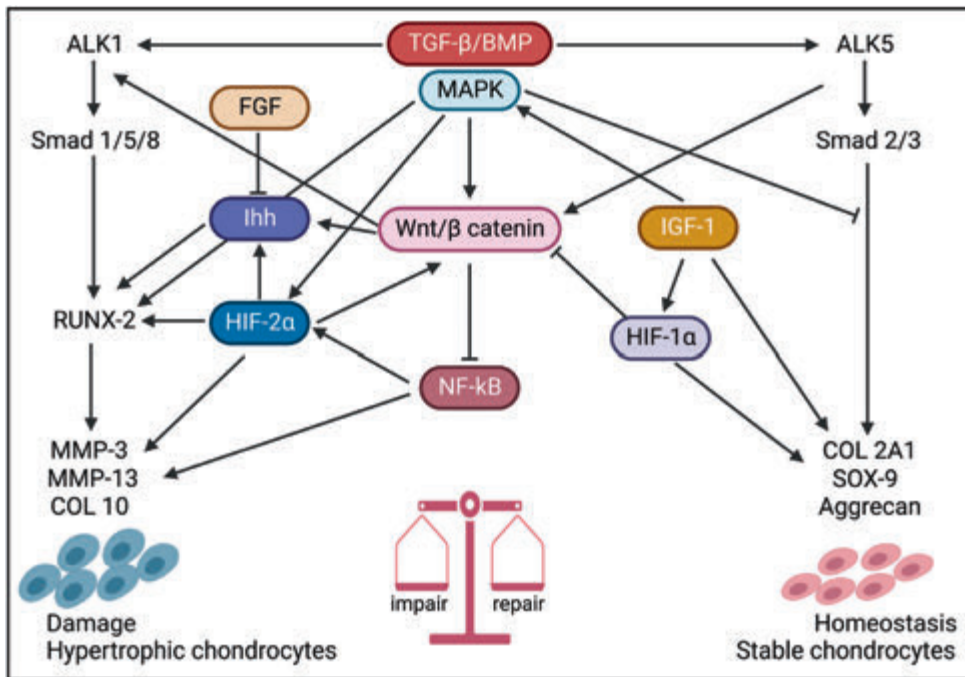


Figure 2. The schematic illustration of the signaling crosstalk of cartilage tissue homeostasis and repair. These signaling mainly comprise mitogen-activated protein kinase (MAPK), transforming growth factor- β (TGF- β), hypoxia-induced factors (HIF), bone morphogenetic proteins (BMPs), nuclear factor kappa B (NF- κ B), Wnt/ β -catenin, and indian hedgehog (Ihh) pathways, which control the balance driving for and catabolic and anabolic activities in AC (Adapted and reproduced from Mariani et al. [41], Copyright 2014, MDPI).

2.2. Joint-resident ESPCs and ESPCs-mediated AC repair

Cells are the building blocks for AC tissue engineering [10]. Many studies utilized *in vitro* manipulated cells and injected or implanted them into cartilage lesions, providing exogenous cell sources for neocartilage formation [42]. Compared with joint-resident ESPCs-mediated AC repair, these approaches result in challenges rooted in acquiring suitable high-quality, preferably sufficient autologous cells and rebuilding essential *in vitro* microenvironmental signaling that regulate *in vivo* tissue development and morphogenesis [10,43,44]. Besides, when using allogeneic or xenogeneic cells, the patients may need long-term immunosuppression therapies, probably impairing the treatment benefits. Moreover, these approaches usually ignore the donor's disease state and other features (e.g. age, ongoing chronic inflammation, and overall health conditions), perhaps influencing the tissue integration as well as the long-term survival of injected cells and engineered AC constructs [45].

Here, we suppose that cell sources for AC repair should be poised for a paradigm shift from exogenous cells or *in vitro* manipulated autologous cells to joint-resident ESPCs thanks to the emergence of advanced technologies of shifting the injured microenvironment into a pro-regenerative environment with reduced inflammation and activation of endogenous repairing signals to some degree. The 'endogeny' portion highlights the induction of optimal endogenous AC healing by ESPCs; whereas reaching this goal needs exogenous intervention more or less, for example, implanting acellular engineered regenerative scaffolds can ameliorate the diseased microenvironment suffered chronic inflammation, low abundance of ESPCs, and dysregulated tissue turnover, into a pro-regenerative scenario [9,27,28]. ESPCs are tissue-specific adult stem/progenitor cells with self-renewal and differential abilities for maintaining AC homeostasis and repairing injured AC [9,27,28]. In recent decades, ESPCs have been identified and explored as eligible cell sources for *in vivo* AC regeneration [9,28]. Residing in specific niches of knee joints, ESPCs' activation relies on biophysical and biochemical cues within the niches. These niches are from AC and intra- or peri-articular tissues, such as bone marrow, synovial fluid, synovium, ranvier groove, fat pad, cartilage, subchondral bone, periosteum, and meniscus [28] (Figure 3). Niches can provide ESPCs with instructive microenvironments that regenerative biomaterials can re-establish. Typically, a cell niche comprises ECM, cells, and soluble factors. ECM usually functions as a physical scaffold for signaling molecules and cells and is a major regulator and determinant of stem cell fate [46]. Within the ECM, various secreted proteins interact with resident cells dynamically. Distinct cell receptors (e.g. cadherins and integrins) can mediate cell-ECM interactions. Receptors are crucial adhesion molecules for ESPCs' migration, localization, survival, and differentiation.

Different subpopulations of ESPCs possess varied surface markers and chondrogenic differentiation abilities (as indicated in Table 1). For example, synovium-derived MSCs (S-MSCs) have been reported to possess the optimal chondrogenic capacity *in vitro* with a lower potential for hypertrophy among the mesenchymal tissue-derived cells [47,48]. Many studies have provided evidence of the recruitment and migration of ESPCs for cartilage repair *in vivo* [49-51]. Ma et al. (bio)fabricated the macro-porous SA/HAexo-PLGAKGN hydrogel scaffolds which exhibited desirable results of regulating inflammation homeostasis and recruiting endogenous bone marrow mesenchymal stem cells (BM-MSCs) for AC repair in rats via the sequentially deliver of LPS/BG-exo and Kartogenin (KGN) [52].

Huang et al. injected the BM-MSCs affinity peptide sequence PFSSTKT (PFS)-modified chondrocyte ECM particles combined with methacrylated gelatin (GelMA) hydrogel into a rabbit cartilage defect model [53]. The results showed the GelMA/ECM-PFS functional scaffolds promoted the recruitment of ESPCs from the defect site two weeks post-operation and generated hyaline cartilage *in vivo*, whereas the control treatment mostly led to fibrocartilage formation. The possible migration routes (PMRs) of joint-resident ESPCs for AC repair are graphically displayed in Figure 3. There might be different ESPCs involved in the repairing process depending on the category of chondral damages [28]. For adults, BM-MSCs can make direct contributions to regenerating full-thickness AC defects. Yet it remains unclear how BM-MSCs migrate to the superficial area. Additionally, experimental evidence has confirmed the direct migration of SF-MSCs, S-MSCs, and C-SPCs to superficial chondral defects. IFP-SCs may function after being recruited toward the adjacent synovial fluid and synovial lining. The PMR of Rg-MSCs along the perichondrium has also been explored in rabbit knee joints.

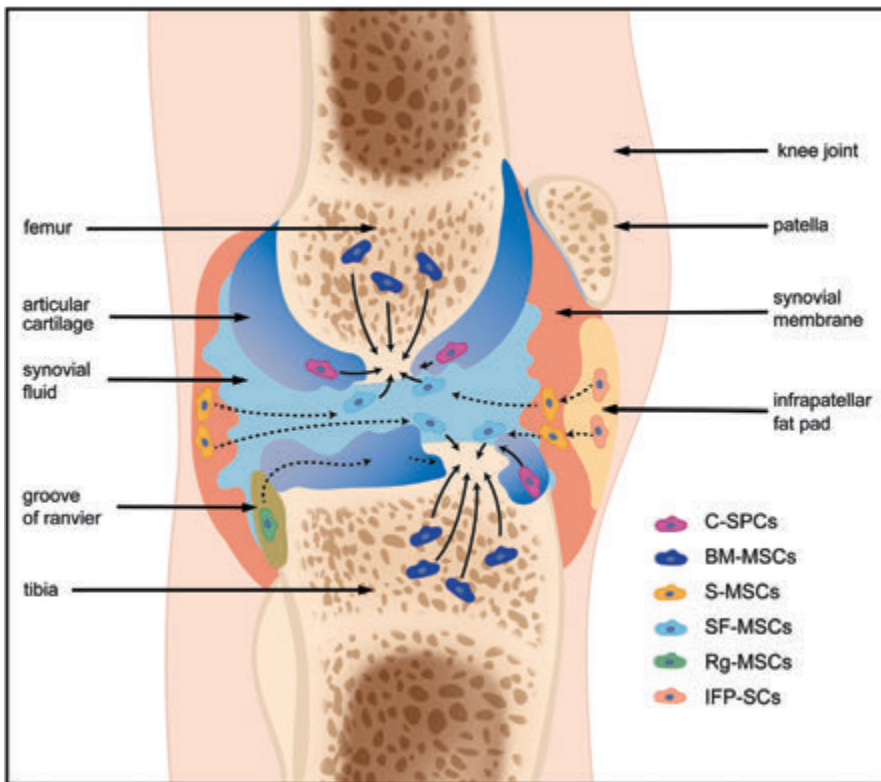


Figure 3. The possible migration routes (PMRs) of native joint-resident ESPCs for AC repair. Within the knee joint, there exist several different cell populations of ESPCs, including cartilage-derived C-SPCs, bone marrow-derived BM-MSCs, synovium tissue-derived S-MSCs, synovial fluid-derived SF-MSCs, ranvier groove-derived Rg-MSCs, infrapatellar fat pad-derived IFP-SCs, and so on. To date, there are huge knowledge gaps in the specific roles of different ESPCs during cartilage healing and the underlying mechanisms.

Table 1. Subpopulations and characteristics of native joint-resident ESPCs.

Cell Types	Location	Specific positive surface markers	Chondrogenic potential and effects on AC repair	Year of first reported
BM-MSCs	Perivascular niches in bone marrow	CD29 ⁺ , CD44 ⁺ , CD73 ⁺ , CD90 ⁺ , CD105 ⁺ , CD147 ⁺ , CD166 ⁺ , CD271 ⁺	Multilineage potential includes chondrogenesis [54]; however, they hold a high tendency to cause hypertrophic chondrocytes and bone formation [55]. CD271+ CD56+ BM-MSCs (localized in the bone-lining regions) have a better chondrogenic capacity compared to CD271+ CD56- BM-MSCs (found in the perivascular regions) [56].	1969
S-MSCs	Synovium of joint	CD10 ⁺ , CD13 ⁺ , CD14 ⁺ , CD34 ⁺ , CD44 ⁺ , CD45 ⁺ , CD49a ⁺ , CD62e ⁺ , CD73 ⁺ , HLA-DR ⁺ , CD90 ⁺ , CD105 ⁺ , CD147 ⁺ , CD166 ⁺	Reported as the best chondrogenesis potential among mesenchymal tissue-derived cells [47]. Limited potential for hypertrophy compared to BM-MSCs, IFP-SCs, and SM-MSCs [48]. CD73+CD90- S-MSCs have a better chondrogenic capacity compared to CD73+CD90+ S-MSCs [57].	2001
SF-MSCs	Synovial fluid of joint	CD40 ⁺ , CD44 ⁺ , CD44 ⁺ , CD55 ⁺ , CD73 ⁺ , CD90 ⁺ , CD105 ⁺ , CD140 ⁺ , CD147 ⁺ , CD273 ⁺	High capacity to differentiate into chondrocytes, and a lower capacity for adipogenic, osteogenic, and neurogenic differentiation [58].	2004
Rg-MSCs	Perichondria I groove of ranvier	Stro-1 ⁺ , BMP1a ⁺ , Patched ⁺ , Notch1 ⁺ , integrin β 1 ⁺ , N-cadherin ⁺ , EGFL7 ⁺	They can maintain their progenitor properties and localization and migrate to the AC surface [59].	1977
IFP-SCs	Intra-articular fat pad	CD9 ⁺ , CD10 ⁺ , CD13 ⁺ , CD29 ⁺ , CD44 ⁺ , CD49 ⁺ , CD59 ⁺ , CD90 ⁺ , CD105 ⁺ , CD104 ⁺ , CD105 ⁺ , CD147 ⁺ , CD166 ⁺	They can maintain their chondrogenic potential for a longer period [60]. A better chondrogenic potency compared with BM-MSCs.	1996
C-SPCs	Mainly in the superficial zone of AC	CD29 ⁺ , CD44 ⁺ , CD54 ⁺ , CD73 ⁺ , CD90 ⁺ , CD105 ⁺ , CD166 ⁺ , Stro-1 ⁺ , Notch-1 ⁺	Superficial cells of the nascent joint are self-renewing chondrocyte progenitors and undergo both symmetric and asymmetric cell division [61]; Stronger chondrogenic differentiation capacity than the IFP-SCs and chondrocytes [62]; Cells migrate during the development and remodeling of AC [63].	2001
CS-PCs	Subchondral cancellous bone	CD44 ⁺ , CD73 ⁺ , CD90 ⁺ , CD105 ⁺ , CD166 ⁺	They showed chondrogenic differentiation potential [64].	2008
M-SPCs	Meniscus red zone	CD29 ⁺ , CD44 ⁺ , CD73 ⁺ , CD90 ⁺ , Sca-1 ⁺ , CD105 ⁺ , CD166 ⁺	Comparable chondrogenic potential to C-SPCs [65];	2009
SM-MSCs	Muscle	NGFR ⁺ , CD44 ⁺ , CD49e ⁺ , CD73 ⁺ , CD90 ⁺ , CD105 ⁺ , CD147 ⁺ , CD54 ⁺ , CD166 ⁺	SM-MSCs harvested from traumatized muscle display a similar phenotype to BM-MSCs [66].	1961
P-MSCs	Periosteum	CD10 ⁺ , CD44 ⁺ , VEGFR-2 ⁺ , CD10 ⁺ , CD44 ⁺ , CD54 ⁺ , CD90 ⁺ , CD105 ⁺ , CD147 ⁺ , CD166 ⁺	The similar multipotency to BM-MSCs [67]; Highest calcification potential compared to BM-MSCs, S-MSCs, IFP-MSCs, and SM-MSCs [68].	1990

S-MSCs: synovium-derived MSCs; SF-MSCs: synovial fluid-derived MSCs; Rg-MSCs: MSCs in the groove of Ranvier; IFP-SCs: Intra-articular fat pad-derived stem cells; C-SPCs: cartilage-derived stem/progenitor cells; CS-PCs: Cortico-spongious progenitor cells; M-SPCs: meniscus stem/progenitor cells; P-MSCs: periosteum-derived MSCs; SM-MSCs: skeletal muscle-derived MSCs; *: characterized on human-derived tissue/primary

cells; #: characterized on animal-derived tissue/primary cells; &: characterized on tissue; ^: characterized on expanded cells *in vitro*.

2.3. CCGs for ESPCs-mediated AC repair

The migration of ESPCs is a prerequisite for endogenous AC repair [9]. Many CCGs are involved in the complicated process of recruiting ESPCs from their previous niches. GFs are polypeptide extracellular signaling molecules that play vital roles in regulating cell migration, proliferation, differentiation, and survival [9,69]. Numerous GFs function synergistically to regulate AC development and homeostasis. The expression of GFs by chondrocytes is increased after injury [70,71]. In recent years, several GFs, such as insulin-like growth factor (IGF), platelet-derived growth factor (PDGF), and TGF- β have been intensively explored for their physiological effects on chondral repair both *in vitro* and *in vivo* [72-74]. Chemokines are small proteins (8-10 kDa) expressed in tissues in response to injury or infection. On the basis of the number and spacing of cysteine residues, they can be categorized into four subfamilies: CC, CXC, XC, and CX3C [75]. ESPCs can be attracted by the activation of chemokines to migrate along the chemotactic gradients and are involved in various following repair stages [75]. ESPCs express various receptors for chemokines, such as CXC chemokine receptors 1 and 2 (CXCR1 and CXCR2), CC chemokine receptor 1 (CCR1) and CCR2, and receptors of GFs such as PDGF receptors a (PDGFR-a) and b (PDGFR-b). Besides, inflammatory cytokines are crucial for regulating the inflammation balance of the defect site. The detailed information of CCGs regarding the members and the potential regulatory effects for ESPCs-mediated cartilage repair are listed in Table 2.

Table 2. The effects of endogenous CCGs on guiding ESPCs for AC regeneration.

Guiding factors	CCGs	Family members	Regulatory effects	Reference
Recruitment factors	chemokines	CCL2 (MCP-1), CCL5 (RANTES), CCL17 (TARC), CCL19 (MIP-3 β), CCL20 (MIP-3 α), CCL21 (SLC), CCL22 (MDC), CCL25 (TECK), CCL28 (MEC), CXCL7 (NAP-2), CXCL8 (IL-8), CXCL10 (IP-10), CXCL11 (I-TAC), CXCL12 (SDF-1), CXCL13 (BLC), CXCL16 (SR-PSOX), XCL1 (Lptn)	To stimulate the chemotaxis of ESPCs	[9,28,29]
	GFs	PDGF-AA, PDGF-AB, PDGF-BB, IGF-1, IGF-2, IGFBP-5, TGF- β 1, TGF- β 3, BMP-2, BMP-4, BMP-7, VEGF-A, FGF-2, HGF, EGF, HB-EGF		
Proliferation factors	GFs	IGF-1, TGF- β 1, TGF- β 3, BMP-2, BMP-4, BMP-7, TGF- β , FGF-2, FGF-9, FGF-18	To stimulate the cell proliferation of ESPCs	[9,76]
Differentiation factors	GFs	TGF- β 1, TGF- β 3, BMP-2, BMP-6, BMP-7, FGF-9, FGF-18, Ihh, PTHrP, Wnt-4, Wnt-8, VEGF	To stimulate ESPCs' chondrogenesis	[9,76]
Inflammatory factors	cytokines	TGF- β , IL-10, IL-4 (anti-inflammation) IL-1 β , IL-6, TNF- α , IL-8, IL-17, IL-18, IFN- γ (pro-inflammation)	To modulate the inflammatory balance	[77]

MCP-1: monocyte chemoattractant protein-1; RANTES: regulated on activation, normal T cell expressed and secreted; TARC: thymus- and activation-regulated chemokine; MIP: macrophage inflammatory protein; SLC: secondary lymphoid-tissue chemokine; MDC: macrophage-derived chemokine; TECK: thymus-expressed chemokine; MEC: mucosae-associated epithelial chemokine; LEC: liver-expressed chemokine; CTACK: cutaneous T-cell attracting chemokine; PARC: pulmonary and activation-regulated chemokine; NAP-2: neutrophil-activating peptide; IL-8: interleukin-8; IP-10: interferon-inducible protein-10; I-TAC: interferon-inducible T cell alpha chemoattractant; SDF-1: the stromal cell-derived factor-1; BLC: B lymphocyte chemoattractant; SR-PSOX: scavenger receptor for phosphatidylserine and oxidized lipoprotein; ENA-78:

epithelial-derived neutrophil-activating peptide; GRO- α : growth-regulated oncogene-alpha; LPtn: lymphotactin; PDGF: platelet-derived growth factor; IGF: insulin-like growth factor; TGF: transforming growth factor; BMP: bone morphogenetic protein; VEGF: vascular endothelial growth factor; FGF: fibroblast growth factors; HGF: hepatocyte growth factor; EGF: epidermal growth factor; HB-EGF: Heparin-binding epidermal growth factor.

3. MACRO/MICRO-POROUS REGENERATIVE SCAFFOLDS FUNCTION AS INSTRUCTIVE BIOREACTORS FOR ESPCS AND THEIR CURRENT CHALLENGES FOR EPSC-BASED AC REPAIR

More recently, macro/micro-porous regenerative biomaterials-based therapy has evolved as a potentially powerful paradigm in cartilage regenerative medicine [78,79]. Typically, these cell-free scaffolds, serving as instructive bioreactors of ESPCs, can promote ESPCs-mediated AC repair on their own or in combination with biologics. With optimized biochemical and biophysical cues, they can be fabricated into varied shapes, sizes, and formulations [15]. These cues play fundamental roles in providing a pro-regenerative microenvironment, open porous structures allowing for coaxing the directional cell homing and infiltration of ESPCs, and supporting cell adhesion, proliferation, and chondrogenesis [15]. For example, the study from Levinson et al. demonstrated that adhesive HA-transglutaminase (HA-TG) hydrogel with chondrogenic properties in a collagen scaffold could allow for ESPCs invasion and promote ESPCs-mediated cartilage repair in an ovine model [80]. The ideal regenerative scaffolds should possess non-toxic, non-immunogenic, and satisfactory biocompatible and biodegradable properties [13,32]. They should be easily manufactured and ease in handling [15]. In the past decades, a plethora of regenerative scaffolds has been (bio)fabricated and assessed for AC repair in the form of bioglasses [81], sponges [82], hydrogels [11], electrospun fibers [83], micro/nanoparticles [49,84], etc. An overview of the pros and cons, as well as specific applications for cartilage repair of various regenerative biomaterials is summarized in another review from Duarte Campos et. al [14]. Naturally-derived biomaterials have been demonstrated several advantages compared to synthetic biomaterials: They hold better biocompatibility, biodegradability, and remodeling properties compared to synthetic biomaterials [14]. For example, animals or human-derived collagen and fibrin consist of cell adhesion ligands and can be vulnerably proteolytically cleaved and degraded, enabling cell infiltration and remodeling. These scaffolds interact with cells by specific surface ligands, contributing to ESPCs migration, proliferation, and matrix deposition [15]. Synthetic biodegradable polymers (e.g. PCL, PLA, PLGA, PLLA, PVA, and PEG) offer some advantages over natural materials, including high reproducibility, controlled degradation rate *in vivo*, easy manipulation into specific shapes, and high mechanical strength; nevertheless, such scaffolds lack the cell recognition signals [14,15]. Thus, synthetic scaffolds are often modified with proteins and peptides to support ESPCs infiltration. Containing two or more different constituent biomaterials or phases on a microscopic or macroscopic size scale, composite biomaterials consisting of natural and synthetic materials can combine the advantages of synthetic polymeric materials with that of natural materials to achieve excellent mechanical properties, bio-functionality, and tunable degradability. Even though tremendous progress in AC repair has been achieved by synthetic and composite regenerative scaffolds, only a few of these scaffolds are now in

clinical use or practice. The commercially available biomaterial products for AC repair are still primarily based on natural biomaterials such as collagen (MaioRegen Chondro+), HA (Chondrotissue® and Hyalofast®), and fibrin glue (Tisseel®) [10,85].

From the scope of preclinical studies, challenges in AC repair often arise after the implantation of engineered regenerative biomaterials into defects. Poor integration with adjacent tissues, undesirable biomechanics for joint locomotion, excessive inflammatory environment, phenotypic instability in the longer run, insufficient recruitment of ESPCs, unfavorable degradable characteristics, high cytotoxicity as well as nerves and blood vessels invasion [2,10,86] impede the further translational potentials of these regenerative biomaterials (Figure 4). To address the above limitations and challenges of current regenerative biomaterials, considerable efforts have been made to reinforce the integration with native cartilage or/and bone, achieve desirable biomechanics, improve anti-inflammation and immunity control, maintain cartilaginous phenotype stability, recruit and guide enough ESPCs, possess favorable degradability, increase biocompatible properties, and seek for anti-angiogenesis coupling with anti-neurogenesis strategies [9,11,28,87]. Some of them have achieved desirable preclinical results. However, regarding the ultimate clinical translation of the established optimal regenerative scaffolds-based ESPCs-mediated cartilage repair, it still has a long way to move forward.

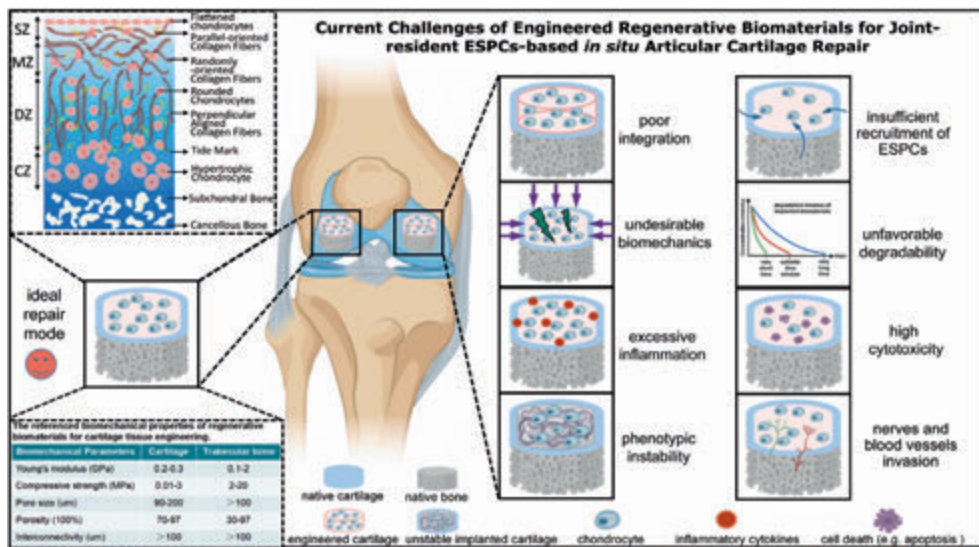


Figure 4. Current challenges of engineered regenerative biomaterials-based guiding of ESPCs for cartilage repair. Eight major challenges faced from the bench to bedside include poor integration with adjacent cartilage, undesirable biomechanics for joint locomotion, excessive inflammatory environment, phenotypic instability over a longtime window, insufficient recruitment of ESPCs, unfavorable degradable characteristics, high cytotoxicity as well as nerves and blood vessels invasion. For the ideal repair mode, the implanted regenerative scaffolds should possess various favorable biochemical cues coupled with biophysical support to promote neocartilage formation whose both anatomical structure and biomechanical characteristics are comparable with surrounding healthy hyaline cartilage. (Partially created by BioRender. The diagram of AC stratified structure is reproduced from Zhou et al. [10], Copyright 2020, John Wiley and Sons).

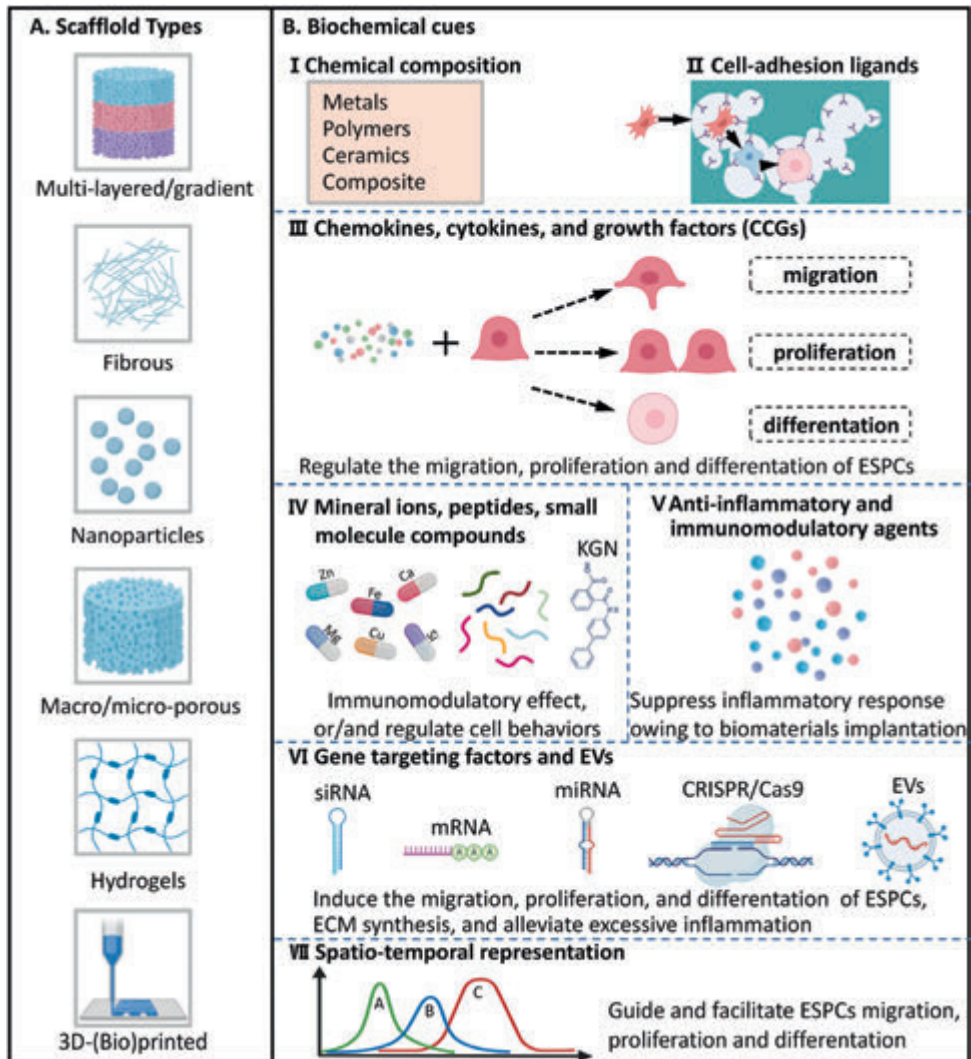


Figure 5. Innovative (bio)design and (bio)fabrication of regenerative biomaterials with favorable biochemical cues to guide joint-resident ESPCs for AC repair. (A) Several examples of regenerative scaffolds, including multi-layered/gradient scaffolds, fibrous scaffolds, nanoparticles, microporous scaffolds, hydrogels, and 3D-printed scaffolds, have been widely explored to harness the innate regenerative ability of cartilaginous tissues in preclinical studies. (B) Engineering regenerative scaffolds with appropriate biochemical cues through (I) chemical composition and (II) surface/interface chemistry modification of biomaterials to produce cell-adhesion ligands. These biochemical cues mainly include (III) CCGs, (IV) peptides, mineral ions, and small-molecule compounds, (V) anti-inflammatory and immunomodulatory agents, (VI) gene targeting factors and EVs (mRNA, messenger RNA; miRNA, microRNA; siRNA, small interfering RNA; and extracellular vesicles, EVs). The combination of regenerative scaffolds and engineered biochemical cues are usually presented as (VII) spatiotemporal delivery/release modalities. (Created by BioRender).

Table 3. Examples of engineered regenerative biomaterials with various favorable biochemical cues to guide ESPCs for AC repair.

Engineered biochemical cues	Specific examples	Other biologics & biomaterials	<i>In vitro/vivo</i>	Influences on SPCs or/and potential applications for ESPCs-mediated AC repair	Reference
Chemical composition	Composition ratios of Gel/HA hybrid hydrogels	N/A	<i>in vitro</i>	Different chemical composition ratios of Gel/HA hybrid hydrogels affected cell adhesion and chondrogenesis. The Gel/HA composite hydrogel (30%/70%) seemed the most promising matrix for chondrogenesis with balanced cell proliferation and adhesion.	[18]
	Lithium incorporation	Li ₂ Ca ₄ Si ₄ O ₁₃ bioceramic	<i>in vitro</i>	A lithium-containing biomaterial promoted chondrogenesis of iPSCs with reduced hypertrophy.	[92]
	Composition ratios of PEG:CS:MMP-pep	N/A	<i>in vitro</i>	Unique biomaterial compositions (PEG:CS:MMP-pep) directed BMSCs into specific chondrocyte phenotypes corresponding to the various zones of AC.	[93]
(Surface/interface) chemical modification	Hydrophilic coating	PLGA scaffold	<i>in vitro</i>	The hydrophilic surface of biomaterials had beneficial effects on chondrocyte activity and matrix synthesis.	[94]
	Gelatin, collagen, chitosan coating	PLLA membrane	<i>in vitro</i>	PLLA membrane surfaces modified with natural macromolecule layers could enhance chondrocyte attachment, proliferation rate, and cell activity.	[95]
	HA modification	PLGA scaffold	<i>in vitro</i>	HA-coated wells and HA-modified PLGA scaffolds could enhance the chondrogenesis of human ADSCs.	[96]
	HA modification	PGA scaffold	<i>in vitro</i>	HA coating of PGA scaffolds could significantly improve biocompatibility and cartilage formation.	[97]
	Hydrophilic coating	PLLA scaffold	<i>in vitro</i>	Hydrophilic coating using two or more natural macromolecules (CS and Collagen) on scaffolds may synergistically enhance chondrogenesis.	[98]
	CS surface grafting	PLLA fiber	<i>in vivo</i> ; rabbit model	An aligned PLLA fiber scaffold grafting with a biomimetic CS surface for accelerating cartilage repair	[19]
	NB coating	SF microparticle	<i>in vivo</i> ; rabbit model	JS-Paint is mainly composed of NB-coated silk fibroin microparticles and possesses optimal cell adhesion, migration, and proliferation properties for promoting AC regeneration.	[99]
Chemokines, Cytokines, and GFs (CCGs)	CXCL12	fibrin/HA hydrogel	<i>ex vivo</i> ; bovine OC explant	CXCL12-loaded fibrin/HA hydrogel networks could achieve functional repair of full-thickness bovine AC defect via homing chondrogenic progenitor cells.	[100]
	IL-8- and MIP-3 α	PLA/ β -TCP scaffold	<i>in vivo</i> ; beagle model	IL-8 and MIP-3 α significantly enhanced the chemotaxis of BMSCs. IL-8- and MIP-3 α -containing scaffolds recruited ESPCs for knee AC regeneration.	[101]

	IL-4 and IL-13	Gelatin/genipin microspheres	<i>in vitro</i>	Exposure of the IL-4 and IL-13 loaded microspheres reduced the inflammation of chondrocytes up to 80%. The microsphere format allowed for minimally invasive delivery of anti-inflammatory cytokines for cartilage repair.	[102]
	IL-4	GelMA/PCL-HA scaffold	<i>in vivo</i> ; rabbit model	The upper layer with IL-4 relieved the adverse effects of inflammation on chondrocytes. IL-4-loaded bi-layer scaffold promoted the regeneration of both cartilage and subchondral bone.	[103]
	TGF-β3	PLCL scaffold	<i>in vivo</i> ; nude mice model	TGF-β3 encapsulated PLCL scaffold could help to yield hyaline cartilage-specific lacunae structures and prevent hypertrophic chondrocyte formation.	[104]
	TGF-β1	HA/HAp/PEG-PCL scaffold	<i>in vivo</i> ; rabbit model	TGF-β1 containing composite scaffold could enhance the healing of cartilage and subchondral bone through improved effects on EPSCs adhesion, proliferation, and differentiation.	[20]
	PDGF-BB and TGF-β3	HAMA/HepMA microgel	<i>in vivo</i> ; rat model	Stem cell-recruiting injectable microgels loaded with PDGF-BB and TGF-β3 for repairing cartilage.	[73]
	PRPs	PLPMH scaffold	<i>in vivo</i> ; rabbit model	PRP-loaded macro-porous hydrogel scaffold recruited endogenous M2 macrophages in large numbers and long-time duration (42 days) to provide a local anti-inflammatory microenvironment for AC repair.	[51]
Mineral ions	Mg ²⁺	N/A	<i>in vitro/vivo</i> ; rabbit model	Mg ²⁺ enhanced the adherence and cartilage formation of S-MSCs through integrins; Mg ²⁺ enhanced the chondrogenesis of MSCs by inhibiting activated macrophage-induced inflammation.	[87,105]
	Mg ²⁺	Mg-Nd-Zn-Zr alloy@PDA	<i>in vitro</i>	The Mg-based scaffolds could recruit MSCs, enhance chondrogenesis, attenuate local inflammatory responses by improving M2 macrophage polarization, and down-regulating NF-κB signaling.	[21]
	Sr ²⁺ , Cu ²⁺ , Mn ²⁺ , Zn ²⁺ , Si ⁴⁺	N/A	<i>in vitro/vivo</i>	Strontium, copper, manganese, zinc, and silicon-based scaffolds could improve cartilage formation.	[81],[106],[107],[108],[109]
Chondroinductive/chondroconductive peptides	CK2.1	β-GP/CS-HAp/CS	<i>in vivo</i> ; rabbit model	CK2.1-coated β-glycerophosphate chitosan composite scaffolds for cartilage repair in a rabbit model through the recruitment and induced chondrogenesis of EPSCs.	[23]
	PFSSTKT	dECM/RAD peptide	<i>in vivo</i> ; rabbit model	Increased recruitment of EPSCs and chondrogenic differentiation by a composite scaffold loaded with bone marrow homing peptides for repairing AC.	[110]
	GGGHAVDI	NC/PdBT/GHK	<i>in vivo</i> ; rabbit model	Hydrogels containing a chondrogenic peptide sequence could obtain higher histological assessments of overall defect filling, GAGs, cell contents, and cartilage surface regularity.	[89]
	DHLSDN YTLDHD RAIH	N/A	<i>in vitro</i>	Link protein N-terminal peptide significantly enhanced migration and chondrogenesis of PSCs <i>in vitro</i> .	[111]

Biochemical cues to enhance endogenous repair

	Ec peptide	TGF-β1	<i>in vitro</i>	Ec could facilitate <i>in vitro</i> hMSC mobilization and chondrogenesis and enhance the role of TGF-β1.	[112]
Small molecule compounds	Dexamethasone	PLGA/agarose	<i>in vivo</i> ; canine model	Sustained delivery of low-dose dexamethasone (up to 99 days) via a PLGA microsphere-embedded agarose implant to attenuate inflammation and improve pro-anabolic effect for AC repair.	[113]
	KGN	SDF-1/PLGA/HA	<i>in vivo</i> ; rabbit model	A cell-free therapy for AC repair based on synergistic delivery of SDF-1 & KGN (more than two months) with HA injectable hydrogel.	[22]
	Icariin	N/A	<i>in vivo</i> ; rabbit model	Icariin promoted proliferation, and chondrogenic differentiation of BMSCs <i>in vitro</i> and rabbit knee cartilage defects repair via the BMP/Smad pathway.	[114]
Gene targeting factors and EVs	antimiR-221	fibrin/HA	<i>ex vivo</i> ; bovine OC explant	Hydrogel loaded with antimiR-221/lipofectamine could drastically enhance AC regeneration through ESPCs.	[24]
	miR-29b-5p	(SKPPGTSS) SAP hydrogel	<i>in vivo</i> ; mice model	Sustained miR-29b-5p delivery and recruitment of S-MSCs and their subsequent differentiation into chondrocytes led to successful cartilage repair and chondrocyte rejuvenation.	[115]
	hWJMSC-Exos	dECM scaffold	<i>in vivo</i> ; rat/rabbit model	hWJMSC-Exos could promote cell proliferation, migration, and polarization <i>in vitro</i> . hWJMSC-Exos injection could inhibit inflammation in the joint cavity and improve cartilage repair.	[116]
	DNA aptamer	SF/HA-Tyr hydrogel	<i>in vivo</i> ; rabbit model	Apt19S-functionalized bilayer scaffold could dramatically enhance BM-MSCs migration <i>in vitro</i> and support AC repair by recruiting ESPCs toward the defect sites of rabbits.	[117]
	rAAV vector	PEO-PPO-PEO hydrogel	<i>in vivo</i> ; minipig model	The PEO-PPO-PEO poloxamers-based thermosensitive hydrogels allowed for a controlled in situ release of rAAVs to repair chondral defects effectively.	[118]
Anti-inflammatory & immunomodulatory agents	Celebrex	N/A	<i>in vivo</i> ; rat model	Celecoxib acted as chondroprotective and anti-inflammatory effects on AC both <i>ex vivo</i> and <i>in vivo</i> .	[119]
	Squid collagen II	N/A	<i>in vivo</i> ; rat model	Squid collagen II promoted cartilage repair via inhibiting apoptosis and hypertrophy of chondrocytes and immunomodulating activation of M2 macrophages.	[120]
	GM-HPCH+TGFβ1	N/A	<i>in vivo</i> ; rat model	The GM-HPCH + TGFβ1 hydrogels effectively improved AC repair by immunoregulating macrophages, recruiting ESPCs, and facilitating chondrogenesis.	[25]
	PRP-GelMA	N/A	<i>in vivo</i> ; rabbit model	20% of PRP-GelMA hydrogels improved the chemotaxis and chondrogenesis of ESPCs, immune regulation, and macrophage polarization shift from M1-to-M2, which were suitable for AC repair.	[91]

MMP-pep: matrix metalloproteinase-sensitive peptides; *NB*: N-(2-aminoethyl)-4-(4-(hydroxymethyl)-2-methoxy-5-nitrosophenoxy) butanamide; *HAp*: hydroxyapatite; *KGN*: kartogenin; *HAMA/HepMA*: methacrylated HA and heparin; *PLPMH*: platelet lysate-rich plasma macro-porous hydrogel; *β-GP*: β-glycerophosphate; *OC*: osteochondral; *PRP*: platelet-rich plasma; *SAP*: self-assembling peptide; *silk fibroin*: SF; *NC/PdBT/GHK*: N-cadherin/poly(glycolic acid)-di(but-2-yne-1,4-dithiol)/glycine-histidine-lysine; *hWJMSC-Exos*: human umbilical cord Wharton's jelly MSC-derived exosomes; *rAAVs*: recombinant adeno-associated virus; *PEO-PPO-PEO*: poly(ethylene oxide)-poly(propylene oxide)-poly(ethylene oxide); *GM-HPCH*: glycidyl methacrylate-modified hydroxypropyl chitin.

4. REGENERATIVE IMPLANTS WITH FAVORABLE BIOCHEMICAL CUES MAGNIFY THE HEALING EFFECT OF ESPCS FOR AC REPAIR

Due to their intrinsic characteristics, traditional biomaterials have shown limited capabilities in promoting cell recruitment, proliferation, and differentiation. Moreover, traditional biomaterial treatment might bring inadequate cartilaginous matrix deposition and maturation, a lack of natural anisotropic structures, and excessive inflammation [11,14]. However, advanced regenerative scaffolds with optimized biophysical and biochemical properties can overcome the above-mentioned challenges to some degree. It has been shown that biophysical and biochemical cues function synergistically to facilitate AC regeneration [88]. In this review, we only focus on tunable biochemical messages. Across the intracellular and extracellular environment, the gradient presence of biochemical cues is able to respond to multiple cell functional requests [9,88]. Many exogenous biochemical cues can be incorporated into biomaterials to regulate ESPCs' physiological activities, i.e. enhancing cell migration. Therefore, we think that an exquisite (bio)design and (bio)fabrication of regenerative scaffolds with appropriate biochemical cues holds the potential to guide ESPCs-mediated cartilage repair. A variety of multi-layered/gradient, fibrous, nanoparticle, macro/micro-porous, and hydrogel scaffolds have been constructed through many emerging cutting-edge technologies and concepts including 3D-(bio)printing [49,52,89-91] (Figure 5A). Their beneficial biochemical signals are usually rooted in chemical composition (Figure 5B (I)), (surface/interface) biochemical modification (Figure 5B (II)), CCGs (Figure 5B (III)), mineral ions, peptides, small molecule compounds (Figure 5B (IV)), gene-targeting factors and EVs (Figure 5B (V)), anti-inflammatory and immunomodulatory agents (Figure 5B (VI)), and spatiotemporal scaffold-based drug delivery systems (SDDS) (Figure 5B (VII)). Some specific examples are listed below in Table 3. Novel regenerative scaffolds should ideally possess one or more features beyond conventional biomaterials, offering a pro-regenerative microenvironment for ESPCs' homing and chondrogenesis as well as matrix production and maturation, and responding to dynamic changes in the environment throughout the neocartilage formation.

4.1. Chemical compositions and chemistry modifications

A judicious selection of cartilage-mimicking biomaterials with varying tailored chemical compositions and/or (surface/interface) chemistry modifications can impact the amount or phenotype of resulting cartilage. For example, different chemical composition ratios of gelatin/HA hybrid hydrogels affected the cell behaviors of hMSCs [18] (Figure 6A). It has been shown that pure gelatin enabled good cell adhesion without notable *in vitro* chondrogenesis of MSCs, while pure HA induced chondrogenesis without cell spreading

[18]. The hydrated gelatin/HA scaffolds, particularly with more contents of HA, enhanced cell adhesion, proliferation, and chondrogenic differentiation [18]. More GAG contents were observed with elevated expression of chondrogenic markers such as sox-9, aggrecan, and collagen II [18]. Compared with naturally derived biomaterials, biologically inert synthetic biomaterials lack cell-adhesion ligands, namely cell recognition signals, and their hydrophobic nature impedes cell attachment and spreading [121]. To improve the biocompatibility of synthetic biomaterials, chemistry modifications can be utilized to generate cell-biomaterial interfaces which are beneficial for eliciting cell spreading and maintaining differentiated phenotypic expression [122]. Apart from synthetic biomaterials, natural biomaterials, for example, HA and its derivatives, have been widely utilized for EPSC-mediated AC repair [97,100,123]. The abundant -COOH and -OH functional groups support their chemistry modifications and covalent crosslinking via ester and ether linkages. The chemical functionalization of HA-based biomaterials through various functional groups has been well summarized in Ref. [43] (Figure 6B).

Scaffold surface characteristics critically influence cell behaviors and ECM production. The hydrophilic surface has been shown to have a beneficial effect on chondrocyte activity [94]. To enhance the hydrophilic properties of the surface, hydrophilic and reactive groups such as hydroxyl, amide, and carboxyl have been introduced onto the scaffold surface by plasma treatment, ozone oxidation, aminolysis, and photo-induced grafting copolymerization of hydroxyethyl methacrylate (HEMA) or methacrylic acid (MAA) [83]. These hydrophilic groups can be used to immobilize biologically active ligands further to produce bioactive surfaces [124]. Ren et al. fabricated an aligned PLLA fiber scaffold with a biomimetic surface for accelerating cartilage repair [19] (Figure 6C). CS was grafted on the fiber surfaces using polydopamine (PDA) as an adhesive polymeric bridge. The PLLA/PDA/CS scaffolds were implanted into cartilage defects drilled in the middle area of rabbit femoral condyles. The *in vivo* macroscopic and histological assessment results suggested that the PLLA/PDA/CS scaffolds obviously improved defects filling and hyaline AC formation compared to PLLA, PLLA/PDA scaffolds. Zhang et al. fabricated a ready-to-use tissue-adhesive joint surface paint (JS-Paint) in favor of repairing AC [99] (Figure 6D). The JS-Paint mainly consists of N-(2-aminoethyl)-4-(4-(hydroxymethyl)-2-methoxy-5-nitrosophenoxy) butanamide (NB)-coated silk fibroin (SF) microparticles and possesses excellent properties to facilitate cell spreading, migration, and proliferation. NB-modified SF microparticles can attach directly to AC and yield a smooth layer on the surface through the photogenerated aldehyde group of NB reacting with the -NH₂ groups of AC tissues. At six weeks post-surgery, the JS-Paint-treated groups indicated considerable improvements in repairing rabbit partial-thickness AC defects and forming smoothed surfaces. Chen et al. immobilized quercetin (QUE) on the poly (3-hydroxybutyric acid-co-3-hydroxyvaleric acid) (PHBV) scaffold through the esterification reaction to improve its bioactivity required for cartilage regeneration [125]. Chen et al. introduced carboxyl groups on the surface of PLLA nanofibers via oxygen plasma, followed by covalent grafting of cationized gelatin molecules onto the fiber surface to make it more conducive to cell attachment and spreading [83].

Additionally, surface coating of some natural macromolecules such as proteoglycans, HA, and collagen was also reported [95-97,126]. Ma et al. immobilized three types of natural macromolecules (collagen, gelatin, or chitosan) on the PLLA membrane surface using a

grafting-coating method to improve its biocompatibility [95]. Results confirmed that this layer of natural macromolecule attached tightly to the PLLA membrane surface. Chondrocytes cultured on this modified PLLA membranes held better cell attachment, proliferation rate, and viability. Lin et al. uncovered the improved biocompatibility and cartilage formation by HA coating on polyglycolic acid (PGA) in a rabbit model [97]. *In vitro* characterization demonstrated that HA coating enhanced cell adhesion to PGA scaffolds. This might be due to the binding between cells and the biomaterials through HA and CD44, a receptor for HA. Besides, a less inflammatory reaction was exhibited on the HA-coated scaffold *in vitro* and *in vivo* [97]. Moreover, hydrophilic coating using two or more natural macromolecules on scaffolds may have a synergistic effect. Chang et al. reported the best hydrophilicity, degradation rates, and upregulation of cell activity on HA/CS-coated PLGA scaffold compared to HA or chitosan alone [94]. Gong et al. assembled biocompatible CS and collagen I onto PLLA scaffolds layer by layer for enhancing the cell-biomaterial interactions [98]. Significant improvement in cell attachment, proliferation, cytoviability, and GAGs secretion on the PLLA/CS/collagen scaffold was achieved.

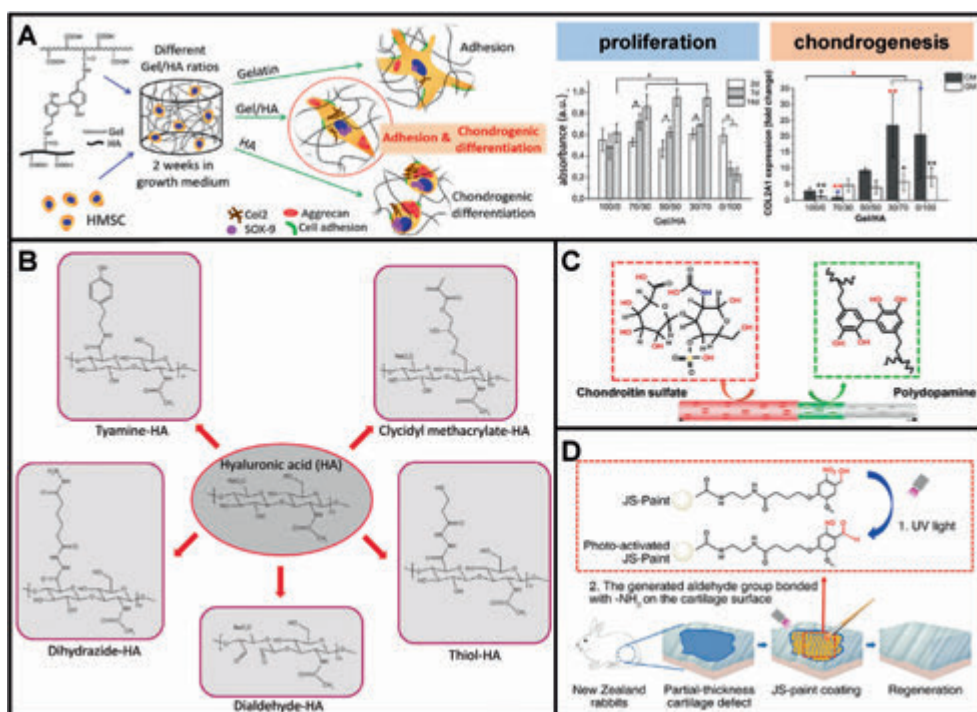


Figure 6. Chemical compositions and chemical modifications of regenerative scaffolds could provide favorable biochemical cues for cell adhesion, proliferation, chondrogenesis, and ESPCs-mediated AC repair. (A) Different chemical composition ratios of gelatin/HA hybrid hydrogels affected cell behaviors of hMSCs regarding adhesion and chondrogenic differentiation (adapted and reproduced from et al. [18], Copyright 2017, ACS). (B) A selection of chemical modifications of HA (reproduced from Ivirico et al. [43], Copyright 2017, Elsevier). (C) Chondroitin sulfate (CS) was grafted on the surface of an aligned porous fibrous membrane through PDA coatings to accelerate cartilage regeneration (reproduced from Ren et al. [19], Copyright 2019, Elsevier). (D) NB-modified SF microparticles-based tissue-adhesive paint for articular surface cartilage regeneration (reproduced from Zhang et al. [99], Copyright 2020, ACS).

4.2. Exogenous chemokines, cytokines, and growth factors (CCGs)

As discussed in section 2.3, inadequate endogenous CCGs would lead to failed endogenous cartilage healing. Therefore, engineering regenerative biomaterials with exogenous favorable CCGs emerged as a promising way for promoting AC repair process. Via these sufficient cues, the implant could recruit more ESPCs with cartilage regeneration capacities from adjacent niches and guide further tissue repair. Many previous studies have investigated the cell-recruiting abilities of chemokines, such as CCL2, CCL5, CCL21, CCL25, CXCL8, CXCL12, and CXCL13 [100,127-129]. Joutoku et al. found that exogenous CCL21 delivery to adults diminished scar-forming healing and improved hyaline-like AC formation in a rabbit OCD model. Their results showed that the CCL21/CCR7 axis might be crucial for the molecular control mechanism of juvenile AC repair, raising the possibility that agents modulating the production of CCL21 *in vivo* could enhance the quality of newly-formed cartilage among adults [130]. In a bovine explant model, Yu et al. delivered rhSDF-1 α through fibrin and HA hydrogels to treat full-thickness chondral defects [100] (Figure 7A). Using rhSDF-1 α dramatically improved the recruitment of ESPCs to the defect area on day 12. It achieved significantly better cell morphology, matrix deposition, tissue ultrastructure, and mechanical properties at six weeks [100]. Besides, since acute, local inflammation and systemic inflammation appeared to hold detrimental effects on chondrogenesis and chondral healing [131], exogenous anti-inflammatory cytokines administration represented one option for AC repair. Bioresponsive gelatin microspheres loaded with IL-4, IL-10, and IL-13 as anti-inflammatory cytokines reduced inflammation and stimulated a metabolic response for AC repair [102] (Figure 7B).

Apart from chemokines and cytokines, GFs also play crucial roles in cell proliferation and differentiation during EPSC-mediated AC repair. The study by Lee et al. demonstrated that TGF β 3-adsorbed collagen hydrogel recruited 130% more cells in the humeral regenerated AC of skeletally mature rabbits (6-month-old) compared to TGF β 3-free collagen hydrogel [132]. And thereby TGF β 3-treated group yielded hyaline cartilage regeneration and significantly greater thickness on the articular surface [132]. Similar results were reported that TGF- β 1 improved the overall full-thickness cartilage defect repair in 4-month-old rabbits [133]. Nixon et al. treated critical-sized (15 mm in diameter) full-thickness cartilage defects on the lateral trochlear ridge of the distal femur of adult horses with IGF-1 fibrin clots [134]. After six months, the cartilage defects loaded with IGF-1 fibrin clots were filled with hyaline cartilage, while the IGF-1-free fibrin clots resulted in poorly organized collagen (predominantly type I) and fibroblasts. A similar effect of IGF-1 was observed in repairing partial thickness AC defects created in the knee joints of skeletally mature rabbits and mini pigs [135].

Vainieri et al. explored the *in vitro* BMSC migration under different concentrations of PDGF-BB, CCL5, and CXCL12 using a 3D spheroid-based assay and PDGF-BB was chosen as the most promising chemotactic factor [136]. *In vivo* data indicated that both hydrogels strengthened ESPC infiltration and supported a favorable microenvironment for producing neocartilage using an osteochondral explant model implanted subcutaneously in athymic mice. Of note, these processes were best supported in fibrin-HA hydrogels without PDGF-BB [136]. Additionally, combinational utilization of CCGs exhibited some advantages in eliciting its maximal chemotactic performance. Luo et al. combined mechano growth factor (MGF) and TGF- β 3 into silk scaffolds for AC repair in a rabbit model [72] (Figure 7C).

This combination significantly increased cell recruitment ability *in vitro*. The MGF/TGF- β 3-treated group produced more cartilage-like ECM and less fibrillar collagen than MGF- or TGF- β 3-treated group [72]. Lei et al. fabricated a PDGF-BB and TGF- β 3 loaded HAMA and heparin blend microgel for AC repair in a rat model [73] (Figure 7D). The studies showed that the microgel could improve the migration ability of ESPCs and recruit them from surrounding niches by releasing PDGF-BB. Via using HA, the “cell island” microgels provided an amenable microenvironment for cell attachment and spreading. Furthermore, the “cell island” microgels induced chondrogenic differentiation of the recruited ESPCs through releasing TGF- β 3 and presented an excellent repairing potential for cartilage. To date, all these strategies are on preclinical stages and much more efforts are needed for their translation.

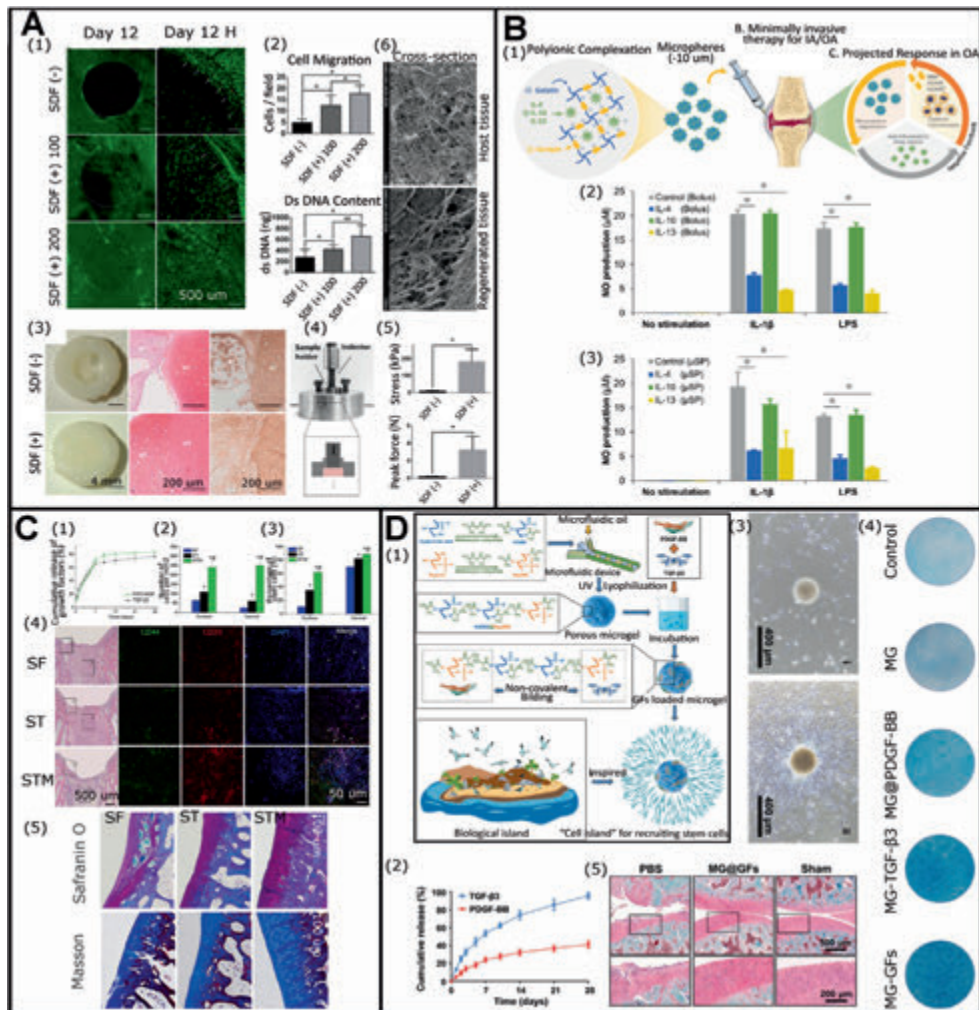


Figure 7. Exogenous CCGs can function as favorable biochemical cues for ESPCs-mediated AC repair. (A) Functional repair of full-thickness bovine AC defect via homing of ESPCs by rhSDF-1 α -loaded fibrin/HA composite hydrogels. Cell migration assay in response to rhSDF-1 α (A1), and quantification of migrated cells and DNA contents (A2). Assessment of cartilage integration of repaired tissues in macroscopic appearance,

safranin O staining, and IHC staining of Col II (A3), mechanical analysis (A4 and A5), and cross-section SEM images (A6) (Adapted and reproduced from Yu et al. [100], Copyright 2015, John Wiley and Sons). (B) Injectable microspheres for AC preservation and repair through on-demand delivery of anti-inflammatory cytokines. (B1) Graphical illustration of this study. (B2 and B3) Cytokine-loaded microspheres could modulate the inflammation status (adapted and reproduced from Park et al. [102], Copyright 2019, John Wiley and Sons). (C) MGF and TGF- β 3 functionalized silk scaffolds to improve articular hyaline cartilage repair in a rabbit model. (C1) Cumulative release profiles of TGF- β 3 and FITC-MGF for 28 days. (C2 and C3) Quantification of cell number of infiltration into the scaffolds and percentage of stem cells (CD29+/CD44+) at 7 days after subcutaneous implantation. (C4) Cell infiltration and multipotent stem cell identification at 7-day post-implantation in articular joint. (C5) Representative safranin O and masson's trichrome staining images of rabbit articular at 3 months after implantation (Adapted and reproduced from Luo et al. [72], Copyright 2015, Elsevier). (D) The combinational use of PDGF-BB and TGF- β 3 for recruiting stem cells and repairing AC. (D1) A brief illustration of the concept of "cell island" microgels by loading with PDGF-BB and TGF- β 3 as a recruiting factor and a differentiation factor of ESPCs, respectively. The injectable porous microgel was developed by photopolymerization of HAMA@HepMA blended pregel droplets generated via microfluidics. Subsequently, PDGF-BB and TGF- β 3 were non-covalently incorporated into the microgels by binding heparin, creating "cell island" microgels with robust recruiting and pro-chondrogenic potentials. (D2) The release curves of TGF- β 3 and PDGF-BB. (D3) The chemotaxis assay showed the cell-homing effect of the microgels. (D4) The representative alcian blue staining images indicated that microgels could promote chondrogenic differentiation *in vitro*. (D5) The representative safranin O-fast green staining images showed improved repair outcomes of MG@GFs. (Adapted and reproduced from Lei et al. [73], Copyright 2021, Wiley-VCH).

4.3. Mineral ions

As cofactors of enzymes or immunomodulators, many mineral ions (e.g. Zinc (Zn), boron (B), selenium (Se), cobalt (Co), calcium (Ca), copper (Cu), magnesium (Mg), manganese (Mn) ions) are involved in the proliferation, attachment, and differentiation of ESPCs, matrix formation, anti-inflammation and tissue homeostasis [137] (Figure 8A). Optimized mineral ions can impart these biochemical cues to implants for enhancing ESPCs-mediated AC repair. Co ions are simulated hypoxia inducers, and the hypoxia-induced transcriptional profile plays a vital role in chondrogenic differentiation [138]. The incorporation of Co ions into alginate scaffolds could support chondrogenesis by mimicking the hypoxia environment following a dose-dependent manner [139,140]. Lv et al. incorporated Co or Ca ions into an injectable GelMA-sodium alginate (SA) hydrogel to promote cartilage formation in an eight-week-old male rat model [140]. After eight weeks, the empty defects were filled with fibrous tissues, while the GelMA-SA-Ca group obtained a better fill-in with a mixture of cartilage-like and fibrous tissues. In comparison, the GelMA-SA-Co group achieved the best cartilage repair with a similar structure to native cartilage. Cu ions could enhance the chondrogenesis of MSCs by promoting the MSCs' cytoskeleton change and up-regulating the chondrogenic gene expression [106,141]. Adding Cu into a porous alginate scaffold improved cartilage formation in adult male mice models [141]. Shimaya et al. reported that Mg ions enhanced cell adherence and cartilage formation by endogenous rabbit S-MSCs through integrins *in vivo* [105]. Further study revealed the effects of different Mg ion concentrations on cell adhesion, migration, and proliferation *in vitro* [142] (Figure 8B). Fluorescent staining showed that medium containing 100 -ppm Mg ions boosted cell-substratum adhesion, and cells in this group showed larger and polygonal cell morphologies. In contrast, the 0 ppm Mg²⁺-treated group exhibited delayed cell-substratum adhesion. The 100 ppm Mg²⁺-treated group demonstrated the highest cell migration velocity and cell proliferation. The study from Zhao et al. develop a porous Mg-Nd-Zn-Zr alloy scaffold coated with PDA and validated their cytocompatibility and impacts

on immunomodulation for AC repair [21] (Figure 8C). This study revealed the advantageous potential of Mg-based implants to expedite chondrogenesis by controlled release of Mg^{2+} in addressing the destructive effect of activated macrophage polarization on chondrocytes. The commercial product MaioRegen also contains Mg in the lower layer of Mg-HA as favorable external biochemical cues to recruit ESPCs and guide AC repair.

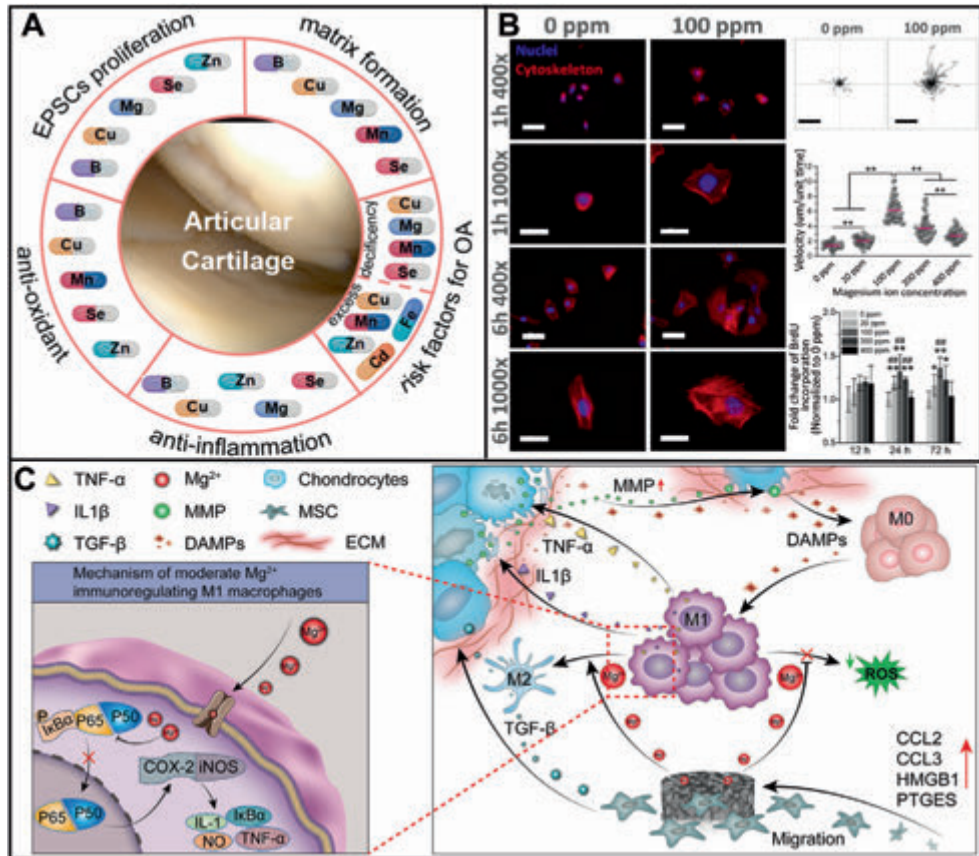


Figure 8. The crucial roles of mineral ions in the example of Mg^{2+} are to regulate cell behaviors of stem/progenitor cells (SPCs) and enhance cartilage repair. (A) Mineral ions play irreplaceable roles in regulating cellular behavior and promoting cartilage healing. (B) Effects of different Mg^{2+} concentrations on cell adhesion, migration, and proliferation in vitro (reproduced from Shen et al. [142], Copyright 2021, Elsevier). (C) Via the controlled release of Mg^{2+} , Mg-based scaffolds could enhance chondrogenesis and eliminate the destructive effects of activated macrophages on chondrocytes (reproduced from Zhao et al. [21], Copyright 2022, Elsevier).

4.4. Chondroinductive/chondroconductive peptides

Peptides are a particular category of bioactive substances which can be engineered into/onto biomaterials to serve as chondroinductive/chondroconductive biochemical cues [143]. Compared with proteinous GFs, chemically synthesized peptides are more advantageous in quantity, efficiency, and purity and can be easily modified for improved functionalities. Other than direct mixture and self-assembly, the chemical conjugation

approaches involve Michael addition and temperature- or UV-induced crosslinking. Therefore, these peptide-functionalized biomaterials showcase great promise in ESPCs-mediated AC repair. Typically, chondroinductive/chondroconductive peptides can be categorized into two types: GF-derived peptides (e.g. CK2.1, BMP, B2A, and SPPEPS peptide) and cell-cell adhesion molecules/ECM components-derived peptides (e.g. N-cadherin mimetic peptide, LPP peptide, RGD, CMP, GFOGER, and Glycopeptide) [143] (Figure 9). They mainly function through BMP, ERK, Smad, TGF- β , and Wnt signaling pathways (indicated in Figure 2) to upregulate the Sox 9, Aggrecan, and Collagen II expression and GAG contents for enhanced AC defect healing. Most peptides are chondroconductive instead of chondroinductive. For some peptides (i.e. 100 nM CK2.1) induce chondrogenesis more efficiently both *ex vivo* (micromass model) and *in vivo* (mice knee AC defects) compared with 40 nM BMP-2 proteins [144]. Moreover, this peptide results in no or much less hypertrophy and mineralization [144], which is of paramount importance for maintaining the hemostasis of neo-cartilage. Liu et al. fabricated CK2.1-coated β -glycerophosphate chitosan (CK2.1@GC) composite scaffolds for AC repair in a rabbit model through the recruitment and induced chondrogenesis of ESPCs [23]. SPPEPS, a TGF- β 3-derived peptide, seemed to be more chondroconductive rather than chondroinductive due to its very mild potency in inducing chondrogenesis and it could only enhance *in vitro* collagen II expression [145]. Future research should concentrate on the (bio)design, (bio)fabrication, and assessment of more potent chondroinductive peptides and peptides-functionalized scaffolds with *in vivo* efficacies to facilitate their clinical translation.

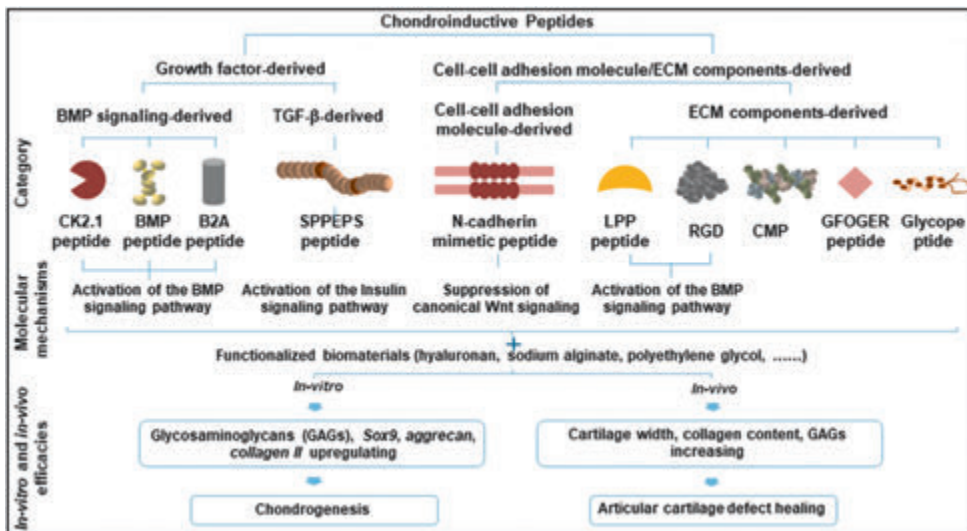


Figure 9. Chondroinductive/chondroconductive peptides can boost the chondrogenesis of ESPCs and AC repair. Growth factor- and cell-cell adhesion molecule/ECM components-derived peptides can activate distinct molecular mechanisms. CMP: collagen mimetic peptide; LPP: link protein N-terminal peptide. (Reproduced from Zhu et al. [143], Copyright 2021, Elsevier).

4.5. Small molecule compound drugs

Small molecule compounds allow for a simple and efficacious approach to enhance chondrocyte proliferation, cell phenotype maintenance, and chondrogenesis of SPCs [146-148]. Accordingly, regenerative biomaterials functionalized with appropriate small-molecule drugs represent a feasible option to enhance ESPCs-mediated AC repair. They can be summarized in two options: (1) promoting chondrocyte proliferation (e.g. Glucosamine, Ascorbic acid, Estrogen, Salidroside, 1,25(OH)₂D₃, Lysophosphatidic acid, AG-041R, Berberine chloride, and Sphingosine-1-phosphate); and (2) inducing chondrogenesis (e.g. KGN, Melatonin, Icariin, TD-198946, Simvastatin, BIO, Resveratrol, Prostaglandin E₂, Dexamethasone, and Staurosporine) [146] (Figure 10A and B). They mainly function via TGF- β , MAPK, Wnt, IGF, and IHH signaling pathways indicated in Figure 2. And they hold several superiorities in rapid, reversible, and dose-dependent bio-effect, chemical modification, large-scale production, cost-effectiveness, and straightforward administration [146-148]. Two disadvantages of small molecule functionalization are multiple targets and unexpected toxicity, impeding their further applicability [146-148]. Of note, currently only glucosamine, icariin, and estrogen have been used in cartilage treatment clinically [146]. The emerging technologies of streamlined high-throughput drug screening platforms bring new hopes, and they can simplify and accelerate the research and development of targeted small molecule compounds, expediting their ultimate translation processes (Figure 10C).

Currently, most of the above-mentioned small molecule compound drugs are still in preclinical stages and have achieved desirable animal results to some degree. For instance, Stefani et al. established a sustained delivery system with low-dose dexamethasone by a PLGA microsphere-embedded agarose implant to markedly enhance AC repair in dogs [113] (Figure 10D). The controlled presentation of dexamethasone (up to 99 days) exhibited dual pro-anabolic and anti-catabolic effects, both facilitating tissue integration whereas also mitigating excess inflammation [113]. KGN and icariin could also function as chondrogenic factors. Xuan et al. (bio)fabricated a chondrogenic and physiological-temperature-triggered shape-memory ternary scaffold for cell-free AC repair in a rat model [149] (Figure 10E). Within the scaffold, poly (glycerol sebacate) (PGS) networks supported shape recovery and elasticity properties; crystallized poly (1,3-propylene sebacate) (PPS) served as switchable phase; and incorporated KGN ensured the scaffold with pro-chondrogenic ability. The *in vitro* scaffold degradation and cumulative release curve indicated that the sustained release of KGN could last at least 12 weeks [149]. The *in vivo* studies suggested that the PPS/PGS/KGN scaffolds enhanced neocartilage regeneration in the absence of exogenous GFs and seeded cells [149]. Besides, icariin could activate HIF- α in chondrocytes and promote AC repair [150] (Figure 10F). The data showed that Icariin may suppress prolyl hydroxylase domain (PHD) activity via competing for cellular iron ions and it might act as an HIF-1 activator to enhance AC regeneration by controlling chondrocyte differentiation, proliferation, and tissue integration [150].

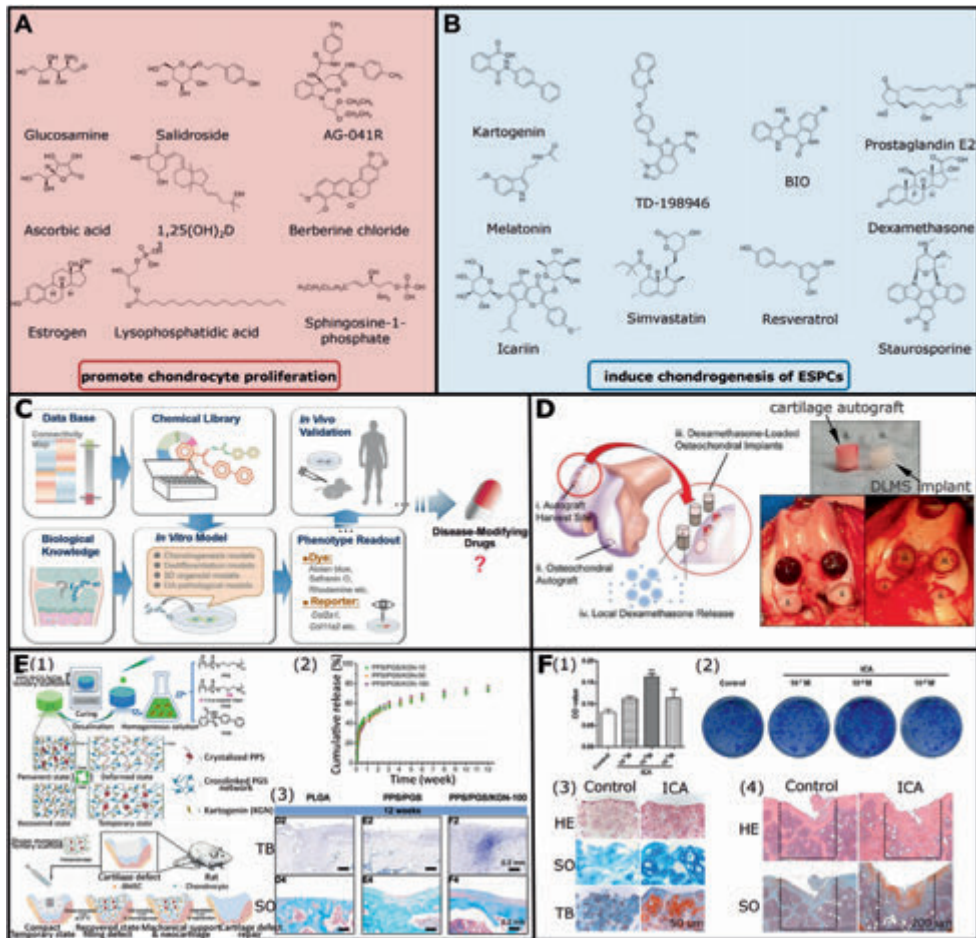


Figure 10. Small molecule compounds can function as favorable biochemical cues for ESCs-mediated AC repair. (A, B) Small molecule compounds could support chondrocyte proliferation and chondrogenesis of progenitor/stem cells (adapted and reproduced from Li et al. [146], Copyright 2020, Elsevier). (C) State-of-the-art screening strategies of small molecular drugs for AC repair (reproduced from Chen et al. [148], Copyright 2021, Springer Nature). (D) Improved AC and subchondral bone repair by a PLGA microspheres-embedded agarose scaffold via sustained delivery of dexamethasone (reproduced from Stefani et al. [113], Copyright 2020, Elsevier) (E) A cell-free strategy for AC repair by biofunctionalized chondrogenic shape-memory ternary PPS/PGS/KGN scaffolds. (E1) Schematic diagram of this study. (E2) KGN release curves of PPS/PGS scaffolds with different original KGN contents. (E3) The representative toluidine blue and safranin O staining images of AC repair in different groups at 12 weeks (adapted and reproduced from Xuan et al. [149], Copyright 2020, Elsevier). (F) Icaritin could activate HIF-1 α in chondrocytes and promote AC repair. (F1) MTT assay for cell viability of chondrocytes and (F2) colony formation assay for chondroprogenitor cells indicated that Icaritin could promote chondrocyte proliferation. (F3) The representative HE, safranin O, and toluidine blue staining images showed that icaritin promotes chondrogenesis in the alginate-chondrocyte 3D culture system. (F4) The representative HE and safranin O staining images showed icaritin could enhance AC regeneration in a mouse OCD model (adapted and reproduced from Wang et al. [150], Copyright 2016, PLOS).

4.6. Gene targeting factors and EVs

Numerous gene targeting factors (e.g. siRNA, mRNA, miRNA, and CRISPR/Cas9) can be engineered into regenerative implants for ESPCs-mediated cartilage repair. Advanced biomaterial-guided delivery of gene vectors is an emerging and highly desirable therapeutic option for AC repair, enabling the spatiotemporally controlled and minimally invasive delivery of vectors and minimizing intra-articular vector spread and potential loss of the therapeutic gene products. Madry et al. fabricated an injectable and thermosensitive PEO-PPO-PEO hydrogel system, capable of repairing full-thickness chondral defects in a minipig model through the controlled release of a therapeutic rAAV vector overexpressing the chondrogenic sox 9 transcription factor [118] (Figure 11A). Additionally, miRNAs can also modulate gene expression via inhibiting translation or triggering mRNA degradation, affecting cell behaviors and even cell fate [151]. miRNAs expression profiles differ during AC development and MSC chondrogenesis, indicating their significant role during cartilage healing. Lolli et al. reported miR-221 as a novel anti-chondrogenic miRNA, and silencing miR-221 in human BM-MSCs could improve chondrogenesis [152,153]. Lolli et al. further silenced miR-221 in ESPCs by fibrin/HA hydrogels loaded with locked nucleic acid (LNA)-microRNA inhibitors via non-viral transfection [24]. AntimiR-221 significantly promoted chondrogenesis and AC repair in a semi-orthotopic model of bovine osteochondral tissues implanted subcutaneously in nude mice [24] (Figure 11B). Even under an inflammation environment, hydrogel-based delivery of miR-29b-5p could stimulate to recruit ESPCs for cartilage repair by suppressing senescence in an OA rat model [115] (Figure 11C). Besides, some *in vitro* experiments confirmed the pro-migratory effects of miRNAs, such as miR-10b [154] and antimiR-375 [155]. Apart from miRNAs, aptamers (single-stranded DNA or RNA) with unique tertiary structures could bind specifically with cognate molecular targets [156]. Wang et al. showed that an Apt19S-functionalized bilayer scaffold could recruit BM-MSCs and support cell adhesion both *in vitro* and *in vivo* for AC repair macroscopically and histologically in a rabbit model [117].

Furthermore, actively released by a variety of cells, EVs are small membrane-enclosed particles [157]. The mRNAs, miRNAs, and DNA carried in EVs can potentially be transferred to neighboring cells, inducing persistent and prolonged genetic reprogramming and modifying their phenotype as well as the microenvironment [158]. On the basis of biogenesis, size, and content, EVs can be divided into three categories: exosomes (40-200 nm), microvesicles/shedding particles (50-1000 nm), and apoptotic bodies (500-2000 nm) [157,159]. Recently, EVs have been proposed as emerging tools for restoring joint homeostasis and improving AC regeneration [159] (Figure 11D). As a result of heterogeneous contents, selecting suitable parental cells and proper therapeutic methods are indispensable for targeting treatment of AC defects [159]. Loading EVs by biomaterials optimizes their effectiveness for cartilage regeneration. A promising tissue patch for rabbit AC regeneration was constructed by Liu et al. through the integration of HA-NB/Gelatin hydrogel glues and stem cell-derived exosomes [160]. Zhang et al. fabricated an injectable mussel-inspired highly adhesive hydrogel for the local delivery of exosomes [50] (Figure 11E). Exosomes released from the AD/CS/RSF/EXO hydrogel maintained their structures and bioactivities. These released exosomes largely contributed to the recruitment and inflation, proliferation, and differentiation of BM-MSCs *in vitro*, and improved rat AC repair

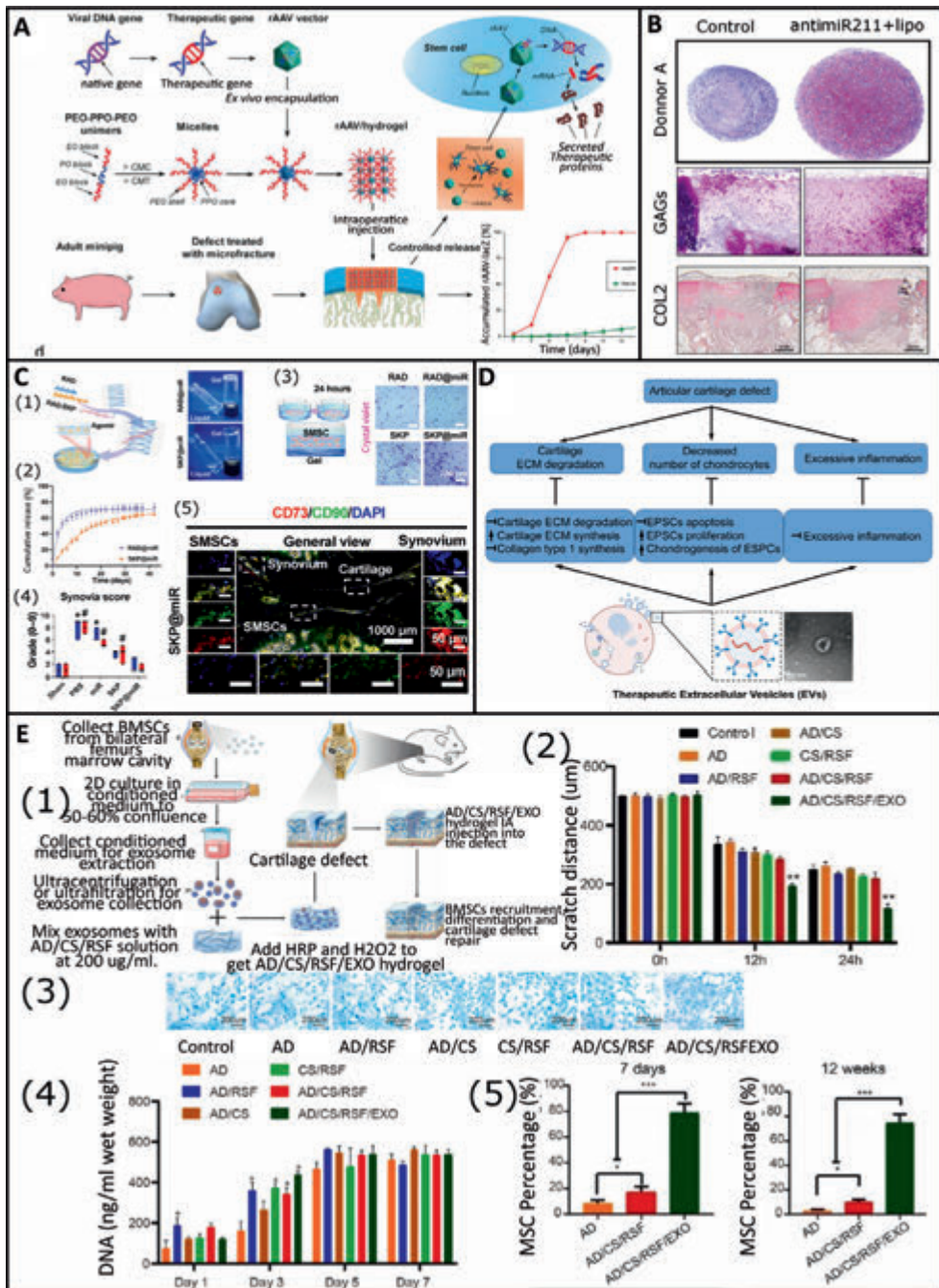


Figure 11. Gene targeting factors and EVs could function as favorable biochemical cues to enhance ESC-mediated cartilage repair. (A) PEO-PPO-PEO poloxamers-based thermosensitive hydrogel loaded with rAAV for efficient gene therapy of AC defects (reproduced from Madry et al. [118], Copyright 2020, Wiley). (B) Hydrogel-based delivery of antimir-221 improved chondral defect repair through ESCs (reproduced from Lolli et al. [24], Copyright 2019, Elsevier). (C) Hydrogel-based delivery of miR-29b-5p to recruit ESCs for

cartilage repair by suppressing senescence in a rat model. A brief illustration of the (C1) fabrication of hydrogel-miRNA constructs. (C2) Cumulative release profiles of agomir-29b-5p at 37 °C. (C3) Transwell assay to monitor ESPCs recruitment *in vitro*. (C4) Synovia scores, and (C5) immunofluorescence staining to show SKP@miR induced ESPCs recruitment and enhanced chondrogenic differentiation *in vivo* (adapted and reproduced from Zhu et al. [115], Copyright 2022, AAAS). (D) Therapeutic EVs as promising cell-free strategies for AC regeneration (adapted and reproduced from Amsar et al. [159], Copyright 2022, Future Science). (E) Injectable mussel-inspired highly adhesive hydrogel with exosomes for recruiting ESPCs and repairing AC defect. (E1) Schematic illustration of this study. (E2) Scratch distance assay to show the migration and infiltration of BMSCs *in vitro*, (E3) Alcian staining to show the effect of pro-chondrogenic differentiation on BMSCs *in vitro*, (E4) DNA concentration analysis to show the improved proliferation effect on BMSCs *in vitro*, and (E5) Semi-quantitative analysis of stem cell percentage to show the enhanced migration and infiltration effect on ESPCs *in vivo* (adapted and reproduced from Zhang et al. [50], Copyright 2021, Elsevier and Fan et al. [163], Copyright 2022, MDPI).

with mature ECM remodeling by recruiting ESPCs *in vivo* [50]. Shen et al. developed a silk hydrogel loaded with hypoxia preconditioned MSCs-derived EVs to repair AC through the miR-205-5p/PTEN/AKT pathway [161]. The hypoxia preconditioned EVs significantly boosted the proliferation, migration, and anabolism of chondrocyte cells and anti-inflammatory effects [161]. This was in accordance with a study by Xue et al. [162]. Despite the promising preclinical results, more in-depth research should focus on addressing the related problems, such as high homogeneous EVs and large-scale production, to facilitate their clinical application.

4.7. Anti-inflammatory and immunomodulatory agents

The inflammation phase of AC repair is pivotal since it orchestrates all the following biological activities. A cascade of reactions is triggered immediately after biomaterials implantation, including a layer of proteins from the surrounding vasculature adsorbs onto the biomaterial surface, infiltration adherence of various immune cells (e.g. platelets, neutrophils, monocytes, and macrophages), the release of physicochemical signals by immune cells to recruit ESPCs, microenvironment remodeling by deposition of nascent proteins by ESPCs, and neocartilage formation (Figure 12A). At present, a critical mode toward the better regeneration of AC is supported by implant-mediated immunomodulation [164]. Studies have indicated that biomaterials can significantly impact the polarization of macrophages and T cells, which hold extensive cell crosstalk with ESPCs [165]. So far, the polarization shift from pro-inflammatory (M1) to anti-inflammatory macrophage (M2) phenotypes has been increasingly investigated to alleviate excessive inflammation, which can be applied to the biomaterial design principles based on the macrophage-mediated immunomodulatory healing of AC [165] (Figure 12B). Thus, many immunomodulation cues can be engineered into regenerative scaffolds to achieve this goal based on the macrophage polarization shift. Yuan et al. fabricated the hydroxypropyl chitin (HPCH) hydrogel and confirmed its function in activating inflammatory responses and recruiting endogenous macrophages to support a suitable inflammation microenvironment [166]. Following this pattern, Ji et al. synthesized a thermosensitive photocrosslinkable glycidyl methacrylate-modified HPCH hydrogel (GM-HPCH) loaded with TGF- β 1 [25] (Figure 12C). The *in vivo* and *in vitro* studies revealed that a GM-HPCH + TGF- β 1 treatment markedly shifted the recruited macrophages from M1 to M2 [25]. The composite hydrogel boosted the expression of chondrogenic genes and the

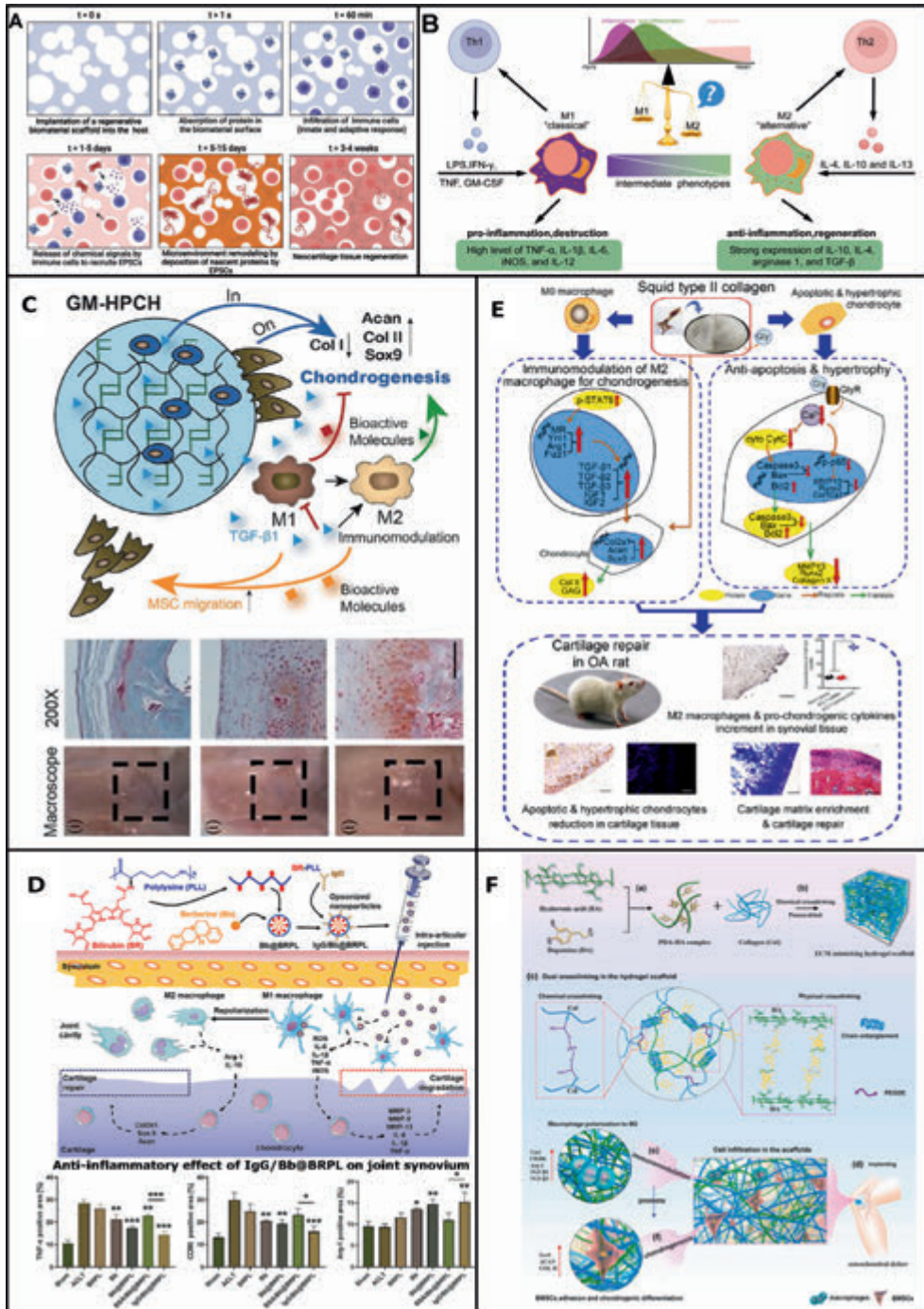


Figure 12. Engineering regenerative biomaterials with optimized biochemical cues with good anti-inflammatory and immunomodulatory effects for ESPCs-mediated AC repair. (A) Immune response following the implantation of regenerative biomaterials (created by BioRender). (B) The delicate polarization shift balance between pro-inflammatory M1 and regenerative M2 macrophages and their distinct effects on

cartilage healing. (C) The thermosensitive photocrosslinkable TGF- β 1-loaded composite hydrogel facilitated AC repair through immunomodulating macrophages, recruiting ESPCs, and expediting chondrogenesis (reproduced from Ji et al. [25], Copyright 2020, Ivyspring). GM-HPCH: glycidyl methacrylate-modified hydroxypropyl chitin. (D) A trapping strategy for AC regeneration via opsonized nanoparticles to selectively target M1 macrophage and promote M1-to-M2 polarization shift (reproduced from Kou et al. [167], Copyright 2022, Elsevier). (E) Under degenerative OA conditions, AC repair was significantly enhanced by squid type II collagen via inhibiting apoptosis and hypertrophy of chondrocytes and immunomodulating activation of M2 macrophages (reproduced from Dai et al. [120], Copyright 2018, Elsevier). (F) A cell- and GF-free AC repair strategy based on the mussel-inspired ECM-mimicking hydrogels with excellent cell affinity and immunomodulation capability (reproduced from Gan et al. [169], Copyright 2022, Elsevier).

migration of BM-MSCs and achieved superior cartilage healing [25]. To treat OA, Kou et al. prepared artificial opsonized nanoparticles (IgG/Bb@BRPL) which can selectively target M1 macrophages to repolarize M1-to-M2 by reactive oxygen species scavenging and NF- κ B pathway deactivation [167] (Figure 12D). Dai et al. developed a squid-derived collagen II (SCII) scaffold that could suppress the pro-inflammatory macrophages via inhibiting the STAT1 signal for cartilage lesions [120,168] (Figure 12E). SCII scaffolds induced the M1 macrophage polarization into the M2 phenotype and promoted macrophages to express pro-chondrogenic genes as well as the production of Collagen II and GAGs *in vitro* [120]. Inspired by mussel, Gan et al. fabricated a ECM-mimicking composite hydrogel with high cell infiltration and immunomodulation capability for GFs-free AC repair in a rabbit model [169] (Figure 12F).

Apart from macrophages, regenerative scaffolds could also impact other immune cells' phenotypes to modulate AC repair. For example, the recruitment of neutrophils is necessary for the onset of inflammation, but sustained neutrophils might result in long-term chronic pro-inflammation and then failed repair. Engineered anti-inflammatory and immunomodulatory cues of biomaterials have significant implications for neutrophils' activation and function [37]. Hoemann et al. proved that chitosan-glycerol phosphate/blood implants could attract more neutrophils *in vitro* and *in vivo* compared to whole blood clots, though both released a similar profile of chemotactic factors (CCL2, CXCL8, PDGF-BB) [170]. And after eight weeks *in vivo*, more uniform and integrated cartilage tissue was observed in the trochlear cartilage defects treated with chitosan-glycerol phosphate/blood implants, indicating the potential roles of neutrophils in AC repair [170]. Such studies highlighted the significance of investigating biomaterials in the framework of immunomodulation of immune cells (i.e. macrophages) and their repair responses in ESPCs-mediated AC regeneration.

4.8. Spatiotemporal delivery/release modalities

Engineered regenerative constructs might address the challenges of traditional drug delivery approaches by improving biochemical cues' delivery, retention, targeting, and bioactivity [171]. To closely recapitulate the innate repairing cascades, controlled sequential release of exogenous bioactive factors to the defect site has been established to enhance ESPCs-mediated cartilage repair [28,113,171]. The (bio)design and (bio)fabrication of innovative scaffold-based drug delivery systems (DDS) offered new possibilities for sophisticated release kinetics of various bioactive substances, including specific drugs, CCGs, mineral ions, small molecule compounds, peptides, anti-inflammatory agents, gene targeting factors and EVs (Figure 13A).

By intra-articular injection-based local delivery, free drugs cannot exist for a very long duration (mostly within hours or days) due to joint clearance. As soon as being injected into joints, drugs get into synovial fluid with a rapid physiological turnover. When it comes to a short therapeutic time frame, some doctors try to reduce the injection frequency, aiming to prolong the drug's residence. Encouragingly, novel DDS technologies demonstrate tremendous potential for addressing the above-mentioned problems. A modest improvement in intra-articular presence can significantly influence the drug's exposure time. Ionic and ECM-based GFs delivery leverage the interaction of positively charged proteins with negatively charged substrates for longer effective days, compared with monolithic carriers releasing GFs by diffusion [69] (Figure 13B). Current efforts are mainly focused on strengthening these bioactive factors' localization, retention, bioactivity, delivery, and targeting [171]. Through physical adsorption, direct blending, surface grafting, drop casting, chemical immobilization, covalent bonding, coaxial electrospinning, and microparticles incorporation, bioactive factors could be combined with biomaterials [172]. For instance, SDF-1 α /TGF- β 1 can be physically absorbed and sustained release from a SF-porous gelatin scaffold [90]. The release kinetics of SDF-1 α /TGF- β 1 encapsulated within hydrogels were controllable via hydrogel properties such as mesh size [173]. However, physical absorption or encapsulation within regenerative scaffolds has shown some disadvantages, such as unexpected burst release at an early time point. Covalently binding to the scaffold surfaces provides accurate and controllable spatiotemporal delivery and avoids burst release. Lee et al. achieved the directional PDGF-AA release using catecholamine adhesion chemistry to develop robust interfacial adhesion covalently, which greatly promoted the recruitment of ESPCs and cartilage repair [174]. However, poorly controlled conjugation can negatively influence the conformation and biological activity of GFs. For example, when BMP-2 was covalently bound to the surface of a PCL scaffold and the conjugation provided a sustained release of BMP-2, negligible alkaline phosphatase deposition and less tissue ingrowth were observed compared to the one by physical absorption, which had a small burst release of BMP-2 [175]. Besides, binding and mimetic peptides of biomaterials could be designed to interact with specific regions of CCGs. This process could be utilized to manipulate the releasing profile of DDS.

However, the release of biochemical cues by regular DDSs only sustained for a relatively short period, which is insufficient for long-term and complete AC regeneration [28]. Innovative DDSs-based strategies, such as nano-carriers, liposomes, and micelles were extensively studied to achieve a prolonged release or even penetration into cartilage [26]. Zhang et al. reported an advanced all-silk-derived sequential DDS through incorporating the tunable drug-loaded SF nanospheres into a SF porous matrix, which could provide a sustained and relatively slow release paradigm of KGN longer than one month [176]. Dong et al. fabricated a chitosan/SF hydrogel with PLGA microspheres to deliver KGN and SDF-1 simultaneously [177] (Figure 13C). PLGA microspheres were evenly spread within the chitosan/SF hydrogel, permitting the sequential release of those two drugs. SDF-1 and KGN served as recruiting factors and chondroinductive factors, respectively. This special (bio)design markedly improved the cell homing and chondrogenic differentiation of ESPCs *in vitro* and *in vivo* and cartilage repair in a rabbit model. Theoretically, the delivery/release profiles of different bioactive substances can meet the timeline of different AC healing stages via taking advantage of the inherent properties of distinct biomaterials and spatially organized components. Unfortunately, an ideal DDS that can sequentially release bioactive

factors in every repairing stage for enhancing AC restoration has rarely been reported. Much more efforts are required to discover an optimal DDS and advance its clinical translation.

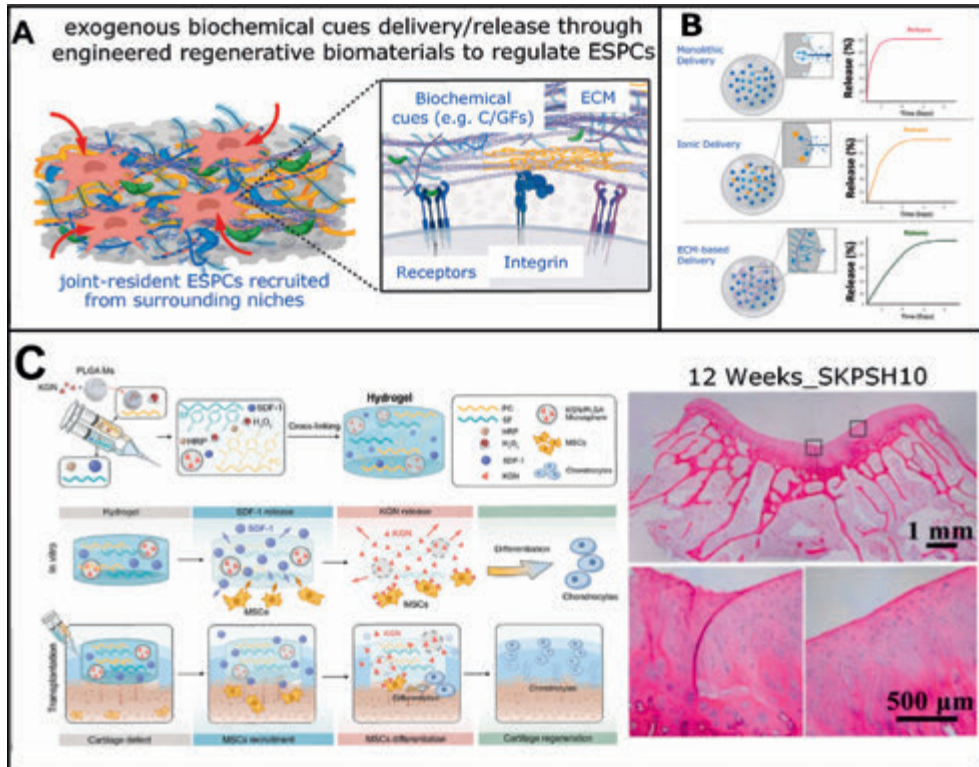


Figure 13. Engineering regenerative biomaterials as spatiotemporal delivery/release modalities of various biochemical cues to guide ESPCs for cartilage repair. (A) Novel regenerative scaffold-based DDS loaded with favorable exogenous biochemical cues to recruit ESPCs from surrounding niches for ESPCs-mediated AC repair (adapted and reproduced from Gresham et al. [69], Copyright 2021, Elsevier). (B) Representative release profiles of GFs-based DDS. Each profile (monolithic, ionic, and ECM-based delivery) is graphically illustrated to reveal its releasing mechanism (reproduced from Gresham et al. [69], Copyright 2021, Elsevier). (C) Sequential delivery of SDF-1/KGN by injectable PC/SF composite hydrogels for spatiotemporal regulation of endogenous cells to improve AC repair (reproduced from Dong et al. [177], Copyright 2021, Springer Nature).

5. CONCLUSION REMARKS AND PERSPECTIVES

Compared with endogenous cartilage healing (i.e. bone marrow stimulation techniques) and *in vitro* manipulated cell-based treatments, cell-free regenerative scaffolds-based strategies exhibited many advantages, such as less donor-site morbidities, the absence of cell selection, delivery, viability, and phenotypic stability issues, the timing of pre-treatments, regulatory issues, and low costs. Meanwhile, several acellular commercial products, such as Agili-C™ and MaioRegen Chondro+ have been approved by regulatory bodies, reinforcing our translational determination and direction. Therefore it is time to highlight and summarize the proposed strategies based on the synergistic effects of endogenous cells and biochemical cues from regenerative scaffolds for cartilage repair. Of

note are the target groups based on EPCs-mediated AC repair strategies are young patients with cartilage defects due to trauma and may not be suited for patients with progressed OA and older patients. The question now is how to stimulate joint-resident ESPCs effectively and adequately for *in vivo* cartilage defect repair. So far, many methodologies have been adopted to (bio)design and (bio)fabricate novel regenerative constructs with optimized biochemical cues and spatiotemporal delivery/release modalities, achieving desirable outcomes to some degree. After implantation, these biomaterials can interact with the adjacent tissues through these biochemical signals, which alter local tissue microenvironments by modulating the immune system and controlling the kinetics and degree of healing by activating and recruiting a large population of joint-resident ESPCs infiltration, guiding their mobilization, proliferation, chondrogenesis, matrix deposition, and remodeling to generate hyaline-like cartilage eventually. This review may provide a basic summary of these biochemical cues for the successful activation and maintenance of ESPCs-mediated AC repair.

Based on the literature review, at present, we cannot conclude which biochemical cue or combination has the most robust effect due to the lack of standardized comparison in the preclinical studies. The preclinical assessments use different animal models, defect locations, defect sizes, histological/CT methods, and scoring/semi-quantification systems. No consensus of standardized and streamlined preclinical evaluation protocols and procedures exist currently to compare different engineered biochemical cues. It is envisioned that more standardized preclinical studies are performed allowing to better compare the results between labs and clinics. The cartilage tissue engineering community has the obligation to tackle this issue soon to facilitate the ultimate translation of acellular regenerative biomaterials with optimized and robustly engineered biochemical cues for cartilage repair via initiating and magnifying the roles of ESPCs. Besides, future research work shall address the following aspects: (1) to investigate the roles of endogenous cells (e.g. different immune cells and joint-resident progenitor/stem cells): and the underlying molecular mechanisms of ESPCs-mediated AC repair; (2) to uncover how these exogenous biochemical cues influence exogenous cell behaviors *in vivo* and how to manipulate and control these biochemical cues properly *in vivo* to satisfy multiple demands of different healing stages; (3) to solve the technical barriers of combining biochemical cues with cartilage-mimicking regenerative scaffolds thoroughly; (4) to innovate more advanced methodologies (i.e. 3D-(bio)printing technology) to (bio)design and (bio)fabricate regenerative implants with excellent biophysical and biochemical properties; (5) to improve the delivery, retention, targeting, and bioactivity of exogenous biochemical cues within the joint via spatiotemporal scaffold-based DDS. Although the journey from bench to bedside is very draining, the multidisciplinary approaches involving material scientists, biologists, engineers, and clinicians seem to be a winning strategy to speed up the translational procedure. Our proposed solutions may represent silver linings for cartilage regeneration.

REFERENCES

- [1] Buckwalter JA. Articular cartilage: injuries and potential for healing. *J Orthop Sports Phys Ther.* 1998;28(4):192-202.
- [2] Makris EA, Gomoll AH, Malizos KN, Hu JC, Athanasiou KA. Repair and tissue engineering techniques for articular cartilage. *Nat Rev Rheumatol.* 2015;11(1):21-34.
- [3] Apostu D, Lucaciu O, Mester A, Oltean-Dan D, Baciut M, Baciut G, Bran S, Onisor F, Piciu A, Pasca RD, Maxim A, Benea H. Systemic drugs with impact on osteoarthritis. *Drug Metabol Rev.* 2019;51(4):498-523.
- [4] Cole BJ, Pascual-Garrido C, Grumet RC. Surgical management of articular cartilage defects in the knee. *JBJS.* 2009;91(7):1778-1790.
- [5] Gomoll AH, Madry H, Knutsen G, van Dijk N, Seil R, Brittberg M, Kon E. The subchondral bone in articular cartilage repair: current problems in the surgical management. *Knee Surg Sports Traumatol Arthrosc.* 2010;18(4):434-447.
- [6] He Y, Dong G, Cui G, Lu H, Lan T, Shen Z, Long W, Yu C, Yan H, Zhang J, Li Y, Xu X. Effect of deposition conditions on the properties of TCO films. *2018 IEEE 7th World Conference on Photovoltaic Energy Conversion, WCPEC 2018 - A Joint Conference of 45th IEEE PVSC, 28th PVSEC and 34th EU PVSEC.* 2018:2018-2020.
- [7] Kraeutler MJ, Aliberti GM, Scillia AJ, McCarty EC, Mulcahey MK. Microfracture versus drilling of articular cartilage defects: a systematic review of the basic science evidence. *Orthopaedic Journal of Sports Medicine.* 2020;8(8):2325967120945313.
- [8] Armiento AR, Alini M, Stoddart MJ. Articular fibrocartilage - Why does hyaline cartilage fail to repair? *Adv Drug Deliv Rev.* 2019;146:289-305.
- [9] Im GI. Endogenous cartilage repair by recruitment of stem cells. *Tissue Eng B Rev.* 2016;22(2):160-171.
- [10] Zhou L, Malda VOGJ, Stoddart MJ, Lai Y, Richards RG, Ki-wai Ho K, Qin L. Innovative tissue-engineered strategies for osteochondral defect repair and regeneration: current progress and challenges. *Advanced Healthcare Materials.* 2020;9(23):2001008.
- [11] Zhou L, Guo P, D'Este M, Tong W, Xu J, Yao H, Stoddart MJ, van Osch GJ, Ho KK, Li Z, Qin L. Functionalized hydrogels for articular cartilage tissue engineering. *Engineering.* 2022;13:71-90.
- [12] Brittberg M. Cellular and acellular approaches for cartilage repair: a philosophical analysis. *Cartilage.* 2015;6(2_suppl):4S-12S.
- [13] Stace ET, Dakin SG, Mouthuy PA, Carr AJ. Translating regenerative biomaterials into clinical practice. *J Cell Physiol.* 2016;231(1):36-49.
- [14] Duarte Campos DF, Drescher W, Rath B, Tingart M, Fischer H. Supporting biomaterials for articular cartilage repair. *Cartilage.* 2012;3(3):205-221.
- [15] Gaharwar AK, Singh I, Khademhosseini A. Engineered biomaterials for in situ tissue regeneration. *Nat Rev Mater.* 2020;5(9):686-705.
- [16] Pot MW, Gonzales VK, Buma P, Int'Hout J, van Kuppevelt TH, de Vries RB, Daamen WF. Improved cartilage regeneration by implantation of acellular biomaterials after bone marrow stimulation: a systematic review and meta-analysis of animal studies. *PeerJ.* 2016;4.
- [17] Geller J. FDA issues several final, device-specific guidance documents. *J Clin Eng.* 2022;47(3):121-123.

- [18] Moulisova V, Poveda-Reyes S, Sanmartín-Masia E, Quintanilla-Sierra L, Salmeron-Sanchez M, Gallego Ferrer G. Hybrid protein-glycosaminoglycan hydrogels promote chondrogenic stem cell differentiation. *ACS Omega*. 2017;2(11):7609-7620.
- [19] Ren X, Li J, Li J, Jiang Y, Li L, Yao Q, Ke Q, Xu H. Aligned porous fibrous membrane with a biomimetic surface to accelerate cartilage regeneration. *Chem Eng J*. 2019;370:1027-1038.
- [20] Hsieh YH, Hsieh MF, Fang CH, Jiang CP, Lin B, Lee HM. Osteochondral regeneration induced by TGF- β loaded photo cross-linked hyaluronic acid hydrogel infiltrated in fused deposition-manufactured composite scaffold of hydroxyapatite and poly (ethylene glycol)-block-poly (ϵ -caprolactone). *Polymers*. 2017;9(5):182.
- [21] Zhao J, Wu H, Wang L, Jiang D, Wang W, Yuan G, Pei J, Jia W. The beneficial potential of magnesium-based scaffolds to promote chondrogenesis through controlled Mg²⁺ release in eliminating the destructive effect of activated macrophages on chondrocytes. *Mater Sci Eng C*. 2022;112719.
- [22] Wu H, Shen L, Zhu Z, Luo X, Zhai Y, Hua X, Zhao S, Cen L, Zhang Z. A cell-free therapy for articular cartilage repair based on synergistic delivery of SDF-1 & KGN with HA injectable scaffold. *Chem Eng J*. 2020;393:124649.
- [23] Liu P, Li M, Yu H, Fang H, Yin J, Zhu D, Yang Q, Ke Q, Huang Y, Guo Y. Biphasic coated β -glycerophosphate chitosan/LL37-modified layered double hydroxide chitosan composite scaffolds enhance coordinated hyaline cartilage and subchondral bone regeneration. *Chem Eng J*. 2021;418:129531.
- [24] Lolli A, Sivasubramaniyan K, Vainieri ML, Oieni J, Kops N, Yayon A, van Osch GJ. Hydrogel-based delivery of anti-miR-221 enhances cartilage regeneration by endogenous cells. *J Contr Release*. 2019;309:220-230.
- [25] Ji X, Lei Z, Yuan M, Zhu H, Yuan X, Liu W, Pu H, Jiang J, Zhang Y, Jiang X. Cartilage repair mediated by thermosensitive photocrosslinkable TGF β 1-loaded GM-HPCH via immunomodulating macrophages, recruiting MSCs and promoting chondrogenesis. *Theranostics*. 2020;10(6):2872.
- [26] Huang H, Lou Z, Zheng S, Wu J, Yao Q, Chen R, Kou L, Chen D. Intra-articular drug delivery systems for osteoarthritis therapy: shifting from sustained release to enhancing penetration into cartilage. *Drug Deliv*. 2022;29(1):767-791.
- [27] Xia H, Li X, Gao W, Fu X, Fang RH, Zhang L, Zhang K. Tissue repair and regeneration with endogenous stem cells. *Nat Rev Mater*. 2018;3(7):174-193.
- [28] Yang Z, Li H, Yuan Z, Fu L, Jiang S, Gao C, Wang F, Zha K, Tian G, Sun Z. Endogenous cell recruitment strategy for articular cartilage regeneration. *Acta Biomater*. 2020;114:31-52.
- [29] Hu H, Liu W, Sun C, Wang Q, Yang W, Zhang Z, Xia Z, Shao Z, Wang B. Endogenous repair and regeneration of injured articular cartilage: a challenging but promising therapeutic strategy. *Aging and Disease*. 2021;12(3):886.
- [30] Elchaninov A, Sukhikh G, Fatkhudinov T. Evolution of regeneration in animals: a tangled story. *Frontiers in Ecology and Evolution*. 2021;9:621686.
- [31] Cosden R, Lattermann C, Romine S, Gao J, Voss S, MacLeod J. Intrinsic repair of full-thickness articular cartilage defects in the axolotl salamander. *Osteoarthritis Cartilage*. 2011;19(2):200-205.
- [32] Mauck RL, Burdick JA. From repair to regeneration: biomaterials to reprogram the meniscus wound microenvironment. *Ann Biomed Eng*. 2015;43(3):529-542.

- [33] Butler MGK, Ambrosi TH, Murphy MP, Chan CK. Aging of skeletal stem cells. *Advances in Geriatric Medicine and Research*. 2022;4(2).
- [34] Matsuoka M, Onodera T, Sasazawa F, Momma D, Baba R, Hontani K, Iwasaki N. An articular cartilage repair model in common C57Bl/6 mice. *Tissue Eng C Methods*. 2015;21(8):767-772.
- [35] Evans CH, Palmer GD, Pascher A, Porter R, Kwong FN, Gouze E, Gouze JN, Liu F, Steinert A, Betz O. Facilitated endogenous repair: making tissue engineering simple, practical, and economical. *Tissue Eng*. 2007;13(8):1987-1993.
- [36] Wei F, Liu S, Chen M, Tian G, Zha K, Yang Z, Jiang S, Li M, Sui X, Chen Z. Host response to biomaterials for cartilage tissue engineering: key to remodeling. *Front Bioeng Biotechnol*. 2021;9:664592.
- [37] Ode Boni B, Lamboni L, Souho T, Gauthier M, Yang G. Immunomodulation and cellular response to biomaterials: the overriding role of neutrophils in healing. *Mater Horiz*. 2019;6:401-419.
- [38] Fernandes TL, Gomoll AH, Lattermann C, Hernandez AJ, Bueno DF, Amano MT. Macrophage: a potential target on cartilage regeneration. *Front Immunol*. 2020;11:111.
- [39] Lepage SI, Robson N, Gilmore H, Davis O, Hooper A, St John S, Kamesan V, Gelis P, Carvajal D, Hurtig M. Beyond cartilage repair: the role of the osteochondral unit in joint health and disease. *Tissue Eng B Rev*. 2019;25(2):114-125.
- [40] Lee CH, Cook JL, Mendelson A, Moioli EK, Yao H, Mao JJ. Regeneration of the articular surface of the rabbit synovial joint by cell homing: a proof of concept study. *Lancet*. 2010;376(9739):440-448.
- [41] Mariani E, Pulsatelli L, Facchini A. Signaling pathways in cartilage repair. *Int J Mol Sci*. 2014;15(5):8667-8698.
- [42] Zhang Y, Zhang J, Chang F, Xu W, Ding J. Repair of full-thickness articular cartilage defect using stem cell-encapsulated thermogel. *Mater Sci Eng C*. 2018;88:79-87.
- [43] Ivirico JLE, Bhattacharjee M, Kuyinu E, Nair LS, Laurencin CT. Regenerative engineering for knee osteoarthritis treatment: biomaterials and cell-based technologies. *Engineering*. 2017;3(1):16-27.
- [44] Roelofs A, Rocke J, De Bari C. Cell-based approaches to joint surface repair: a research perspective. *Osteoarthritis Cartilage*. 2013;21(7):892-900.
- [45] Food, H. Drug Administration. Eligibility determination for donors of human cells, tissues, and cellular and tissue-based products. Final rule. *Fed Regist*. 2004;69(101):29785-29834.
- [46] Lander AD, Kimble J, Clevers H, Fuchs E, Montarras D, Buckingham M, Calof AL, Trumpp A, Oskarsson T. What does the concept of the stem cell niche really mean today? *BMC Biol*. 2012;10(1):1-15.
- [47] Sakaguchi Y, Sekiya I, Yagishita K, Muneta T. Comparison of human stem cells derived from various mesenchymal tissues: superiority of synovium as a cell source. *Arthritis Rheum*. 2005;52(8):2521-2529.
- [48] Jones BA, Pei M. Synovium-derived stem cells: a tissue-specific stem cell for cartilage engineering and regeneration. *18(4)*. 2012;301-311.
- [49] Hakamivala A, Robinson K, Huang Y, Yu S, Yuan B, Borrelli J Jr, Tang L. Recruitment of endogenous progenitor cells by erythropoietin loaded particles for in situ cartilage regeneration. *Bioact Mater*. 2020;5(1):142-152.

- [50] Zhang FX, Liu P, Ding W, Meng QB, Su DH, Zhang QC, Lian RX, Yu BQ, Zhao MD, Dong J. Injectable Mussel-Inspired highly adhesive hydrogel with exosomes for endogenous cell recruitment and cartilage defect regeneration. *Biomaterials*. 2021;278:121169.
- [51] Pan X, Yuan S, Xun X, Fan Z, Xue X, Zhang C, Wang J, Deng J. Long-term recruitment of endogenous M2 macrophages by platelet lysate-rich plasma macroporous hydrogel scaffold for articular cartilage defect repair. *Adv Healthc Mater*. 2022;11(6):2101661.
- [52] Ma Z, Song W, He D, Zhang X, He Y, Li H. Smart μ -fiber hydrogels with macroporous structure for sequentially promoting multiple phases of articular cartilage regeneration. *Adv Funct Mater*. 2022;32(22):2113380.
- [53] Huang B, Li P, Chen M, Peng L, Luo X, Tian G, Wang H, Wu L, Tian Q, Li H. Hydrogel composite scaffolds achieve recruitment and chondrogenesis in cartilage tissue engineering applications. *J Nanobiotechnol*. 2022;20(1):1-17.
- [54] Pittenger MF, Mackay AM, Beck SC, Jaiswal RK, Douglas R, Mosca JD, Moorman MA, Simonetti DW, Craig S, Marshak DR. Multilineage potential of adult human mesenchymal stem cells. *Science*. 1999;284(5411):143-147.
- [55] Sacchetti B, Funari A, Michienzi S, Di Cesare S, Piersanti S, Saggio I, Tagliafico E, Ferrari S, Robey PG, Riminucci M, Bianco P. Self-renewing osteoprogenitors in bone marrow sinusoids can organize a hematopoietic microenvironment. *Cell*. 2007;131(2):324-336.
- [56] Sivasubramaniyan K, Ilas DC, Harichandan A, Bos PK, Santos DL, de Zwart PK, Koevoet WJ, Owston H, Bühring HJ, Jones E. Bone marrow-harvesting technique influences functional heterogeneity of mesenchymal stem/stromal cells and cartilage regeneration. *Am J Sports Med*. 2018;46(14):3521-3531.
- [57] Sivasubramaniyan K, Koevoet WJ, Hakimiyan A, Sande M, Farrell E, Hoogduijn M, Verhaar J, Chubinskaya S, Bühring HJ, van Osch G. Cell-surface markers identify tissue resident multipotential stem/stromal cell subsets in synovial intimal and sub-intimal compartments with distinct chondrogenic properties. *Osteoarthritis Cartilage*. 2019;27(12):1831-1840.
- [58] Xu X, Liang Y, Li X, Ouyang K, Wang M, Cao T, Li W, Liu J, Xiong J, Li B. Exosome-mediated delivery of kartogenin for chondrogenesis of synovial fluid-derived mesenchymal stem cells and cartilage regeneration. *Biomaterials*. 2021;269:120539.
- [59] Karlsson C, Thornemo M, Henriksson HB, Lindahl A. Identification of a stem cell niche in the zone of Ranvier within the knee joint. *J Anat*. 2009;215(3):355-363.
- [60] English A, Jones E, Corscadden D, Henshaw K, Chapman T, Emery P, McGonagle D. A comparative assessment of cartilage and joint fat pad as a potential source of cells for autologous therapy development in knee osteoarthritis. *Rheumatology*. 2007;46(11):1676-1683.
- [61] Li L, Newton PT, Boudierlique T, Sejnohova M, Zikmund T, Kozhemyakina E, Xie M, Krivanek J, Kaiser J, Qian H, Dyachuk V, Lassar AB, Warman ML, Barenus B, Adameyko I, Chagin AS. Superficial cells are self-renewing chondrocyte progenitors, which form the articular cartilage in juvenile mice. *FASEB J*. 2017;31(3):1067-1084.
- [62] Li Y, Zhou J, Yang X, Jiang Y, Gui J. Intermittent hydrostatic pressure maintains and enhances the chondrogenic differentiation of cartilage progenitor cells cultivated in alginate beads. *Dev Growth Differ*. 2016;58(2):180-193.
- [63] Hunziker EB, Kapfinger E, Geiss J. The structural architecture of adult mammalian articular cartilage evolves by a synchronized process of tissue resorption and neof ormation during postnatal development. *Osteoarthritis Cartilage*. 2007;15(4):403-413.

- [64] Neumann K, Dehne T, Endres M, Erggelet C, Kaps C, Ringe J, Sittinger M. Chondrogenic differentiation capacity of human mesenchymal progenitor cells derived from subchondral cortico-spongy bone. *J Orthop Res.* 2008;26(11):1449-1456.
- [65] Seol D, Zhou C, Brouillette MJ, Song I, Yu Y, Choe HH, Lehman AD, Jang KW, Fredericks DC, Laughlin BJ. Characteristics of meniscus progenitor cells migrated from injured meniscus. *J Orthop Res.* 2017;35(9):1966-1972.
- [66] Jackson W, Aragon A, Djouad F, Song Y, Koehler S, Nesti L, Tuan R. Mesenchymal progenitor cells derived from traumatized human muscle. *J Tissue Eng Regen Med.* 2009;3(2):129-138.
- [67] Eyckmans J, Lin GL, Chen CS. Adhesive and mechanical regulation of mesenchymal stem cell differentiation in human bone marrow and periosteum-derived progenitor cells. *Biol Open.* 2012;1(11):1058-1068.
- [68] Yoshimura H, Muneta T, Nimura A, Yokoyama A, Koga H, Sekiya I. Comparison of rat mesenchymal stem cells derived from bone marrow, synovium, periosteum, adipose tissue, and muscle. *Cell Tissue Res.* 2007;327(3):449-462.
- [69] Gresham RC, Bahney CS, Leach JK. Growth factor delivery using extracellular matrix-mimicking substrates for musculoskeletal tissue engineering and repair. *Bioact Mater.* 2021;6(7):1945-1956.
- [70] Bos P, Van Osch G, Frenz D, Verhaar J, Verwoerd-Verhoef G. Growth factor expression in cartilage wound healing: temporal and spatial immunolocalization in a rabbit auricular cartilage wound model. *Osteoarthritis Cartilage.* 2001;9(4):382-389.
- [71] Bos P, Verhaar J, Van Osch G. Age-related differences in articular cartilage wound healing: a potential role for transforming growth factor β 1 in adult cartilage repair. *Tissue Eng.* 2006;297-309.
- [72] Luo Z, Jiang L, Xu Y, Li H, Xu W, Wu S, Wang Y, Tang Z, Lv Y, Yang L. Mechano growth factor (MGF) and transforming growth factor (TGF)- β 3 functionalized silk scaffolds enhance articular hyaline cartilage regeneration in a rabbit model. *Biomaterials.* 2015;52:463-475.
- [73] Lei Y, Wang Y, Shen J, Cai Z, Zeng Y, Zhao P, Liao J, Hu N, Luo X. Stem cell-recruiting injectable microgels for repairing osteoarthritis. *Adv Funct Mater.* 2021;31(48):2105084.
- [74] Zhang Z, Li L, Yang W, Cao Y, Shi Y, Li X, Zhang Q. The effects of different doses of IGF-1 on cartilage and subchondral bone during the repair of full-thickness articular cartilage defects in rabbits. *Osteoarthritis Cartilage.* 2017;25(2):309-320.
- [75] Fortier LA, Barker JU, Strauss EJ, McCarrel TM, Cole BJ. The role of growth factors in cartilage repair. *Clin Orthop Relat Res.* 2011;469(10):2706-2715.
- [76] Oseni AO, Crowley C, Boland MZ, Butler PE, Seifalian AM. Cartilage tissue engineering: the application of nanomaterials and stem cell technology. *Tissue Eng Tissue Organ Regen.* 2011;1:233-267.
- [77] Himly M, Geppert M, Hofer S, Hofstatter N, Horejs-Hock J, Duschl A. When would immunologists consider a nanomaterial to be safe? Recommendations for planning studies on nanosafety. *Small.* 2020;16(21):1907483.
- [78] Liao J, Tian T, Shi S, Xie X, Ma Q, Li G, Lin Y. The fabrication of biomimetic biphasic CAN-PAC hydrogel with a seamless interfacial layer applied in osteochondral defect repair. *Bone Res.* 2017;5(1):1-15.
- [79] Fu L, Li P, Zhu J, Liao Z, Gao C, Li H, Yang Z, Zhao T, Chen W, Peng Y. Tetrahedral framework nucleic acids promote the biological functions and related mechanism of

synovium-derived mesenchymal stem cells and show improved articular cartilage regeneration activity in situ. *Bioact Mater.* 2022;9:411-427.

[80] Levinson C, Cavalli E, von Rechenberg B, Zenobi-Wong M, Darwiche SE. Combination of a collagen scaffold and an adhesive hyaluronan-based hydrogel for cartilage regeneration: a proof of concept in an ovine model. *Cartilage.* 2021;13(2_suppl):636S-649S.

[81] Cai Z, Li Y, Song W, He Y, Li H, Liu X. Anti-inflammatory and prochondrogenic in situ-formed injectable hydrogel crosslinked by strontium-doped bioglass for cartilage regeneration. *ACS Appl Mater Interfaces.* 2021;13(50):59772-59786.

[82] Chen J, Li Y, Wang B, Yang J, Heng BC, Yang Z, Ge Z, Lin J. TGF- β 1 affinity peptides incorporated within a chitosan sponge scaffold can significantly enhance cartilage regeneration. *J Mater Chem B.* 2018;6(4):675-687.

[83] Chen JP, Su CH. Surface modification of electrospun PLLA nanofibers by plasma treatment and cationized gelatin immobilization for cartilage tissue engineering. *Acta Biomater.* 2011;7(1):234-243.

[84] Holland TA, Tabata Y, Mikos AG. In vitro release of transforming growth factor- β 1 from gelatin microparticles encapsulated in biodegradable, injectable oligo (poly (ethylene glycol) fumarate) hydrogels. *J Control Release.* 2003;91(3):299-313.

[85] Wang L, Guo X, Chen J, Zhen Z, Cao B, Wan W, Dou Y, Pan H, Xu F, Zhang Z. Key considerations on the development of biodegradable biomaterials for clinical translation of medical devices: with cartilage repair products as an example. *Bioact Mater.* 2022;9:332-342.

[86] Rahmani Del Bakhshayesh A, Babaie S, Tayefi Nasrabadi H, Asadi N, Akbarzadeh A, Abedelahi A. An overview of various treatment strategies, especially tissue engineering for damaged articular cartilage. *Artif Cells Nanomed Biotechnol.* 2020;48(1):1089-1104.

[87] Hu T, Xu H, Wang C, Qin H, An Z. Magnesium enhances the chondrogenic differentiation of mesenchymal stem cells by inhibiting activated macrophage-induced inflammation. *Sci Rep.* 2018;8(1):1-13.

[88] Li J, Liu Y, Zhang Y, Yao B, Li Z, Song W, Wang Y, Duan X, Yuan X, Fu X. Biophysical and biochemical cues of biomaterials guide mesenchymal stem cell behaviors. *Front Cell Dev Biol.* 2021;9:640388.

[89] Guo JL, Kim YS, Koons GL, Lam J, Navara AM, Barrios S, Xie VY, Watson E, Smith BT, Pearce HA. Bilayered, peptide-biofunctionalized hydrogels for in vivo osteochondral tissue repair. *Acta Biomater.* 2021;128:120-129.

[90] Chen Y, Wu T, Huang S, Su CW, Cheng X, Li J, Hou H, She G, Zhang H, Wang H. Sustained release SDF-1 α /TGF- β 1-loaded silk fibroin-porous gelatin scaffold promotes cartilage repair. *ACS Appl Mater Interfaces.* 2019;11(16):14608-14618.

[91] Jiang G, Li S, Yu K, He B, Hong J, Xu T, Meng J, Ye C, Chen Y, Shi Z. A 3D-printed PRP-GelMA hydrogel promotes osteochondral regeneration through M2 macrophage polarization in a rabbit model. *Acta Biomater.* 2021;128:150-162.

[92] Hu Y, Chen L, Gao Y, Cheng P, Yang L, Wu C, Jie Q. A lithium-containing biomaterial promotes chondrogenic differentiation of induced pluripotent stem cells with reducing hypertrophy. *Stem Cell Res Ther.* 2020;11(1):1-13.

[93] Nguyen LH, Kudva AK, Guckert NL, Linse KD, Roy K. Unique biomaterial compositions direct bone marrow stem cells into specific chondrocytic phenotypes corresponding to the various zones of articular cartilage. *Biomaterials.* 2011;32(5):1327-1338.

- [94] Chang NJ, Jhung YR, Issariyakul N, Yao CK, Yeh ML. Synergistic stimuli by hydrodynamic pressure and hydrophilic coating on PLGA scaffolds for extracellular matrix synthesis of engineered cartilage. *J Biomater Sci Polym Ed.* 2012;23(17):2133-2151.
- [95] Ma Z, Gao C, Gong Y, Ji J, Shen J. Immobilization of natural macromolecules on poly-L-lactic acid membrane surface in order to improve its cytocompatibility. *J Biomed Mater Res.* 2002;63(6):838-847.
- [96] Wu SC, Chang JK, Wang CK, Wang GJ, Ho ML. Enhancement of chondrogenesis of human adipose derived stem cells in a hyaluronan-enriched microenvironment. *Biomaterials.* 2010;31(4):631-640.
- [97] Lin X, Wang W, Zhang W, Zhang Z, Zhou G, Cao Y, Liu W. Hyaluronic acid coating enhances biocompatibility of nonwoven PGA scaffold and cartilage formation. *Tissue Eng C Methods.* 2017;23(2):86-97.
- [98] Gong Y, Zhu Y, Liu Y, Ma Z, Gao C, Shen J. Layer-by-layer assembly of chondroitin sulfate and collagen on aminolyzed poly (L-lactic acid) porous scaffolds to enhance their chondrogenesis. *Acta Biomater.* 2007;3(5):677-685.
- [99] Zhang J, Zhang X, Hong Y, Fu Q, He Q, Mechakra A, Zhu Q, Zhou F, Liang R, Li C. Tissue-adhesive paint of silk microparticles for articular surface cartilage regeneration. *ACS Appl Mater Interfaces.* 2020;12(20):22467-22478.
- [100] Yu Y, Brouillette MJ, Seol D, Zheng H, Buckwalter JA, Martin JA. Use of recombinant human stromal cell-derived factor 1 α -loaded fibrin/hyaluronic acid hydrogel networks to achieve functional repair of full-thickness bovine articular cartilage via homing of chondrogenic progenitor cells. *Arthritis Rheumatol.* 2015;67(5):1274-1285.
- [101] Park MS, Kim YH, Jung Y, Kim SH, Park JC, Yoon DS, Kim SH, Lee JW. In situ recruitment of human bone marrow-derived mesenchymal stem cells using chemokines for articular cartilage regeneration. *Cell Transplant.* 2015;24(6):1067-1083.
- [102] Park E, Hart ML, Rolauffs B, Stegemann JP, Annamalai RT. Bioresponsive microspheres for on-demand delivery of anti-inflammatory cytokines for articular cartilage repair. *J Biomed Mater Res.* 2020;108(3):722-733.
- [103] Li J, Gong L, Zhang J, Pan Z, Liu Y, Zhou F, Hong Y, Hu Y, Bunpetch V, Ouyang H. An Interleukin 4 Loaded Bi-phasic 3D Printed Scaffold Promotes Osteochondral Defect Regeneration. *Available at SSRN.* 2020;3600426.
- [104] Kim SH, Kim SH, Jung Y. TGF- β 3 encapsulated PLCL scaffold by a supercritical CO₂-HFIP co-solvent system for cartilage tissue engineering. *J Control Release.* 2015;206:101-107.
- [105] Shimaya M, Muneta T, Ichinose S, Tsuji K, Sekiya IJ. Magnesium enhances adherence and cartilage formation of synovial mesenchymal stem cells through integrins. *Cartilage.* 2010;18(10):1300-1309.
- [106] Wang Y, Zhang W, Yao Q. Copper-based biomaterials for bone and cartilage tissue engineering. *J Orthop Transl.* 2021;29:60-71.
- [107] Kumar S, Adjei IM, Brown SB, Liseth O, Sharma B. Manganese dioxide nanoparticles protect cartilage from inflammation-induced oxidative stress. *Biomaterials.* 2019;224:119467.
- [108] Khader A, Arinze TL. Biodegradable zinc oxide composite scaffolds promote osteochondral differentiation of mesenchymal stem cells. *Biotechnol Bioeng.* 2020;117(1):194-209.

- [109] Bunpetch V, Zhang X, Li T, Lin J, Maswikiti EP, Wu Y, Cai D, Li J, Zhang S, Wu C. Silicate-based bioceramic scaffolds for dual-lineage regeneration of osteochondral defect. *Biomaterials*. 2019;192:323-333.
- [110] Lu J, Shen X, Sun X, Yin H, Yang S, Lu C, Wang Y, Liu Y, Huang Y, Yang Z. Increased recruitment of endogenous stem cells and chondrogenic differentiation by a composite scaffold containing bone marrow homing peptide for cartilage regeneration. *Theranostics*. 2018;8(18):5039.
- [111] He R, Wang B, Cui M, Xiong Z, Lin H, Zhao L, Li Z, Wang Z, Peggrem S, Xia Z. Link protein N-terminal peptide as a potential stimulating factor for stem cell-based cartilage regeneration. *Stem Cell Int*. 2018;2018.
- [112] Armakolas N, Dimakakos A, Armakolas A, Antonopoulos A, Koutsilieris M. Possible role of the Ec peptide of IGF-1Ec in cartilage repair. *Mol Med Rep*. 2016;14(4):3066-3072.
- [113] Stefani RM, Lee AJ, Tan AR, Halder SS, Hu Y, Guo XE, Stoker AM, Ateshian GA, Marra KG, Cook JL. Sustained low-dose dexamethasone delivery via a PLGA microsphere-embedded agarose implant for enhanced osteochondral repair. *Acta Biomater*. 2020;102:326-340.
- [114] Jiao F, Tang W, Wang J, Liu D, Zhang H, Tang D. Icaritin promotes the repair of bone marrow mesenchymal stem cells in rabbit knee cartilage defects via the BMP/Smad pathway. *Ann Transl Med*. 2022;10(12).
- [115] Zhu J, Yang S, Qi Y, Gong Z, Zhang H, Liang K, Shen P, Huang YY, Zhang Z, Ye W. Stem cell-homing hydrogel-based miR-29b-5p delivery promotes cartilage regeneration by suppressing senescence in an osteoarthritis rat model. *Sci Adv*. 2022;8(13).
- [116] Jiang S, Tian G, Yang Z, Gao X, Wang F, Li J, Tian Z, Huang B, Wei F, Sang X. Enhancement of acellular cartilage matrix scaffold by Wharton's jelly mesenchymal stem cell-derived exosomes to promote osteochondral regeneration. *Bioact Mater*. 2021;6(9):2711-2728.
- [117] Wang X, Song X, Li T, Chen J, Cheng G, Yang L, Chen C. Aptamer-functionalized bioscaffold enhances cartilage repair by improving stem cell recruitment in osteochondral defects of rabbit knees. *Am J Sports Med*. 2019;47(10):2316-2326.
- [118] Madry H, Gao L, Rey-Rico A, Venkatesan JK, Müller-Brandt K, Cai X, Goebel L, Schmitt G, Speicher-Mentges S, Zurakowski D. Thermosensitive hydrogel based on PEO-PPO-PEO poloxamers for a controlled in situ release of recombinant adeno-associated viral vectors for effective gene therapy of cartilage defects. *Adv Mater*. 2020;32(2):1906508.
- [119] Haartmans MJ, Timur UT, Emanuel KS, Caron MM, Jeuken RM, Welting TJ, van Osch GJ, Heeren RM, Cillero-Pastor B, Emans PJ. Evaluation of the anti-inflammatory and chondroprotective effect of celecoxib on cartilage ex vivo and in a rat osteoarthritis model. *Cartilage*. 2022;13(3):19476035221115541.
- [120] Dai M, Sui B, Xue Y, Liu X, Sun J. Cartilage repair in degenerative osteoarthritis mediated by squid type II collagen via immunomodulating activation of M2 macrophages, inhibiting apoptosis and hypertrophy of chondrocytes. *Biomaterials*. 2018;180:91-103.
- [121] Hutmacher DW. Scaffolds in tissue engineering bone and cartilage. *Biomaterials*. 2000;21(24):2529-2543.
- [122] Cui YL, Qi AD, Liu WG, Wang XH, Wang H, Ma DM, Yao KD. Biomimetic surface modification of poly(L-lactic acid) with chitosan and its effects on articular chondrocytes in vitro. *Biomaterials*. 2003;24(21):3859-3868.

- [123] Park SH, Seo JY, Park JY, Park YB, Ji K, Kim HS, Choi S, Choi JH, Kim BH, Min BH, Kim MS. An injectable, click-crosslinked, cytomodulin-modified hyaluronic acid hydrogel for cartilage tissue engineering. *NPG Asia Mater.* 2019;11(1):1-16.
- [124] Nakajima K, Hirano Y, Iida T, Nakajima A. Adsorption of plasma proteins on Arg-gly-Asp-ser peptide-immobilized poly(vinyl alcohol) and ethylene-acrylic acid copolymer films. *Polym J.* 1990;22(11):985-990.
- [125] Chen W, Li Y, Huang Y, Dai Y, Xi T, Zhou Z, Liu H. Quercetin modified electrospun PHBV fibrous scaffold enhances cartilage regeneration. *J Mater Sci Mater Med.* 2021;32(8):92.
- [126] Ma Z, Gao C, Gong Y, Shen J. Cartilage tissue engineering PLLA scaffold with surface immobilized collagen and basic fibroblast growth factor. *Biomaterials.* 2005;26(11):1253-1259.
- [127] Stich S, Loch A, Leinhase I, Neumann K, Kaps C, Sittinger M, Ringe J. Human periosteum-derived progenitor cells express distinct chemokine receptors and migrate upon stimulation with CCL2, CCL25, CXCL8, CXCL12, and CXCL13. *Eur J Cell Biol.* 2008;87(6):365-376.
- [128] D'Este M, Sprecher C, Kyllonen L, Milz S, Schmid T, Alini M, Eglin D. SDF-1 and CCL5 delivered from thermoresponsive hyaluronan hydrogel induce cell homing in an osteochondral defect repair model in rabbit. *Acta Biomater.* 2020;128:120-129.
- [129] Joutoku Z, Onodera T, Matsuoka M, Homan K, Momma D, Baba R, Hontani K, Hamasaki M, Matsubara S, Hishimura R. CCL21/CCR7 axis regulating juvenile cartilage repair can enhance cartilage healing in adults. *Sci Rep.* 2019;9(1):5165.
- [130] Joutoku Z, Onodera T, Matsuoka M, Homan K, Momma D, Baba R, Hontani K, Hamasaki M, Matsubara S, Hishimura R, Iwasaki N. CCL21/CCR7 axis regulating juvenile cartilage repair can enhance cartilage healing in adults. *Sci Rep.* 2019;9(1):1-12.
- [131] van der Kraan PM. The interaction between joint inflammation and cartilage repair. *Tissue Eng Regen Med.* 2019;16(4):327-334.
- [132] Lee CH, Cook JL, Mendelson A, Moiola EK, Yao H, Mao JJ. Regeneration of the articular surface of the rabbit synovial joint by cell homing: a proof of concept study. *Lancet.* 2010;376(9739):440-448.
- [133] Diao H, Wang J, Shen C, Xia S, Guo T, Dong L, Zhang C, Chen J, Zhao J, Zhang J. Improved cartilage regeneration utilizing mesenchymal stem cells in TGF- β 1 gene-activated scaffolds. *Tissue Eng.* 2009;15(9):2687-2698.
- [134] Nixon AJ, Fortier LA, Williams J, Mohammed H. Enhanced repair of extensive articular defects by insulin-like growth factor-I-laden fibrin composites. *J Orthop Res.* 1999;17(4):475-487.
- [135] Hunziker EB, Rosenberg LC. Repair of partial-thickness defects in articular cartilage: cell recruitment from the synovial membrane. *J Bone Joint Surg Am.* 1996;78(5):721-735.
- [136] Vainieri ML, Lolli A, Kops N, D'atri D, Eglin D, Yayon A, Alini M, Grad S, Sivasubramanian K, Van Osch GJ. Evaluation of biomimetic hyaluronic-based hydrogels with enhanced endogenous cell recruitment and cartilage matrix formation. *Acta Biomater.* 2020;101:293-303.
- [137] Mourino V, Cattalini JP, Boccaccini AR. Metallic ions as therapeutic agents in tissue engineering scaffolds: an overview of their biological applications and strategies for new developments. *J R Soc Interface.* 2012;9(68):401-419.

- [138] Taheem DK, Foyt DA, Loaiza S, Ferreira SA, Ilic D, Auner HW, Grigoriadis AE, Jell G, Gentleman E. Differential regulation of human bone marrow mesenchymal stromal cell chondrogenesis by hypoxia inducible factor-1 α hydroxylase inhibitors. *Stem Cell*. 2018;36(9):1380-1392.
- [139] Focaroli S, Teti G, Salvatore V, Orienti I, Falconi M. Calcium/cobalt alginate beads as functional scaffolds for cartilage tissue engineering. *Stem Cell Int*. 2016;2016.
- [140] Lv Q, Ma C. A novel protocol for injectable artificial cartilage constructs based on programmed shape-morphing hydrogels for cartilage regeneration. *Chem Eng J*. 2022;446:137109.
- [141] Xu C, Chen J, Li L, Pu X, Chu X, Wang X, Li M, Lu Y, Zheng X. Promotion of chondrogenic differentiation of mesenchymal stem cells by copper: implications for new cartilage repair biomaterials. *Mater Sci Eng C*. 2018;93:106-114.
- [142] Shen J, Chen B, Zhai X, Qiao W, Wu S, Liu X, Zhao Y, Ruan C, Pan H, Chu PK. Stepwise 3D-spatio-temporal magnesium cationic niche: nanocomposite scaffold mediated microenvironment for modulating intramembranous ossification. *Bioact Mater*. 2021;6(2):503-519.
- [143] Zhu M, Zhong W, Cao W, Zhang Q, Wu G. Chondroinductive/chondroconductive peptides and their-functionalized biomaterials for cartilage tissue engineering. *Bioact Mater*. 2022;9:221-238.
- [144] Akkiraju H, Bonor J, Nohe A. CK2. 1, a novel peptide, induces articular cartilage formation in vivo. *J Orthop Res*. 2017;35(4):876-885.
- [145] Mahzoon S, Townsend JM, Lam TN, Sjoelund V, Detamore MS. Effects of a bioactive SPPEPS peptide on chondrogenic differentiation of mesenchymal stem cells. *Ann Biomed Eng*. 2019;47(11):2308-2321.
- [146] Li T, Liu B, Chen K, Lou Y, Jiang Y, Zhang D. Small molecule compounds promote the proliferation of chondrocytes and chondrogenic differentiation of stem cells in cartilage tissue engineering. *Biomed Pharmacother*. 2020;131:110652.
- [147] Lo KWH, Jiang T, Gagnon KA, Nelson C, Laurencin CT. Small-molecule based musculoskeletal regenerative engineering. *Trends Biotechnol*. 2014;32(2):74-81.
- [148] Chen Y, Sun H, Yao X, Yu Y, Tian T, Xu W, Zhou Y, Ouyang H. Pharmaceutical therapeutics for articular regeneration and restoration: state-of-the-art technology for screening small molecular drugs. *Cell Mol Life Sci*. 2021;78(24):8127-8155.
- [149] Xuan H, Hu H, Geng C, Song J, Shen Y, Lei D, Guan Q, Zhao S, You Z. Biofunctionalized chondrogenic shape-memory ternary scaffolds for efficient cell-free cartilage regeneration. *Acta Biomater*. 2020;105:97-110.
- [150] Wang P, Zhang F, He Q, Wang J, Shiu HT, Shu Y, Tsang WP, Liang S, Zhao K, Wan C. Flavonoid compound icariin activates hypoxia inducible factor 1 α in chondrocytes and promotes articular cartilage repair. *PLoS One*. 2016;11(2).
- [151] Bartel DP. MicroRNAs: genomics, biogenesis, mechanism, and function. *Cell*. 2004;116(2):281-297.
- [152] Lolli A, Lambertini E, Penolazzi L, Angelozzi M, Morganti C, Franceschetti T, Pelucchi S, Gambari R, Piva R. Pro-chondrogenic effect of miR-221 and slug depletion in human MSCs. *Stem Cell Rev Rep*. 2014;10(6):841-855.
- [153] Lolli A, Narcisi R, Lambertini E, Penolazzi L, Angelozzi M, Kops N, Gasparini S, van Osch GJ, Piva R. Silencing of antichondrogenic microRNA-221 in human mesenchymal stem cells promotes cartilage repair in vivo. *Stem Cell*. 2016;34(7):1801-1811.

- [154] Zhang F, Jing S, Ren T, Lin J. MicroRNA-10b promotes the migration of mouse bone marrow-derived mesenchymal stem cells and downregulates the expression of E-cadherin. *Mol Med Rep.* 2013;8(4):1084-1088.
- [155] Song J, Kim D, Chun CH, Jin EJ. MicroRNA-375, a new regulator of cadherin-7, suppresses the migration of chondrogenic progenitors. *Cell Signal.* 2013;25(3):698-706.
- [156] Zhu G, Chen X. Aptamer-based targeted therapy. *Adv Drug Deliv Rev.* 2018;134:65-78.
- [157] Thery C, Witwer KW, Aikawa E, Alcaraz MJ, Anderson JD, Andriantsitohaina R, Antoniou A, Arab T, Archer F, Atkin-Smith GK. Minimal information for studies of extracellular vesicles 2018 (MISEV2018): a position statement of the International Society for Extracellular Vesicles and update of the MISEV2014 guidelines. *J Extracell Vesicles.* 2018;7(1):1535750.
- [158] Nawaz M, Fatima F, Vallabhaneni KC, Penfornis P, Valadi H, Ekstrom K, Kholia S, Whitt JD, Fernandes JD, Pochampally R. Extracellular vesicles: evolving factors in stem cell biology. *Stem Cell Int.* 2016;2016.
- [159] Amsar RM, Wijaya CH, Ana ID, Hidajah AC, Notobroto HB, Kencana Wungu TD, Barlian A. Extracellular vesicles: a promising cell-free therapy for cartilage repair. *Future Sci OA.* 2022;8(2).
- [160] Liu X, Yang Y, Li Y, Niu X, Zhao B, Wang Y, Bao C, Xie Z, Lin Q, Zhu L. Integration of stem cell-derived exosomes with in situ hydrogel glue as a promising tissue patch for articular cartilage regeneration. *Nanoscale.* 2017;9(13):4430-4438.
- [161] Shen K, Duan A, Cheng J, Yuan T, Zhou J, Song H, Chen Z, Wan B, Liu J, Zhang X. Exosomes derived from hypoxia preconditioned mesenchymal stem cells laden in a silk hydrogel promote cartilage regeneration via the miR-205-5p/PTEN/AKT pathway. *Acta Biomater.* 2022;143:173-188.
- [162] Xue K, Jiang Y, Zhang X, Wu J, Qi L, Liu K. Hypoxic ADSCs-derived EVs promote the proliferation and chondrogenic differentiation of cartilage stem/progenitor cells. *Adipocyte.* 2021;10(1):322-337.
- [163] Fan Y, Li Z, He Y. Exosomes in the pathogenesis, progression, and treatment of osteoarthritis. *Bioengineering.* 2022;9(3):99.
- [164] Zhang B, Su Y, Zhou J, Zheng Y, Zhu D. Toward a better regeneration through implant-mediated immunomodulation: harnessing the immune responses. *Adv Sci.* 2021;8(16):2100446.
- [165] Chen Z, Klein T, Murray RZ, Crawford R, Chang J, Wu C, Xiao Y. Osteoimmunomodulation for the development of advanced bone biomaterials. *Mater Today.* 2016;19(6):304-321.
- [166] Yuan M, Bi B, Huang J, Zhuo R, Jiang X. Thermosensitive and photocrosslinkable hydroxypropyl chitin-based hydrogels for biomedical applications. *Carbohydr Polym.* 2018;192:10-18.
- [167] Kou L, Huang H, Tang Y, Sun M, Li Y, Wu J, Zheng S, Zhao X, Chen D, Luo Z. Opsonized nanoparticles target and regulate macrophage polarization for osteoarthritis therapy: a trapping strategy. *J Control Release.* 2022;347:237-255.
- [168] Dai M, Liu X, Wang N, Sun J. Squid type II collagen as a novel biomaterial: isolation, characterization, immunogenicity and relieving effect on degenerative osteoarthritis via inhibiting STAT1 signaling in pro-inflammatory macrophages. *Mater Sci Eng C.* 2018;89:283-294.

- [169] Gan D, Jiang Y, Hu Y, Wang X, Wang Q, Wang K, Xie C, Han L, Lu X. Mussel-inspired extracellular matrix-mimicking hydrogel scaffold with high cell affinity and immunomodulation ability for growth factor-free cartilage regeneration. *J Orthop Transl.* 2022;33:120-131.
- [170] Hoemann CD, Chen G, Marchand C, Tran-Khanh N, Thibault M, Chevrier A, Sun J, Shive MS, Fernandes MJ, Poubelle PE. Scaffold-guided subchondral bone repair: implication of neutrophils and alternatively activated arginase-1+ macrophages. *Am J Sports Med.* 2010;38(9):1845-1856.
- [171] Patel JM, Saleh KS, Burdick JA, Mauck RL. Bioactive factors for cartilage repair and regeneration: improving delivery, retention, and activity. *Acta Biomater.* 2019;93:222-238.
- [172] Shalumon K, Chen JP. Scaffold-based drug delivery for cartilage tissue regeneration. *Curr Pharm Des.* 2015;21(15):1979-1990.
- [173] Holland TA, Tabata Y, Mikos AG. In vitro release of transforming growth factor- β 1 from gelatin microparticles encapsulated in biodegradable, injectable oligo (poly(ethylene glycol) fumarate) hydrogels. *J Control Release.* 2003;91(3):299-313.
- [174] Lee JM, Ryu JH, Kim EA, Jo S, Kim BS, Lee H, Im GI. Adhesive barrier/directional controlled release for cartilage repair by endogenous progenitor cell recruitment. *Biomaterials.* 2015;39:173-181.
- [175] Patel JJ, Flanagan CL, Hollister SJ. Bone morphogenetic protein-2 adsorption onto poly- ϵ -caprolactone better preserves bioactivity in vitro and produces more bone in vivo than conjugation under clinically relevant loading scenarios. *Tissue Eng C Methods.* 2015;21(5):489-498.
- [176] Zhang W, Ling C, Zhang A, Liu H, Jiang Y, Li X, Sheng R, Yao Q, Chen J. An all-silk-derived functional nanosphere matrix for sequential biomolecule delivery and in situ osteochondral regeneration. *Bioact Mater.* 2020;5(4):832-843.
- [177] Dong Y, Liu Y, Chen Y, Sun X, Zhang L, Zhang Z, Wang Y, Qi C, Wang S, Yang Q. Spatiotemporal regulation of endogenous MSCs using a functional injectable hydrogel system for cartilage regeneration. *NPG Asia Mater.* 2021;13(1):71.

3

Modulating design parameters to drive cell invasion into hydrogels for osteochondral tissue formation

Andrea Schwab[#], Marinus A Wesdorp[#], [Jietao Xu](#), Florencia Abinzano, Claudia Loebel, Marc Falandt, Riccardo Levato, David Eglin, Roberto Narcisi, Martin J Stoddart, Jos Malda, Jason A Burdick, Matteo D'Este, Gerjo J V M van Osch

[#]Authors contributed equally to this work

J Orthop Translat. 2023 Sep 4;41:42-53.

ABSTRACT

Background

The use of acellular hydrogels to repair osteochondral defects requires cells to first invade the biomaterial and then to deposit extracellular matrix for tissue regeneration. Due to the diverse physicochemical properties of engineered hydrogels, the specific properties that allow or even improve the behaviour of cells are not yet clear. The aim of this study was to investigate the influence of various physicochemical properties of hydrogels on cell migration and related tissue formation using *in vitro*, *ex vivo* and *in vivo* models.

Methods

Three hydrogel platforms were used in the study: Gelatine methacryloyl (GelMA) (5% wt), norbornene hyaluronic acid (norHA) (2% wt) and tyramine functionalised hyaluronic acid (THA) (2.5% wt). GelMA was modified to vary the degree of functionalisation (DoF 50% and 80%), norHA was used with varied degradability via a matrix metalloproteinase (MMP) degradable crosslinker and THA was used with the addition of collagen fibrils. The migration of human mesenchymal stromal cells (hMSC) in hydrogels was studied *in vitro* using a 3D spheroid migration assay over 48h. In addition, chondrocyte migration within and around hydrogels was investigated in an *ex vivo* bovine cartilage ring model (three weeks). Finally, tissue repair within osteochondral defects was studied in a semi-orthotopic *in vivo* mouse model (six weeks).

Results

A lower DoF of GelMA did not affect cell migration *in vitro* ($p = 0.390$) and led to a higher migration score *ex vivo* ($p < 0.001$). The introduction of a MMP degradable crosslinker in norHA hydrogels did not improve cell infiltration *in vitro* or *in vivo*. The addition of collagen to THA resulted in greater hMSC migration *in vitro* ($p = 0.031$) and *ex vivo* ($p < 0.001$). Hydrogels that exhibited more cell migration *in vitro* or *ex vivo* also showed more tissue formation in the osteochondral defects *in vivo*, except for the norHA group. Whereas norHA with a degradable crosslinker did not improve cell migration *in vitro* or *ex vivo*, it did significantly increase tissue formation *in vivo* compared to the non-degradable crosslinker ($p < 0.001$).

Conclusion

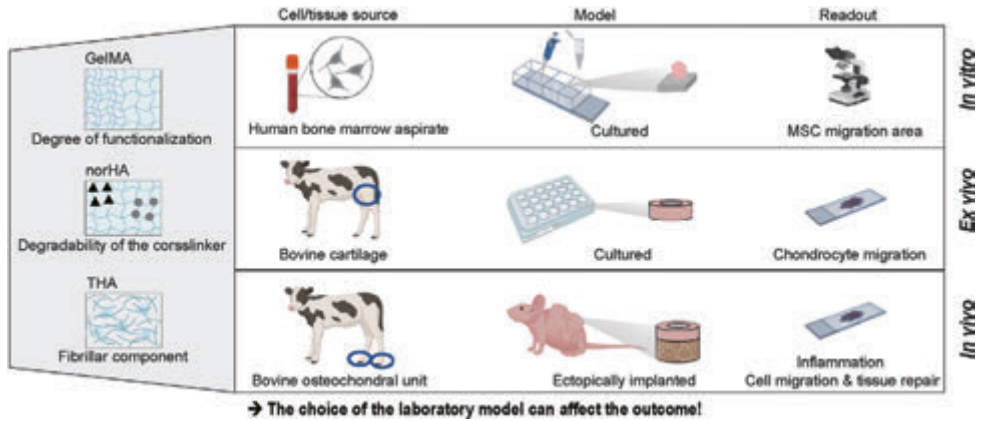
The modification of hydrogels by adapting DoF, use of a degradable crosslinker or including fibrillar collagen can control and improve cell migration and tissue formation for osteochondral defect repair. This study also emphasizes the importance of performing both *in vitro* and *in vivo* testing of biomaterials, as, depending on the material, the results might be affected by the model used.

The Translational Potential of this Article

The translational potential of this article: This article highlights the potential of using acellular hydrogels to repair osteochondral defects, which are common injuries in orthopaedics. The study provides a deeper understanding of how to modify the properties of hydrogels to control cell migration and tissue formation for osteochondral defect repair. The results of this article also highlight that the choice of the used laboratory model can

affect the outcome. Testing hydrogels in different models is thus advised for successful translation of laboratory results to the clinical application.

Keywords: cartilage; cells; hydrogels; regenerative medicine; tissue engineering



1. INTRODUCTION

Current matrix-based approaches for the repair of (osteo-) chondral defects, like autologous matrix-induced chondrogenesis (AMIC, a combination of microfracture with a collagen scaffold) and matrix-assisted chondrocyte implantation (MACI), have improved clinical outcomes and lowered revision rates when compared to microfracture alone [1-3]. Although these treatments lead to improved function and reduced pain, they fail to repair defects fully functional for the long-term [4]. Acellular biomaterial-assisted approaches are an attractive alternative to cell-based procedures for the treatment of small focal defects, particularly due to the elimination of donor-site morbidity and the possibility of a single-stage procedure [5]. Importantly, it has been shown that biomaterials help to improve the preservation of the cartilage tissue surrounding the defect [6]. However, to repair cartilage fully, improved mobilisation and infiltration of cells residing in the knee into the biomaterials are needed [7-9].

Injectable hydrogels are one promising group of biomaterials to fill complex defects of any shape and location through a minimally invasive approach [10,11]. Despite the extensive research performed *in vitro* on the chondro-inductive properties of hydrogels, these biomaterials often fail upon implantation *in vivo*. Failure is related to the challenge of retaining the material in the defect area, which limits cell invasion [12]. Integration of the biomaterial with the tissues adjacent to the defect, results mainly from the infiltration of host cells, followed by matrix deposition [13]. Thus, rapid cell infiltration is an important step in an integrative defect repair strategy [14]. Cell infiltration is not only relevant for acellular hydrogel-assisted repair, but also of interest for approaches where cells are encapsulated within a hydrogel to integrate the repair tissue into the host tissue [15]. This highlights the need to understand how physicochemical properties of hydrogels influence cell migration and which modifications may improve cell migration from surrounding tissues for osteochondral defect repair.

Since collagen and glycosaminoglycan are major components in the ECM of connective tissue, collagen and hyaluronic acid (HA) based hydrogels have attracted interest in cartilage tissue engineering approaches [16]. Gelatine, the product of denatured collagen, modified with methacryloyl groups (GelMA), is an emerging and widely used hydrogel that exhibits tunable material properties while maintaining regions with cell adhesives (e.g. arginine-glycine-aspartate (RGD)) and degradable sequences [17,18]. The crosslinking density in GelMA hydrogels is controlled by the degree of functionalisation (DoF), which is the extent of functionalisation with methacryloyl groups that alters crosslinking. GelMA at a fixed concentration, but an increase in DoF leads to a higher crosslinking density and thus a smaller mesh size [19]. More recently, a lower degree of functionalization of the GelMA50 has been associated with a faster enzymatic degradation kinetic [20]. For endothelial cells it has been shown that a lower DoF supports greater endothelial cell derived capillary-like-network formation [21]. Whether this hydrogel modification also improves cell migration in the osteochondral environment and supports tissue repair has not yet been studied.

The most widely used proteoglycan hydrogels in biomedicine are HA and its derivatives. HA-based biomaterials are often functionalised with biochemical cues (e.g., chondroinductive or chondroconductive peptides, the addition of fibrous components)

and/or biophysical cues (mechanical properties, mesh size, porosity) to stimulate (endogenous) cell infiltration and cartilaginous matrix deposition [14,22,23]. To improve the tunability of mechanical properties, the interaction with the host tissue or the rheological properties and printability, functionalization of HA-based hydrogels (e.g. with thiol-norbornene or tyramine) have been introduced [24-26]. Norbornene hyaluronic acid (norHA) is an attractive biomaterial due to its excellent printability, tunable properties and the ability for in situ crosslinking [27]. Tyramine functionalized HA (THA) is characterized by its enhanced binding to the cartilage host tissue via the formation of di-tyrosine bonds between THA and cartilage ECM [28]. Together with its tunable properties, THA is also an attractive hydrogel for bioprinting [29-31]. The main limitation of HA-based materials is the limited cell adhesion [32,33]. One approach to overcome this is to combine THA with either RGD, collagen or gelatine to increase cell attachment and cell spreading [30,34,35]. Beyond the possibility of varying RGD concentration, the use of a degradable crosslinker, specifically the use of a matrix metalloproteinase (MMP) cleavable crosslinker, has allowed mesenchymal stromal cells (MSC) spreading and mechano-response when embedded in the hydrogel [36].

The above-introduced hydrogel biomaterials (GelMA, norHA and THA) are attractive for (osteo-) chondral repair due to their chondrogenic potential and printability [27-30,34,36-41]. Thus, this study aimed to investigate the effect of selected hydrogel modifications on human hMSC and chondrocyte migration *in vitro* and related tissue formation for (osteo-) chondral defect repair *in vivo*. We hypothesised that a lower crosslinking density in GelMA, use of a degradable crosslinker with norHA precursors, as well as the addition of collagen fibrils in THA hydrogels would increase cell migration and improve tissue formation. Cell migration into the hydrogel was investigated using three models: (1) hMSC spheroids seeded within hydrogels for *in vitro* migration, (2) endogenous chondrocyte migration in a cartilage ring model *ex vivo*, and (3) cell migration and tissue formation in a semi-orthotopic mouse model *in vivo*. While the first two models focus on a single cell type, the *in vivo* model was chosen to study the interplay of multiple cell types within the osteochondral defect environment.

2. MATERIALS AND METHODDS

2.1. Biomaterial preparation and characterization

2.1.1. Hydrogel preparation

Two HA-based materials (THA, norHA) and a gelatine-based material (GelMA) were evaluated by MSC cell migration *in vitro*, chondrocyte migration from cartilage explants *ex vivo*, cell migration, and osteochondral defect repair in a semi-orthotopic model *in vivo* (Figure 1). For the *in vitro* migration study, hydrogels were crosslinked in an 8-well plate prior to cell seeding. For the *in vivo* and *ex vivo* model, hydrogel precursors were injected in the defects of either cartilage rings or osteochondral explants and photo-crosslinked.

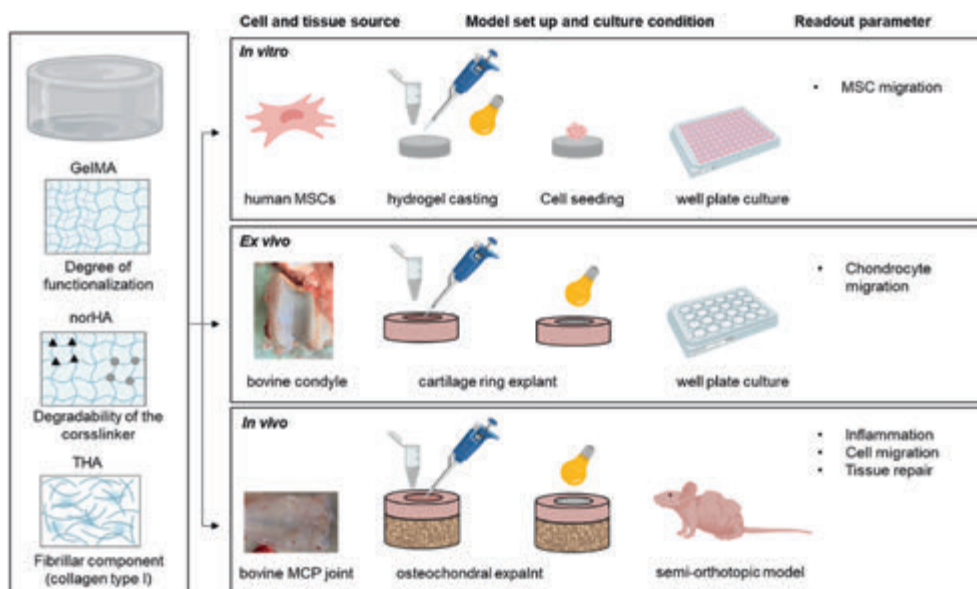


Figure 1. Graphical illustration of the in vitro, ex vivo and in vivo models to evaluate acellular hydrogels for (osteo-) chondral repair. Three hydrogel types were evaluated for cell migration and tissue formation in osteochondral defects. Comparisons included the degree of functionalization (50% and 80%) for gelatine methacryloyl (GelMA hydrogels), the degradability of matrix metalloprotease (MMP) degradable versus non-degradable (1,4-Dithiothreitol, DTT) crosslinkers for norbornene-modified hyaluronic acid (HA) and the addition of fibrillar collagen on tyramine modified HA (THA) hydrogels. Images were created with Biorender.com.

2.1.1.1. Gelatine methacryloyl (GelMA)

GelMA was synthesized with a DoF of 50% (GelMA50) and 80% (GelMA80). Based on the protocol described by Melchels et al., 0.6 g methacrylic anhydride (Sigma Aldrich 92%) per g of gelatine (type A from porcine skin, 300 g Bloom, Sigma Aldrich) was used (10% gelatine in PBS, 50°C, 1h) for GelMA80. For GelMA50, 0.036 g methacrylic anhydride per g of gelatine was used [42,43]. GelMA (50 mg/ml) was reconstituted at 60°C before adding the photo crosslinker ruthenium (0.5 mM) and sodium persulfate (5.0 mM) with subsequent photo-crosslinking (15 min, 3 cm distance, AVIDE lamp). The variable of the two GelMA formulations used in this study were the DoF (50% or 80%).

2.1.1.2. Norbornene hyaluronic acid (norHA)

NorHA was synthesized as previously described and reconstituted with either a non-degradable 1,4-Dithiothreitol (DTT, 0.22 mg/ml, Sigma Aldrich, Saint Louis, USA) crosslinker or a MMP cleavable crosslinker (2.55 mg/ml, GCNSVPMS↓MRGGSNCG, Lot: U1432DL070-1/PE2401, GenScript, Piscataway Township, USA) [41,44]. NorHA was reconstituted at a final polymer concentration of 20 mg/ml. NorHA precursors (norHA-DTT and norHA-MMP) contained thiolated RGD sequences (GCGYGRGDSPG, 1.0 mM, U0140DA260-1, Lot: 94230930001/PE8559, GenScript). Photo-crosslinking (20 min, 3 cm distance, AVIDE lamp) was achieved using photo-initiators ruthenium and sodium persulfate (Advanced Biomatrix, 5248-1KIT) followed by hydrogel gelation. The choice of

the crosslinker (MMP degradable or non-degradable DTT) was the variable to prepare two norHA formulations.

2.1.1.3. Tyramine modified hyaluronic acid (THA)

THA with a degree of substitution of 6% was synthesized as described previously [45]. THA was reconstituted (25 mg/ml) and photoinitiator Eosin Y (0.02 mg/ml, Sigma Aldrich) was added. THA (25 mg/ml final concentration) and THA-collagen (THA 12.5 mg/ml and 2.5 mg/ml collagen 1 isolated from rat tails, Corning, Bedford, USA) hydrogels were enzymatically crosslinked using peroxidase from horseradish (0.3 U/ml, Sigma Aldrich) and hydrogen peroxide (120 ppm, Carl Roth, Karlsruhe, Germany) with subsequent photo-crosslinking (10 min, 3 cm distance, AVIDE lamp, Well-Com Vertriebs GmbH, Gelsenkirchen, Germany) [34]. The variable for the two THA formulations was the addition of the fibrillary component (THA-col) compared to THA alone.

2.1.2. Nuclear magnetic resonance (NMR) spectrum

The hydrogel precursor materials were characterized by ^1H NMR spectroscopy to confirm the molecular structure, and to assess purity and degree of functionalization. All materials were dissolved in deuterium oxide (D_2O).

2.1.3. Dynamic mechanical analysis

Hydrogel mechanical properties were assessed using a dynamic mechanical analyzer (DMA Q800, TA Instruments, The Netherlands). Hydrogels in phosphate buffered saline (PBS, Sigma Aldrich) were analysed in unconfined uniaxial compression test (room temperature, $n = 5$ samples per condition) to measure their compressive moduli. A preload of 0.01 N was applied to the hydrogels, followed by a ramp force of 2 N/m until a maximum force of 8 N was reached. The compressive modulus (Young's modulus) was calculated as the slope of the linear elastic range of the stress/strain curve. To measure the stress-relaxation response, a constant strain was applied (preload of 0.001 N, room temperature, $n = 5$ samples per condition) to hydrogels. After applying a constant strain of 20% for 2 min, the hydrogel response was measured over a period of 1 min. The relaxation of the material was calculated as the ratio of minimum and maximum stress after 2 min of 20% strain.

2.1.4. Rheological characterization

Photo rheology experiments on the hydrogel precursor solutions (GelMA DOF 50 and DOF80, norHA MMP and norHA DTT) to determine the crosslinking kinetics was measured using a DHR2 rheometer (TA Instruments, The Netherlands). Samples were prepared fresh (100 μl measuring volume, $n = 3$) before loaded onto the rheometer for oscillatory time sweep experiments (frequency of 1.0 Hz, angular frequency of 6.28 rad/s, with 5.0% constant strain at 37C, preset measuring gap size of 300 μm , 20.0 mm parallel EHP stainless steel plate). After 30 s of measuring, the visible light source was turned on to allow photo crosslinking of the hydrogels for the remaining time of the experiment and storage (G') and loss moduli (G'') were recorded.

2.2. *In vitro* hMSC migration assay

2.2.1. hMSC isolation and expansion

hMSC were isolated from bone marrow of patients undergoing total hip replacement after informed consent (approved by the local Medical Ethical Committees of Erasmus MC: protocol MEC-2015-644) as described earlier [46]. hMSCs were thawed, and expanded in media composed of alpha-Minimum Essential Medium (α -MEM, Gibco, California, USA) supplemented with 10% fetal bovine serum (FBS, Gibco, California, USA), 50 $\mu\text{g}/\text{mL}$ gentamycin (Gibco), 1.5 $\mu\text{g}/\text{mL}$ fungizone (Gibco), 1 ng/mL fibroblast growth factor 2 (FGF2, AbD Serotec, Puchheim, Germany) and 25 $\mu\text{g}/\text{mL}$ ascorbic acid-2-phosphate (AA-2-P, Sigma-Aldrich) in a humidified atmosphere with media replacement twice per week. Cells at 80-90% confluency were sub-cultured using 0.25% Trypsin/1x EDTA (Gibco). hMSCs were fluorescently labelled according to the manufacturer's instructions (Vybrant CFDA-SE Cell tracer Kit, Thermo Fisher) to visualize cell location after seeding on the hydrogels (see 2.2.2).

2.2.2. *In vitro* migration assay set up

hMSC migration was evaluated by measuring the migration area of the cells in a 3D migration assay after 48h of culture *in vitro* [47]. Micro-moulds (Micro Tissues 3D Petri Dish, Sigma Aldrich) were casted with agarose to form 256 circular micro-wells. After the micro-moulds gelled, they were transferred to a 12-well-plate containing α -MEM (Gibco) supplemented with 10% foetal bovine serum (FBS, Gibco) and 25 $\mu\text{g}/\text{mL}$ ascorbic acid-2-phosphate (Sigma-Aldrich) and incubated in a humidified atmosphere (37 °C, 5% CO₂) for 1h. Cell spheroids (500 cells per spheroid) were prepared by dropwise seeding the CFDA labelled cell suspension (0.128 \times 10⁶ cells/190 μL) into the 3D agarose moulds and then cultured in a humidified atmosphere for 24 h to form spheroids. Spheroid formation was assessed by a standard inverted microscope and irregular sized spheroids were discarded. To harvest the spheroids, the 3D agarose moulds were transferred and inverted into a new 12-well plate containing media and cells and were centrifuged (5 min at 120g). The medium containing the spheroids was transferred to a falcon tube and again centrifuged (30 s at 300 g). Spheroids were resuspended in the assay media composed of α -MEM supplemented with 1% insulin, transferrin and selenium (ITS+, Sigma Aldrich), and 25 $\mu\text{g}/\text{mL}$ ascorbic acid-2-phosphate (Sigma-Aldrich) Next, 125 μL of each hydrogel precursor was casted in each well of a chamber slide (Nunc cell culture imaging 8-welllls, Thermo Fisher), crosslinked and washed three times with serum free α -MEM. Afterwards, 5-10 spheroids were seeded on each hydrogel in each well. Cell spheroids were cultured on the hydrogels for 48h with assay media supplemented with platelet-derived growth factor BB (50 ng/ml, PDGF-BB, Peprotech, NJ, USA) to stimulate cell migration. To quantify cell migration, confocal imaging (Leica SP5, FITC channel, 10x magnification) was performed with the acquisition of z-stacks to monitor the spheroid migration from the top to the bottom of the hydrogel. Cell migration area of hMSC was measured on the different hydrogel compositions (n = 6, n = 5 for THA-col) using the earlier described macro with Fiji image processing software [47]. The migration area of the migrating cells was calculated to obtain the total migratory area in a radius of 760 μm .

2.3. *Ex vivo* migration assay to assess chondrocyte migration

2.3.1. Cartilage ring isolation and *ex vivo* explant culture

Cartilage explants were isolated from the patellar groove of bovine knee joints (six months old calves, Angst AG, Switzerland) using a biopsy punch (8 mm, KAI medical, Arnold Bott AG, Opfikon, Switzerland). Cartilage was separated from the subchondral bone with a scalpel. Explants were washed with DMEM HG (Gibco) supplemented with 1% antibiotics (10 U/ml penicillin, 10 µg/ml streptomycin, Gibco). After defect creation (4 mm, KAI medical, Arnold Bott AG, Switzerland) in the centre of the explant, the defects were filled with the hydrogel precursors (described in Figure 1), and then gelled in the defect to ensure optimal integration between the hydrogel and the cartilage tissue. All samples were transferred into a 24 well plate (TPP, Trasadingen, Switzerland) containing DMEM HG enriched with 10% FBS, 50 µg/ml ascorbic acid and 1% antibiotics. Samples were cultured *ex vivo* for 21 days (37 °C, 5% CO₂) with media change every 2-3 days.

2.3.2. Cell viability staining of *ex vivo* samples

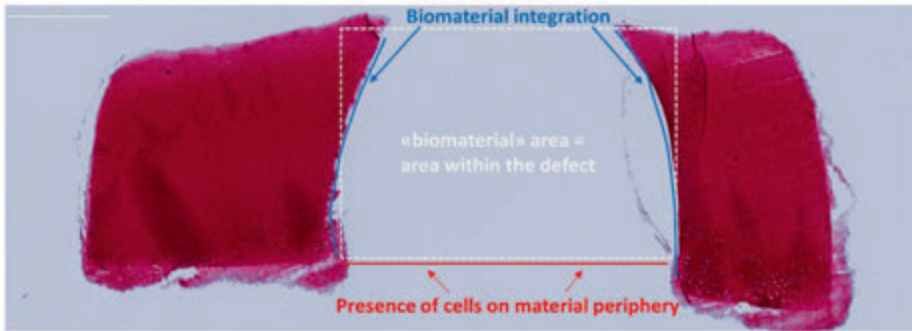
After 21 days of culture, metabolic activity of cartilage explants was assessed with 3-(4,5-dimethylthiazol-2-yl)-2,5-diphenyltetrazoliumbromid (MTT, 1 mg/ml, 1h incubation at 37 °C, Sigma Aldrich). Samples were imaged with bright field microscope (Zeiss). Samples were also stained for live-dead assessment (Sigma Aldrich) with Ethidium homodimer (4 µM) and Calcein-AM (2 µM) according to manufacturer's instructions, washed with PBS after 25 min incubation and kept in culture media for microscopic assessment (Zeiss confocal microscope, LSM800).

2.3.3. Histological processing, staining and scoring of *ex vivo* samples

Samples were harvested at day 21, fixed with formalin (4%, Formafix AG, Hittnau, Switzerland), washed with PBS, immersed with sucrose (150 mg/ml and 300 mg/ml, Sigma-Aldrich), embedded in freezing media (Leica, Nussloch, Germany) and snap frozen with liquid nitrogen. Sections of 8 µm were cut with a cryostat microtome (HM 500 OM; Zeiss) and stored at -20 °C.

Safranin-O staining was performed to visualize proteoglycans. Cryosections were washed with deionized water to remove freezing media, incubated for 10 min with Weigert's hematoxylin (Sigma Aldrich), blued with tap water and incubated with fast green (0.02%, 6 min, Sigma Aldrich). After washing with acetic acid (1%, Fluka), slides were incubated in safranin-O (0.01%, 15 min, Sigma Aldrich) and differentiated with ethanol (70%, Alcosuisse, Rüti bei Büren, Switzerland) with subsequent dehydration (ethanol 96%, ethanol absolute, Xylene) and cover slipping (Eukitt, Sigma Aldrich). Bright-field microscopic images (Olympus BX63, Olympus) were acquired for cell migration analysis.

A migration score was introduced to semi-quantitatively evaluate chondrocyte migration from the explant towards the acellular hydrogels. Safranin-O stained slices of the samples at day 21 (n = 3 samples per biomaterial, n = 2 samples empty defect control, n = 2 sections) were scored by three independent observers blinded for the condition (Figure 2). The individual scores were visually inspected and in case of differences, discussed to reach consensus between observers.



Scoring criteria	0	1	2	3
Explant-biomaterial integration	No integration, gaps formed between material and tissue	Limited integration. Material-tissue contact (<25%) less than half	Local integration with cartilage tissue (> 50%)	Nearly full integration, no gaps between material and tissue (>90%)
Presence of cells on material periphery	No cells	Single cells present (locally)	Parts are covered with cells (>20%)	Full layer of cells on materials (>90%)
Presence of cells within biomaterial	No cells	Few (local) cells	Moderate cell density, inhomogeneous distribution	Many cells, "homogenous" distribution

Figure 2. Scoring criteria to assess chondrocyte migration in the ex vivo cartilage ring model. Safranin-O staining of cartilage explant with defect in the centre (white dashed line). The areas of interest are indicated for the biomaterial integration (blue line) and presence of cells (red line). (For interpretation of the references to color in this figure legend, the reader is referred to the Web version of this article.)

2.4. Semi-orthotopic model to assess osteochondral defect repair in vivo

2.4.1. In vivo subcutaneous osteochondral defect model

To evaluate the capacity of the hydrogels to support endogenous cell migration and osteochondral repair, an *in vivo* semi-orthotopic osteochondral defect model was used, where tissues are implanted subcutaneously in mice [48]. This animal experiment was approved by the ethics committee for laboratory animal use (under license AVD101002016691, protocol #EMC16-691-07) and following the ARRIVE (Animal Research: Reporting of *In Vivo* Experiments) guidelines. Bovine osteochondral biopsies (8 mm diameter, 5 mm height) were harvested with a dental trephine from metacarpal-phalangeal joints of 3-8 months old calves from a local slaughterhouse and provided by LifeTec Group (Eindhoven, Netherlands). Osteochondral defects (4 mm diameter, 4 mm depth) were created in the centre of the biopsies using a hand drill to avoid thermal damage. The defect created into the subchondral bone will allow bone marrow and subchondral bone hosting cells to infiltrate the defect area. The osteochondral biopsies were kept overnight in α -MEM (Gibco, USA) supplemented with 10% fetal bovine serum (FBS, Gibco), 1.5 μ g/mL fungizone (Gibco), and 50 μ g/mL gentamycin (Gibco) to ensure sterility. The hydrogel precursors were used to fill the defects and then photo crosslinked

before implantation. All hydrogel-loaded osteochondral constructs were covered with a circular 8 mm Neuro-Patch membrane (Braun, Melsungen, Germany) on the cartilage to prevent the ingrowth of host cells.

Thirteen 11-week-old female NMRI-Foxn1 nu/nu mice (Janvier Labs, St. Berthevin, France) were used in this study. The mice were allowed to adapt to the conditions of the animal facility for seven days before implantation surgery. The mice were housed under specific-pathogen-free conditions with a regular day/night light cycle and food and water were available ad libitum. Four osteochondral constructs were randomly implanted subcutaneously on the back of each mouse under 2.5-3.0% isoflurane anaesthesia (Laboratories Karizoo, Barcelona, Spain). To minimise the risk of infection, the mice received 25 mg/kg bodyweight of ampicillin (Dopharma, Raamsdonksveer, Netherlands) subcutaneously during surgery. Staples (AgnTho's, Lidingö, Sweden) were used to close the incisions and were removed one week after implantation. To ensure pre- and postoperative analgesia, the mice received a subcutaneous injection of 0.05 mg/kg body weight of buprenorphine (Chr. Olesen & Co, Copenhagen, Denmark) 1 h before surgery and 6 h after surgery. After ten days (n = 3 samples per condition) and six weeks (n = 5 samples per condition), mice were killed by cervical dislocation and the osteochondral constructs were harvested.

2.4.2. Histological processing, staining and scoring

The osteochondral constructs were fixed in 4% formalin for 1 week, followed by decalcification using 10% ethylenediaminetetraacetic acid (EDTA, pH 7.4, Sigma Aldrich) for up to 4 weeks. Six-week samples were processed for routine paraffin embedding and sectioned (microtome, Leica). Dewaxed slides were stained with hematoxylin and eosin (HE) to study general cell and tissue morphology. Images were taken with a slide scanner (NanoZoomer, Hamamatsu). Ten-week samples were processed for cryo embedding (OCT, Sakura, Nagano, Japan) and cutting (Cryostat, Leica, Nussloch, Germany) after demineralization.

Image analysis (NDP.View2 software, version 2.8.24, 2020 Hamamatsu Photonics K.K.) was used to assess tissue formation. The area of the newly formed tissue was measured by manually selecting the tissue regions. The percentages of the defects covered with cartilage-like, bone-like and other tissue were measured separately (Supplementary Figure S4D), with the defect area set to 100%. The tissue volume of three sections that were taken at depths of 1, 1.5 and 2 mm for each sample was averaged for further analyses. All slides were scored by an investigator blinded to the experimental condition.

2.5. Statistical analysis

Mechanical characterization and *ex vivo* migration are presented as box plots (min to max value with a line presenting the median). *In vitro* MSC migration area and tissue volume in % are presented as mean \pm standard deviation (SD). For each of the hydrogel groups (THA, GelMA, norHA) the results of the two modifications were compared. All statistical analyses were performed using SPSS (version 28.0.1.0, IBM Corporation, USA). Student t-tests were performed for mechanical characterization, *in vitro* MSC migration and *in vivo* tissue formation and two-sided p-values are reported. In case the variances between the two modifications were significantly different, p-value of equal variances not assumed is

reported and marked with a *. Mann-Whitney U tests were used to assess statistical significance in the *ex vivo* migration scores. For all statistical analyses, a p-value < 0.05 was considered statistically significant and marked with a *.

3. RESULTS

3.1. Lower crosslinking density of GelMA hydrogels increases cell migration

Compression moduli (E-moduli) of GelMA hydrogels with DoF of 50% and 80% crosslinked under the same conditions after equilibrating in PBS were respectively 6.8 ± 1.3 kPa and 7.3 ± 1.7 kPa, $p = 0.637$, revealing no significant difference between the two DoF (Figure 3A). Stress recovery of GelMA80 (0.8 ± 0.1) was similar to that of GelMA50 (0.7 ± 0.1 , $p = 0.236$).

The ^1H NMR spectrum confirms the different DOF (Supplementary Figure S1). GelMA50 had slower photo-crosslinking kinetics than GelMA80, both with a final storage modulus around 1 kPa (Supplementary Figure S2).

hMSCs migrated out of the spheroid in both GelMA formulations. The migration area (Figure 3B) of hMSC seeded in GelMA50 ($42,050 \pm 15,335 \mu\text{m}^2$) was similar to the migration in GelMA80 ($28,010 \pm 34,241 \mu\text{m}^2$, $p = 0.390^*$) trending towards more migration in the lower DoF. In the *ex vivo* migration assay, the chondrocytes in the cartilage explant remained metabolic active (as indicated by MTT staining Figure 3C) and a few metabolically active chondrocytes invaded both GelMA formulations (Supplementary Figure S6A). Most of the cells were observed on top of the hydrogels. GelMA50 had a significantly higher chondrocyte migration score (min/max:2.5/7, median:5) than GelMA80 (min/max:1/5, median:3, $p < 0.001$). The hydrogels with both DoF remained inside the cartilage defect. In general, a slight shrinkage was observed during culture resulting in a gap between the hydrogel and the surrounding defect.

Hydrogels were implanted in the semi-orthotopic *in vivo* model. After ten days, infiltration of a few multinucleated cells was observed in GelMA80 (2 out of 3 samples) and GelMA50 (1 out of 3 samples), indicating a low inflammatory response (Supplementary Figure S3). After six weeks the average area of remaining hydrogel implanted in the osteochondral defect was $11.3\% \pm 9.7\%$ for GelMA50 and $16.4\% \pm 12.3\%$ for GelMA80 (values calculated relative to respective total defect area). This means that the hydrogel was degraded upon implantation. The infiltration of cells and newly formed osteochondral tissue were mostly present in the deep zone and at the lateral sides of the osteochondral defects (Figure 3D). In GelMA80 a cell-free area within the hydrogel was still present, even in the samples with the highest invasion (see Supplementary Figure S4A and S5A). GelMA50 and GelMA80 both allowed osteochondral defect repair ($70.5\% \pm 21.3\%$ vs $48.0\% \pm 23.0\%$, $p = 0.149$). The repair consisted of cartilage-like tissue ($0.04\% \pm 0.09\%$ vs $5.3\% \pm 6.3\%$, $p = 0.135^*$), bone-like tissue ($5.4\% \pm 7.1\%$ vs $12.8\% \pm 12.6\%$, $p = 0.284$) and other tissues ($52.4\% \pm 11.9\%$ vs $42.6\% \pm 20.2\%$, $p = 0.379$).

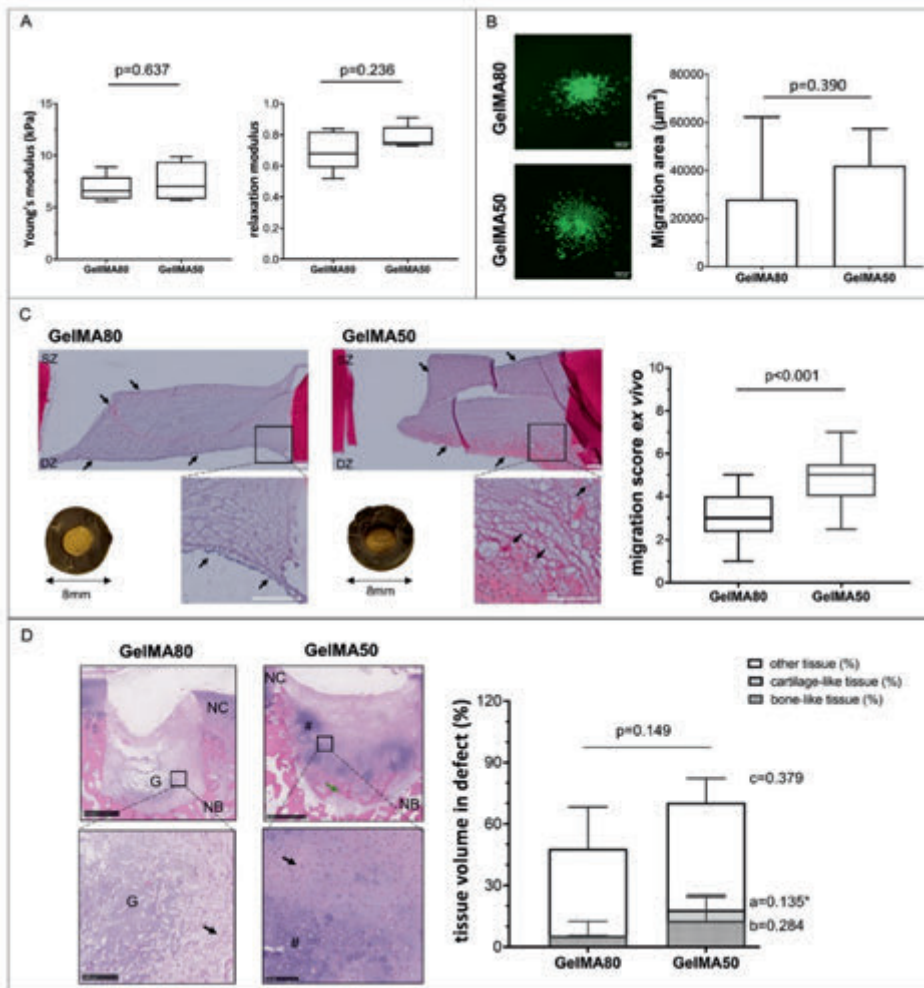


Figure 3. Effect of lowering the degree of functionalization (DoF) from 80% to 50% in gelatine methacryloyl (GelMA) hydrogels on cell migration and tissue formation. A) the Young's modulus and stress-relaxation to characterize hydrogel recovery after swelling in PBS ($n = 5$ per group). B) In vitro cell migration of hMSCs out of spheroids seeded on top of hydrogels ($n = 6$ per group). hMSC labelled with membrane dye are shown in green. Scale bar 200 μm . C) Chondrocyte migration and migration score in the ex vivo cartilage ring model (min to max score with median). Macroscopic (explant diameter 8 mm) and microscopic image of MTT stained samples, the safranin-O stained section of the hydrogel and migration score with a maximum score of 9 ($n = 3$ samples per group, $n = 2$ slides per sample). Scale bar 200 μm . D) Cell migration and related tissue formation in acellular hydrogels implanted in osteochondral explants in a semi-orthotopic mouse model ($n = 5$ samples per biomaterial). Hematoxylin and eosin-stained cross-sections of one representative sample are shown. Tissue volume in osteochondral defect (OCD) is presented as bone-like tissue, cartilage-like tissue and other tissue (mean \pm SD) relative to total tissue volume. Scale bar low magnification image 1 mm, higher magnification image 100 μm . NC: native cartilage, NB: native bone, G: hydrogel, # indicated newly formed cartilage-like tissue, green arrow indicates newly formed bone-like tissue, black arrow indicates infiltrated cells within the defects, blue arrow indicates the integration of newly formed bone and native bone. Statistical significance comparing means between hydrogel formulations: a: cartilage-like, b: bone-like, c: other tissue, p: total tissue volume. * equal variances not assumed. (For interpretation of the references to color in this figure legend, the reader is referred to the Web version of this article.)

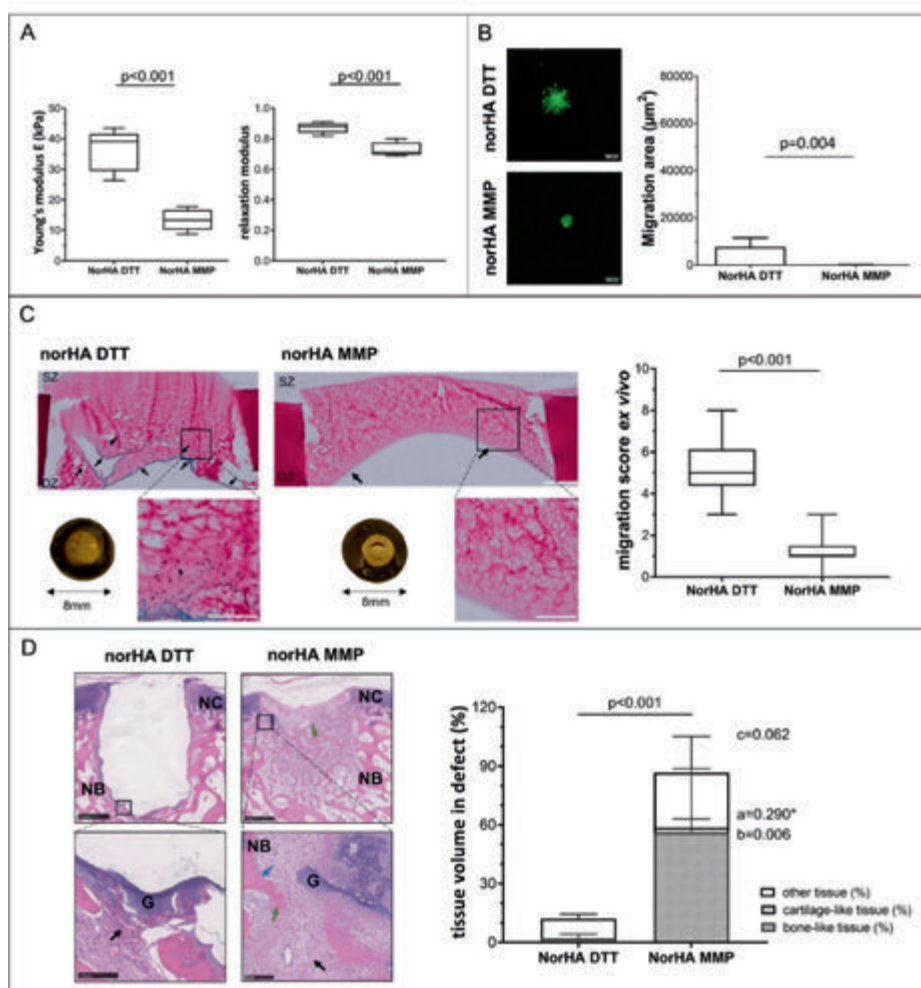


Figure 4. Effect of crosslinker degradability (MMP degradable vs non-degradable DTT) on norbonene modified hyaluronic acid hydrogel (norHA) cell migration and tissue formation. A) Young's modulus and stress-relaxation to characterize hydrogel recovery after swelling in PBS ($n = 5$ per group) are shown. B) In vitro cell migration of hMSCs out of spheroids seeded on top of hydrogels ($n = 6$ per group). hMSC labelled with membrane dye are shown in green. Scale bar $200 \mu\text{m}$. C) Chondrocyte migration and migration score in the ex vivo cartilage ring model (min to max score with median). Macroscopic (explant diameter 8 mm) and microscopic image of MTT stained samples, the safranin-O stained section of the hydrogel and migration score with a maximum score of 9 ($n = 3$ samples per group, $n = 2$ slides per sample). Scale bar $200 \mu\text{m}$ low magnification $500 \mu\text{m}$. D) Cell migration and related tissue formation in acellular hydrogels implanted in osteochondral explants in a semi-orthotopic mouse model ($n = 5$ samples per biomaterial). Hematoxylin and eosin-stained cross-sections of one representative sample are shown. Tissue volume in osteochondral defect (OCD) is presented as bone-like tissue, cartilage-like tissue and other tissue (mean \pm SD) relative to total tissue volume. Scale bar low magnification image 1 mm , higher magnification image $100 \mu\text{m}$. NC native cartilage, NB native bone, G: hydrogel, green arrow indicates newly formed bone-like tissue, black arrow indicates infiltrated cells within the defects, blue arrow indicates the integration of newly formed bone and native bone. Statistical significance comparing means between hydrogel formulations: a: cartilage-like, b: bone-like, c: other tissue, p: total tissue volume. * equal variances not assumed. (For interpretation of the references to color in this figure legend, the reader is referred to the Web version of this article.)

3.2. MMP cleavable norHA hydrogels limit cell migration *in vitro* and *ex vivo* but increase tissue formation *in vivo*

The two norHA hydrogel formulations differed by the presence of either a MMP degradable crosslinker or a non-degradable (DTT) crosslinker. The modulus of norHA MMP (13.4 ± 3.5 kPa) was significantly lower than the modulus of norHA DTT (36.3 ± 6.8 kPa, $p < 0.001$) after swelling and equilibrating in PBS (Figure 4). The stress recovery was significantly higher in norHA DTT (0.9 ± 0.0) compared to norHA MMP (0.7 ± 0.1 , $p < 0.001$). The ^1H NMR spectrum of norHA confirms the functionalization of HA with norbornene groups (Supplementary Figure S1). The results of the photo rheological characterization (Supplementary Figure S2) showed a similar trend to the DMA measurement with a higher storage modulus for norHA DTT (1.5 kPa) compared to norHA MMP (0.2 kPa).

Both NorHA hydrogel formulations showed limited migration of MSC into the hydrogel *in vitro*. Less hMSC migration (Figure 4B) was observed when a norHA MMP degradable crosslinker ($44 \pm 68 \mu\text{m}^2$) was used, compared to a norHA non-degradable DTT crosslinker ($7742 \pm 3772 \mu\text{m}^2$, $p = 0.004$). NorHA MMP was also invaded by less chondrocytes than norHA DTT after three weeks of *ex vivo* culture (Figure 4C, Supplementary Figure S8A, B). A significantly lower migration score was observed for the norHA material with a degradable crosslinker (norHA MMP, min/max: 0/3, median: 1) compared to norHA with a non-degradable crosslinker (norHA DTT, min/max:3/8, median:5, $p < 0.001$). Both hydrogel formulations remained in the defect during 21 days of culture.

After ten days of implantation *in vivo* (Figure 4D) no cell invasion was present in norHA DTT hydrogels (0 out of 3 samples) while the group with the MMP degradable crosslinker exhibited invading cells even in the deeper regions of the hydrogels (3 out of 3 samples (Supplementary Figure S3)). After six weeks of implantation total tissue formation was significantly higher in norHA MMP than norHA DTT ($86.6\% \pm 15.9\%$ vs. $12.1\% \pm 3.7\%$, $p < 0.001$). The average percentage of remaining hydrogel in the defect was $0.7\% \pm 0.5\%$ for norHA MMP and $8.5\% \pm 9.7\%$ for norHA DTT (values calculated relative to respective defect area). The infiltrated cells and newly formed tissue were mostly in the deeper parts and at the sides of the osteochondral defects in the periphery of the hydrogels (Figure 4D). Cartilage-like tissue ($2.4\% \pm 4.5\%$ vs $0.0\% \pm 0.0\%$, $p = 0.290^*$) was observed with areas of proteoglycan-rich matrix (Supplementary Figure S5B). Significantly more bone-like tissue ($56.1\% \pm 32.6\%$ vs $2.0\% \pm 2.3\%$, $p = 0.006$) and a tendency towards more other-like tissue ($28.1\% \pm 18.4\%$ vs $10.1\% \pm 2.4\%$, $p = 0.062$) was formed in the norHA MMP compared to norHA DTT.

3.3. The addition of collagen fibres to THA improves cell migration *in vitro* and *ex vivo*

Moduli (Figure 5A) of THA-col (60.4 ± 24.9 kPa) were similar to THA (38.3 ± 8.5 kPa, $p = 0.121$). The stress recovery was significantly increased in THA compared to THA-col (0.9 ± 0.1 vs 0.6 ± 0.2 , $p = 0.042^*$). The ^1H NMR spectrum of THA confirm the functionalization of HA with tyramine (Supplementary Figure S1).

THA-col had significantly more MSC migration *in vitro* (Figure 5B) ($37,647 \pm 23,532 \mu\text{m}^2$) than THA only ($3737 \pm 4243 \mu\text{m}^2$, $p = 0.031^*$). Only a few metabolic active chondrocytes were present in the THA hydrogel, and more cells were present in THA-col hydrogel in the *ex vivo* model (Figure 5C, Supplementary Figure S6A). This was also visible from the

chondrocyte migration score that was significantly higher in THA-col (chondrocyte migration score min/max; 2/5.5, median 4) than in THA (min/max: 0/5.5, median 1, $p < 0.001$). Hydrogels of both formulations remained in the cartilage defect during the 21 days of culture.

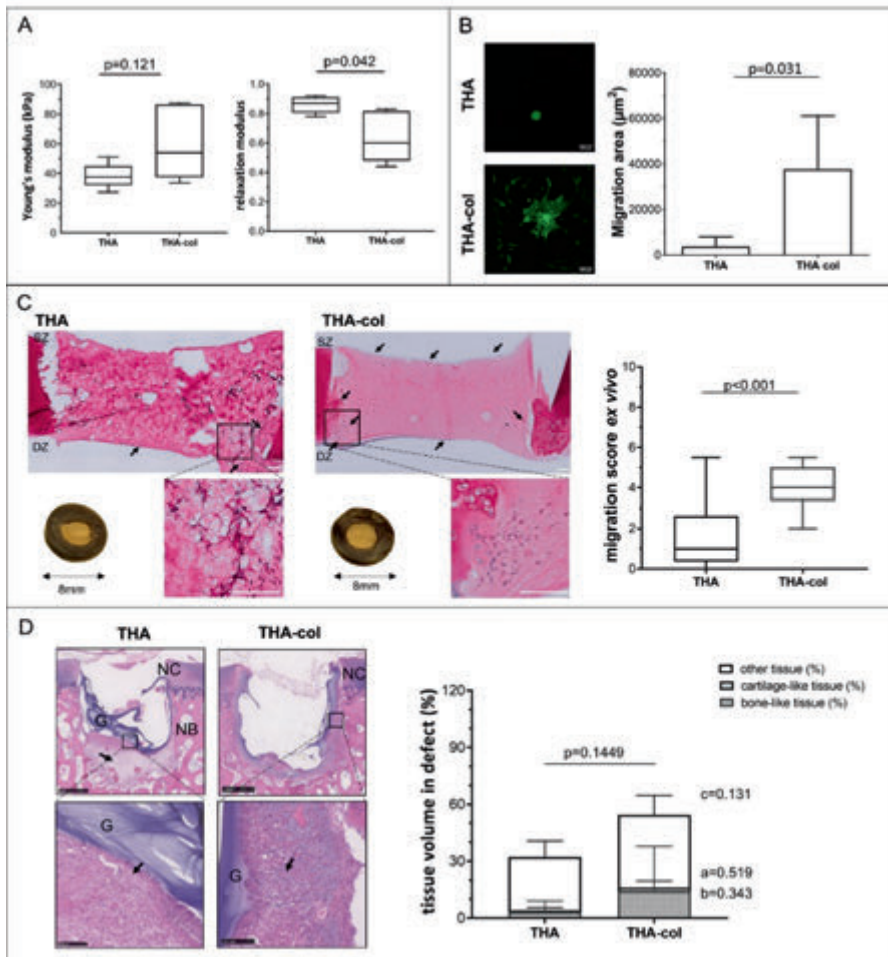


Figure 5. Effect of the addition of fibrillary collagen (col) to tyramine modified hyaluronic acid (THA) hydrogels on cell migration and tissue formation. A) Young's modulus and stress-relaxation to characterize hydrogel recovery after swelling in PBS ($n = 5$ per group). B) In vitro cell migration of hMSCs out of spheroids seeded on top of hydrogels ($n = 6$ THA, $n = 5$ THA-col). hMSC labelled with membrane dye shown in green. Scale bar 200 μm . C) Chondrocyte migration and migration score in the ex vivo cartilage ring model (min to max score with median). Macroscopic (explant diameter 8 mm) and microscopic image of MTT stained samples, the safranin-O stained section of the hydrogel and migration score with a maximum score of 9 ($n = 3$ samples per group, $n = 2$ slides per sample). Scale bar 200 μm . D) Cell migration and related tissue formation in acellular hydrogels implanted in osteochondral explants in a semi-orthotopic mouse model ($n = 5$ samples per biomaterial). Haematoxylin and eosin-stained cross-sections of one representative sample are shown. Tissue volume in osteochondral defect (OCD) is presented as bone-like tissue, cartilage-like tissue and other tissue (mean \pm SD) relative to total tissue volume. Scale bar low magnification image 1 mm, higher magnification image 100 μm . NC native cartilage, NB native bone, G: hydrogel, black arrow indicates

*infiltrated cells within the defects, blue arrow indicates the integration of newly formed bone and native bone. Statistical significance comparing means between hydrogel formulations: a: cartilage-like, b: bone-like, c: other tissue, p: total tissue volume. * equal variances not assumed. (For interpretation of the references to color in this figure legend, the reader is referred to the Web version of this article.)*

Ten days after implantation *in vivo*, a few inflammatory cells were observed on the hydrogels (THA: 2 out of 3 samples, THA-col: 2 out of 3 samples, Supplementary Figure S3), located at the hydrogel periphery and inside the hydrogels. After six weeks of implantation, the average amount of remaining hydrogel in the defect was $9.7\% \pm 3.0\%$ for THA-col and $15.2\% \pm 9.1\%$ for THA (values calculated relative to respective defect area). For THA materials, limited cell migration and total osteochondral tissue repair (THA-col: $54.4\% \pm 26.4\%$ vs. THA: $32.3\% \pm 15.4\%$, $p = 0.144$) was observed in the defects of the osteochondral explants. In line with the *in vitro* hMSC migration and *ex vivo* chondrocyte migration, a trend for an increased amount of cartilage-like tissue ($1.8\% \pm 3.5$ vs $0.7\% \pm 1.5\%$, $p = 0.519$), bone-like tissue ($14.3\% \pm 23.6\%$ vs $3.4\% \pm 5.7\%$, $p = 0.343$) and other tissue ($38.3\% \pm 10.3\%$ vs $28.3\% \pm 8.4\%$ $p = 0.131$) were observed in the defects filled with THA-col composite compared to THA alone (Figure 5D, Supplementary Figure S4C and S5C).

4. DISCUSSION

Material-based cell-free approaches to treat cartilage and osteochondral defects have shown promising results [5,49,50]. These approaches are of interest due to the limited availability of autologous chondrocytes. Infiltration of cells from the adjacent tissues into the biomaterial is a critical step in this approach, as these migrating cells play a pivotal role in depositing the extracellular matrix and facilitating tissue repair [15]. However, data on which biomaterial properties influence cell infiltration and related tissue formation is limited since most studies use only one material or modification, and different studies use different models for their evaluation. Focus of this study was to evaluate different materials and modifications in an *in vitro* assay for MSC migration, an *ex vivo* assay for chondrocyte migration and an *in vivo* model to assess cell infiltration, inflammatory response and tissue formation. Our findings indicate significant differences between the three hydrogel groups across the various assays, and the outcomes may be extended to other materials and modifications.

Lowering DoF from 80% to 50% (GelMA80 vs. GelMA50) showed a higher migration index and thus a higher number of chondrocytes migrating into the hydrogel *ex vivo*. It has also been described that the hydraulic permeability and mechanical properties of GelMA can be controlled by the DoF, polymer concentration and crosslinking time [51]. The mechanical behaviour of the two formulations during the rheology tests was not significantly different and did not allow estimation of the permeability of the gels. The lower degree of functionalization of GelMA50 has been previously associated with a faster enzymatic degradation kinetic [20], which is known to promote cell migration. A higher cell migration and more tissue formation compared to the higher DoF group was only observed in the *ex vivo* migration assay. The MSCs in the *in vitro* assay were spreading and migrating in both, GelMA50 and GelMA80. This partially aligns with a previous *in vitro* study comparing GelMA (5% wt) with different DoF, which showed spreading of encapsulated adipose-derived MSCs in the samples with a DoF of 30% and 50%, but not above 70%

[21,43]. In the *ex vivo* assay, the difference in migration score between the two DoF was more prominent. Although the chondrocytes retained a round morphology, they seem to prefer invasion into the lower DoF hydrogel. This finding highlights that different models and/or the cell types used, influence migration behaviour. A tendency of overall more tissue formation was observed in GelMA50 compared to GelMA80 after six weeks of implantation. Although GelMA has some potential to stimulate cell migration and cartilage-like-tissue formation, the shrinking of the hydrogel when cultured in the cartilage ring model is a drawback. Nguyen et al. described that GelMA with a lower DoF degrades faster by collagenase-loaded micro-particles [19]. This shrinkage leads to limited integration with the surrounding tissue and resulting in gap formation that cells might not be able to bridge.

A different approach to control the degradability of a hydrogel and to increase cell migration is the use of a MMP degradable crosslinker with a norHA hydrogel. In contrast to our original hypothesis, that the use of a MMP cleavable crosslinker would improve cell migration, the addition of the MMP degradable crosslinker did not improve cell migration *in vitro* or in the *ex vivo* setting. It is possible that the proteases secreted by the MSCs and the cartilage explants in these settings were not capable of sufficiently degrading the VPMSMRGG peptide of the crosslinker in our study. It has been investigated before that the VPMSMRGG is most sensitive to MMP1 [52,53]. It is likely that there are more MMPs present in the *in vivo* model that lead to a faster degradation. In addition, it is plausible that the *ex vivo* model prompts the secretion of tissue inhibitors of matrix metalloproteinases, which hinder the activity of MMPs and, as a result, impede the degradation of the hydrogel [54,55]. Although no differences in MSCs [41], and (lung) epithelial cells [56] were observed in previous studies, future studies will need to investigate whether specific MMPs are responsible to degrade these bonds in the norHA-MMP gels. Furthermore, the more than three-fold lower bulk mechanical properties of norHA-MMP could have limited cell attachment and thus migration. In the *in vivo* model, however, the MMP-sensitive crosslinker clearly showed more tissue formation in the gels crosslinked with the non-degradable DTT crosslinker. The formation of various tissue types, including cartilage-like and bone-like tissue, in the semi-orthotopic model aligns with prior literature, which has reported that in norHA hydrogels that incorporate non-degradable crosslinkers, matrix deposition is confined to the pericellular region after 28 days [27]. Additionally, research on maleimide modified HA (1.2% wt) crosslinked with an MMP-sensitive crosslinker (CRDVPMSQMRGGDRCG) has shown that a greater amount of cartilage-like tissue is formed compared to gels with protease-insensitive DTT crosslinkers [57]. Thus, our study verifies the benefit of using MMP-cleavable crosslinker to promote the formation of repair tissue and cartilage-like matrix deposition. Furthermore, our study underscores the importance of utilizing multiple assays and selecting an appropriate experimental design to evaluate the performance of a hydrogel.

Besides using a MMP degradable crosslinker, the addition of RGD peptides is another approach to control cell spreading. Collagen type I and, to some extent, GelMA contains natural RGD sites that are characterized by cell-instructive properties [58]. We found that the addition of collagen in a THA hydrogel enhanced the migration of MSCs and chondrocytes in all three models examined. Furthermore, the incorporation of type 1 collagen into the THA hydrogel leads to the development of a fibrillary network, which

induces bio-instructive properties sensed by the cells, thereby providing an additional advantage. It has been shown that these micro-structural features in THA-col can be used to orient collagen fibres via 3D bioprinting [39]. Whether the fibrillar component, the RGD sites or a combination of both are the most driving factor promoting cell migration remains unknown and a focus for future studies. Although THA-col composite did positively influence MSC migration and MSC chondrogenesis *in vitro* [59,60], still only 60% of the defect volume was filled with newly formed tissue, and limited cartilage-like tissue was formed in the *in vivo* setting. Further optimization of this hydrogel is needed to achieve more cell invasion and support cartilage-like tissue formation.

Cell-material interaction and thus mechanosensing contributes to cell spreading and migration. The results suggest that cell migration is not primarily controlled by the bulk mechanical properties as it has been proposed in other studies. It is rather a combination of different material properties that control cell behaviour [47,61,62]. THA and THA-col had similar Young's moduli and the higher cell migration in the THA-col compared to THA is likely due to the presence of RGD sequences. Storage moduli of THA and THA-col have been shown to be similar [34,39]. GelMA80 and GelMA50 both naturally contain RGD sequences and in this study the young's moduli as well as final storage moduli were comparable [43]. Yet, migration on GelMA50 was better in the *ex vivo* model compared to GelMA80. This indicates that the lower DOF can have a positive effect on cell migration and tissue formation. Both norHA hydrogels contained RGD for cell adhesion. In the *in vitro* and the *ex vivo* model, more cell invasion was found in the stiffer norHA DTT hydrogel compared to norHA MMP. Caliri et al. have shown that MSC spreading depends on the substrate stiffness of norHA hydrogels, and found that stiffer hydrogels (20 kPa) stimulated MSC spreading in 2D, whereas in 3D cell spreading was seen only in the least stiff hydrogel (1 kPa) [36]. This discrepancy with our results in norHA gels indicates that the dimensionality of the model and hydrogel stiffness are not the only parameters influencing cell migration. Instead, a complex interplay of multiple parameters might affect cell migration in hydrogels. More research is needed to understand the underlying mechanisms of bioinstructive properties to increase cell infiltration and improve biochemical and biophysical properties of biomaterials for cell free tissue repair.

Evaluating the samples implanted for only ten days in the semi-orthotopic mouse model, we identified only a few inflammatory cells on and within the hydrogels, highlighting that there was no strong foreign body reaction related to any of the hydrogels used. Although a strong foreign body response can cause unwanted effects, this inflammation is also known to influence cell migration as well as matrix degradation and therefore can be stimulating the ingrowth of cells in a hydrogel [7,14,63,64]. In the design and modification of biomaterials such a positive effect of inflammation should be considered as well. To pre-screen biomaterials and modifications on their pro- or anti-inflammatory response, different *in vitro* models are available. Wesdorp et al. showed a similar response of neutrophils seeded on THA, THA-col (2.5% wt THA, 0.25% wt col) and GelMA (15% wt, DoF 50%) in terms of myeloperoxidase, neutrophil elastase and cytokine secretion [65]. In light of the 3R principle (refinement, reduction, and replacement), an initial screening may be conducted *in vitro* to assess the potential impact of hydrogel modifications on inflammation, which could alter the cell infiltration behavior of the hydrogel.

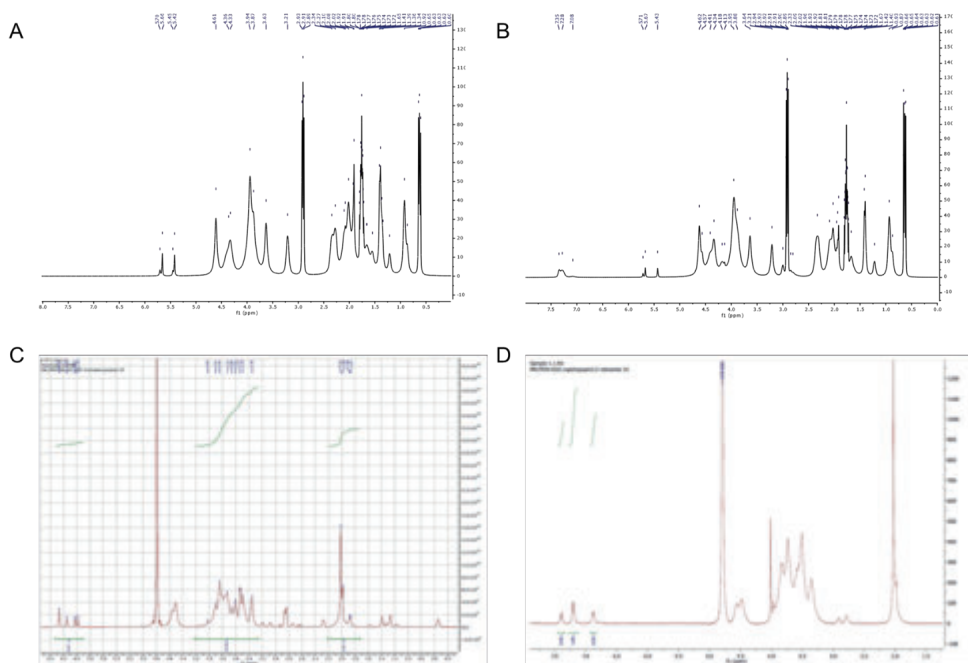
Cell type specific differences in response to the materials as a function of the mechanical properties, chemical composition and mesh size have been reported [26,66,67]. The screening of the hydrogels in the three models covers different cell types, namely MSCs, chondrocytes and cells residing in the subchondral bone and bone marrow of the osteochondral explants. Results of the here reported *in vitro*, *ex vivo* and *in vivo* testing together with findings related to how cells respond to different materials suggest that the specific hydrogel formulations tested in this study were not selective for different mesenchymal cell types present in the osteochondral environment. This study further showed that with a single modification in either a HA or gelatine-based hydrogel, cell invasion can be stimulated. A limitation of the present study is that for each formulation multiple characteristics of the matrices (total polymer concentration, crosslinking density, mesh size) are simultaneously modified, limiting the ability to decouple findings. Since each modification will have different effects on hydrogel swelling, secondary structure, degradation and most likely the cell-biomaterial interaction, a direct comparison would have been not very practical. The current approach prevented this direct comparison and solely demonstrated the possible effects of one specific chemical modification within three selected hydrogel types on cell migration and tissue formation. More fundamental knowledge on how different material properties influence cell behaviour is required to optimize the design of hydrogels for osteochondral tissue repair.

The success of acellular hydrogel approaches to repair (osteo-) chondral defects is limited in treating larger defects. In this case, the relatively low number of cells invading the biomaterial implanted in the defect might not allow for complete defect repair. One approach to increase the invasion distance might be the use of chemotactic factors. If this is not feasible, a combined approach of encapsulating patient-derived cells and a hydrogel stimulating the migration and invasion of cells from surrounding tissue can be considered. Moreover, good bonding and minimal lateral delamination of the hydrogel from the surrounding tissue are a prerequisite allowing for endogenous cell migration and related matrix deposition [68]. To address this research question, different models including push out tests are available for quantitative measures of integration [69,70]. DMA has been proposed to study the adhesion strength between the tissue and hydrogel [71]. Before taking this next step, a more in-depth understanding is needed to improve cell invasion further and to understand the mechanisms driving or limiting cell migration.

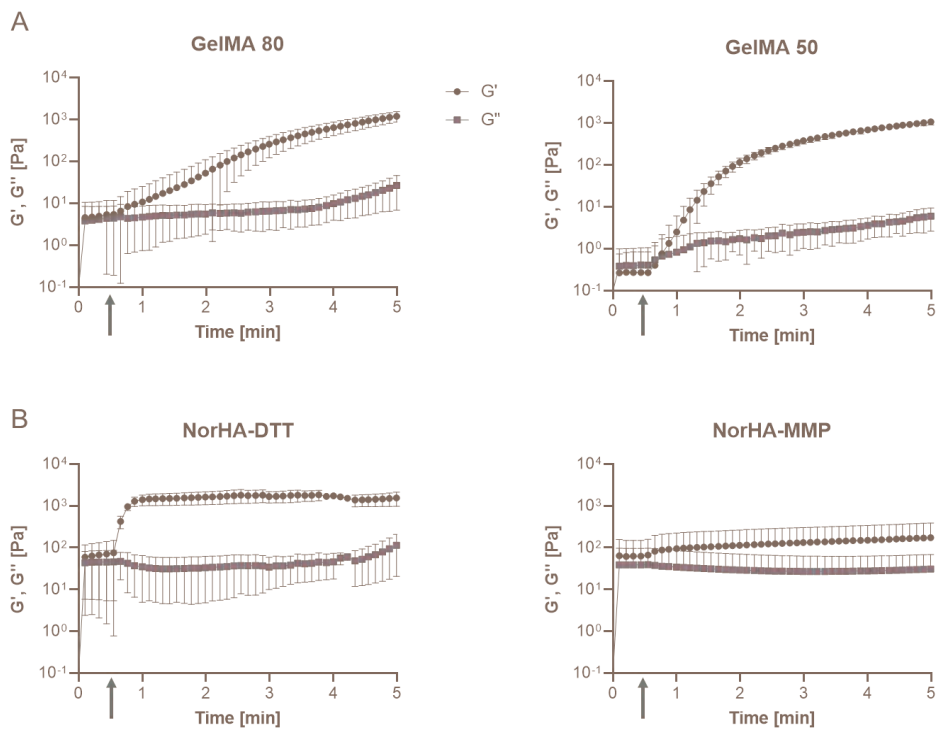
5. CONCLUSION

Migration of cells with chondrogenic potential into hydrogels is the first step to improve cell free repair of (osteo-) chondral defects. While cell free approaches would fail in the absence of cell invasion, cell-based treatments would also benefit from enhanced integration of the implant to the surrounding tissue. Our study shows that cell migration is dependent on multiple material characteristics, including physicochemical and bio-instructive properties. Moreover, this study also highlights the need for screening biomaterials in different models *in vitro*, *ex vivo* and *in vivo* since results might differ depending on the model used. The three hydrogel groups and modifications screened in this study, do support cartilage-like and bone-like tissue formation making them suitable candidates for further optimization and use in osteochondral repair.

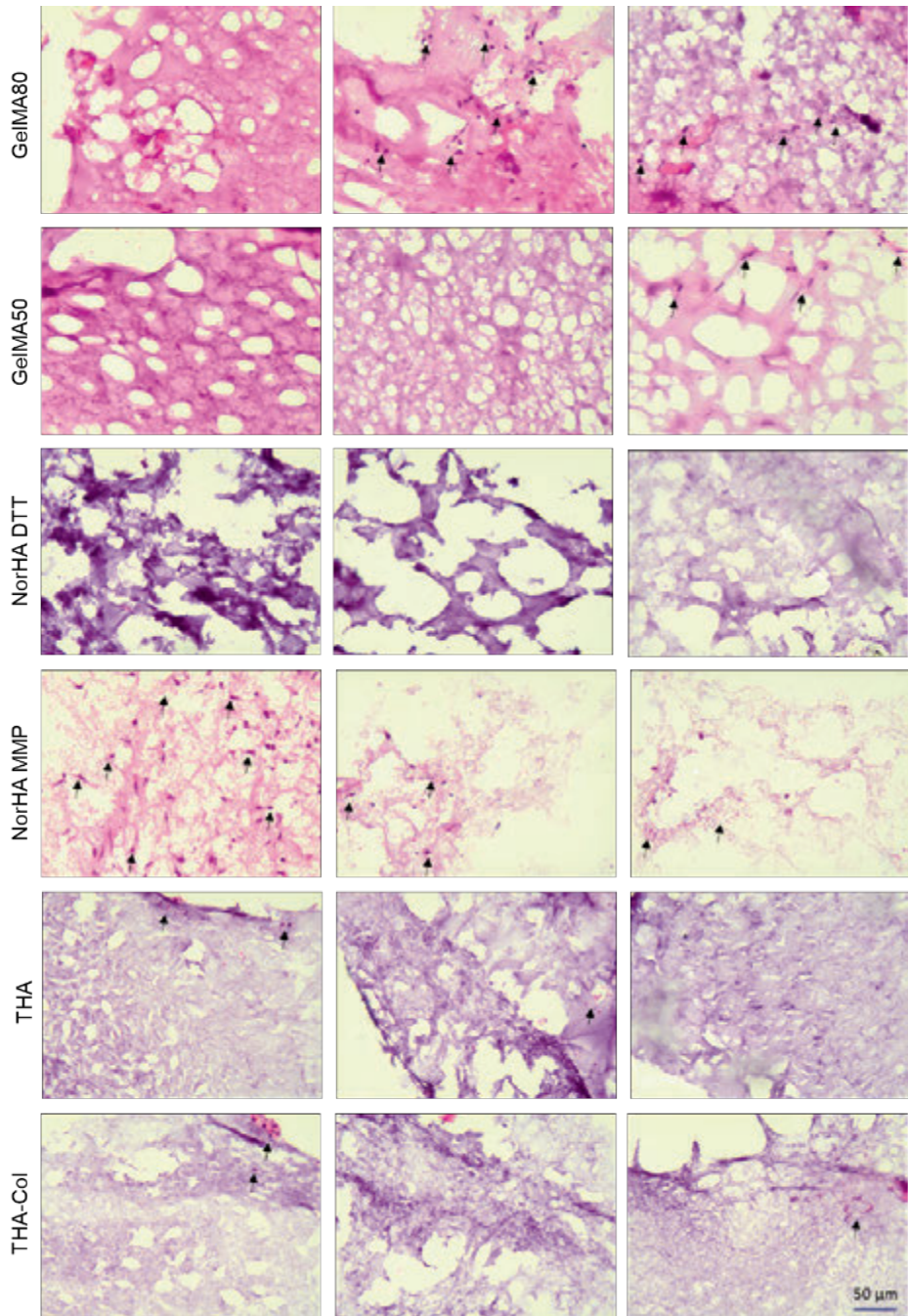
SUPPLEMENTARY MATERIALS



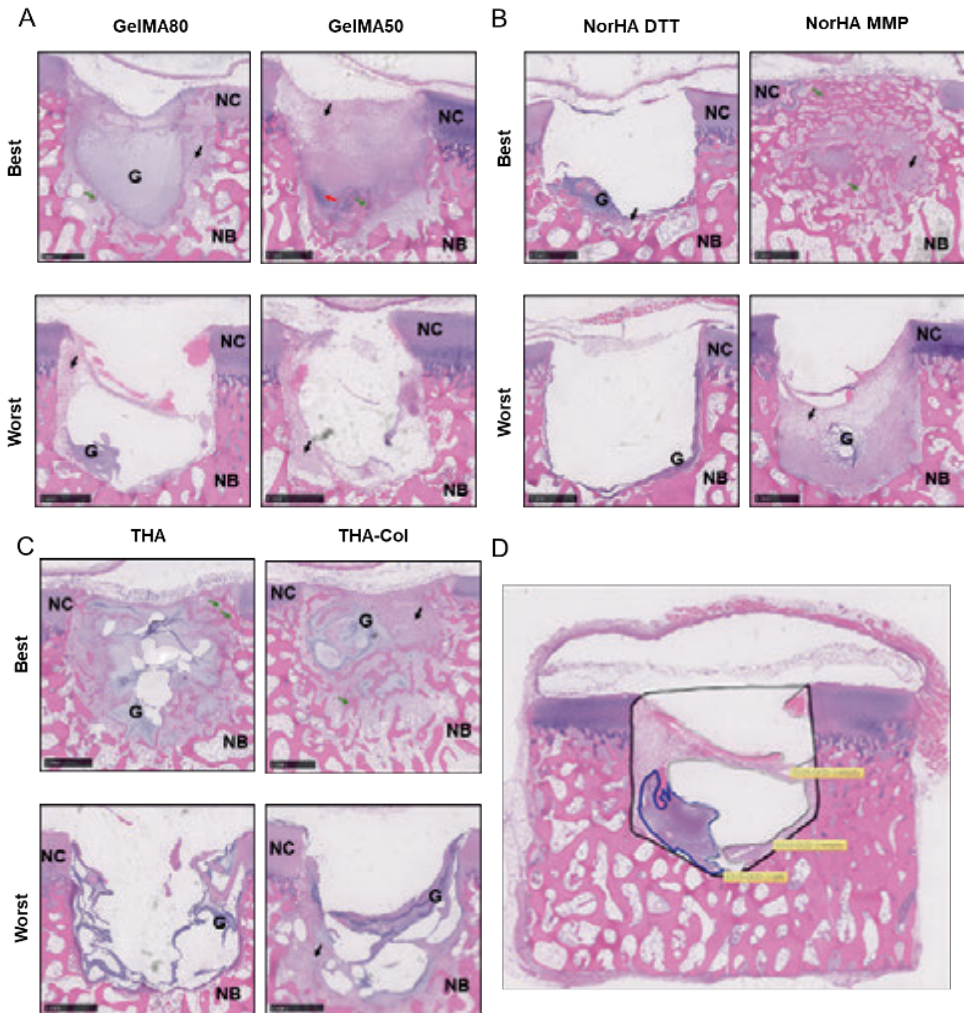
Supplementary Figure S1: ^1H NMR spectrum of hydrogel precursors. (A, B) Gelatine methacryloyl (GelMA) in D_2O (4% concentration, with 0.5 mg/ml of 3-(Trimethylsilyl)-1-propanesulfonic acid sodium salt). NMR spectra of (A) GelMA50 and (B) GelMA80 confirm the methacrylation of the gelatine backbone. At 5.5 and 6.0 ppm the peaks corresponding to the protons belonging to the double bond of the methacrylate moiety with a shorter peak in GelMA50 compared to GelMA80. A small peak for lysine at 3.0 ppm was still present on the GelMA50 but it is missing on the GelMA80 sample. (C) Norbornene-functionalized hyaluronic acid (NorHA) in D_2O (5wt%). Modification of HA with norbornene (30%) determined by integration of vinyl protons (2x2H) relative to the sugar ring of HA (10H). NorHA precursor was the same for preparing, norHA-DTT and norHAMMP. (D) Tyramine functionalized hyaluronic acid (THA) in D_2O (3%w/v in D_2O containing 0.4 mg/ml hyaluronidase). The NMR spectrum conforms to the structure of the tyramine derivative of HA, showing a singlet corresponding to the N-acetyl group around 2ppm, and a broad multiplet between 3.2 and 4.0 ppm corresponding to various protons on the saccharide rings. The three peaks around 7 ppm corresponding to the aromatic resonances of the tyramine groups are visible (Loebel, Stauber et al. 2017). THA precursor was the same to prepare THA-collagen.



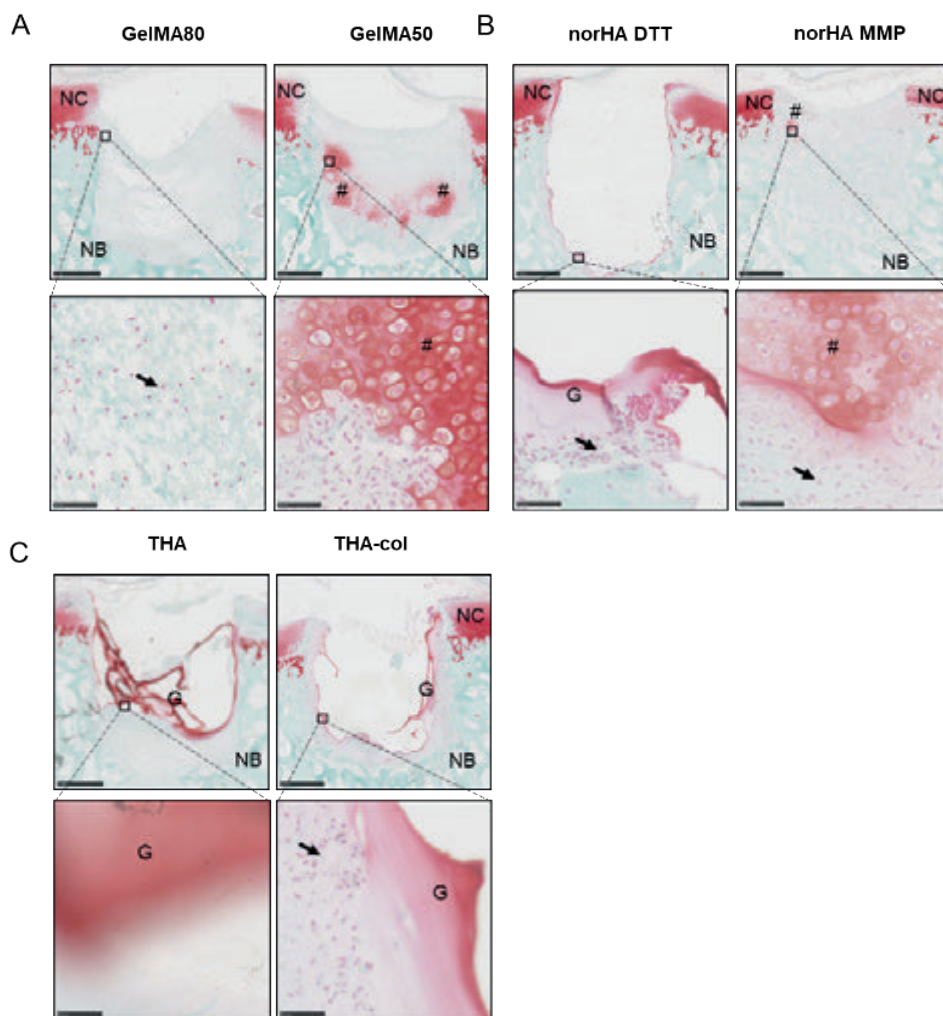
Supplementary Figure S2. Potorheology of gelatin methacryloyl (50% and 80% degree of functionalization, DOF) and norbornene functionalized hyaluronic acid (norHA) crosslinked with either a non-degradable (DTT) or MMP degradable crosslinker. Blue arrow indicates the time (30 sec) when the light was turned on for photo-crosslinking the hydrogel precursors.



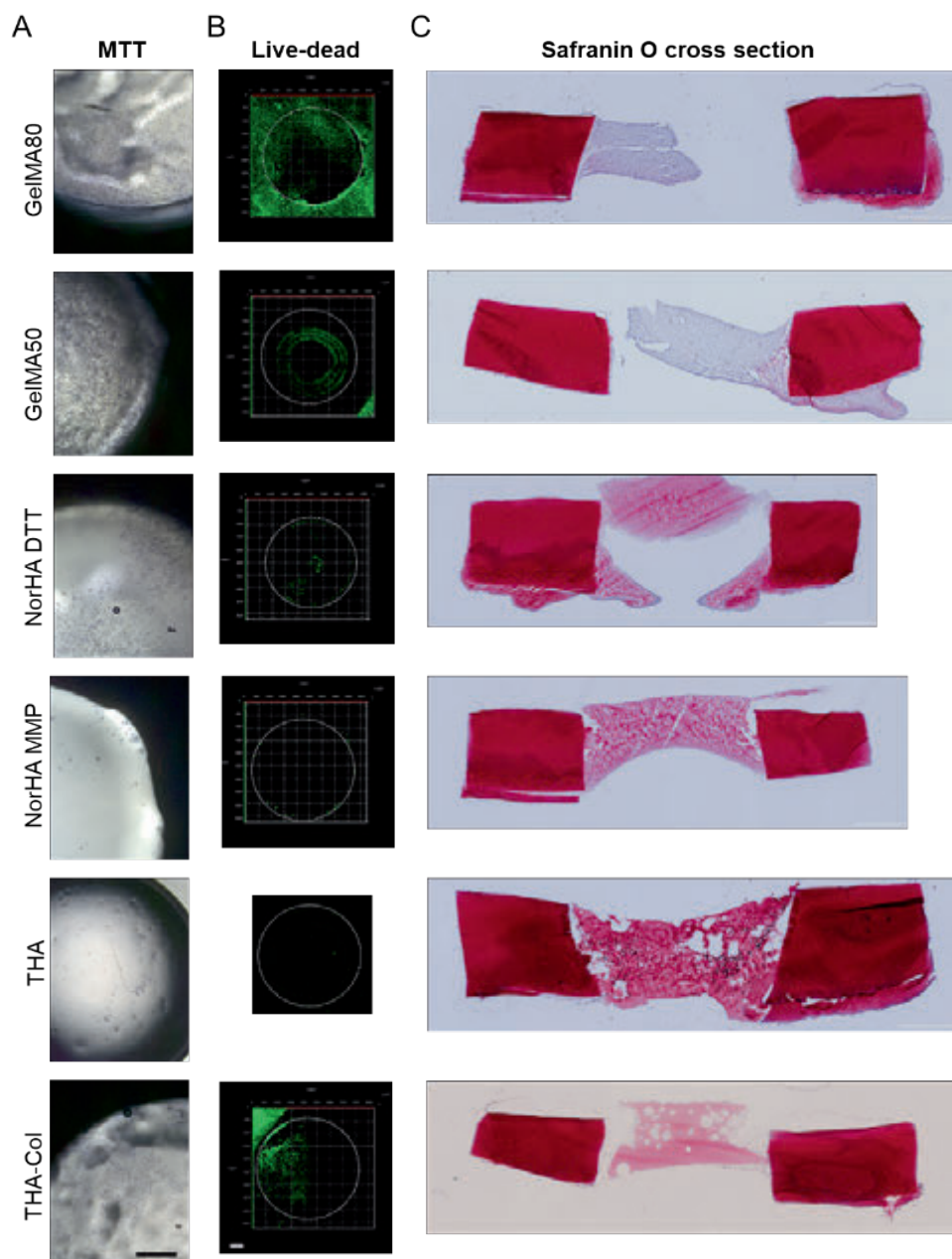
Supplementary Figure S3. Cell infiltration into hydrogels after 10 days implantation in semi-orthotopic model. HE staining of acellular hydrogels were polymerized in osteochondral defects and implanted in nude mice ($n = 3$ samples per biomaterial). Most cells were observed in GelMA 80% and 50% as well as norHA MMP gels. Only single cells were present in the other hydrogel groups. Arrows indicate (multinucleated) cells. Scale bar 50 μm .



Supplementary Figure S4. Tissue regeneration in osteochondral defects filled with the hydrogels in an *in vivo* subcutaneous implantation mouse model. The best and worst repair constructs stained with H&E showing the *in-situ* hydrogels and tissue regeneration within the osteochondral defects after 6 weeks of implantation. A) GelMA degree of functionalization 50% and 80%, B) norHA with protease (MMP) cleavable and non-degradable DTT crosslinker, C) THA and THA-collagen. Scale bars indicate 1 mm. Black arrows indicated infiltrated cells within the defects. Red arrows indicated newly formed cartilage-like tissue. Green arrows indicated newly formed bone-like tissue. NC: native cartilage; NB: native bone; G: hydrogel. D) Example on defining the defect region (black line), hydrogel selection (blue line) and newly formed tissue formation (grey line) for quantification of tissue formation mice ($n = 5$ samples per biomaterial).



Supplementary Figure S5. Representative images of the repair constructs stained with Safranin O showing the in-situ hydrogels and tissue regeneration within the osteochondral defects after 6 weeks of implantation. A) GelMA degree of functionalization 50% and 80%, B) norHA with protease (MMP) cleavable and non-degradable DTT crosslinker, C) THA and THA-collagen. Scale bars indicate 1 mm (lower magnification) and 50 μm (higher magnification). Black squares indicated the magnified areas. Black arrows indicated infiltrated cells within the defects. NC: native cartilage; NB: native bone; G: hydrogel; #: cartilage-like tissue.



Supplementary Figure S6. Ex vivo cartilage explant model after 21 days of culture. A) Microscopic image of metabolic active chondrocytes migrating on the biomaterials (MTT staining). Scale bar 500 μm . B) Live-dead staining (green: alive cells, red: dead cells). Scale bar 500 μm . C) Safranin O staining of representative cartilage explants treated with biomaterials. Scale bar 1 mm. THA: tyramine modified hyaluronic acid (HA), THA-col, norHA DTT: norbonene functionalized HA with non-degradable crosslinker, norHA MMP: norHA with Matrix Metalloproteinase degradable crosslinker, GelMA 50: gelatine methacryloyl with 50% degree of functionalization (DoF), GelMA 80: GelMA 80% DoF.

REFERENCES

- [1] Volz M, Schaumburger J, Frick H, Grifka J, Anders S. A randomized controlled trial demonstrating sustained benefit of Autologous Matrix-Induced Chondrogenesis over microfracture at five years. *Int Orthop*. 2017;41(4):797-804.
- [2] Migliorini F, Maffulli N, Baroncini A, Bell A, Hildebrand F, Schenker H. Autologous matrix-induced chondrogenesis is effective for focal chondral defects of the knee. *Sci Rep*. 2022;12(1):9328.
- [3] Brittberg M. New frontiers for cartilage repair, joint preservation and prevention. *J Cartilage Joint Preservation*. 2022;2(2):100060.
- [4] Brittberg M, Recker D, Ilgenfritz J, Saris DBF, Group SES. Matrix-Applied Characterized Autologous Cultured Chondrocytes Versus Microfracture: Five-Year Follow-up of a Prospective Randomized Trial. *Am J Sports Med*. 2018;46(6):1343-1351.
- [5] Brittberg M. Cellular and Acellular Approaches for Cartilage Repair: A Philosophical Analysis. *Cartilage*. 2015;6(2 Suppl):4S-12S.
- [6] Levinson C, Cavalli E, von Rechenberg B, Zenobi-Wong M, Darwiche SE. Combination of a Collagen Scaffold and an Adhesive Hyaluronan-Based Hydrogel for Cartilage Regeneration: A Proof of Concept in an Ovine Model. *Cartilage*. 2021;13(2_suppl):636S-649S.
- [7] Zhang S, Hu B, Liu W, Wang P, Lv X, Chen S, et al. Articular cartilage regeneration: The role of endogenous mesenchymal stem/progenitor cell recruitment and migration. *Semin Arthritis Rheum*. 2020;50(2):198-208.
- [8] Yang Z, Li H, Yuan Z, Fu L, Jiang S, Gao C, et al. Endogenous cell recruitment strategy for articular cartilage regeneration. *Acta Biomater*. 2020;114:31-52.
- [9] Moroni L, Elisseeff JH. Biomaterials engineered for integration. *Materials Today*. 2008;11(5):44-51.
- [10] Spector M, Lim TC. Injectable biomaterials: a perspective on the next wave of injectable therapeutics. *Biomed Mater*. 2016;11(1):014110.
- [11] Jeon O, Lee YB, Lee SJ, Guliyeva N, Lee J, Alsborg E. Stem cell-laden hydrogel bioink for generation of high resolution and fidelity engineered tissues with complex geometries. *Bioact Mater*. 2022;15:185-193.
- [12] Sennett ML, Friedman JM, Ashley BS, Stoeckl BD, Patel JM, Alini M, et al. Long term outcomes of biomaterial-mediated repair of focal cartilage defects in a large animal model. *Eur Cell Mater*. 2021;41:40-51.
- [13] Wei F, Liu S, Chen M, Tian G, Zha K, Yang Z, et al. Host Response to Biomaterials for Cartilage Tissue Engineering: Key to Remodeling. *Front Bioeng Biotechnol*. 2021;9:664592.
- [14] Qu F, Guilak F, Mauck RL. Cell migration: implications for repair and regeneration in joint disease. *Nat Rev Rheumatol*. 2019;15(3):167-179.
- [15] Pabbruwe MB, Esfandiari E, Kafienah W, Tarlton JF, Hollander AP. Induction of cartilage integration by a chondrocyte/collagen-scaffold implant. *Biomaterials*. 2009;30(26):4277-4286.
- [16] Zhang Z, Schon L. The Current Status of Clinical Trials on Biologics for Cartilage Repair and Osteoarthritis Treatment: An Analysis of ClinicalTrials.gov Data. *Cartilage*. 2022;13(2):19476035221093065.

- [17] Sun M, Sun X, Wang Z, Guo S, Yu G, Yang H. Synthesis and Properties of Gelatin Methacryloyl (GelMA) Hydrogels and Their Recent Applications in Load-Bearing Tissue. *Polymers (Basel)*. 2018;10(11).
- [18] Van Den Bulcke AI, Bogdanov B, De Rooze N, Schacht EH, Cornelissen M, Berghmans H. Structural and rheological properties of methacrylamide modified gelatin hydrogels. *Biomacromolecules*. 2000;1(1):31-38.
- [19] Nguyen AH, McKinney J, Miller T, Bongiorno T, McDevitt TC. Gelatin methacrylate microspheres for controlled growth factor release. *Acta Biomater*. 2015;13:101-110.
- [20] Li X, Chen S, Li J, Wang X, Zhang J, Kawazoe N, et al. 3D Culture of Chondrocytes in Gelatin Hydrogels with Different Stiffness. *Polymers (Basel)*. 2016;8(8).
- [21] Klotz BJ, Lim KS, Chang YX, Soliman BG, Pennings I, Melchels FPW, et al. Engineering of a complex bone tissue model with endothelialised channels and capillary-like networks. *Eur Cell Mater*. 2018;35:335-348.
- [22] Nicolas J, Magli S, Rabbachin L, Sampaolesi S, Nicotra F, Russo L. 3D Extracellular Matrix Mimics: Fundamental Concepts and Role of Materials Chemistry to Influence Stem Cell Fate. *Biomacromolecules*. 2020;21(6):1968-1994.
- [23] Xia H, Li X, Gao W, Fu X, Fang RH, Zhang L, et al. Tissue repair and regeneration with endogenous stem cells. *Nat Rev Mater*. 2018;3(7):174-193.
- [24] Kim YS, Guilak F. Engineering Hyaluronic Acid for the Development of New Treatment Strategies for Osteoarthritis. *Int J Mol Sci*. 2022;23(15).
- [25] Kim IL, Mauck RL, Burdick JA. Hydrogel design for cartilage tissue engineering: a case study with hyaluronic acid. *Biomaterials*. 2011;32(34):8771-8782.
- [26] Petta D, D'Amora U, Ambrosio L, Grijpma DW, Eglin D, D'Este M. Hyaluronic acid as a bioink for extrusion-based 3D printing. *Biofabrication*. 2020;12(3):032001.
- [27] Galarraga JH, Kwon MY, Burdick JA. 3D bioprinting via an in situ crosslinking technique towards engineering cartilage tissue. *Sci Rep*. 2019;9(1):19987.
- [28] Behrendt P, Ladner Y, Stoddart MJ, Lippross S, Alini M, Eglin D, et al. Articular Joint-Simulating Mechanical Load Activates Endogenous TGF-beta in a Highly Cellularized Bioadhesive Hydrogel for Cartilage Repair. *Am J Sports Med*. 2020;48(1):210-221.
- [29] Petta D, Armiento AR, Grijpma D, Alini M, Eglin D, D'Este M. 3D bioprinting of a hyaluronan bioink through enzymatic-and visible light-crosslinking. *Biofabrication*. 2018;10(4):044104.
- [30] Petta D, Grijpma DW, Alini M, Eglin D, D'Este M. Three-Dimensional Printing of a Tyramine Hyaluronan Derivative with Double Gelation Mechanism for Independent Tuning of Shear Thinning and Postprinting Curing. *ACS Biomater Sci Eng*. 2018;4(8):3088-3098.
- [31] Loebel C, Stauber T, D'Este M, Alini M, Zenobi-Wong M, Eglin D. Fabrication of cell-compatible hyaluronan hydrogels with a wide range of biophysical properties through high tyramine functionalization. *J Mater Chem B*. 2017;5(12):2355-2363.
- [32] Shu XZ, Ghosh K, Liu Y, Palumbo FS, Luo Y, Clark RA, et al. Attachment and spreading of fibroblasts on an RGD peptide-modified injectable hyaluronan hydrogel. *J Biomed Mater Res A*. 2004;68(2):365-375.
- [33] Lam J, Truong NF, Segura T. Design of cell-matrix interactions in hyaluronic acid hydrogel scaffolds. *Acta Biomater*. 2014;10(4):1571-1580.
- [34] Staubli F, Stoddart MJ, D'Este M, Schwab A. Pre-culture of human mesenchymal stromal cells in spheroids facilitates chondrogenesis at a low total cell count upon

embedding in biomaterials to generate cartilage microtissues. *Acta Biomater.* 2022;143:253-265.

[35] Lei Y, Gojgini S, Lam J, Segura T. The spreading, migration and proliferation of mouse mesenchymal stem cells cultured inside hyaluronic acid hydrogels. *Biomaterials.* 2011;32(1):39-47.

[36] Caliarì SR, Vega SL, Kwon M, Soulas EM, Burdick JA. Dimensionality and spreading influence MSC YAP/TAZ signaling in hydrogel environments. *Biomaterials.* 2016;103:314-323.

[37] Mouser VH, Melchels FP, Visser J, Dhert WJ, Gawlitta D, Malda J. Yield stress determines bioprintability of hydrogels based on gelatin-methacryloyl and gellan gum for cartilage bioprinting. *Biofabrication.* 2016;8(3):035003.

[38] Loebel C, Szczesny SE, Cosgrove BD, Alini M, Zenobi-Wong M, Mauck RL, et al. Cross-Linking Chemistry of Tyramine-Modified Hyaluronan Hydrogels Alters Mesenchymal Stem Cell Early Attachment and Behavior. *Biomacromolecules.* 2017;18(3):855-864.

[39] Schwab A, Helary C, Richards RG, Alini M, Eglin D, D'Este M. Tissue mimetic hyaluronan bioink containing collagen fibers with controlled orientation modulating cell migration and alignment. *Mater Today Bio.* 2020;7:100058.

[40] Loebel C, Kwon MY, Wang C, Han L, Mauck RL, Burdick JA. Metabolic Labeling to Probe the Spatiotemporal Accumulation of Matrix at the Chondrocyte-Hydrogel Interface. *Adv Funct Mater.* 2020;30(44):1909802.

[41] Loebel C, Mauck RL, Burdick JA. Local nascent protein deposition and remodelling guide mesenchymal stromal cell mechanosensing and fate in three-dimensional hydrogels. *Nat Mater.* 2019;18(8):883-891.

[42] Melchels FPW, Dhert WJA, Huttmacher DW, Malda J. Development and characterisation of a new bioink for additive tissue manufacturing. *J Mater Chem B.* 2014;2(16):2282-2289.

[43] Pepelanova I, Kruppa K, Scheper T, Lavrentieva A. Gelatin-Methacryloyl (GelMA) Hydrogels with Defined Degree of Functionalization as a Versatile Toolkit for 3D Cell Culture and Extrusion Bioprinting. *Bioengineering (Basel).* 2018;5(3).

[44] Gramlich WM, Kim IL, Burdick JA. Synthesis and orthogonal photopatterning of hyaluronic acid hydrogels with thiol-norbornene chemistry. *Biomaterials.* 2013;34(38):9803-9811.

[45] Loebel C, D'Este M, Alini M, Zenobi-Wong M, Eglin D. Precise tailoring of tyramine-based hyaluronan hydrogel properties using DMTMM conjugation. *Carbohydr Polym.* 2015;115:325-333.

[46] Wesdorp MA, Bastiaansen-Jenniskens YM, Capar S, Verhaar JAN, Narcisi R, Van Osch GJVM. Modulation of Inflamed Synovium Improves Migration of Mesenchymal Stromal Cells *in vitro* Through Anti-Inflammatory Macrophages. *Cartilage.* 2022;13(1):19476035221085136.

[47] Vainieri ML, Lolli A, Kops N, D'Atri D, Eglin D, Yayon A, et al. Evaluation of biomimetic hyaluronic-based hydrogels with enhanced endogenous cell recruitment and cartilage matrix formation. *Acta Biomater.* 2020;101:293-303.

[48] de Vries-van Melle ML, Tihaya MS, Kops N, Koevoet WJ, Murphy JM, Verhaar JA, et al. Chondrogenic differentiation of human bone marrow-derived mesenchymal stem cells in a simulated osteochondral environment is hydrogel dependent. *Eur Cell Mater.* 2014;27:112-123; discussion 123.

- [49] Ricci M, Tradati D, Maione A, Uboldi FM, Usellini E, Berruto M. Cell-free osteochondral scaffolds provide a substantial clinical benefit in the treatment of osteochondral defects at a minimum follow-up of 5 years. *J Exp Orthop*. 2021;8(1):62.
- [50] Kon E, Filardo G, Perdisa F, Venieri G, Marcacci M. Acellular Matrix-Based Cartilage Regeneration Techniques for Osteochondral Repair. *Operative Techniques in Orthopaedics*. 2014;24(1):14-18.
- [51] Miri AK, Hosseinabadi HG, Cecen B, Hassan S, Zhang YS. Permeability mapping of gelatin methacryloyl hydrogels. *Acta Biomater*. 2018;77:38-47.
- [52] Chen W, Zhou Z, Chen D, Li Y, Zhang Q, Su J. Bone Regeneration Using MMP-Cleavable Peptides-Based Hydrogels. *Gels*. 2021;7(4).
- [53] Turk BE, Huang LL, Piro ET, Cantley LC. Determination of protease cleavage site motifs using mixture-based oriented peptide libraries. *Nat Biotechnol*. 2001;19(7):661-667.
- [54] Cawston T, Billington C, Cleaver C, Elliott S, Hui W, Koshy P, et al. The regulation of MMPs and TIMPs in cartilage turnover. *Ann N Y Acad Sci*. 1999;878:120-129.
- [55] Raeszadeh-Sarmazdeh M, Do LD, Hritz BG. Metalloproteinases and Their Inhibitors: Potential for the Development of New Therapeutics. *Cells*. 2020;9(5).
- [56] Loebel C, Weiner AI, Eiken MK, Katzen JB, Morley MP, Bala V, et al. Microstructured Hydrogels to Guide Self-Assembly and Function of Lung Alveolospheres. *Adv Mater*. 2022;34(28):2202992.
- [57] Feng Q, Zhu M, Wei K, Bian L. Cell-mediated degradation regulates human mesenchymal stem cell chondrogenesis and hypertrophy in MMP-sensitive hyaluronic acid hydrogels. *PLoS One*. 2014;9(6).
- [58] Gavenis K, Schneider U, Maus U, Mumme T, Muller-Rath R, Schmidt-Rohlfing B, et al. Cell-free repair of small cartilage defects in the Goettinger minipig: which defect size is possible? *Knee Surg Sports Traumatol Arthrosc*. 2012;20(11):2307-2314.
- [59] Heino J. The collagen family members as cell adhesion proteins. *Bioessays*. 2007;29(10):1001-1010.
- [60] Davis GE. Affinity of integrins for damaged extracellular matrix: $\alpha\beta3$ binds to denatured collagen type I through RGD sites. *Biochem Biophys Res Commun*. 1992;182(3):1025-1031.
- [61] Matellan C, del Río Hernández AE. Engineering the cellular mechanical microenvironment - from bulk mechanics to the nanoscale. *J Cell Sci*. 2019;132(9).
- [62] Zan F, Wei Q, Fang L, Xian M, Ke Y, Wu G. Role of Stiffness versus Wettability in Regulating Cell Behaviors on Polymeric Surfaces. *ACS Biomater Sci Eng*. 2020;6(2):912-922.
- [63] Li M, Yin H, Yan Z, Li H, Wu J, Wang Y, et al. The immune microenvironment in cartilage injury and repair. *Acta Biomater*. 2022;140:23-42.
- [64] van der Kraan PM. The Interaction between Joint Inflammation and Cartilage Repair. *Tissue Eng Regen Med*. 2019;16(4):327-334.
- [65] Wesdorp MA, Schwab A, Bektas EI, Narcisi R, Eglin D, Stoddart MJ, et al. A culture model to analyze the acute biomaterial-dependent reaction of human primary neutrophils *in vitro*. *Bioact Mater*. 2023;20:627-637.
- [66] Caliarì SR, Burdick JA. A practical guide to hydrogels for cell culture. *Nat Methods*. 2016;13(5):405-414.
- [67] Levato R, Jungst T, Scheuring RG, Blunk T, Groll J, Malda J. From Shape to Function: The Next Step in Bioprinting. *Adv Mater*. 2020;32(12):1906423.

- [68] Khan IM, Gilbert SJ, Singhrao SK, Duance VC, Archer CW. Cartilage integration: evaluation of the reasons for failure of integration during cartilage repair. A review. *Eur Cell Mater.* 2008;16:26-39.
- [69] Iseki T, Rothrauff BB, Kihara S, Sasaki H, Yoshiya S, Fu FH, et al. Dynamic Compressive Loading Improves Cartilage Repair in an *in vitro* Model of Microfracture: Comparison of 2 Mechanical Loading Regimens on Simulated Microfracture Based on Fibrin Gel Scaffolds Encapsulating Connective Tissue Progenitor Cells. *Am J Sports Med.* 2019;47(9):2188-2199.
- [70] van de Breevaart Bravenboer J, In der Maur CD, Bos PK, Feenstra L, Verhaar JAN, Weinans H, et al. Improved cartilage integration and interfacial strength after enzymatic treatment in a cartilage transplantation model. *Arthritis Res Ther.* 2004;6(5):R469.
- [71] Lim KS, Abinzano F, Bernal PN, Albillos Sanchez A, Atienza-Roca P, Otto IA, et al. One-Step Photoactivation of a Dual-Functionalized Bioink as Cell Carrier and Cartilage-Binding Glue for Chondral Regeneration. *Adv Healthc Mater.* 2020;9(15):e1901792.

4

Incorporating strontium enriched amorphous calcium phosphate granules in collagen/collagen-magnesium- hydroxyapatite osteochondral scaffolds improves subchondral bone repair

Jietao Xu[#], Jana Vecstaudza[#], Marinus A. Wesdorp, Margot Labberté, Nicole Kops, Manuela Salerno, Joeri Kok, Marina Simon, Marie-Françoise Harmand, Karin Vancíková, Bert van Rietbergen, Massimiliano Maraglino Misciagna, Laura Dolcini, Giuseppe Filardo, Eric Farrell, Gerjo J.V.M. van Osch, Janis Locs, Pieter A.J. Brama

[#]Authors contributed equally to this work

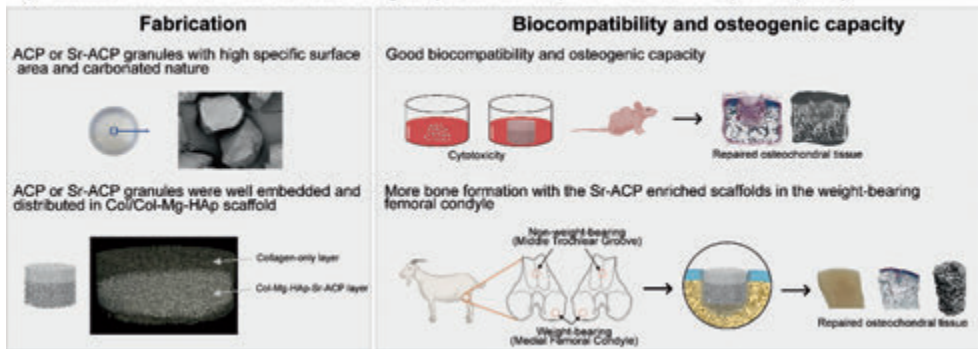
Mater Today Bio. 2024 Jan 20;25:100959.

ABSTRACT

Osteochondral defect repair with a collagen/collagen-magnesium-hydroxyapatite (Col/Col-Mg-HAp) scaffold has demonstrated good clinical results. However, subchondral bone repair remained suboptimal, potentially leading to damage to the regenerated overlying neocartilage. This study aimed to improve the bone repair potential of this scaffold by incorporating newly developed strontium (Sr) ion enriched amorphous calcium phosphate (Sr-ACP) granules (100-150 μm). Sr concentration of Sr-ACP was determined with ICP-MS at 2.49 ± 0.04 wt%. Then 30 wt% ACP or Sr-ACP granules were integrated into the scaffold prototypes. The ACP or Sr-ACP granules were well embedded and distributed in the collagen matrix demonstrated by micro-CT and scanning electron microscopy/energy dispersive x-ray spectrometry. Good cytocompatibility of ACP/Sr-ACP granules and ACP/Sr-ACP enriched scaffolds was confirmed with *in vitro* cytotoxicity assays. An overall promising early tissue response and good biocompatibility of ACP and Sr-ACP enriched scaffolds were demonstrated in a subcutaneous mouse model. In a goat osteochondral defect model, significantly more bone was observed at 6 months with the treatment of Sr-ACP enriched scaffolds compared to scaffold-only, in particular in the weight-bearing femoral condyle subchondral bone defect. Overall, the incorporation of osteogenic Sr-ACP granules in Col/Col-Mg-HAp scaffolds showed to be a feasible and promising strategy to improve subchondral bone repair.

Keywords: tissue engineering; regenerative medicine; osteochondral defect; amorphous calcium phosphate; strontium

→ Addition of Sr-ACP into a Col/Col-Mg-HAp scaffold improves its bone repair capacity



1. INTRODUCTION

Pain and restriction-free movement of joints is possible when the osteochondral unit is well preserved. The native osteochondral unit is composed of two main tissue types: articular cartilage and subchondral bone which are connected via calcified cartilage. Healthy articular cartilage ensures joint lubrication and stress reduction, and the subchondral bone is crucial for underlying mechanical support. These functions can be altered if the complex structure of the osteochondral unit is damaged by traumatic injuries, chronic diseases, and age-related degeneration. Endogenous osteochondral defect repair is limited due to the lack of a vascular/nerve supply in the cartilage and the complex multiphasic structure of the osteochondral unit [1,2]. Due to its limited self-healing capacity, osteochondral defects may progress into osteoarthritis without effective and timely intervention. To regenerate osteochondral tissue in the lesion site, surgical interventions, such as autologous chondrocyte implantation, osteochondral grafting, and microfracture have been extensively applied. Regenerated tissue, however, mainly consists of a mixture of fibrous tissue and fibrocartilage [3,4], leading to poor resistance to shear forces and deterioration at long-term follow-up [5,6].

To improve osteochondral tissue repair, biomaterial-based scaffolds have shown promising results in regenerating damaged tissues. To mimic the native osteochondral composition and structure, biomaterial-based bilayered scaffolds have been developed and tested [7]. Among these, a scaffold with a superficial collagen-only layer and a deep layer of collagen mixed with magnesium-containing hydroxyapatite (Mg-HAp) represents a promising substitute [8,9]. Each side of the scaffold provides unique chemical (e.g., biomimetic chemical composition) and physical (e.g., stiffness, elasticity) cues for chondrogenesis and osteogenesis. Specifically, collagen is a biologically derived protein and therefore an efficient biomaterial to support cellular activities and promote osteochondral repair [10]. Next, bioactive magnesium (Mg) ions have been introduced in the mineral phase of HAp to enhance the affinity of HAp with natural bone and promote an increase in cell osteogenic activity [11]. Clinically, this collagen/collagen-magnesium-hydroxyapatite (Col/Col-Mg-HAp) scaffold has demonstrated good stability and clinically relevant improvement in knee function [12-14]. However, subchondral bone repair remained suboptimal in comparison to the cartilage repair capacity of this scaffold in clinical follow-up [14]. The unrepaired subchondral bone may affect the biomechanical properties of the osteochondral unit, which might lead to damage to the regenerated overlying neocartilage and joint pain for the patient. Well-healed subchondral bone is, therefore, critical to support long-term survival of the overlying neocartilage [15].

We hypothesize that addition of extra calcium phosphate (CaP) to the Col/Col-Mg-HAp scaffold would enhance the regeneration of the subchondral bone. That extra CaP could be the well-known hydroxyapatite (HAp, $\text{Ca}_{10}(\text{PO}_4)_6(\text{OH})_2$) which is a close chemical analogue to the biological apatite present in bone [16]. However, the stoichiometric HAp, in comparison with biological apatite, has low solubility and resorbability [17]. Limitations of HAp could be overcome by additionally using amorphous calcium phosphate (ACP). ACP is a hydrated CaP with an amorphous structure, allowing different Ca/P molar ratios (1.2-2.2), and a high specific surface area [18,19]. The presence of an amorphous phase, hydrated structure and high specific surface area of ACP are shared with the biological

apatite [20], and it ensures ACP's bioactivity, solubility, and excellent adsorption properties of biologically relevant ions and molecules [18].

As ACP's amorphous structure can accommodate other ions besides calcium and phosphate [21], it can be modified to include other ions for an additional bone regenerative effect. Bioinorganic ions such as strontium (Sr) are cost-effective and easy to use as a local delivery tool [22] having less risk than bone morphogenetic protein (BMP) strategies used for improved regeneration of bone [23]. Previously Sr has been introduced in forms of a Sr ranelate drug or as a dopant in the biomaterial of choice [24-26], this includes CaPs as well. On a cellular level, Sr ions have a dual mode of action: stimulation of osteoblasts and inhibition of osteoclasts [27,28]. Sr promotes formation of extracellular matrix (ECM) proteins produced by osteoblasts [29]. These effects might be useful in repair of the subchondral bone as well. In the available studies the use of Sr containing biomaterials in bone defect repair is already well established [22,30,31] and it leads to improved or at least unchanged new bone formation compared to the Sr-free groups [32]. However, the specific effects of Sr and even ACP on subchondral bone regeneration are still yet to be provided.

In particular, the combination of a recently developed ACP with high specific surface area ($>100 \text{ m}^2/\text{g}$) [33-36] and Sr ions might provide excellent cues for ECM formation and subchondral bone tissue regeneration through sustaining of an ion-rich microenvironment. Upon contact with the biological environment, dissolution of strontium, calcium and phosphate ions is expected, which are favouring cues for ECM production and bone formation [37]. The Sr ion effect on chondrogenesis is less studied, however, it has been found that the Sr ions upregulate cartilage-specific gene expression and thus facilitate differentiation towards chondrogenic cell lineage [38,39].

In this study, we modified the synthesis technology of ACP for incorporation of Sr, and developed a method to incorporate ACP/Sr-ACP granules into the Col/Col-Mg-HAp scaffold (upper cartilaginous layer with the average 100-150 μm pore diameter, the lower bony layer with the average 250-450 μm pore diameter [12]). Then we characterized physicochemical properties and the *in vitro* cytocompatibility of ACP or Sr-ACP granules and ACP/Sr-ACP enriched Col/Col-Mg-HAp scaffolds. To evaluate the osteogenic potential in osteochondral defects, we first investigated the biocompatibility and osteogenic effect of ACP/Sr-ACP enriched scaffold in an *in vivo* semi-orthotopic mouse model at the early phases of repair. Finally, the osteogenic effect of the Sr-ACP enriched Col/Col-Mg-HAp scaffold was investigated *in vivo* in a translational large animal (goat) osteochondral defect model.

2. MATERIALS AND METHODDS

2.1. Synthesis of ACP and Sr-ACP

ACP and Sr-ACP granules used in the study were prepared from materials synthesized according to a wet precipitation technology developed previously [34]. Here, the synthesis technology was modified (use of calcium oxide instead of hydroxyapatite), and a novel synthesis procedure of ACP/Sr-ACP was developed as described below.

First, 2.71 g of CaO (calcined $\text{Ca}(\text{OH})_2$ (Jost Chemical Co., USA)) and 0.438 g of $\text{Sr}(\text{NO}_3)_2$ (Sigma-Aldrich, Germany) were mixed in deionized water (300 mL). The amount of Sr within Sr-ACP was chosen to be 50x the maximum amount reported of Sr in bone mineral (0.05 wt% [40] i.e., 2.5 wt%). The mixing was done with an overhead mixer MM-1000 (Biosan, Latvia) equipped with a propeller stirrer at 300-400 rpm at 20 ± 2 °C. Then 14.48 mL of 2 M H_3PO_4 (75 %, "Latvijas Kimija" Ltd.) was admixed and the suspension was stirred for 30 min. Next, 32.3 mL 3 M HCl (Merck EMSURE®, Austria) at a rate of 5 mL/min was added. Resulting in dissolution of reagents, and thus a transparent solution containing calcium, phosphate, strontium, and nitrate ions was obtained. Next, after 30 min the mixing speed was increased to 450-550 rpm and an equimolar amount of 2 M NaOH (Merck EMSURE®, Germany) was rapidly admixed to raise the pH and to induce precipitation of Sr-ACP. Then the stirring was continued for another 5 min until the reading of the pH electrode stabilized (pH 10-11). Next, the precipitated Sr-ACP was separated by vacuum filtration. During the filtration, the Sr-ACP was washed with deionized water (1.5-2.0 L) to remove any formed water-soluble by-products, e.g., NaCl, from the precipitates. The presence of NaCl was tested by adding a few drops of 0.1 M silver nitrate to the solution that had passed the filter. When the formation of an opaque precipitate was not observed after the addition of the silver nitrate, it was considered that the solution did not contain NaCl. Then, the washed Sr-ACP was transferred onto glass Petri dishes, spread evenly, and dried at 80 °C for 1 h in a drying oven with forced air circulation (UFE 400, Memmert, Germany). A schematic overview of the synthesis is shown in Figure 1. Synthesis of ACP was analogous but without the addition of $\text{Sr}(\text{NO}_3)_2$.

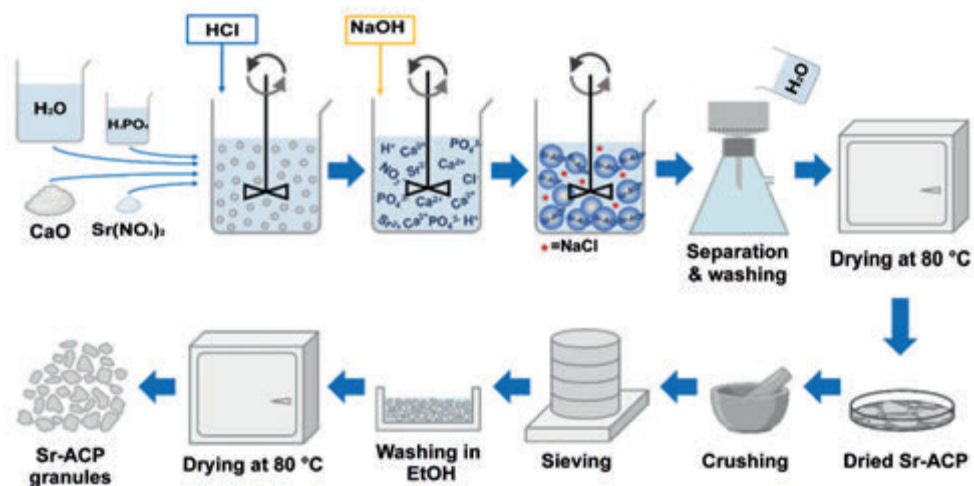


Figure 1. Schematic overview of the Sr-ACP synthesis procedure (top) and dry granulation technology (bottom) for obtaining Sr-ACP granules.

2.2. Production and characterization of ACP and Sr-ACP granules

ACP/Sr-ACP granules were manufactured using dry granulation technology (Figure 1) which involved milling of the synthesized ACP/Sr-ACP followed by sieving of the milled material to the desired range of granule size. In brief, the dried ACP/Sr-ACP precipitates

were in the form of flat agglomerates (< 3 mm thick). The agglomerates were manually crushed in a mortar and further sieved using sieves and a vibratory sieve shaker Analysette 3 (Fritsch GmbH, Germany). The sieving resulted in ACP/Sr-ACP granules in a size range of 100-150 μm . The debris that was formed during granulation was removed by rinsing the granules with ethanol (96 %). The rinsed granules were dried in a drying oven (UFE 400, Memmert, Germany) with forced air circulation at 80 °C (3 h). The manufactured ACP/Sr-ACP granules were characterized for their physicochemical properties as described below.

Phase composition of the synthesized ACP/Sr-ACP products was analysed using x-ray diffraction (XRD) with an X'Pert Pro (Malvern Panalytical B.V., The Netherlands) diffractometer. The diffractometer was equipped with a Cu tube run at 40 kV and 30 mA. In the path of diffracted x-rays, a Ni filter was installed to minimize Cu K β radiation. The XRD patterns were acquired in 2Theta range 10-70° with a step size of 0.0334° and time per step of 30.48 s. Powdered samples were put on a front-loading sample holder with a low background Si insert.

Information about chemical groups was gathered using a Fourier-transform infrared spectrometer (Varian 800 FT-IR, Scimitar Series, USA) in an attenuated reflectance (ATR, GladiATR™, Pike technologies, USA) mode. Samples were finely ground and analysed in the form of a powder. FT-IR spectra were obtained at 4 cm^{-1} resolution co-adding 50 scans over a range of wavenumbers from 400 cm^{-1} to 4000 cm^{-1} . Before each FT-IR measurement, a background spectrum was taken and later deducted from the sample spectrum.

Specific surface area (SSA) of the granules was determined by using an N₂ adsorption system Quadrasorb SI Kr (Quantachrome Instruments, USA) with Autosorb Degasser AD-9 (Quantachrome Instruments, USA). Samples (0.5 g, n = 3) were degassed at room temperature to remove any adsorbed volatiles. Calculation of the SSA was done according to Brunauer-Emmett-Teller (BET) theory. Next, the calculated particle size (d_{BET}) was found using the following equation: $d_{\text{BET}} = 6000/(\text{SSA} \times \text{density})$, assuming particles to be spherical.

Granule morphology was visualized using a field emission scanning electron microscope (SEM) Mira (Tescan, Czech Republic). SEM imaging was done at an accelerating voltage of 5 kV with both scanning electron (SE) and backscattered electron (BSE) detectors. Before the SEM imaging, samples were attached to sample holders with double-sided carbon tape and then coated with a layer of gold using sputter coater K550X (Quorum technologies, UK). Sputtering parameters were 25 mA for 180 s in an argon atmosphere with a sample rotation to obtain a homogenous coating. Additionally, the scaffolds were analysed with an energy dispersive x-ray spectrometer (EDS) X-MaxN 150 (Oxford Instruments, UK) to obtain element distribution maps. To obtain element maps the electron gun was operated at 15 kV. The mapping area was selected by drawing a rectangle over the image of the sample. The EDS mapping was done with Inca software (Oxford Instruments, UK).

Strontium concentration in Sr-ACP granules was determined using an inductively coupled plasma-optical emission spectrometry (ICP-OES, Thermo Scientific iCAP 7400, Waltham, MA, USA). The sample was dissolved in nitric acid (65 v/v%). The content (ppm) in the samples was determined by comparison with a predetermined standard curve. Sr (wt%) was calculated on the basis of the sample weight.

2.3. Preparation and characterization of ACP/Sr-ACP granule containing collagen/collagen-magnesium-hydroxyapatite osteochondral scaffolds

Col/Col-Mg-HAp with/without ACP or Sr-ACP granules are biomimetic scaffolds that have a porous, 3-dimensional composite structure. The scaffold is composed of two layers: the cartilaginous layer consisting of Type I collagen and the bone layer consisting of a combination of Type I collagen (60 %) and magnesium-hydroxyapatite (40 %, Mg-HAp). Each layer of the scaffold was synthesized separately by a standardised process from an atelocollagen aqueous solution (1 wt%) in acetic acid, isolated from equine tendon. The upper non-mineralised chondral layer of the scaffold was obtained by dissolving an acetic solution of Type I collagen in bi-distilled water by adding NaOH. The bone layer of the scaffold was obtained by nucleating nanostructured Mg-HAp into self-assembling collagen fibres, as occurs in the natural biological neo-ossification process. To stabilize the scaffold, the fibrous structures were chemically cross-linked for 16 h at room temperature. After chemical cross-linking, ACP or Sr-ACP granules were added through a deposition by vacuum directly into the bone layer during the pre-filtration phase. The two layers were superimposed and afterwards they are freeze-dried. Finally, the scaffolds were gamma sterilized at 25 KGy.

ACP/Sr-ACP granule integration within the Col/Col-Mg-HAp scaffolds was evaluated using SEM/EDS and micro-CT techniques. Prior SEM imaging and EDS element mapping samples were cross sectioned with a scalpel. Further, the sample preparation procedure was the same as described above for ACP/Sr-ACP granules alone (section 2.2).

Further micro-CT analysis of the scaffolds was performed with a micro-CT 50 instrument (Scanco Medical, Wangen-Brüttisellen, Switzerland). A sample holder with a diameter of 14 mm was used in which the scaffold was fixed with PU foam. Parameters of micro-CT control file were: energy 70 KV; intensity 114 μ A; resolution - native; field of view 15.2 mm; voxel size 3.4 μ m; integration time 2000 s. Scans were done under a 0.5 mm thick Al filter. The instrument was calibrated against a hydroxyapatite phantom.

2.4. *In vitro* cytotoxicity

To assess the possible cytotoxicity of the developed ACP/Sr-ACP granules and scaffolds, the *in vitro* cell viability was assessed. Granules or scaffolds were incubated in Dulbecco's Modified Eagle Medium high glucose (DMEM, high glucose, Gibco, Waltham, MA, USA) supplemented with 10 % fetal bovine serum (FBS, Gibco, Waltham, MA, USA) under gentle agitation for 24 h at 37 °C to obtain extracts. An extraction ratio of 0.2 g/mL for granules and 3 cm²/mL for scaffolds was considered, according to ISO 10993-12. Balb/c 3T3 clone A31 were seeded at 15,000 cells/cm² then incubated for 24 h at 37 °C before exposition to the extracts. 30 % Sr-ACP/Sr-ACP granules (in weight of the scaffold) will be incorporated into the scaffold. And 30 % Sr-ACP/Sr-ACP granules in weight of the scaffold are equivalent to 8 % ACP or Sr-ACP extract dilutions. Therefore, cells were incubated in culture medium with ACP or Sr-ACP extracts (25 % and successive dilutions 15 %, 8 % and 2.5 %) or scaffold extracts (100 % and successive dilutions 40 %, 16 % and 6.4 %) for 48 h at 37 °C in a humidified atmosphere with 5 % CO₂. Negative control (complete culture medium) and positive control for cytotoxicity (Phenol) were run in parallel. At the end of the incubation period, culture medium was removed and discarded. Cells were detached using trypsin

solution. Then, a Trypan Blue solution with 10 % FBS was added. Living cells were counted using a haemocytometer.

2.5. *In vivo* osteochondral defect mice model

To evaluate the biocompatibility and osteogenic capacity of ACP/Sr-ACP granules incorporated into the Col/Col-Mg-HAp scaffold *in vivo*, a semi-orthotopic osteochondral defect model established by our group was used (Figure 2A) [41]. In order to model several larger critical sized bone defects using a small animal model, we created a semi-orthotopic osteochondral defect model by implanting bovine osteochondral explants subcutaneously in mice. Briefly, osteochondral defects (4 mm in diameter, 4 mm in depth) were created in the explants (8 mm in diameter, 5 mm in height) harvested from metacarpal-phalangeal joints of 6-8 months old calves (LifeTec, Eindhoven, The Netherlands) with a hand drill. The osteochondral explants were cultured overnight in alpha-Minimum Essential Medium (α -MEM; Gibco, Massachusetts, USA) supplemented with 10 % fetal bovine serum (FBS, Gibco, Massachusetts, USA), 50 μ g/mL gentamycin (Gibco, Massachusetts, USA), and 1.5 μ g/mL fungizone (Gibco, Massachusetts, USA). Then the osteochondral defects were fitted with: (1) Col/Col-Mg-HAp scaffold-only (n = 6, osteochondral scaffold, Finceramica, Italy, diameter: 4 mm, height: 4 mm), or (2) ACP enriched Col/Col-Mg-HAp scaffold (n = 7), or (3) Sr-ACP enriched Col/Col-Mg-HAp scaffold (n = 7). All osteochondral explants were covered with a circular 8 mm Neuro-Patch membrane (Braun, Melsungen, Germany) to prevent the ingrowth of host cells from the top.

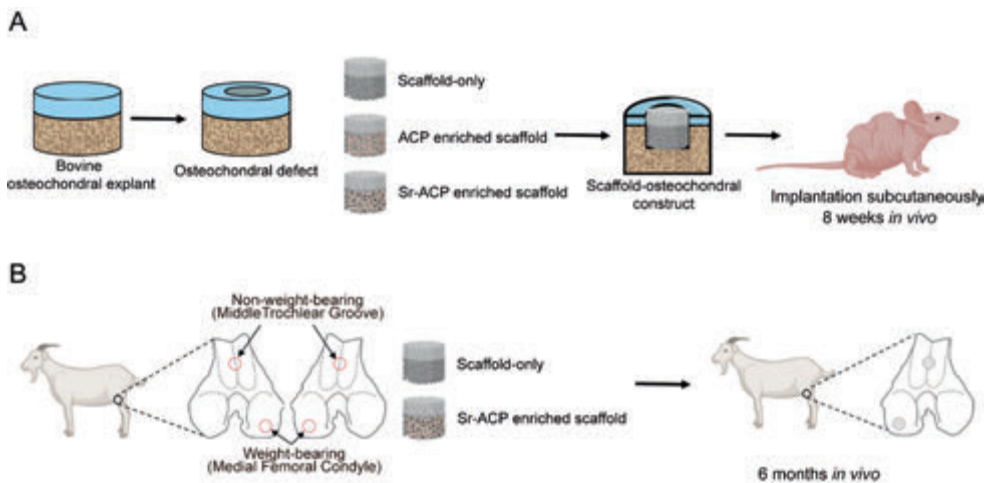


Figure 2. Schematic experiment setup of *in vivo* models. (A) *In vivo* osteochondral defect model in the mouse. (B) *In vivo* osteochondral defect model in the goat.

Five 12-week-old NMRI-Fox1nu female mice (Taconic, New York, USA) were randomly assigned and housed under specific-pathogen-free conditions with a regular day/night light cycle. Food and water were available ad libitum. The mice were allowed to adapt to the conditions of the animal facility for 7 days. The osteochondral explants were implanted subcutaneously on the back of the mice under 2.5-3% isoflurane anesthesia (1000 mg/g, Laboratorios Karizoo, Maharashtra, India). 4 osteochondral explants were implanted in 4

pockets per mouse respectively. Staples (Fine Science Tools, Vancouver, Canada) were used to close the incisions and were removed 1 week after implantation. To ensure pre- and post-operative analgesia, the mice received a subcutaneous injection of 0.05 mg/kg bodyweight of buprenorphine (Ividior, North Chesterfield, Virginia, USA) 1 h before surgery and 6-8 h after surgery. Mice received a subcutaneous prophylactic antibiotic injection of 25 mg/kg body weight of Amoxicillin (Dopharma, Raamsdonksveer, Netherlands).

After 8 weeks, mice were euthanized by cervical dislocation under 2.5-3% isoflurane anesthesia and the osteochondral explants were harvested. All the samples were fixed in 4 % formalin for 1 week for further processing. This animal experiment complied with the ARRIVE guidelines and was approved by the Ethics Committee for Laboratory Animal Use (AVD101002016991; protocol #EMC 16-691-05).

2.6. *In vivo translational large animal osteochondral defect model*

A validated preclinical large animal bilateral osteochondral defect model was used to assess the osteogenic effect of the developed Sr-ACP enriched Col/Col-Mg-HAp scaffold. A gender balanced (6 castrated male goats and 6 female goats) experimental unit of 12 skeletally mature Saanen goats (age: 2-3 years, weight: 35.8 ± 6.6 kg) was subjected to a bilateral arthrotomy under general anesthesia as described before [42-44]. In short: all animals received a prophylactic antibiotic injection with amoxycillin clavulanic acid 8.75 mg/kg intramuscular (Noroclav, Norbrook, Ireland) and were intravenously sedated with butorphanol (0.2 mg/kg, Butador, Chanelle Pharma, Ireland) and diazepam (0.2 mg/kg, Diazemuls; Accord Healthcare, UK). A lumbosacral epidural block with lidocaine (2 mg/kg, Lidocaine HCl 2 %, B. Braun Medical Inc., EU, Melsungen, Germany) and morphine (0.2 mg/kg, Morphine Sulphate 10 mg/mL, Kalceks, Latvia) was performed with the animal in sternal recumbency. Anesthesia was induced with propofol IV to effect (max. 6 mg/kg, Propofol-Lipuro 1 %, B. Braun Medical Inc., Melsungen, Germany) and was maintained with isoflurane (Vetflurane, Virbac Animal Health, Suffolk, UK) in 100 % oxygen via a circle rebreathing system. All animals received analgesia with meloxicam IV (0.5 mg/kg, Rheumocam, Chanelle, Galway, Ireland); and morphine IV (0.2 mg/kg, Morphine sulphate, Mercury Pharmaceuticals, Dublin, Ireland) 90 min after the epidural block.

An arthrotomy of each stifle joint was performed in dorsal recumbency using a lateral parapatellar approach. Under constant irrigation with saline, a pointed 6 mm drill bit was used to drill an approximate 3-4 mm deep non-weight-bearing defect in the transition of the distal 1/3 to the middle 1/3 of the trochlear groove and in the central weight-bearing part of the medial femoral condyle. Subsequently, a custom-made flattened drill bit and a depth guide were used to create an exact flat 6 mm deep by 6 mm wide circular critical-sized osteochondral defect in the non-weight-bearing and weight-bearing location. The joint was flushed with saline to remove any debris, and the defects were press fit with a similar-sized selected scaffold before surgical closure as described before. The left and right stifle joints of each goat were randomly assigned to one of the two treatment groups (within animal controlled) (Figure 2B): 1) Col/Col-Mg-HAp scaffold-only, and 2) Sr-ACP enriched Col/Col-Mg-HAp scaffold.

Following surgery, postoperative analgesia was provided (meloxicam 5 days) and goats were housed in indoor pens for daily postoperative welfare monitoring and scoring. Two weeks postoperatively, following the removal of skin sutures, animals were released to

pasture or loose housing (weather dependent) for the remainder of the study period with daily health checks. An orthopaedic assessment (Table S1) was performed on the day of humane euthanasia under sedation with a barbiturate overdose at the predetermined endpoint at 6 months after surgery. Subsequently, all the joints, surrounding joint tissues, and synovial fluids were scored (Table S2), dissected, and photographed (Body Canon EOS R5, lens: Canon EF 100 mm f/2.8 L Macro IS USM, flash: Macro Ring lite MR-14EX II). Biopsies 1 cm by 1 cm square containing the entire osteochondral defects were harvested with an oscillating saw.

This animal experiment complied with the ARRIVE guidelines. Ethical evaluation and approval were provided by the Health Products Regulatory Authority of Ireland (AE1898217/P142), the Animal Research Ethics Committee of University College Dublin (AREC-18-17-Brama) and the Lyons Animal Welfare Board (Health, Husbandry and Monitoring plans; 201,907).

2.7. Macroscopic assessment of osteochondral defect repair

The quality of defect repair was assessed semi-quantitatively using the International Cartilage Repair Society (ICRS) macroscopic evaluation system (Table S3) [45] and a macroscopic scoring system (Table S4) developed by Goebel et al. [46]. The ICRS scoring system rates cartilage repair tissue as Grade IV (severely abnormal), Grade III (abnormal), Grade II (nearly normal) or Grade I (normal). The Goebel Score describes articular cartilage repair with five major evaluation categories. The quality of defect repair was scored blinded on fresh samples by two independent assessors, and the scores were averaged for further calculation. All the samples were fixed in 4 % formalin for 10 days after the macroscopic assessment.

2.8. Micro-computed tomography of subchondral bone defect repair

The harvested samples underwent micro-CT scans (Quantum GX2, Perkin Elmer, USA) after fixation in 4 % formalin *ex vivo*. For the bovine explants from the mouse model, the settings were: energy 90 KV, intensity 88 μ A, 18 mm FOV, 36 μ m isotropic voxel size. The micro-CT scan settings for goat samples were: energy 90 KV, intensity 88 μ A, 36 mm FOV, 72 μ m isotropic voxel size. All the scans were under an x-ray filter of Cu (thickness = 0.06 mm) and Al (thickness = 0.5 mm), and were calibrated using phantoms with a known density of 0.75 g/cm³, which were additionally scanned before and after each scan. A high-resolution mode was set, and a scan time of 4 min was used. Image processing included modest Gauss filtering (sigma = 0.8 voxel, width = 1 voxel) and segmentation using a single threshold. A cylindrical region (4 mm diameter and 5 mm height) in the defect was selected as a volume of interest (VOI). In this VOI the following morphometric parameters were measured: bone volume per total volume (BV/TV), trabecular thickness (Tb-Th), trabecular number (Tb-N), and trabecular separation (TB.Sp). Morphological analyses were performed using IPL (Scanco Medical AG, Wangen-Brüttisellen, Switzerland).

2.9. Histology of osteochondral defect repair

After micro-CT scanning, the bovine osteochondral explants from the mouse model were decalcified using 10 % ethylenediaminetetraacetic acid (EDTA) for 4 weeks. The goat samples were decalcified for 3 weeks using 10 % formic acid. Subsequently, all samples

were embedded in paraffin and sectioned in 6 μm thin sections. To study general cell and tissue morphology, H&E staining was performed with Hematoxylin (Sigma, Saint Louis, USA) and Eosin Y (Merck, Kenilworth, USA). Safranin-O staining was performed with 0.1 % Light green O (Fluka, Buchs, Switzerland) and 0.1 % Safranin-O (Fluka, Buchs, Switzerland) to visualize glycosaminoglycans in the extracellular matrix (ECM). To demonstrate the osteoclasts in the defects, Tartrate-resistant acid phosphatase (TRAP) staining was performed. Briefly, dewaxed sections were pre-incubated in sodium acetate (Sigma, Saint Louis, USA) and L (+) tartaric acid (Acros Organics, NJ, USA) buffer at room temperature for 20 min. Then naphthol AS-BI phosphate (Sigma, Saint Louis, USA) and fast red TR salt (Sigma, Saint Louis, USA) were added to the buffer and the slides were further incubated for 3 h at 37 °C. To discriminate between calcified and non-calcified osteochondral tissue, RGB staining was performed using Alcian Blue (Sigma, Saint Louis, USA), Fast Green (Sigma, Saint Louis, USA), and Picrosirius Red (Sigma, Saint Louis, USA).

NDP Software View2 (version 2.8.24, 2020 Hamamatsu Photonics K.K.) was used to measure the tissue volume in the osteochondral defect at three sections that were taken at the centre of the defect, and 0.5 mm and 1 mm from the centre for bovine explants from the mouse model or at the centre of the defect for the goat samples (Supplementary Figure S1). The percentage of the defect covered with newly formed osteochondral tissue was calculated (Supplementary Figure S2). Tissue volume in goat samples was independently measured by two investigators blinded to the experimental condition. The measurements of the two investigators were averaged for each section.

2.10. Statistical analysis

All statistical tests were performed using SPSS software 28.0 (SPSS inc., Chicago, USA). Comparisons in cytotoxicity assessment were analysed by a Kruskal-Wallis test. Multiple comparisons between scaffold-only, ACP enriched scaffold and Sr-ACP enriched scaffold groups in bovine explants from the mouse model were analysed by a One-Way ANOVA test or a Kruskal-Wallis test (depending on normality tested by a Shapiro-Wilk test). Statistically significant differences between the scaffold-only group and the Sr-ACP enriched scaffold group, or between trochlear groove and femoral condyle groups in goat samples were determined by a Paired T test or a Wilcoxon signed-rank test (depending on normality tested by a Shapiro-Wilk test). A p-value ≤ 0.05 was considered statistically significant.

3. RESULTS

3.1. Characterization of ACP/Sr-ACP granules

The modified wet precipitation technology successfully yielded ACP and Sr-ACP materials. An overview of ACP/Sr-ACP granule physicochemical characteristics are given in Table 1, Figure 3, Figure 4. The XRD patterns confirmed the amorphous character of the obtained products (Figure 3A). The experimental Sr concentration of Sr-ACP (Table 1) was determined with ICP-MS at 2.49 ± 0.04 wt% ($n = 3$), which compared well with the theoretical value of 2.5 wt%. SEM-EDS mapping of chemical elements demonstrated homogenous Sr distribution within the Sr-ACP granules (Figure 4C and D). The FT-IR spectra demonstrated the hydrated and carbonated nature both of ACP and Sr-ACP (Figure 3B).

Introduction of Sr ions in the given concentration for the as-synthesized materials did not reveal any structural changes that could be observed with XRD and FT-IR. Additionally, XRD and FT-IR measurements were performed on the same materials 3.5 years after manufacturing to check stability of the amorphous phase (Figure 3C and D). The obtained XRD patterns demonstrated that ACP has started to crystallize while Sr-ACP has remained amorphous. In the FT-IR spectra of ACP, phosphate band shifts from 1002 cm^{-1} to 1010 cm^{-1} and from 549 cm^{-1} to 554 cm^{-1} were detected in parallel with the appearance of a band shoulder at 594 cm^{-1} for the 3.5-year-old sample. The band shoulder at 594 cm^{-1} confirms crystallization of ACP to some extent as already demonstrated by the XRD data as splitting of phosphate bands around 1000 cm^{-1} and 550 cm^{-1} usually indicates crystallization of ACP materials [47]. The specific surface area of both ACP and Sr-ACP granules was high ($>100\text{ m}^2/\text{g}$) with particle size d_{BET} being 20-21 nm (Table 1). The dry granulation technology produced irregular shape granules with sharp edges (Figure 4A and B). The sharp edges of the granules originate from the milling of the ACP agglomerates. Granule surfaces at the macro level were smooth and non-porous. By measuring granule dimensions from the SEM images, an average value of the experimental granule size was determined to be $187 \pm 35\ \mu\text{m}$ (at least 100 granules were measured for each sample).

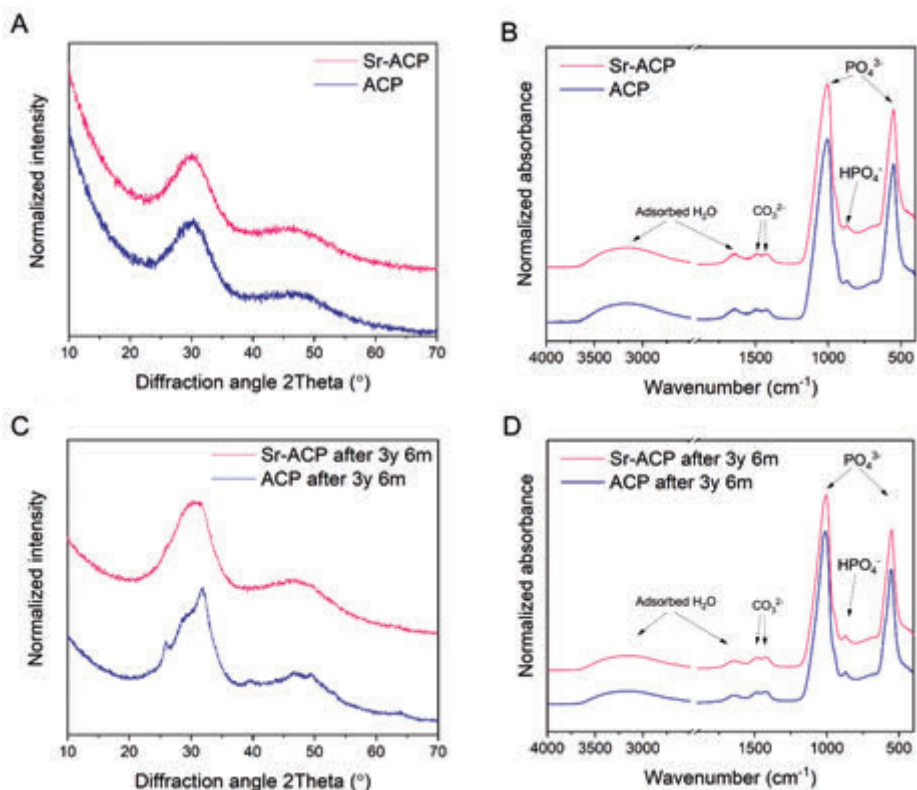


Figure 3. Phase and chemical group composition of ACP and Sr-ACP. (A) XRD patterns showing wide diffraction maxima indicative of the amorphous phase of the as-synthesized ACP and Sr-ACP, (B) FT-IR spectra demonstrating chemical group information, hydrated and amorphous nature of ACP and Sr-ACP, (C) XRD patterns and (D) FT-IR spectra of ACP and Sr-ACP after 3.5 years of storage in air at room temperature ($20 \pm 2\text{ }^{\circ}\text{C}$) in a sealed container.

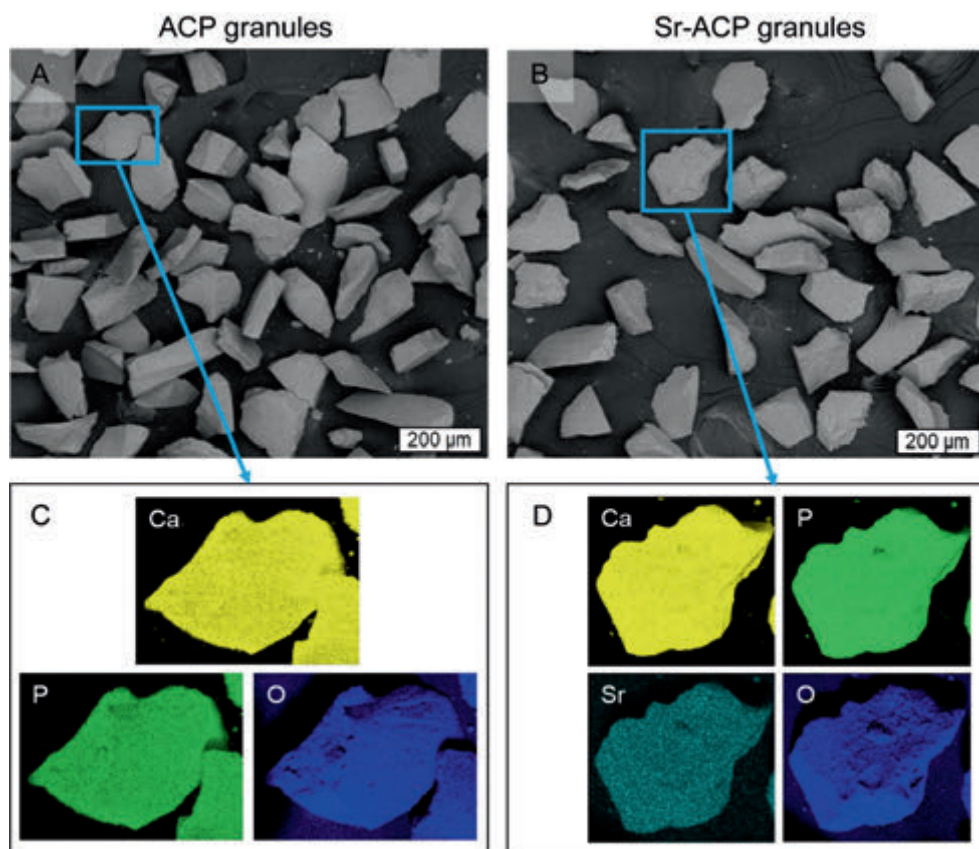


Figure 4. Morphology and chemical element distribution of ACP and Sr-ACP granules. SEM images of ACP (A) and Sr-ACP (B) irregularly shaped granules. SEM-EDS element maps of selected ACP (C) and Sr-ACP (D) granules demonstrate homogenous chemical composition, where each material's main elements are shown.

Table 1. Values of Sr concentration, specific surface area (SSA), and calculated particle size d_{BET} for ACP and Sr-ACP granules.

	Sr conc., wt%	SSA, m ² /g	d_{BET} , nm
ACP	0.01	113 ± 2	21
Sr-ACP	2.49 ± 0.04	115 ± 2	20

The final step of the granule production was granule washing with ethanol to remove any debris that may have originated from the granulation process. To assess whether the rinsing procedure has an impact on the structure of the ACP materials, granules were characterized with FT-IR (Supplementary Figure S3). No differences in FT-IR spectra of ACP granules before and after the rinsing with ethanol were detected.

Before *in vitro* and *in vivo* experiments, materials must be sterilized; in this study, gamma irradiation was used. To ensure amorphous granule composition remained unaffected

post-sterilization, phase and chemical composition were analysed using XRD and FT-IR. Obtained results demonstrated that gamma irradiation sterilization of ACP granules was effective, with no detectable changes in composition or crystallinity (Supplementary Figure S4).

3.2. ACP/Sr-ACP granule containing Col/Col-Mg-HAp scaffolds

The addition of ACP/Sr-ACP granules to the Col/Col-Mg-HAp scaffold is an additional step for the manufacturing process of the scaffolds. The newly developed ACP/Sr-ACP granule containing Col/Col-Mg-HAp scaffolds were examined with two-dimensional SEM and three-dimensional micro-CT analyses to assess granule 3D distribution within the ACP granule containing scaffolds. The Sr-ACP granules were well and homogeneously distributed in the bottom layer of scaffold (Figure 5A). The SEM image (Figure 5B) shows the bilayered structure of the scaffold as well: collagen-only layer on top and Col-Mg-HAp-Sr-ACP layer on the bottom. Both layers of the freeze-dried scaffold have a porous structure, which is governed by collagen. In the bottom layer the incorporated micron-sized Sr-ACP granules can be seen, while the nanoparticles of Mg-HAp cannot be visualized at given magnification. The shown SEM-EDS element maps of Ca, P, Sr, C, and Mg of Sr-ACP enriched Col/Col-Mg-HAp scaffolds (Figure 5C) and ACP enriched Col/Col-Mg-HAp (supplementary Figure S5) demonstrate localization of the chemical elements within the scaffolds. EDS element maps of the same area (Figure 4C) confirm the presence of the Sr-ACP granules as well. As Ca and P are the main constituents of Sr-ACP, the high contrast areas in Ca and P element maps match Sr-ACP granule placement in the SEM image (Figure 5B). The presence of Sr is detected as well. The EDS map of Mg designates the location of the biomimetically deposited Mg-HAp nanoparticles onto the fibers of the collagen scaffold's bottom layer (Figure 5C). The EDS map of C demonstrates the presence of collagen throughout the mapped area; higher intensity area of C is visible for the top layer which contains only collagen and no calcium phosphates (Figure 5C). SEM inspection of Sr-ACP granule containing scaffolds showed that the granules have a good compatibility with the scaffold's main component - collagen. SEM images (Figure 5D), showed that the ACP granules were incorporated in the collagen fibers of the scaffold. Collagen fibers were attached to the surface of the granules and stretched across it.

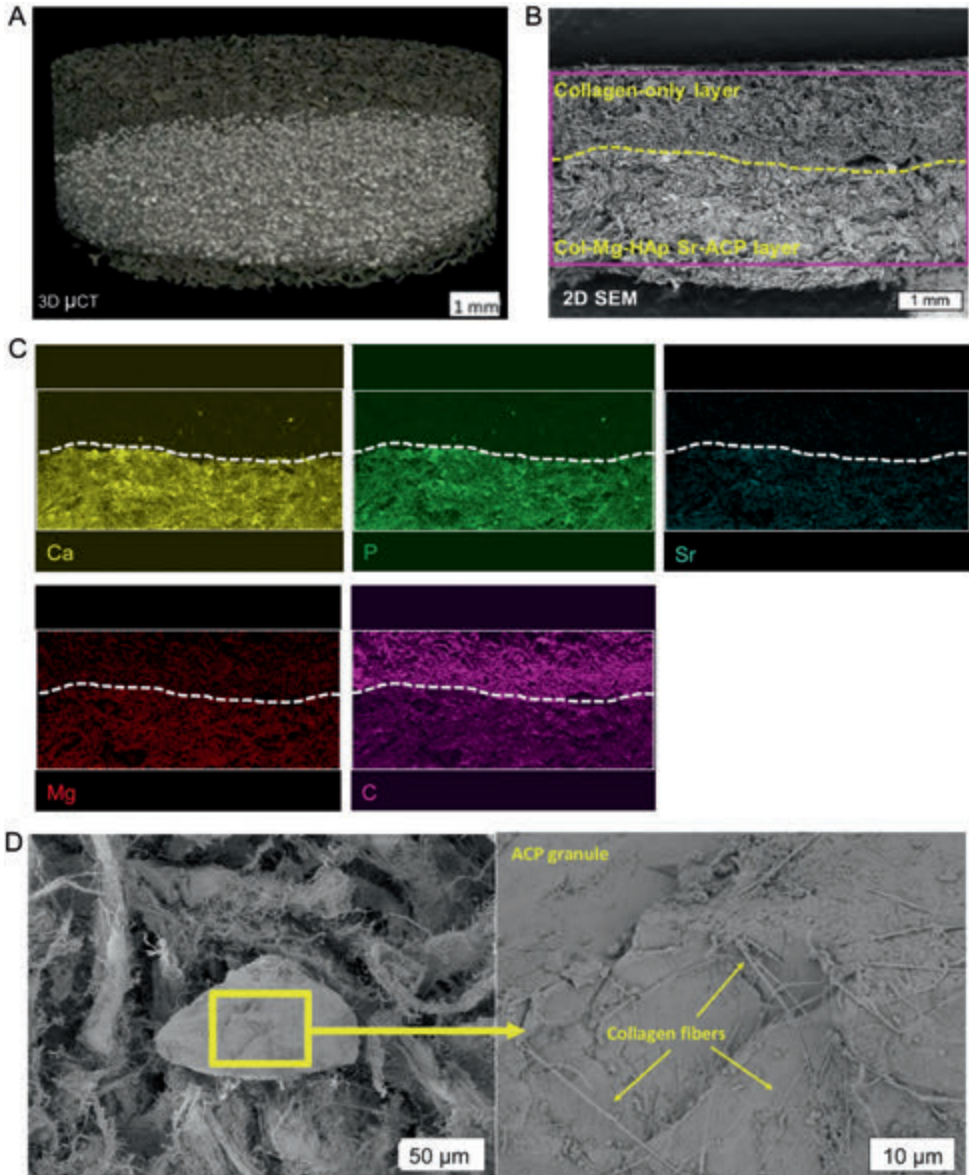


Figure 5. Characterization of Sr-ACP enriched Col/Col-Mg-HAp scaffold. Representative three-dimensional micro-CT image (A) of Sr-ACP granule containing Col/Col-Mg-HAp scaffold. SEM image in backscattered electron (BSE) detector mode (B) of cross-section of the Sr-ACP granule containing Col/Col-Mg-HAp scaffold, where the top layer is collagen and the bottom layer is Col-Mg-HAp layer enriched with Sr-ACP granules, and where the drawn rectangle marks EDS mapping area. EDS element (Calcium, Ca - yellow, Phosphorus, P - green, Strontium, Sr - light blue, Magnesium, Mg - red, Carbon, C - magenta) maps (C) of the scaffold visualized on (B), where the dashed line shows the border between both layers and the brightest areas in Ca and P maps represent positions of the Sr-ACP granules SEM images of Sr-ACP granule containing scaffold (D) where single ACP granule (left) and close-up view of the surface of the Sr-ACP granule covered in collagen fibers (right) is shown.

3.3. Cytotoxicity assessment

The *in vitro* cell viability was assessed to evaluate the possible cytotoxicity of the developed ACP/Sr-ACP granules. The 25 %, 15 %, 8 % and 2.5 % dilutions of extracts that were harvested after 24-h incubation of ACP or Sr-ACP (2.49 wt% Sr) granules were not cytotoxic (Figure 6A). To assess the biocompatibility of ACP or Sr-ACP enriched Col/Col-Mg-HAp scaffolds, scaffolds with 30 wt% ACP or Sr-ACP granules were prepared for cytotoxicity assessment. 100 % extracts from all the scaffolds were cytotoxic, and ACP or Sr-ACP enriched Col/Col-Mg-HAp scaffolds reached a non-cytotoxic level from dilution 16 % (Figure 6B).

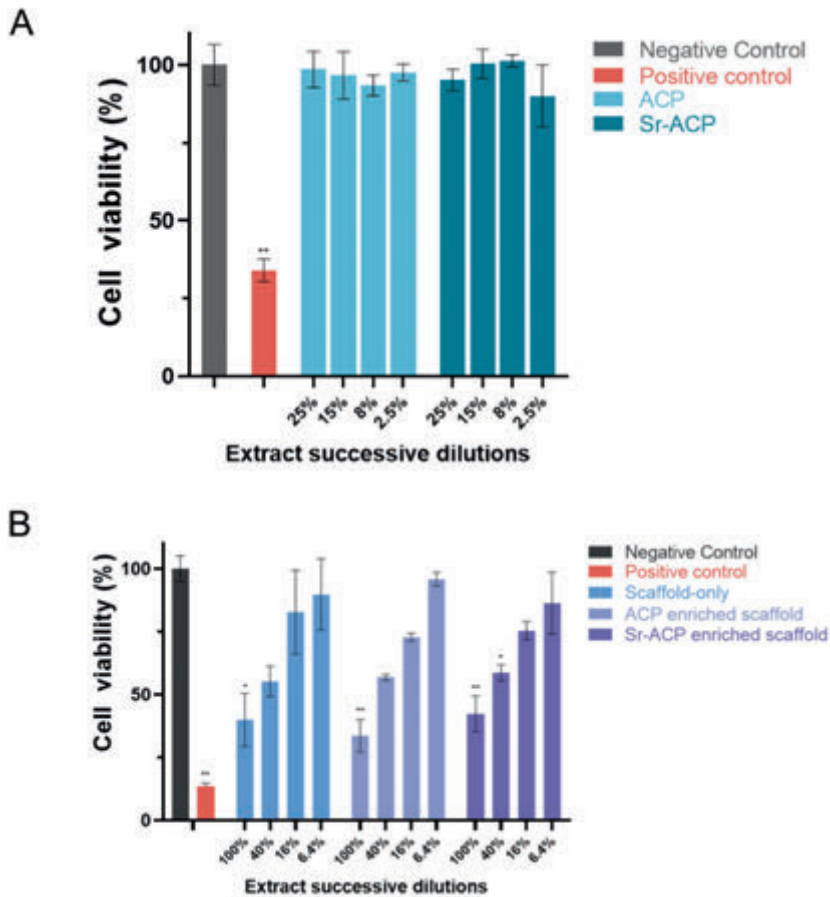


Figure 6. Cytotoxicity of the developed ACP/Sr-ACP granules and scaffolds. Cytocompatibility evaluation of Balb/c 3T3 clone A31 cells exposed to ACP/Sr-ACP granules extraction (A, $n = 4$) and ACP/Sr-ACP enriched scaffold extraction (B, $n = 3$). Cell viability (%) is the ratio of test condition and negative control. Negative control is complete culture medium only. Phenol was added in the positive control. ** $P < 0.01$, * $P < 0.05$ compared to negative control.

3.4. Effect of ACP and Sr-ACP addition to the scaffold on osteochondral defect repair in an *in vivo* mouse subcutaneous model

An *in vivo* early osteochondral repair phase semi-orthotopic mouse model was used to assess the *in vivo* compatibility and osteogenic effect of ACP or Sr-ACP enriched Col/Col-Mg-Hap scaffolds. After 8 weeks, remnants of the collagen-only layer were observed in the cartilage region of the defect, while the Col-Mg-HAp layer in the subchondral bone defect was mostly degraded and replaced by bone-like tissue (Figure 7A). Notably, ACP or Sr-ACP granules can still be seen after 8 weeks, and were well distributed in the newly formed tissues (Figure 7A). Some osteoclasts attaching to the granules in the bone tissue were demonstrated by TRAP staining (Figure 7A). The subchondral bone defects were filled with newly formed osteochondral tissue, indicating good biocompatibility and osteogenic property of ACP and Sr-ACP granules. Slightly more osteochondral repair tissue was found in the osteochondral defects loaded with Sr-ACP enriched scaffolds ($89.3 \pm 7.2\%$) compared to the scaffold-only ($87.2 \pm 11.1\%$) or ACP enriched scaffolds ($80.2 \pm 21.5\%$), although no significant differences in tissue volumes were found (Figure 7B).

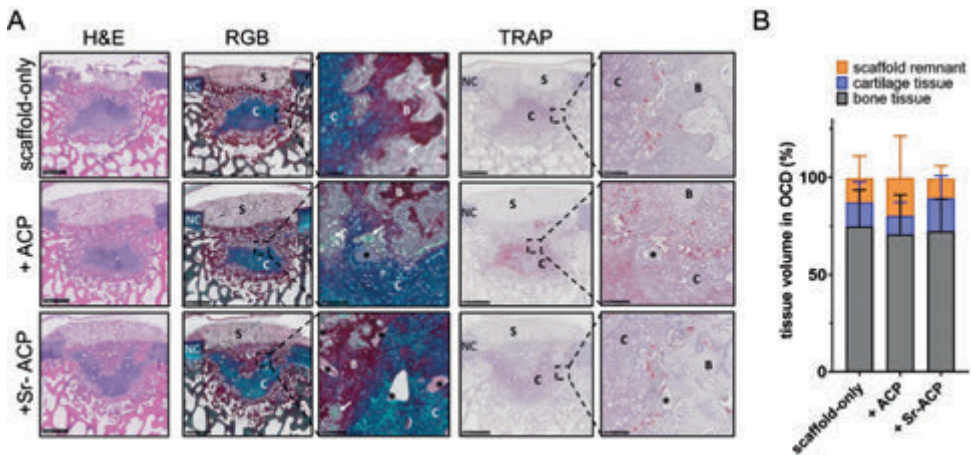


Figure 7. ACP and Sr-ACP showed a good biocompatibility for osteochondral repair *in vivo*. (A) Representative images of the 8-week repair constructs stained with H&E (Hematoxylin and Eosin), RGB (Alcian Blue, Fast Green, and Picosirius Red) and Tartrate-resistant acid phosphatase (TRAP) staining. Scale bars indicate 1 mm and 100 μ m, respectively. NC: native cartilage; C: newly formed cartilage-like tissue; B: newly formed bone-like tissue; S: remnants of the scaffolds; *: ACP or Sr-ACP granules. (B) The percentage of tissue volume calculated in the osteochondral defects (OCD). The repair tissue volume was expressed as mean \pm standard deviation (SD). No significant difference was found among the three conditions.

3.5. Effect of Sr-ACP on osteochondral defect repair in an *in vivo* large animal translational model

3.5.1. Clinical observations and scaffold implantation

The Sr-ACP enriched Col/Col-Mg-HAp scaffold demonstrated good repair in the mouse model and therefore the osteogenic capacity of Sr-ACP granules was further investigated in a validated translational goat osteochondral defect model in the knee. Scaffolds were successfully implanted into osteochondral defects created in the trochlear groove (a non-weight-bearing location) and the medial femoral condyle (a weight-bearing location) of both knees. All animals recovered well postoperatively except for one goat that died 2 weeks post-surgery due to clostridium disease unrelated to the surgery or the experiment.

The macroscopic appearance 2 weeks post-surgery showed that scaffolds were stable at both medial femoral condyle and trochlear groove osteochondral defect sites (Supplementary Figure S6A). The two layers of the scaffold can clearly be seen in the osteochondral defects histologically at two weeks (Supplementary Figure S6B). Another two goats died at 4- and 5-months post-surgery, again caused by clostridium disease despite vaccination and unrelated to the surgery and the experiment. The remaining eight goats were in good health throughout the study. At the predetermined 6-month endpoint the orthopedic exam demonstrated normal locomotion and excellent joint mobility in all goats.

All the joints, surrounding joint tissues, and synovial fluid were scored macroscopically on opening of the joints. There was no evidence of inflammatory responses or construct delamination in the treated joints at the time of retrieval. No joint swelling, effusion, mobility abnormalities or adhesions were found. Synovial fluid and membrane were normal and no indications of patellar instability/luxation were found.

3.5.2. Tissue repair in the osteochondral defects

The samples from the goats that unexpectedly died at 4 and 5 months post scaffold implantation revealed that the scaffolds had been degraded completely, and the osteochondral defects were mostly filled with repair tissue demonstrated by H&E, Safranin-O and RGB staining (Supplementary Figure S7). Overall, at 6 months, well-structured subchondral trabecular bone was observed in most trochlear groove and femoral condyle subchondral bone defects demonstrated by reconstructed micro-CT images, macroscopic sectional view and histology (Figure 8, Figure 9, Supplementary Figure S8). Reconstructed subchondral bone defect images showed an area with no trabecular bone either underneath or at the bottom of the defects unrelated to the defect location or the scaffold type. Histological images demonstrated that these areas found in micro-CT images were filled with bone marrow and were dissimilar to cysts.

In the non-weight-bearing trochlear groove location reconstructed micro-CT images showed no significant difference in the BV/TV, Tb. Th, Tb. N and Tb. Sp within animals between subchondral bone defects filled with scaffold only or Sr-ACP enhanced scaffolds (Figure 8A and B). The macroscopic cross-sectional view and histology further confirmed the well-repaired subchondral bone (Figure 9C). Bone-like tissue (including the bone marrow) was quantified on RGB stained histology. After 6 months, slightly more bone tissue ($98.0 \pm 29.0\%$ vs. $92.7 \pm 11.9\%$, $P = 0.499$) was found in the subchondral bone defects when the Sr-ACP was incorporated into the scaffolds compared to the scaffold-only, although no statistically significant difference was found (Figure 9D).

In the weight-bearing femoral condyle location no significant difference in the BV/TV, Tb. Th, Tb. N, and Tb. Sp was observed at 6 months within animals between subchondral bone defects filled with scaffold only or Sr-ACP enhanced scaffolds (Figure 9A and B). Overall, $96.9 \pm 3.8\%$ (scaffold-only group) and $96.0 \pm 5.6\%$ (Sr-ACP enriched scaffold) of the subchondral bone defects were filled with osteochondral tissue (Figure 8C and D). However, when looking specifically at the study target, the bone layer of the osteochondral unit, significantly more bone tissue was found ($P = 0.029$, Figure 8D) in the subchondral defects loaded with Sr-ACP enriched scaffold ($88.6 \pm 7.6\%$) compared to scaffold-only ($76.7 \pm 11.4\%$).

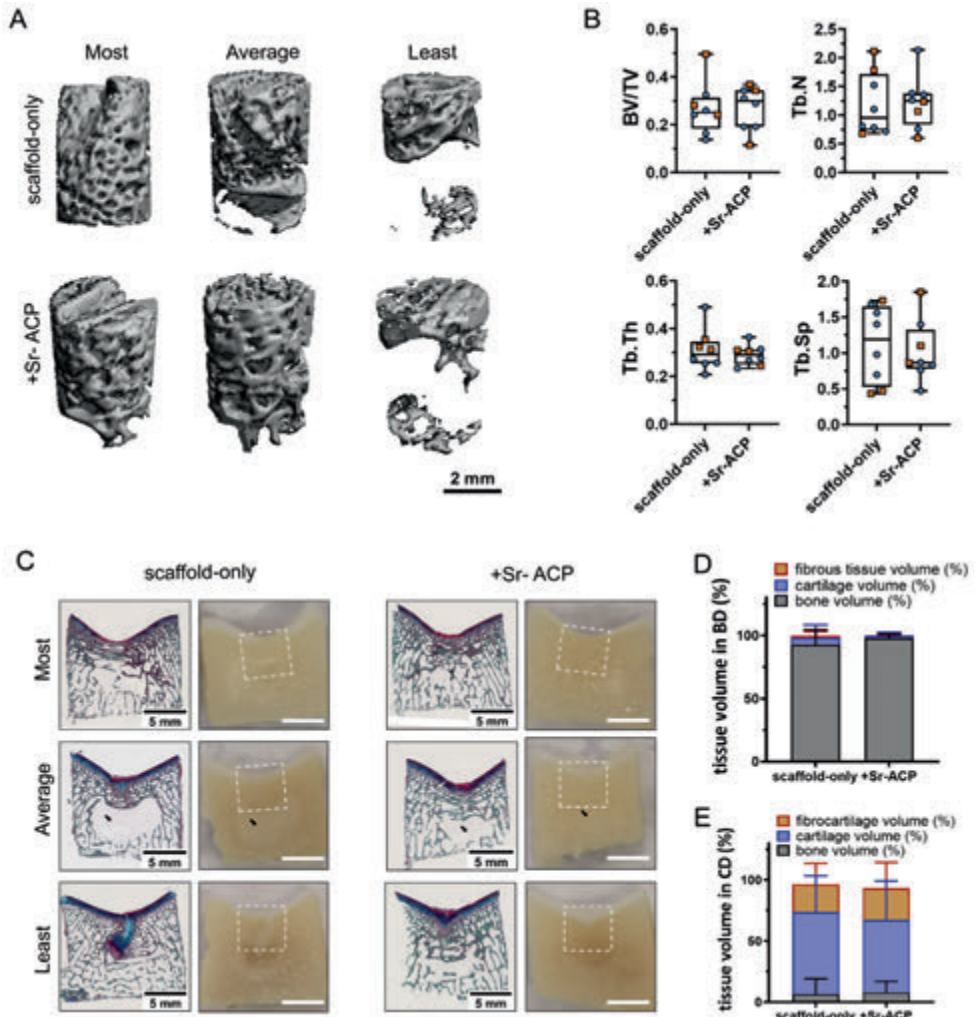


Figure 8. Tissue repair in the trochlear groove defect sites. (A) Representative micro-CT reconstructions treated with either scaffold-only or Sr-ACP enriched scaffold. Samples with most, average, and least bone volume are presented. The scale bar indicated 2 mm. (B) BV/TV, trabecular thickness (Tb. Th [mm]), trabecular number (Tb. N [1/mm]), and trabecular separation (Tb. Sp [mm]) in the bone defects after 6 months. Blue circles indicate castrated male goats, orange squares indicate female goats. The box plots indicate the minimum, first quartile, median, third quartile, and maximum. No significant difference was found between the two conditions. (C) RGB (Alcian Blue, Fast Green, and Picrosirius Red) staining and macroscopically sectional view of osteochondral defects treated with either scaffold-only or Sr-ACP enriched scaffold. H&E staining and Safranin-O staining of the same samples are presented in Supplementary Figure S8. Samples with most, average, and least bone-like tissue in bone defects are presented. White squares indicated 6*6 mm osteochondral defects. Black arrows indicated the structure with only bone marrow. The scale bar indicates 5 mm. (D) The percentage of tissue volume calculated in the subchondral bone defects (BD). The repair tissue volume was expressed as mean \pm standard deviation (SD). (E) The percentage of tissue volume calculated in the cartilage defects (CD). The repair tissue volume was expressed as mean \pm standard deviation (SD). No significant difference in tissue volume in both cartilage defects and bone defects was found between the two conditions.

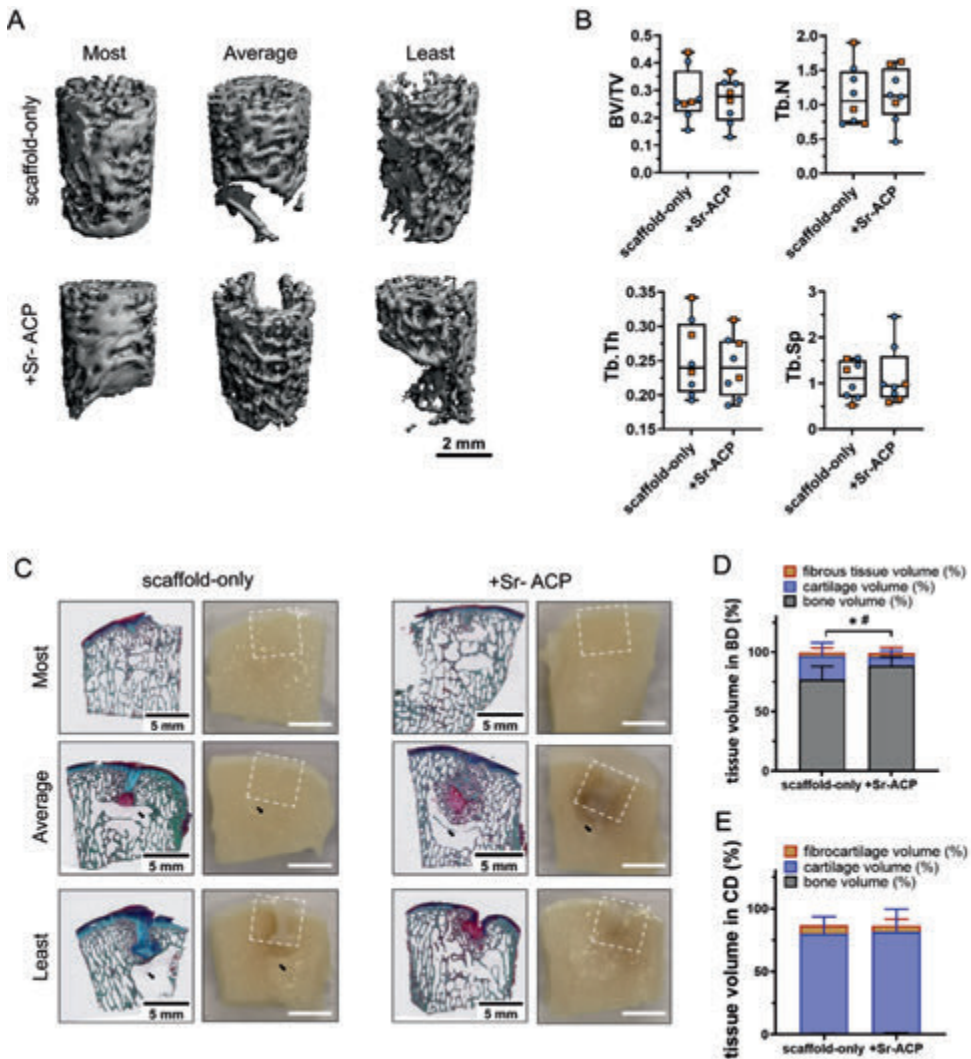


Figure 9. Tissue repair in the femoral condyle defect sites. (A) Representative micro-CT reconstructions treated with either scaffold-only or Sr-ACP enriched scaffold. Samples with most, average, and least bone volume are presented. The scale bar indicates 2 mm. (B) BV/TV, trabecular thickness (Tb. Th [mm]), trabecular number (Tb. N [1/mm]), and trabecular separation (Tb. Sp [mm]) in the subchondral bone defects after 6 months. Blue circles indicate castrated male goats, orange squares indicate female goats. The box plots indicate the minimum, first quartile, median, third quartile, and maximum. No significant difference was found between the two conditions. (C) RGB (Alcian Blue, Fast Green, and Picrosirius Red) staining and macroscopic images of osteochondral defects treated with either scaffold-only or Sr-ACP enriched scaffold. H&E staining and Safranin-O staining of the same samples are presented in Supplementary Figure S8. Samples with most, average, and least bone-like tissue in bone defects are presented. White squares indicated 6*6 mm osteochondral defects. Black arrows indicated the structure with only bone marrow. The scale bar indicated 5 mm. (D) The percentage of tissue volume calculated in the subchondral bone defects (BD). The repair tissue volume was expressed as mean \pm standard deviation (SD). * $P < 0.05$ in cartilage-like tissue, # $P < 0.05$ in bone-like tissue. (E) The percentage of tissue volume calculated in the cartilage defects (CD). The repair tissue volume was expressed as mean \pm standard deviation (SD). No significant difference in tissue volume in cartilage defects was found between the two conditions.

Interestingly, more bone-like tissue was regenerated in the trochlear groove subchondral bone defect sites compared to the medial femoral condyle subchondral bone defect sites when scaffold-only ($92.7 \pm 11.9\%$ vs. $76.7 \pm 11.4\%$, $P = 0.062$) or Sr-ACP enriched scaffolds (bone-like tissue: $98.0 \pm 2.9\%$ vs. $88.6 \pm 7.6\%$, $P = 0.025$) were implanted in the osteochondral defects.

The cartilage part of the defects treated with either scaffold was repaired well with good integration into the surrounding native tissue macroscopically at 6 months post-implantation (Supplementary Figure S9). Only small, scattered fissures or cracks were observed on some surfaces of the defects and no noticeable depressions were observed overall. In trochlear groove defects (Supplementary Figure S9A), the macroscopic ICRS and Goebel scores for the scaffold-only group had a median score of 10.19 ± 1.65 out of 12 and 17.19 ± 3.39 out of 20, respectively (Supplementary Figure S9B). All the samples were classified as normal (grade I) or nearly normal (grade II) cartilage except for one sample (grade III). For the Sr-ACP enriched scaffold group, the macroscopic ICRS and Goebel scores were 9.50 ± 2.98 and 16.63 ± 3.93 , respectively (Supplementary Figure S9B). Two defects repaired with the Sr-ACP enriched scaffold were classified as abnormal (grade III). Macroscopic assessment of femoral condyle defects repaired (Supplementary Figure S9C) with the scaffold-only resulted in median ICRS scores of 10.13 ± 0.83 , and median Goebel scores of 18.69 ± 0.37 at 6 months (Supplementary Figure S9D). The defects fitted with the Sr-ACP enriched scaffold were scored median ICRS scores of 9.94 ± 1.27 , and median Goebel scores of 18.56 ± 1.02 (Supplementary Figure S9D). All the samples were classified as nearly normal (grade II) cartilage. Overall, no significant difference was observed in cartilage repair between these two conditions with both scoring systems. Histologically, cells with a rounded morphology within the cartilage region were found residing within lacunae and with alignment typical of native cartilage. Both scaffolds demonstrated cartilaginous tissue formation by positive GAG staining on RGB (Figure 8, Figure 9C) and Safranin-O (Supplementary Figure S8) but no significant differences could be found between the scaffolds (Figure 8, Figure 9E).

4. DISCUSSION

The main finding of this study is that the addition of Sr-ACP granules into a clinically used osteochondral scaffold is a feasible and effective strategy to improve its bone repair capacity in *in vivo* osteochondral defects. The subcutaneous mouse osteochondral defect model demonstrated good biocompatibility and an overall good early tissue response of both ACP and Sr-ACP enriched Col/Col-Mg-HAp scaffolds, whereas a better bone formation was obtained in subchondral bone defects treated with the Sr-ACP enriched scaffolds in a weight-bearing subchondral bone defect at 6 months in a translational goat model.

The new strategy proposed in this study is based on the modification of a clinically used Col/Col-Mg-HAp scaffold through the incorporation of ACP or Sr-ACP granules with a high specific surface area ($>100 \text{ m}^2/\text{g}$) and a hydrated and carbonated nature. A simple, fast, cost-effective, and scalable method for the preparation of ACP was used in this study and further modified for the preparation of Sr-ACP. Further, the manufactured ACP or Sr-ACP granules with a large specific surface area and hydrated and carbonated nature were well distributed in the Col/Col-Mg-HAp scaffold. Due to the potent effects of calcium and phosphate ions on bone cells, and their presence in large quantities in bone tissue, calcium

phosphates (CaPs) are of high interest in the bone repair biomaterial field [48]. ACP is involved in the early stages of bone mineralization [49] and the formation of complex CaP structures during bone mineral shaping and structuring [48,50]. Previous studies on ACP have demonstrated excellent biocompatibility and bioactivity of this product *in vitro* [51] as well as good biodegradability, osteoconductivity, and osteogenic potential also in *in vivo* osteochondral defect models [52,53]. On the other hand, the main inorganic component of bone is low crystalline apatite that highly resembles the chemical structure of HAp [54-56]. The addition of HAp into the bone layer can further improve the osteogenic potential of a collagen-based scaffold *in vivo* [57-61]. Therefore, the combination of ACP and HAp materials in a biphasic manner was expected to improve bone regeneration in osteochondral defects. The high crystallinity and stoichiometry of HAp contribute to rather slow rates of dissolution, thereby improving mechanical properties of the scaffold and long-term bone regeneration [62]. ACP, in the meantime, can favour the onset of bone deposition in the early stages of remodelling with its high solubility and amorphous structure [50].

In addition, we have successfully combined an alternative local Sr²⁺ delivery carrier in the form of ACP granules within the Col/Col-Mg-HAp scaffold to further improve bone regeneration. Sr and Ca are chemically very similar in ion size and have the same charge (+2) [63], thus Sr incorporation in calcium rich materials can be achieved. The majority of *in vitro* studies support a dual effect of Sr²⁺ on bone tissue: 1) stimulating bone formation by increasing proliferation and differentiation of osteoblasts, and inhibiting their apoptosis [24,64-66]; 2) hindering bone resorption by inhibiting the formation and differentiation of osteoclasts and promoting their apoptosis [65-67]. Our *in vivo* mouse study showed good osteochondral defect repair with ACP or Sr-ACP enriched scaffolds after 8 weeks with osteoclasts attaching to the granules.

The possible structural transformation of ACP into other calcium phosphate compounds raised problems for mass production, processing and storage [50]. The synthesis route for the preparation of amorphous calcium phosphates we used in this study enabled stability of ACP in air in a dried state for at least 7 months [34]. Trace amounts of various ions have been corroborated to affect ACP transformation [68,69]. Mg²⁺ is an effective inhibitor for the ACP phase transformation by changing the internal structure of ACP and reducing solubility [70-72]. Furthermore, Sr²⁺ can stabilize ACP as well [68]. Interestingly, the presence of Sr²⁺ was reported to significantly enhance the stabilization effect of Mg²⁺ on ACP due to a synergic effect, which might be due to that Sr²⁺ promotes the exclusion of Mg during HAp nucleation from ACP [69]. In the current study, prolonged investigation of ACP and Sr-ACP stability was performed. Sr-ACP with 2.5 wt% of Sr was found to have amorphous phase stability in a dry state of at least 3.5 years while ACP without Sr demonstrated signs of crystalline transformation. Therefore, a relatively stable phase of ACP was expected in a Col/Col-Mg-HAp-Sr-ACP scaffold before implantation. After implantation Sr-ACP/ACP granules eventually would transform into a poorly crystalline calcium phosphate phase resembling bone mineral. Our *in vivo* studies demonstrated that incorporated granules were still present after 8 weeks in mice, and were degraded after 4 months in goats, when there was already sufficient bone regeneration, although the composition (Sr-ACP/ACP granules or calcium phosphate phase) of the granules found on histology was not confirmed.

Here, the Col/Col-Mg-HAp scaffolds modified with ACP and Sr-ACP were investigated on the sequential use for osteochondral defects in *in vivo* models, from a small animal model to a translational large animal model. These two models, used together, allowed us to investigate the possible effect of incorporating ACP or Sr-ACP into the Col/Col-Mg-HAp scaffold used for osteochondral repair and to bring our approach a step closer to the physiological and mechanical conditions in the human osteochondral environment. Firstly, we confirmed biocompatibility and osteogenic properties of the modified Col/Col-Mg-HAp scaffolds in the mouse model as the first screening. The semi-orthotopic model allows a minimally invasive surgery and a multiple graft testing possibility [73], in line with the increasing ethical requirements on animal experiments. The results showed that, after 8 weeks, the bone-like layer in the subchondral bone defect was mostly degraded and replaced by bone-like tissue. The presence of repaired bone tissue together with the lack of side effects in all the experimental groups demonstrated a safe and good repair capacity of both ACP and Sr-ACP enriched scaffolds. In fact, both the native osteochondral Col/Col-Mg-HAp scaffold and the incorporated inorganic granules have been shown to be biocompatible and biodegradable [51-53,59,74,75]. The three treatment groups showed the presence of repair tissue. There is no significant difference among the different scaffolds. This indicates that the granule insertion did not interfere with the healing process. The scaffold-only condition also demonstrated excellent bone healing after 8 weeks in the mouse model. Smaller animals tend to heal quickly if compared with larger animals due to the intrinsic nature of osteochondral lesions [76]. Consequently, 8 weeks represents a relatively late time point in this model. Therefore, considering the quick repair response, and also the lack of synovial fluid, mechanical loading and complete immune system in the mouse [73], the use of a more advanced translational large animal model, suitable for comparison with human conditions, was a logical subsequent step. Thus, after the preliminary evaluation in mice, the most promising scaffold modification, the addition of Sr-ACP granules, was selected to be tested in a goat translational osteochondral defect model.

The goat model is a fully immune competent model using outbred animals, and offers advantages regarding joint size, cartilage and subchondral bone thickness, accessibility for surgical procedures, and limited intrinsic healing capacity [77]. Sex-balance was included in the experimental set up of this study as appropriate to enhance scientific rigor, but sadly unexpected and experimental unrelated animal deaths prevented a sufficiently powered analyses of sex differences. Therefore, no sex difference in subchondral bone repair was observed. The validated goat model provides the opportunity to assess tissue regeneration in paired knee joints within the same goat to reduce individual variation effects and enhance statistical power (within animal controls). The model also allows studying two different mechanical loading environments within the same joint. In particular, the Col/Col-Mg-HAp and the Sr-ACP enriched Col/Col-Mg-HAp scaffolds were successfully implanted in the trochlear groove, with no/low direct mechanical loading, and in the medial femoral condyle, with direct mainly compressional mechanical loading [78]. In this goat model, significantly more bone was regenerated after 6 months in the subchondral bone defects of the biomechanically more challenging femoral condyle lesions when Sr-ACP was incorporated into the scaffold compared to scaffold-only. In fact, during its metabolism, bone incorporates and releases various trace elements (Na, Mg, Sr, Zn, Si etc.) into the cellular microenvironment [63]. Similar element/ion release in the cellular

microenvironment was expected when Sr-ACP was incorporated into the Col/Col-Mg-HAp scaffold, where Sr^{2+} , Mg^{2+} , Ca^{2+} , and PO_4^{3-} should be released from the scaffold during the healing process, favouring chemotaxis, scaffold colonization, and the cell mineralization process, since this bone layer of the scaffold has a porous nano-structured composition aimed at the efficient delivery of ions [37].

In this study, our primary objective was to improve subchondral bone repair of osteochondral defects by incorporating newly developed Sr-ACP granules into the bone-like layer of the Col/Col-Mg-HAp scaffold. The cartilage-like layer of this scaffold has already been studied extensively and the excellent chondrogenic capacity of this Col/Col-Mg-HAp scaffold has been confirmed [79-81]. Briefly, the cartilage layer that consists of type I collagen-only demonstrated 3D support for the attachment and proliferation of human MSCs. Human MSCs seeded on the cartilage part of this scaffold changed toward chondrocytes, as evidenced by cell morphology and the formation of extracellular matrix demonstrated by the synthesis of type II Collagen (immunohistochemistry) and GAGs [79-81]. In the presented study, the cartilage part of the defects treated with either scaffold was repaired well with good integration into the surrounding native tissue, which is consistent with previous *in vitro*, preclinical and clinical results [12-14,79-81].

The overall good osteochondral regeneration obtained with the scaffold-only may have hindered the possibility to detect a significant improvement in this model, which did not show the same criticalities observed in terms of osteochondral regeneration in humans. In the more challenging and translational goat model, the incorporation of Sr-ACP into the scaffold was significantly more effective in regenerating bone tissue compared to the scaffold-only, as shown by the histological analysis. Overall, the scaffold-only and Sr-ACP enriched scaffolds regenerated a similar volume of osteochondral tissues, which means more cartilage-like tissue was present in the subchondral bone defect with the scaffold-only. These cartilage-like tissues might be ossified afterwards. In other words, there might be an acceleration effect of Sr-ACP at the earlier stage of repair. However, in this study, bone repair at only one time-point was assessed in the goat model. Therefore, the early cellular responsiveness that leads to a potential acceleration at this stage of repair, or long-term osteogenesis, which is known to end within 10-12 months [82], was not investigated. An effect could have been missed at its full extent by having a study focus of 6 months. This may also explain how, unlike what was observed by histological analysis, no significant difference in bone volume was found by micro-CT analysis.

5. CONCLUSION

Modification of the ACP structure with 2.5 wt% of Sr ensures prolonged amorphous phase stability of Sr-ACP in the dry state for at least 3.5 years making it a more feasible component of medical devices compared to pure ACP. Furthermore, the incorporation of Sr-ACP granules improves the subchondral bone formation capacity of a Col/Col-Mg-HAp scaffold in weight-bearing areas during osteochondral defect repair. We propose the use of Sr-ACP granules in the bone layer of a bilayered osteochondral scaffold to enhance osteochondral defect repair.

SUPPLEMENTARY MATERIALS

Table S1: Clinical Orthopedic Assessment. This tool is to evaluate the clinical health of goat joints.

Parameter	Variables	Score
Lameness	Walks normally	5
	Slightly lame when walking	4
	Moderately lame when walking	3
	Severely lame when walking	2
	Reluctant to rise and will not walk more than five paces	1
Joint mobility	Full range of motion	5
	Mild limitation (10-20%) in ROM; no crepitus	4
	Mild limitation (10-20%) in ROM; with crepitus	3
	Moderate limitation (20-50%) in ROM; \pm crepitus	2
	Severe limitation (>50%) in ROM; \pm crepitus	1
Pain on knee palpation and movement	None	5
	Mild signs; Goat turns head in recognition	4
	Moderate signs; Goat pulls limb away	3
	Severe signs; Goat vocalises or becomes aggressive	2
	Goat will not allow palpation	1
Weight-bearing	Equal on all limbs standing and walking	5
	Normal standing; favours affected limb when walking	4
	Partial weight-bearing standing and walking	3
	Part. weight-bearing standing; non-weight-bearing walk	2
	Non-weight-bearing standing and walking	1
Overall score of clinical condition	Not affected	5
	Mildly affected	4
	Moderately affected	3
	Severely affected	2
	Very severely affected	1
Total score		25

Table S2: Macroscopic joint Assessment. This tool is to evaluate the macroscopic normalization of goat joints when the joints were opened.

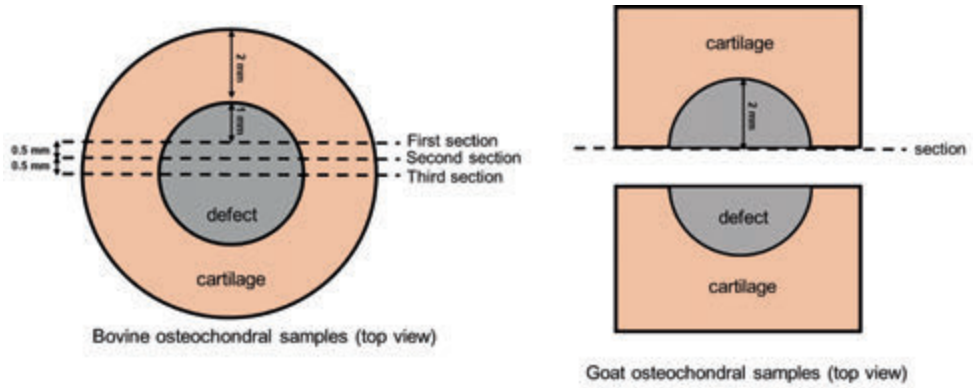
Parameter	Variables	Score
Wound healing abnormal	Yes	0
	No	1
Swelling of soft tissues surrounding joints	Yes	0
	No	1
Effusion of the joints	Yes	0
	No	1
Patellar luxation	Yes	0
	No	1
Joint mobility abnormal	Yes	0
	No	1
Adhesions in the joint	Yes	0
	No	1
Erosions of the joint	Yes	0
	No	1
Synovial fluid abnormal	Yes	0
	No	1
Synovial membrane abnormal	Yes	0
	No	1
Lesion on the opposite cartilage surface (trochlear groove vs patella)	Yes	0
	No	1
Lesion on the opposite cartilage surface (medial femoral condyle vs meniscus/tibia plateau)	Yes	0
	No	1
	Total	0-11

Table S3: International Cartilage Repair Society (ICRS) cartilage repair scoring system. This tool is to evaluate the macroscopic appearance of cartilage repair tissue.

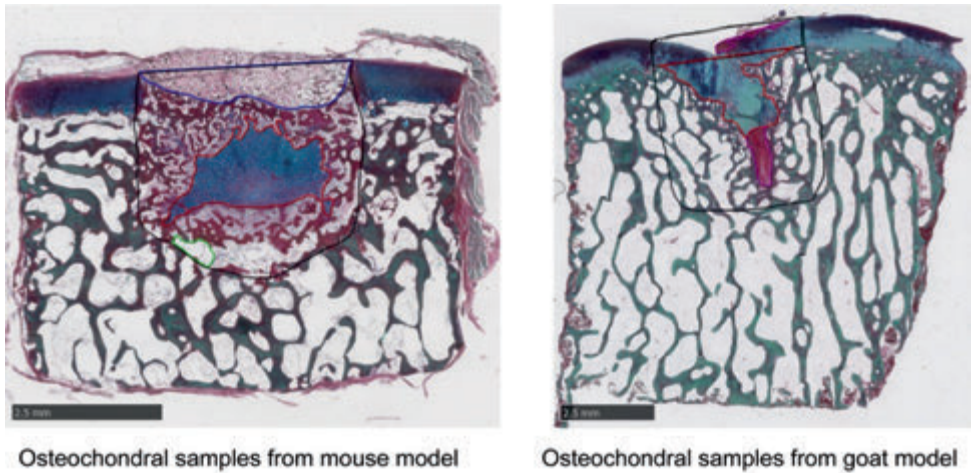
Parameter	Variables	Scores
Degree of defect repair	In level with surrounding cartilage	4
	75% repair of defect depth	3
	50% repair of defect depth	2
	25% repair of defect depth	1
	0% repair of defect depth	0
Integration to border zone	Complete integration with surrounding cartilage	4
	Demarcating border < 1 mm	3
	¼ of graft integrated, ¼ with a notable border > 1 mm	2
	1/2 of graft integrated with surrounding cartilage, 1/2 with a notable border > 1 mm	1
	From no contact to ¼ of graft integrated with surrounding cartilage	0
Macroscopic appearance	Intact smooth surface	4
	Fibrillated surface	3
	Small, scattered fissures or cracks	2
	Several, small or few but large fissures	1
	Total degeneration of grafted area	0
Overall	Grade I normal	12
	Grade II nearly normal	11-8
	Grade III abnormal	7-4
	Grade IV severely abnormal	3-1

Table S4: A semi-quantitative macroscopic scoring system developed by Goebel et al. for the macroscopic description of articular cartilage repair.

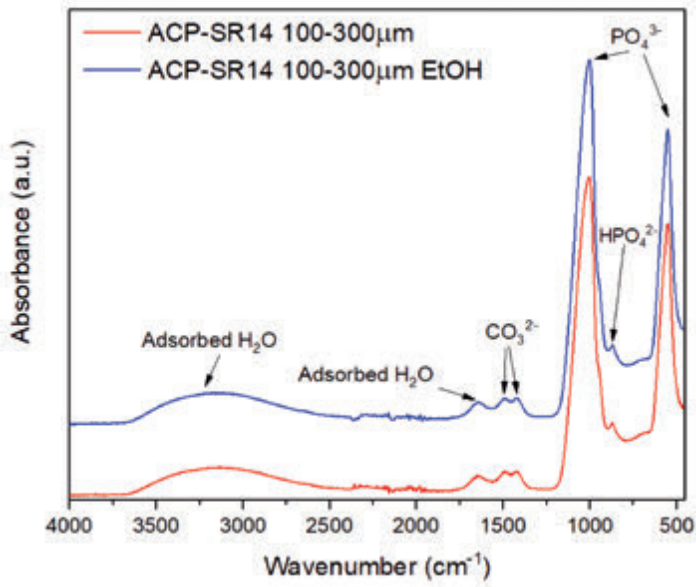
Parameter	Variables	Scores
Color of the repair tissue	Hyaline or white	4
	Predominantly white (>50%)	3
	Predominantly translucent (>50%)	2
	Translucent	1
	No repair tissue	0
Presence of blood vessels in the repair tissue	No	4
	Less than 25% of the repair tissue	3
	25-50% of the repair tissue	2
	50-75% of the repair tissue	1
	More than 75% of the repair tissue	0
Degeneration of adjacent articular cartilage	Normal	4
	Cracks and/or fibrillations in integration zone	3
	Diffuse osteoarthritic changes	2
	Extension of defect into the adjacent cartilage	1
	Subchondral bone damage	0
Surface of the repair tissue	Smooth, homogeneous	4
	Smooth, heterogeneous	3
	Fibrillated	2
	Incomplete new repair tissue (rough)	1
	No repair tissue	0
Percentage defect filling	80-100 %	4
	60-80 %	3
	40-60 %	2
	20-40%	1
	0-20 %	0
Total Scores		20



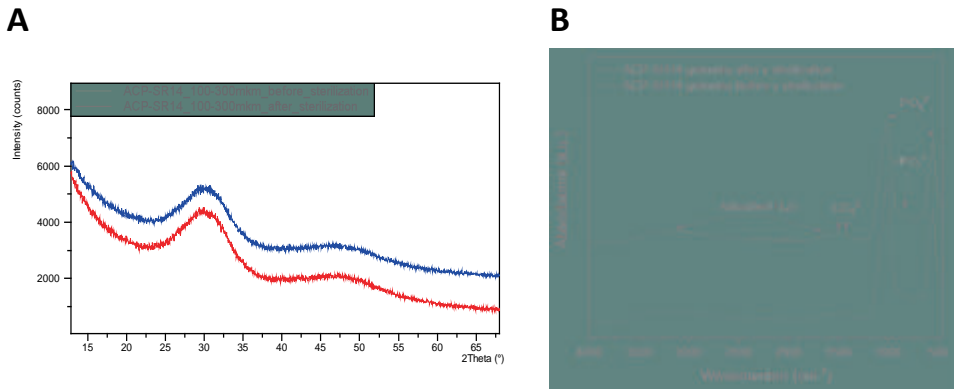
Supplementary Figure S1. Collection of sections from mouse model and goat model for histology.



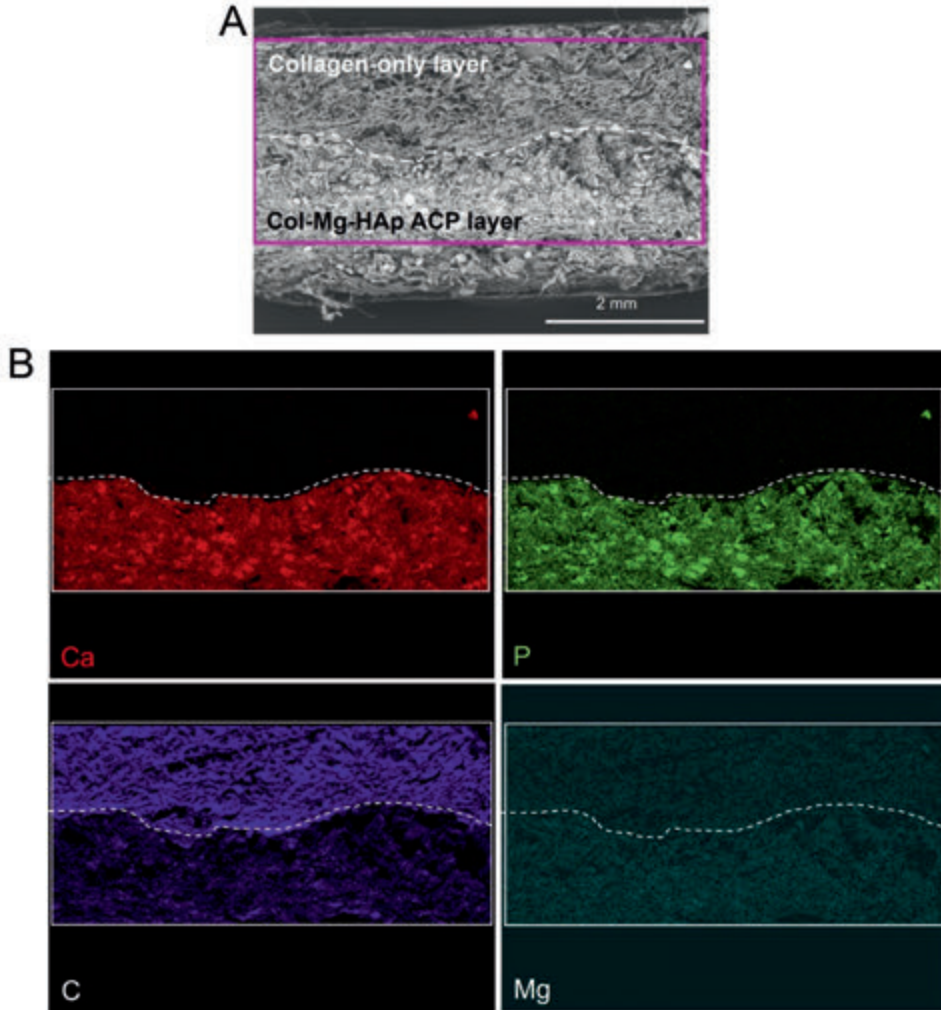
Supplementary Figure S2. Example on defining the defect region, newly formed cartilage-like tissue formation, bone-like tissue formation, fibrous-like tissue formation, remnants of the scaffold for quantification. Scale bars indicated 2.5 mm.



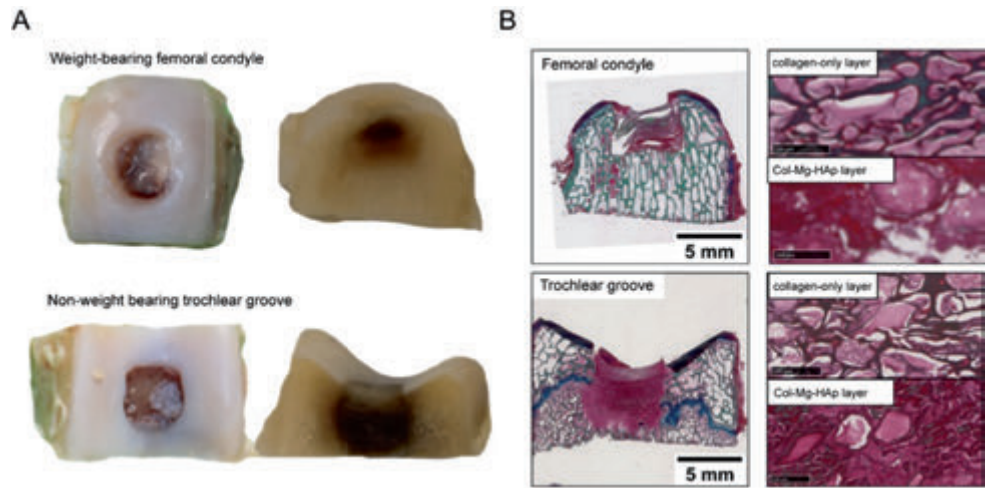
Supplementary Figure S3: FT-IR spectra of ACP granules before and after rinsing in EtOH to remove debris resulted from dry milling process.



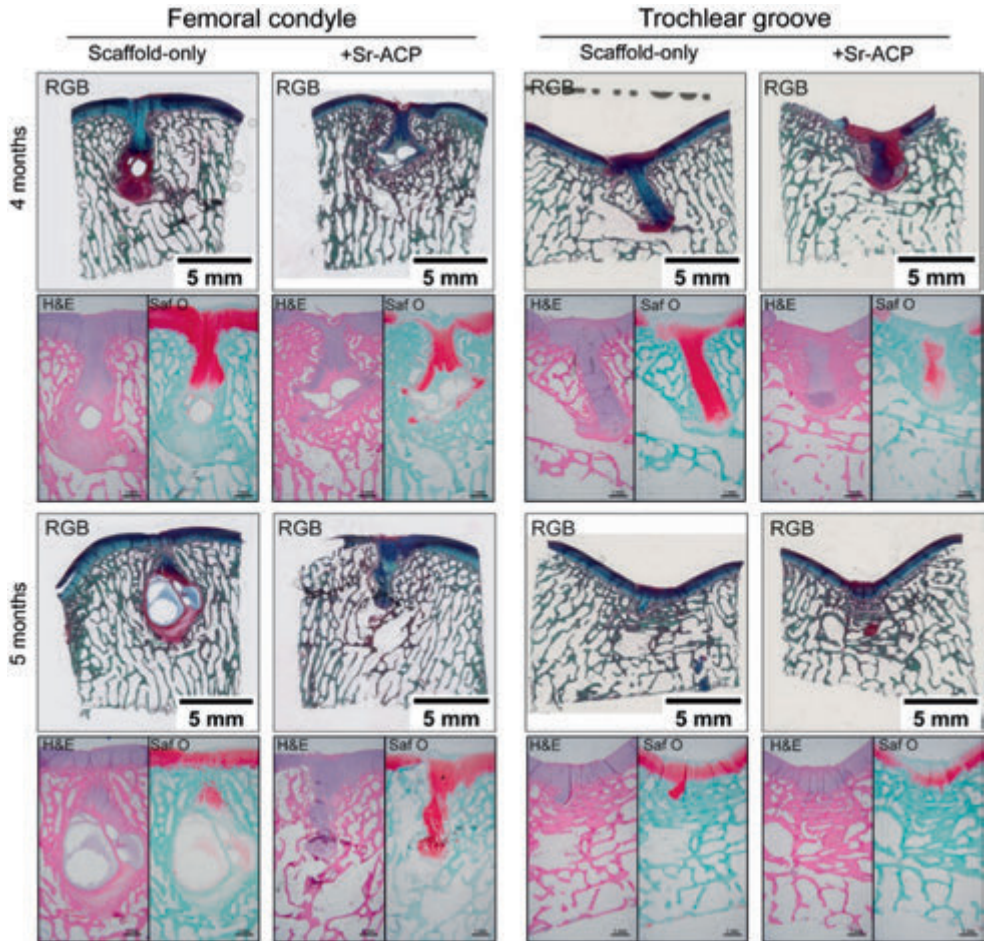
Supplementary Figure S4: XRD patterns (A) and (FT-IR) spectra of ACP granules before and after γ sterilization.



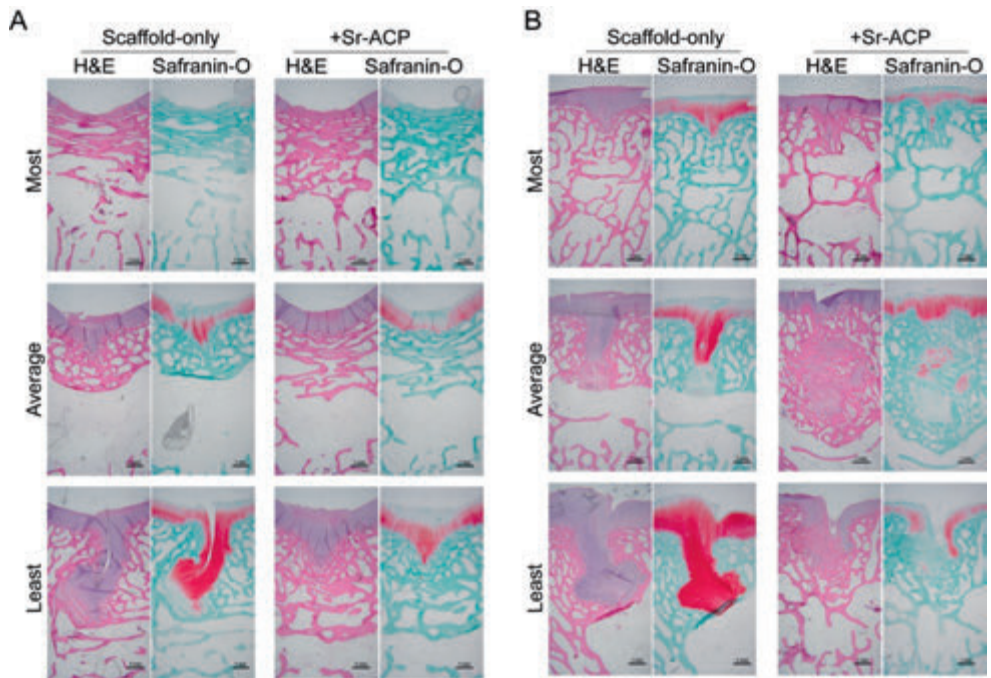
Supplementary Figure S5: Morphological and chemical characterization of ACP enriched Col/Col-Mg-HAp scaffold. (A) SEM image in backscattered electron (BSE) detector mode of cross-section of the ACP granule containing Col/Col-Mg-HAp scaffold, where the top layer is collagen and the bottom layer is collagen-Mg-HAp layer enriched with ACP granules. EDS element (Calcium, Ca - red, Phosphorus, P - green, Magnesium, Mg - dark green, Carbon, C - purple) maps of the scaffold visualized on (A), where the dashed line shows the border between both layers and the brightest areas in Ca and P maps represent positions of the ACP granules.



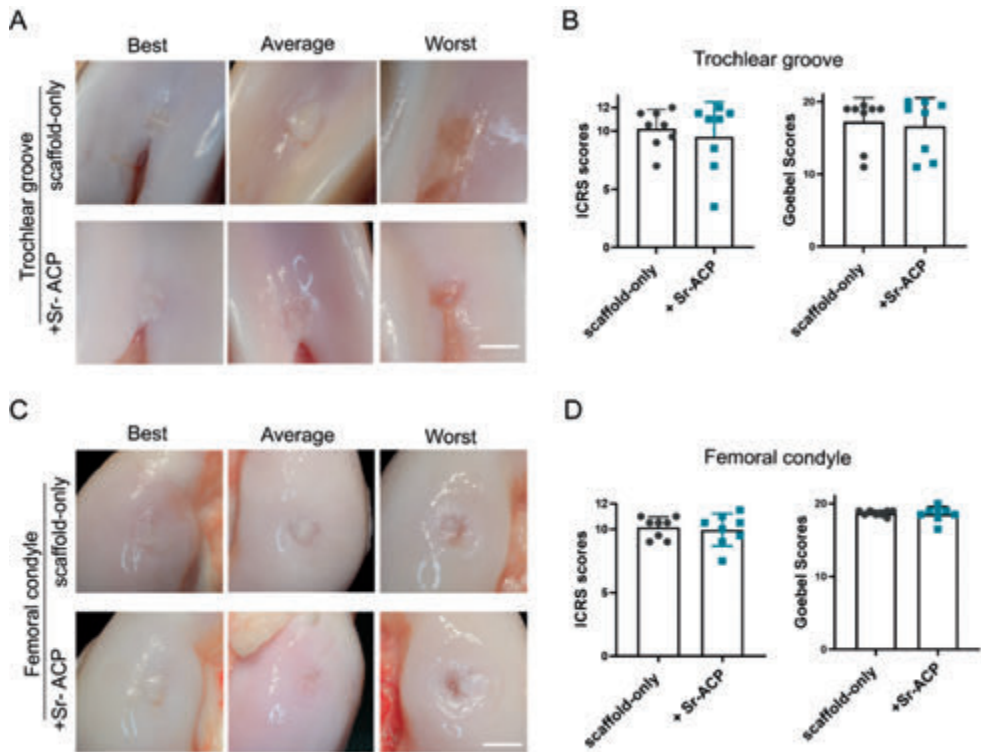
Supplementary Figure S6: (A) The macroscopic appearance of a femoral condyle defect and a trochlear groove defect 2 weeks after implantation. (B) Two layers of the scaffold implanted in the femoral condyle defect after 2 weeks (stained with Alcian Blue, Fast Green, and Picrosirius Red). The scale bar indicates 5 mm and 100 μ m.



Supplementary Figure S7: Osteochondral repair at 4- or 5-month post-surgery. RGB (Alcian Blue, Fast Green, and Picrosirius Red) staining, H&E staining, and Safranin-O staining of femoral condyle defects and trochlear groove defects treated with either scaffold-only or scaffold + Sr-ACP.



Supplementary Figure S8: Osteochondral repair at 6 months post-surgery. H&E staining and Safranin-O staining of trochlear groove (A) and femoral condyle (B) defects treated with either scaffold-only or scaffold + Sr-ACP. Samples with most, average, and least bone-like tissue in bone defects are presented. The scale bar indicates 1 mm.



Supplementary Figure S9: Macroscopic assessment of trochlear groove and femoral condyle defect repair. (A) Representative examples of trochlear groove defect sites treated with scaffold-only or Sr-ACP enriched scaffold after 6 months. Best, average, and worst samples were determined according to the ICRS scores. (B) Macroscopic scores of repair tissue in the trochlear groove defects. (C) Representative examples of femoral condyle defect sites treated with scaffold-only or scaffold with Sr-ACP after 6 months. Best, average, and worst samples were determined according to the ICRS scores. (D) Macroscopic scores of repair tissue in femoral condyle defects. The maximum score for ICRS is 12 (indicating the best), and the maximum score for Goebel score is 20 (indicating the best).

REFERENCES

- [1] Temenoff JS, Mikos AG. Review: tissue engineering for regeneration of articular cartilage. *Biomaterials*. 2000;21(5):431-440.
- [2] Mano JF, Reis RL. Osteochondral defects: present situation and tissue engineering approaches. *Journal of Tissue Engineering and Regenerative Medicine*. 2007;1(4):261-273.
- [3] McCarrel TM, Pownder SL, Gilbert S, Koff MF, Castiglione E, Saska RA, Bradica G, Fortier LA. Two-Year Evaluation of Osteochondral Repair with a Novel Biphasic Graft Saturated in Bone Marrow in an Equine Model. *Cartilage*. 2017;8(4):406-416.
- [4] Mahmoud EE, Kamei N, Kamei G, Nakasa T, Shimizu R, Harada Y, Adachi N, Misk NA, Ochi M. Role of Mesenchymal Stem Cells Densities When Injected as Suspension in Joints with Osteochondral Defects. *Cartilage*. 2019;10(1):61-69.
- [5] Kreuz PC, Steinwachs M, Erggelet C, Krause SJ, Ossendorf C, Maier D, Ghanem N, Uhl M, Haag M. Classification of graft hypertrophy after autologous chondrocyte implantation of full-thickness chondral defects in the knee. *Osteoarthritis and Cartilage*. 2007;15(12):1339-1347.
- [6] Gomoll AH, Madry H, Knutsen G, van Dijk N, Seil R, Brittberg M, Kon E. The subchondral bone in articular cartilage repair: current problems in the surgical management. *Knee Surgery, Sports Traumatology, Arthroscopy*. 2010;18(4):434-447.
- [7] Kon E, Delcogliano M, Filardo G, Fini M, Giavaresi G, Francioli S, Martin I, Pressato D, Arcangeli E, Quarto R, Sandri M, Marcacci M. Orderly osteochondral regeneration in a sheep model using a novel nano-composite multilayered biomaterial. *J Orthop Res*. 2010;28(1):116-124.
- [8] Kon E, Filardo G, Perdisa F, Venieri G, Marcacci M. Clinical results of multilayered biomaterials for osteochondral regeneration. *J Exp Orthop*. 2014;1(1):10.
- [9] Sessa A, Romandini I, Andriolo L, Di Martino A, Busacca M, Zaffagnini S, Filardo G. Treatment of Juvenile Knee Osteochondritis Dissecans with a Cell-Free Biomimetic Osteochondral Scaffold: Clinical and MRI Results at Mid-Term Follow-up. *Cartilage*. 2021;13(1_suppl):1137s-1147s.
- [10] Xue X, Hu Y, Deng Y, Su J. Recent advances in design of functional biocompatible hydrogels for bone tissue engineering. *Advanced Functional Materials*. 2021;31(19):2009432.
- [11] Antonia I, Paltanea VM, Paltanea G, Antoniac A, Nemoianu IV, Petrescu MI, Dura H, Bodog AD. Additive Manufactured Magnesium-Based Scaffolds for Tissue Engineering. *Materials (Basel)*. 2022;15(23):8693.
- [12] Kon E, Delcogliano M, Filardo G, Pressato D, Busacca M, Grigolo B, Desando G, Marcacci M. A novel nano-composite multi-layered biomaterial for treatment of osteochondral lesions: technique note and an early stability pilot clinical trial. *Injury*. 2010;41(7):693-701.
- [13] Perdisa F, Filardo G, Sessa A, Busacca M, Zaffagnini S, Marcacci M, Kon E. One-Step Treatment for Patellar Cartilage Defects With a Cell-Free Osteochondral Scaffold: A Prospective Clinical and MRI Evaluation. *The American Journal of Sports Medicine*. 2017;45(7):1581-1588.
- [14] Di Martino A, Perdisa F, Filardo G, Busacca M, Kon E, Marcacci M, Zaffagnini S. Cell-Free Biomimetic Osteochondral Scaffold for the Treatment of Knee Lesions: Clinical and

Imaging Results at 10-Year Follow-up. *The American Journal of Sports Medicine*. 2021;49(10):2645-2650.

[15] Dhollander AA, Huysse WC, Verdonk PC, Verstraete KL, Verdonk R, Verbruggen G, Almqvist KF. MRI evaluation of a new scaffold-based allogenic chondrocyte implantation for cartilage repair. *European Journal of Radiology*. 2010;75(1):72-81.

[16] Von Euw S, Wang Y, Laurent G, Drouet C, Babonneau F, Nassif N, Azaïs T. Bone mineral: new insights into its chemical composition. *Scientific Reports*. 2019;9(1):8456.

[17] Ratnayake JTB, Mucalo M, Dias GJ. Substituted hydroxyapatites for bone regeneration: A review of current trends. *J Biomed Mater Res B Appl Biomater*. 2017;105(5):1285-1299.

[18] Combes C, Rey C. Amorphous calcium phosphates: synthesis, properties and uses in biomaterials. *Acta Biomaterialia*. 2010;6(9):3362-3378.

[19] Dorozhkin SV. Synthetic amorphous calcium phosphates (ACPs): preparation, structure, properties, and biomedical applications. *Biomater Sci*. 2021;9(23):7748-7798.

[20] Bertolotti F, Carmona FJ, Dal Sasso G, Ramírez-Rodríguez GB, Delgado-López JM, Pedersen JS, Ferri F, Masciocchi N, Guagliardi A. On the amorphous layer in bone mineral and biomimetic apatite: A combined small- and wide-angle X-ray scattering analysis. *Acta Biomaterialia*. 2021;120:167-180.

[21] Degli Esposti L, Iafisco M. Amorphous calcium phosphate, the lack of order is an abundance of possibilities. *Biomater Biosyst*. 2022;5:100037.

[22] Lodoso-Torrecilla I, Klein Gunnewiek R, Grosfeld EC, de Vries RBM, Habibović P, Jansen JA, van den Beucken J. Bioinorganic supplementation of calcium phosphate-based bone substitutes to improve *in vivo* performance: a systematic review and meta-analysis of animal studies. *Biomater Sci*. 2020;8(17):4792-4809.

[23] Wan B, Wang R, Sun Y, Cao J, Wang H, Guo J, Chen D. Building Osteogenic Microenvironments With Strontium-Substituted Calcium Phosphate Ceramics. *Front Bioeng Biotechnol*. 2020;8:591467.

[24] Pilmane M, Salma-Ancane K, Loca D, Locs J, Berzina-Cimdina L. Strontium and strontium ranelate: Historical review of some of their functions. *Mater Sci Eng C Mater Biol Appl*. 2017;78:1222-1230.

[25] Gavinho SR, Pádua AS, Holz LIV, Sá-Nogueira I, Silva JC, Borges JP, Valente MA, Graça MPF. Bioactive Glasses Containing Strontium or Magnesium Ions to Enhance the Biological Response in Bone Regeneration. *Nanomaterials (Basel)*. 2023;13(19):2717.

[26] Kostka K, Hosseini S, Epple M. *In Vitro* Cell Response to Strontium/Magnesium-Doped Calcium Phosphate Nanoparticles. *Micro*. 2023;3(1):156-171.

[27] Bose S, Fielding G, Tarafder S, Bandyopadhyay A. Understanding of dopant-induced osteogenesis and angiogenesis in calcium phosphate ceramics. *Trends Biotechnol*. 2013;31(10):594-605.

[28] Dommeti VK, Roy S, Pramanik S, Merdji A, Ouldyyerou A, Özcan M. Design and Development of Tantalum and Strontium Ion Doped Hydroxyapatite Composite Coating on Titanium Substrate: Structural and Human Osteoblast-like Cell Viability Studies. *Materials (Basel)*. 2023;16(4):1499.

[29] Schumacher M, Gelinsky M. Strontium modified calcium phosphate cements - approaches towards targeted stimulation of bone turnover. *J Mater Chem B*. 2015;3(23):4626-4640.

- [30] Jiménez M, Abradelo C, San Román J, Rojo L. Bibliographic review on the state of the art of strontium and zinc based regenerative therapies. Recent developments and clinical applications. *J Mater Chem B*. 2019;7(12):1974-1985.
- [31] Zhang S, Dong Y, Chen M, Xu Y, Ping J, Chen W, Liang W. Recent developments in strontium-based biocomposites for bone regeneration. *J Artif Organs*. 2020;23(3):191-202.
- [32] Neves N, Linhares D, Costa G, Ribeiro CC, Barbosa MA. *In Vivo* and clinical application of strontium-enriched biomaterials for bone regeneration: A systematic review. *Bone Joint Res*. 2017;6(6):366-375.
- [33] Vecstaudza J, Locs J. Effect of synthesis temperature and Ca/P ratios on specific surface area of amorphous calcium phosphate. *Key Engineering Materials*. Trans Tech Publ; 2017. p. 172-176.
- [34] Vecstaudza J, Locs J. Novel preparation route of stable amorphous calcium phosphate nanoparticles with high specific surface area. *Journal of Alloys and Compounds*. 2017;700:215-222.
- [35] Vecstaudza J, Gasik M, Locs J. Amorphous calcium phosphate materials: Formation, structure and thermal behaviour. *Journal of the European Ceramic Society*. 2019;39(4):1642-1649.
- [36] Rubenis K, Zemjane S, Vecstaudza J, Biteniekis J, Locs J. Densification of amorphous calcium phosphate using principles of the cold sintering process. *Journal of the European Ceramic Society*. 2021;41(1):912-919.
- [37] Pagani S, Salerno M, Filardo G, Locs J, van Osch GJVM, Vecstaudza J, Dolcini L, Borsari V, Fini M, Columbaro M. Human Osteoblasts' Response to Biomaterials for Subchondral Bone Regeneration in Standard and Aggressive Environments. *Int J Mol Sci*. 2023;24(19):14764.
- [38] Cai Z, Li Y, Song W, He Y, Li H, Liu X. Anti-Inflammatory and Prochondrogenic *In Situ*-Formed Injectable Hydrogel Crosslinked by Strontium-Doped Bioglass for Cartilage Regeneration. *ACS Applied Materials & Interfaces*. 2021;13(50):59772-59786.
- [39] Yu H, Liu Y, Yang X, He J, Zhang F, Zhong Q, Guo X. Strontium ranelate promotes chondrogenesis through inhibition of the Wnt/ β -catenin pathway. *Stem Cell Res Ther*. 2021;12(1):296.
- [40] Elliott JC. Structure and Chemistry of the Apatites and Other Calcium Orthophosphates. 1994.
- [41] de Vries-van Melle ML, Narcisi R, Kops N, Koevoet WJ, Bos PK, Murphy JM, Verhaar JA, van der Kraan PM, van Osch GJ. Chondrogenesis of mesenchymal stem cells in an osteochondral environment is mediated by the subchondral bone. *Tissue Engineering Part A*. 2014;20(1-2):23-33.
- [42] Levingstone TJ, Ramesh A, Brady RT, Brama PAJ, Kearney C, Gleeson JP, O'Brien FJ. Cell-free multi-layered collagen-based scaffolds demonstrate layer specific regeneration of functional osteochondral tissue in caprine joints. *Biomaterials*. 2016;87:69-81.
- [43] Browe DC, Burdis R, Díaz-Payno PJ, Freeman FE, Nulty JM, Buckley CT, Brama PAJ, Kelly DJ. Promoting endogenous articular cartilage regeneration using extracellular matrix scaffolds. *Materials Today Bio*. 2022;16:100343.
- [44] Burdis R, Chariyev-Prinz F, Browe DC, Freeman FE, Nulty J, McDonnell EE, Eichholz KF, Wang B, Brama P, Kelly DJ. Spatial patterning of phenotypically distinct microtissues to engineer osteochondral grafts for biological joint resurfacing. *Biomaterials*. 2022;289:121750.

- [45] Van den Borne M, Raijmakers N, Vanlauwe J, Victor J, De Jong S, Bellemans J, Saris D. International Cartilage Repair Society (ICRS) and Oswestry macroscopic cartilage evaluation scores validated for use in Autologous Chondrocyte Implantation (ACI) and microfracture. *Osteoarthritis and Cartilage*. 2007;15(12):1397-1402.
- [46] Goebel L, Orth P, Müller A, Zurakowski D, Bückler A, Cucchiari M, Pape D, Madry H. Experimental scoring systems for macroscopic articular cartilage repair correlate with the MOCART score assessed by a high-field MRI at 9.4 T--comparative evaluation of five macroscopic scoring systems in a large animal cartilage defect model. *Osteoarthritis and Cartilage*. 2012;20(9):1046-1055.
- [47] Querido W, Shanas N, Bookbinder S, Oliveira-Nunes MC, Krynska B, Pleshko N. Fourier transform infrared spectroscopy of developing bone mineral: from amorphous precursor to mature crystal. *Analyst*. 2020;145(3):764-776.
- [48] Habraken W, Habibovic P, Epple M, Bohner M. Calcium phosphates in biomedical applications: materials for the future? *Materials Today*. 2016;19(2):69-87.
- [49] Mahamid J, Sharir A, Addadi L, Weiner S. Amorphous calcium phosphate is a major component of the forming fin bones of zebrafish: Indications for an amorphous precursor phase. *Proc Natl Acad Sci U S A*. 2008;105(35):12748-12753.
- [50] Combes C, Rey C. Amorphous calcium phosphates: Synthesis, properties and uses in biomaterials. *Acta Biomaterialia*. 2010;6(9):3362-3378.
- [51] Gao Y, Weng W, Cheng K, Du P, Shen G, Han G, Guan B, Yan W. Preparation, characterization and cytocompatibility of porous ACP/PLLA composites. *J Biomed Mater Res A*. 2006;79(1):193-200.
- [52] Nagano M, Nakamura T, Kokubo T, Tanahashi M, Ogawa M. Differences of bone bonding ability and degradation behaviour *in vivo* between amorphous calcium phosphate and highly crystalline hydroxyapatite coating. *Biomaterials*. 1996;17(18):1771-1777.
- [53] Huang X, Yang D, Yan W, Shi Z, Feng J, Gao Y, Weng W, Yan S. Osteochondral repair using the combination of fibroblast growth factor and amorphous calcium phosphate/poly(L-lactic acid) hybrid materials. *Biomaterials*. 2007;28(20):3091-3100.
- [54] Olszta MJ, Cheng X, Jee SS, Kumar R, Kim Y-Y, Kaufman MJ, Douglas EP, Gower LB. Bone structure and formation: A new perspective. *Materials Science and Engineering: R: Reports*. 2007;58(3-5):77-116.
- [55] Pryor LS, Gage E, Langevin C-J, Herrera F, Breithaupt AD, Gordon CR, Afifi AM, Zins JE, Meltzer H, Gosman A. Review of bone substitutes. *Craniofacial Trauma & Reconstruction*. 2009;2(3-4):151-160.
- [56] Dorozhkin SV. Calcium orthophosphates (CaPO₄): occurrence and properties. *Progress in Biomaterials*. 2016;5(1):9-70.
- [57] Gleeson JP, Plunkett NA, O'Brien FJ. Addition of hydroxyapatite improves stiffness, interconnectivity and osteogenic potential of a highly porous collagen-based scaffold for bone tissue regeneration. *European Cells & Materials*. 2010;20:218-230.
- [58] Vines JB, Lim DJ, Anderson JM, Jun HW. Hydroxyapatite nanoparticle reinforced peptide amphiphile nanomatrix enhances the osteogenic differentiation of mesenchymal stem cells by compositional ratios. *Acta Biomaterialia*. 2012;8(11):4053-4063.
- [59] Tampieri A, Sandri M, Landi E, Pressato D, Francioli S, Quarto R, Martin I. Design of graded biomimetic osteochondral composite scaffolds. *Biomaterials*. 2008;29(26):3539-3546.

- [60] Sosio C, Di Giancamillo A, Deponti D, Gervaso F, Scalera F, Melato M, Campagnol M, Boschetti F, Nonis A, Domeneghini C, Sannino A, Peretti GM. Osteochondral repair by a novel interconnecting collagen-hydroxyapatite substitute: a large-animal study. *Tissue Engineering Part A*. 2015;21(3-4):704-715.
- [61] Levingstone TJ, Thompson E, Matsiko A, Schepens A, Gleeson JP, O'Brien FJ. Multi-layered collagen-based scaffolds for osteochondral defect repair in rabbits. *Acta Biomaterialia*. 2016;32:149-160.
- [62] Fulmer MT, Ison IC, Hankermayer CR, Constantz BR, Ross J. Measurements of the solubilities and dissolution rates of several hydroxyapatites. *Biomaterials*. 2002;23(3):751-755.
- [63] Bose S, Fielding G, Tarafder S, Bandyopadhyay A. Understanding of dopant-induced osteogenesis and angiogenesis in calcium phosphate ceramics. *Trends in Biotechnology*. 2013;31(10):594-605.
- [64] Radzki RP, Bieńko M, Filip R. Wpływ ranelinianiu strontu na mineralizację i wytrzymałość mechaniczną kości udowej orchidektomizowanych szczurów. *Med Weter*. 2007;63:163-164.
- [65] Marx D, Rahimnejad Yazdi A, Papini M, Towler M. A review of the latest insights into the mechanism of action of strontium in bone. *Bone Rep*. 2020;12:100273.
- [66] Kołodziejaska B, Stępień N, Kolmas J. The Influence of Strontium on Bone Tissue Metabolism and Its Application in Osteoporosis Treatment. *International Journal of Molecular Sciences*. 2021;22(12):6564.
- [67] Saidak Z, Marie PJ. Strontium signaling: molecular mechanisms and therapeutic implications in osteoporosis. *Pharmacology & Therapeutics*. 2012;136(2):216-226.
- [68] Root MJ. Inhibition of the amorphous calcium phosphate phase transformation reaction by polyphosphates and metal ions. *Calcified Tissue International*. 1990;47(2):112-116.
- [69] Jin W, Liu Z, Wu Y, Jin B, Shao C, Xu X, Tang R, Pan H. Synergic Effect of Sr²⁺ and Mg²⁺ on the Stabilization of Amorphous Calcium Phosphate. *Crystal Growth & Design*. 2018;18(10):6054-6060.
- [70] Boskey AL, Posner AS. Magnesium stabilization of amorphous calcium phosphate: a kinetic study. *Materials Research Bulletin*. 1974;9(7):907-916.
- [71] Blumenthal NC, Betts F, Posner AS. Stabilization of amorphous calcium phosphate by Mg and ATP. *Calcified Tissue Research*. 1977;23(1):245-250.
- [72] Ding H, Pan H, Xu X, Tang R. Toward a detailed understanding of magnesium ions on hydroxyapatite crystallization inhibition. *Crystal Growth & Design*. 2014;14(2):763-769.
- [73] de Vries-van Melle ML, Tihaya MS, Kops N, Koevoet WJ, Murphy JM, Verhaar JA, Alini M, Eglin D, van Osch GJ. Chondrogenic differentiation of human bone marrow-derived mesenchymal stem cells in a simulated osteochondral environment is hydrogel dependent. *European Cells & Materials*. 2014;27:112-123; discussion 123.
- [74] Kon E, Delcogliano M, Filardo G, Busacca M, Di Martino A, Marcacci M. Novel nano-composite multilayered biomaterial for osteochondral regeneration: a pilot clinical trial. *The American Journal of Sports Medicine*. 2011;39(6):1180-1190.
- [75] Kon E, Muttini A, Arcangeli E, Delcogliano M, Filardo G, Nicoli Aldini N, Pressato D, Quarto R, Zaffagnini S, Marcacci M. Novel nanostructured scaffold for osteochondral regeneration: pilot study in horses. *Journal of Tissue Engineering and Regenerative Medicine*. 2010;4(4):300-308.

- [76] Davis S, Roldo M, Blunn G, Tozzi G, Roncada T. Influence of the Mechanical Environment on the Regeneration of Osteochondral Defects. *Front Bioeng Biotechnol.* 2021;9:603408.
- [77] van Bergen CJ, Kerkhoffs GM, Marsidi N, Korstjens CM, Everts V, van Ruijven LJ, van Dijk CN, Blankevoort L. Osteochondral defects of the talus: a novel animal model in the goat. *Tissue Engineering Part C Methods.* 2013;19(6):449-457.
- [78] Maglio M, Brogini S, Pagani S, Giavaresi G, Tschon M. Current Trends in the Evaluation of Osteochondral Lesion Treatments: Histology, Histomorphometry, and Biomechanics in Preclinical Models. *Biomed Res Int.* 2019;2019:4040236.
- [79] Sartori M, Pagani S, Ferrari A, Costa V, Carina V, Figallo E, Maltarello MC, Martini L, Fini M, Giavaresi G. A new bi-layered scaffold for osteochondral tissue regeneration: *In Vitro* and *In Vivo* preclinical investigations. *Mater Sci Eng C Mater Biol Appl.* 2017;70:101-111.
- [80] Grigolo B, Cavallo C, Desando G, Manferdini C, Lisignoli G, Ferrari A, Zini N, Facchini A. Novel nano-composite biomimetic biomaterial allows chondrogenic and osteogenic differentiation of bone marrow concentrate derived cells. *J Mater Sci Mater Med.* 2015;26:173.
- [81] Manferdini C, Cavallo C, Grigolo B, Fiorini M, Nicoletti A, Gabusi E, Zini N, Pressato D, Facchini A, Lisignoli G. Specific inductive potential of a novel nanocomposite biomimetic biomaterial for osteochondral tissue regeneration. *J Tissue Eng Regen Med.* 2016;10:374-391.
- [82] Siebert CH, Miltner O, Weber M, Sopka S, Koch S, Niedhart C. Healing of osteochondral grafts in an ovine model under the influence of bFGF. *Arthroscopy.* 2003;19(2):182-187.

5

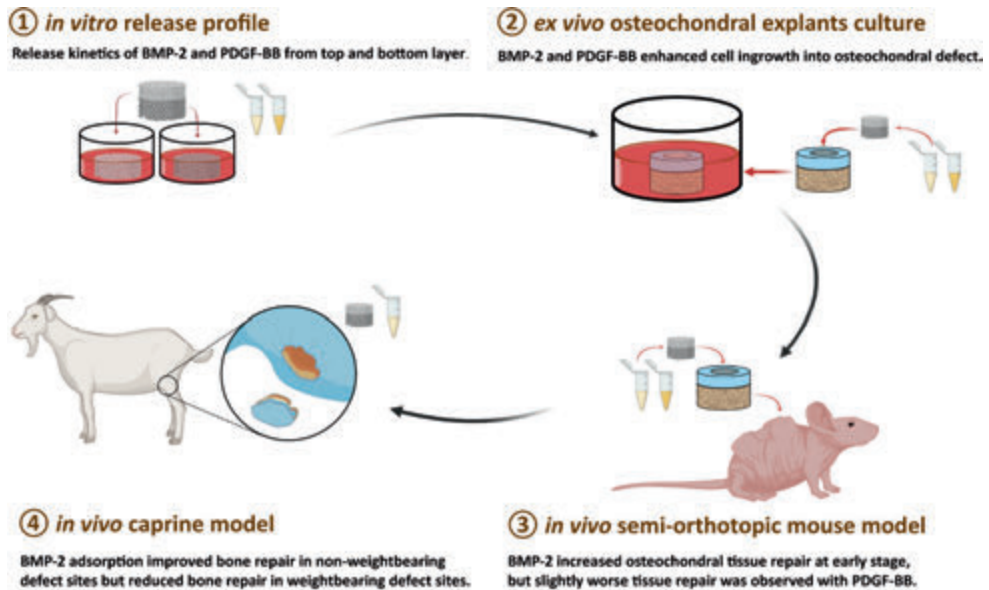
Effectiveness of BMP-2 and PDGF-BB adsorption onto a collagen/collagen-magnesium-hydroxyapatite scaffold in weight-bearing and non-weight-bearing osteochondral defect bone repair: *in vitro*, *ex vivo* and *in vivo* evaluation

Jietao Xu, Shorouk Fahmy-Garcia, Marinus A Wesdorp, Nicole Kops, Lucia Forte, Claudio De Luca, Massimiliano Maraglino Misciagna, Laura Dolcini, Giuseppe Filardo, Margot Labberté, Karin Vancíková, Joeri Kok, Bert van Rietbergen, Joachim Nickel, Eric Farrell, Pieter A.J. Brama, Gerjo J.V. M. van Osch

ABSTRACT

Despite promising clinical results in osteochondral defect repair, a recently developed bi-layered collagen/collagen-magnesium-hydroxyapatite scaffold has demonstrated less optimal subchondral bone repair. This study aimed to improve the bone repair potential of this scaffold by adsorbing bone morphogenetic protein 2 (BMP-2) and/or platelet-derived growth factor-BB (PDGF-BB) onto said scaffold. The *in vitro* release kinetics of BMP-2/PDGF-BB demonstrated that PDGF-BB was burst released from the collagen-only layer, whereas BMP-2 was largely retained in both layers. Cell ingrowth was enhanced by BMP-2/PDGF-BB in a bovine osteochondral defect *ex vivo* model. In an *in vivo* semi-orthotopic athymic mouse model, adding BMP-2 or PDGF-BB increased tissue repair after four weeks. After eight weeks, most defects were filled with bone tissue. To further investigate the promising effect of BMP-2, a caprine bilateral stifle osteochondral defect model was used where defects were created in weight-bearing femoral condyle and non-weight-bearing trochlear groove locations. After six months, the adsorption of BMP-2 resulted in significantly less bone repair compared with scaffold-only in the femoral condyle defects and a trend to more bone repair in the trochlear groove. Overall, the adsorption of BMP-2 onto a Col/Col-Mg-HAp scaffold reduced bone formation in weight-bearing osteochondral defects, but not in non-weight-bearing osteochondral defects.

Keywords: tissue engineering; regenerative medicine; osteochondral lesion; biocompatible materials; bone morphogenetic proteins; platelet-derived growth factor; animal model; weight-bearing



1. INTRODUCTION

Osteochondral tissue is formed by two main tissue types: the articular cartilage, which functions as a low-friction and wear-resistant surface, and the subchondral bone, which plays a crucial mechanically supportive role [1]. Without effective and timely interventions, damage to this osteochondral unit, caused by traumatic injury or disease, may progress to osteoarthritis [2,3]. Bi-layered biomaterial scaffolds have been developed to restore the structural and physiological properties of the entire osteochondral unit and, thus, to support chondrogenesis and osteogenesis simultaneously [4,5]. As a biologically derived protein, collagen is an efficient biomaterial to support cellular activities and promote osteochondral repair [6,7,8]. The addition of hydroxyapatite (HAP) can improve the osteogenic potential of a collagen-based scaffold *in vivo*, and magnesium ions (Mg^{2+}) induce osteogenic differentiation and osteoblast differentiation [9]. Preclinically, bi-layered collagen/collagen-magnesium-HAP (Col/Col-Mg-HAP) scaffolds have successfully reconstructed the articular cartilage and the subchondral bone in animal models [10,11,12]. Clinical cohort studies also demonstrated the excellent stability of this scaffold and clinical improvement in knee function [13,14,15]. However, subchondral bone repair remained suboptimal in some clinical follow-ups in comparison to the cartilage repair capacity of this scaffold [15], which may lead to altered biomechanical properties of the osteochondral unit and thereby affect the long-term survival of the neo-cartilage [16]. This might subsequently lead to renewed osteochondral damage and joint disease [17,18].

Incorporating factors that stimulate bone formation could be a promising approach to overcome this limitation in bone regeneration capacity [19]. Bone morphogenetic protein 2 (BMP-2) has a vital role in osteogenesis and osteoclastogenesis [20,21] and is approved by the Food and Drug Administration (FDA) as an osteogenic protein. The recruitment of stem cells or osteoblasts is necessary for osteogenic initiation, and BMP-2 was reported to facilitate cell ingrowth [22]. Platelet-derived growth factor (PDGF) is potent in stimulating cell ingrowth, angiogenesis, and osteogenesis [23,24,25,26]. The delivery of BMP-2 and PDGF onto biomaterials has been shown to provide an improvement in osteoblast function and bone integration [27,28,29]. Therefore, it might be promising to adsorb BMP-2 and PDGF-BB onto this Col/Col-Mg-HAP scaffold to improve bone healing.

This study aimed to evaluate the osteogenic effectiveness of BMP-2 or PDGF-BB adsorption onto a Col/Col-Mg-HAP scaffold on bone repair in osteochondral defects. We first assessed the release profiles of BMP-2 and PDGF-BB from the two layers of a Col/Col-Mg-HAP scaffold *in vitro*. Next, an *ex vivo* osteochondral culture model was used to investigate the added effect of growth factors on cell ingrowth from adjacent tissues. Then, we investigated the effect of BMP-2 or PDGF-BB incorporated into a Col/Col-Mg-HAP scaffold in an *in vivo* semi-orthotopic mouse model for the early phases of tissue repair. Finally, the effect of BMP-2 incorporated into a Col/Col-Mg-HAP scaffold was investigated in both weight-bearing and non-weight-bearing locations of the knee joint in an established preclinical caprine osteochondral defect model.

2. MATERIALS AND METHODS

2.1. Scaffold fabrication and characterization

Col/Col-Mg-HAp scaffold is a biomimetic scaffold that has a porous, 3-dimensional composite structure. The scaffold is composed of two layers: the cartilaginous layer, consisting of Type I collagen, to maintain joint congruence and the bone layer consisting of a combination of Type I collagen (60%) and magnesium-hydroxyapatite (40%). Each layer of the scaffold is synthesised separately by a standardised process from an atelocollagen aqueous solution (1% w/w) in acetic acid, isolated from equine tendon. The upper non-mineralised chondral layer of the scaffold is obtained by dissolving an acetic solution of Type I collagen in bi-distilled water by adding NaOH. The bone layer of the scaffold is obtained by nucleating nanostructured hydroxyapatite into self-assembling collagen fibres, as occurs in the natural biological neo-ossification process. To stabilise the scaffold, the fibrous structures were chemically cross-linked for 16 hours at room temperature. After chemical cross-linking, the two layers were superimposed and afterwards they are freeze-dried.

The morphology of the scaffold was evaluated by Scanning Electron Microscopy (SEM) performed on a SEM-LEO 438 VP (Carl Zeiss AG, Oberkochen, Germany). The samples were sputter coated with gold prior to examination. The mineral content of the bone layer was evaluated by thermogravimetric analysis (TGA), performed in alumina crucibles in an air atmosphere with a flow rate of 80 mL/min, between 25 and 700 °C (Mettler Toledo DT-TGA/DSC1 Star System, Columbus, OH, USA). The elemental composition of the mineral phase (magnesium-hydroxyapatite) was determined using inductively coupled plasma-optical emission spectrometry (ICP-OES, Thermo Scientific iCAP 7400, Waltham, MA, USA). In particular, the composition is expressed as Ca/P, (Ca+Mg)/P, Mg/Ca% molar ratios. The bone layer was dissolved in hot nitric acid (65 v/v%) in order to completely destroy the collagen matrix and solubilise the inorganic phase. The content (ppm) of magnesium, calcium, and phosphorous in the samples is determined by comparison with a predetermined standard curve: Ca/P = $1.5 \pm 0.1\%$; (Ca+Mg)/P = $1.6 \pm 0.1\%$; Mg/Ca% = $1.5 \pm 0.4\%$. The total porosity of the osteochondral scaffold was determined using Archimedes' principle. The exterior volume (V_s) of the sample was measured using a Vernier calliper. The sample was then immersed in a pycnometer containing 96% ethanol solution. The actual volume (V_a) of the sample is calculated using the formula:

$$V_a = \frac{(W_w - W_o) - (W_t - W_p)}{0.789} \text{ g/cm}^3$$

W_w is the weight of the ethanol and the pycnometer; W_o is the dry weight of the pycnometer; W_t is the combined weight of the ethanol, the pycnometer, and the plug sample; W_p is the combined weight of the dry pycnometer and dry plug sample; and 0.789 g/cm^3 is the density of ethanol solution. The porosity of the scaffold was then determined using the following formula:

$$\text{Total Porosity}(\%) = \frac{V_s - V_a}{V_s} * 100$$

2.2. BMP-2 and PDGF-BB release from the different layers of a Col/Col-Mg-HAp scaffold

To investigate the release kinetics of BMP-2 and PDGF-BB from the different layers of the Col/Col-Mg-HAp scaffold, a time course study was performed (Supplementary Figure S1A). A quantity of 35 μL (28.5 $\mu\text{g/mL}$) BMP-2 or PDGF-BB (Sigma, Saint Louis, MI, USA) was

absorbed into the separated layers (either collagen-only layer or Col-Mg-HAp layer) of a Col/Col-Mg-HAp scaffold (Osteochondral scaffold, Finceramica, Italy) in a low-affinity binding plate at 37 degrees Celsius for 30 min. The concentration of growth factors was determined according to our previous studies [30,31]. After absorption, the medium was harvested from the plate, and the scaffolds were transferred to a new low-affinity binding plate. A quantity of 800 μ L alpha-Minimum Essential Medium (α -MEM, Gibco, Waltham, MA, USA) was added to each scaffold-containing well. At each time point (6, 24, 48, 72, 96, 120, 144, 168 h, 336 h only for BMP-2), the medium was collected and replaced by fresh medium. The collected medium was analysed for BMP-2 by recombinant human BMP-2 (Peprotech, Cranbury, NJ, USA) or PDGF-BB by a recombinant human PDGF-BB DuoSet ELISA kit (R&D Systems, McKinley Place N.E., Minneapolis, MN, USA) according to the manufacturer's instructions.

2.3. Cell recruitment capacity of BMP-2 or PDGF-BB in an *ex vivo* osteochondral defect culture model

To study the effect of BMP-2 and PDGF-BB adsorbed onto a bi-layered Col/Col-Mg-HAp scaffold on cell recruitment capacity, an *ex vivo* osteochondral defect culture model, previously developed and validated in our laboratory, was used [32] (Supplementary Figure S1B). Briefly, osteochondral defects were created in bovine osteochondral biopsies (8 mm diameter, 5 mm height) harvested from metacarpal-phalangeal joints of 6- to 8-month-old calves (LifeTec, Eindhoven, The Netherlands), in which a 4 mm wide and 4 mm high defect was created. The osteochondral plugs were kept overnight in Dulbecco's Modified Eagle Medium high glucose (DMEM, 4.5 g/L glucose, Gibco, Waltham, MA, USA) supplemented with 10% fetal bovine serum (FBS, Gibco, Waltham, MA, USA), 50 μ g/mL gentamycin (Gibco, Waltham, MA, USA), and 1.5 μ g/mL fungizone (Gibco, Waltham, MA, USA). The following day, the Col/Col-Mg-HAp scaffolds (diameter: 4 mm, height: 4 mm) with or without adsorbed growth factors ($n = 4$ for each condition) were inserted into the osteochondral defects. Either 4 μ g (57.1 μ g/mL) BMP-2 solution or 100 ng (1.4 μ g/mL) PDGF-BB was adsorbed onto the scaffold. Each construct was cultured in 3.5 mL medium in a new 12-well plate at 37 °C and 5% CO₂. The medium was refreshed on the first day and subsequently every two days. After 3 weeks, the osteochondral constructs were harvested and fixed in 4% formalin for 1 week with subsequent further histological analysis.

2.4. *In vivo* osteochondral defect model in mice

To assess the effect of BMP-2 and PDGF-BB in the Col/Col-Mg-HAp scaffolds on bone repair, an established *in vivo* subcutaneous mouse model developed previously in our laboratory was used (Supplementary Figure S1C) [33]. Osteochondral biopsies were harvested, and the defects were created as described previously (see under Section 2.3) and kept overnight in α -MEM supplemented with 10% FBS, 50 μ g/mL gentamycin, and 1.5 μ g/mL fungizone until implantation. Eleven 12-week-old NMRI-Fox1nu mice (Taconic, Albany, NY, USA) were used for this study. The animals were randomly assigned and housed under specific-pathogen-free conditions with a regular day/night light cycle and allowed to adapt to the conditions of the animal facility for 7 days. Food and water were available *ad libitum*. Before implantation, 70 μ L of saline solution, or 70 μ L of saline solution containing BMP-2 (57.1 μ g/mL, 4 μ g) or PDGF-BB (28.5 μ g/mL, 2 μ g or 1.4 μ g/mL, 100 ng) was added dropwise onto the Col/Col-Mg-HAp scaffolds. All osteochondral plugs

were covered with a circular 8 mm Neuro-Patch membrane (Braun, Melsungen, Germany) to prevent the ingrowth of host cells from the top. The osteochondral plugs were randomly implanted in subcutaneous pockets on the back of the mice under 2.5-3% isoflurane anaesthesia (1000 mg/g, Laboratorios Karizoo, Maharashtra, India). One osteochondral plug was implanted per pocket, and four osteochondral plugs were implanted per mouse. The incisions were closed with staples (Fine Science Tools, Vancouver, BC, Canada). At 1 h before surgery and at 6-8 h after surgery, 0.05 mg/kg body weight of buprenorphine (Chr. Olesen & Co, Gentofte, Copenhagen, Denmark) was injected subcutaneously to ensure pre- and postoperative analgesia. Mice received a subcutaneous prophylactic antibiotic injection of 25 mg/kg body weight of Amoxicillin (Dopharma, Raamsdonksveer, The Netherlands).

After 4 or 8 weeks, mice were euthanised by cervical dislocation under 2.5-3% isoflurane anaesthesia, and the osteochondral plugs were harvested. All samples were fixed in 4% formalin for 1 week for further analysis. This animal experiment was approved by the Ethics Committee for Laboratory Animal Use (AVD101002016991; protocol #EMC 16-691-05).

2.5. In vivo osteochondral defect caprine model

A validated bilateral osteochondral defect caprine model was used to assess the osteochondral defect repair capacity of BMP-2-supplemented scaffolds in a preclinical large animal model (Supplementary Figure S1D). An experimental unit of 11 skeletally mature female Saanen goats (age: 3 years, weight: 37.9 ± 7.3 kg) was subjected to a bilateral arthrotomy under general anaesthesia as described before [34,35,36]. In short: all animals received a prophylactic antibiotic injection with amoxicillin clavulanic acid 8.75 mg/kg intramuscular (Noroclav, Norbrook, Ireland) and were intravenously sedated with butorphanol (0.2 mg/kg, Butador, Chanelle Pharma, Ireland) and diazepam (0.2 mg/kg, Diazemuls; Accord Healthcare, UK). A lumbosacral epidural block with lidocaine (2 mg/kg, Lidocaine HCl 2%, B. Braun Medical Inc., EU, Melsungen, Germany) and morphine (0.2 mg/kg, Morphine Sulphate 10 mg/mL, Kalceks, Latvia) was performed with the animal in sternal recumbency. Anaesthesia was induced with propofol IV to effect (max. 6 mg/kg, Propofol-Lipuro 1%, B. Braun Medical Inc., Melsungen, German) and was maintained with isoflurane (Vetflurane, Virbac Animal Health, Suffolk, UK) in 100% oxygen via a circle rebreathing system. All animals received analgesia with meloxicam IV (0.5 mg/kg, Rheumocam, Chanelle, Galway, Ireland); and morphine IV (0.2 mg/kg, Morphine sulphate, Mercury Pharmaceuticals, Dublin, Ireland) 90 min after the epidural block.

An arthrotomy of each stifle joint was performed in dorsal recumbency using a lateral parapatellar approach. Under constant irrigation with saline, a pointed 6 mm drill bit was used to drill an approximate 3-4 mm deep non-weight-bearing defect in the transition of the distal 1/3 to the middle 1/3 of the trochlear groove and in the weight-bearing part of the medial femoral condyle. Subsequently, a custom-made flattened drill bit and a depth guide were used to create an exact flat 6 mm deep by 6 mm wide circular critical-sized osteochondral defect in a non-weight-bearing and a weight-bearing location. The joint was flushed with saline to remove any debris, and the defects were press fit with a similar-sized selected scaffold before surgical closure as described before. Each stifle joint was randomly assigned to one of the two treatment groups (Supplementary Figure S1D): (1)

Col/Col-Mg-HAp scaffold-only (6 mm diameter, 6 mm height, Osteochondral scaffold, Finceramica, Italy), and (2) Col/Col-Mg-HAp scaffold adsorbed with BMP-2 (57.1 µg/mL).

Following surgery, postoperative analgesia was provided (meloxicam 5 days) and goats were housed in indoor pens for daily postoperative welfare monitoring and scoring. Two weeks postoperatively, following the removal of skin sutures, animals were released to pasture or loose housing (weather dependent) for the remainder of the study period with daily health checks. An orthopaedic assessment (Table S1) was performed on the day of humane euthanasia under sedation with a barbiturate overdose at the predetermined endpoint at 6 months after surgery. Subsequently, all the joints, surrounding joint tissues, and synovial fluids were scored (Table S2), dissected, and photographed (Body Canon EOS R5, lens: Canon EF 100 mm f/2.8 L Macro IS USM, flash: Macro Ring lite MR-14EX II). Biopsies 1 cm by 1 cm square containing the entire defects were harvested with an oscillating saw.

Ethical evaluation and approval were provided by the Health Products Regulatory Authority of Ireland (AE1898217/P032), the Animal Research Ethics Committee of University College Dublin (AREC-P-12-71) and the Lyons Animal Welfare Board (Health, Husbandry and Monitoring plans).

2.6. Macroscopic assessment of the defect repair in the caprine model

The quality of the cartilage repair in the caprine samples was assessed semi-quantitatively using the International Cartilage Repair Society (ICRS) macroscopic evaluation system (Table S3) [37] and a macroscopic scoring system (Table S4) developed by Goebel et al. [38]. The ICRS scoring system evaluates the macroscopic appearance of cartilage repair tissue as Grade IV (severely abnormal), Grade III (abnormal), Grade II (nearly normal), or Grade I (normal). The Goebel Score describes macroscopic articular cartilage repair with five major evaluation categories. The quality of defect repair was scored blinded on fresh samples by two independent assessors, and the scores were averaged for further analysis. All the samples were fixed in 4% formalin for 10 days after macroscopic assessment for further analysis.

2.7. Micro-computed tomography

From the mouse model, the retrieved bovine osteochondral plugs were scanned (Quantum GX, Perkin Elmer, Akron, OH, USA) with the following settings after fixation in 4% formalin: energy 90 KV, intensity 88 µA, 18 mm FOV, 36 µm isotropic voxel size. All the scans above were under an X-ray filter of Cu (thickness = 0.06 mm) and Al (thickness = 0.5 mm) and were calibrated using a phantom with a known density of 0.75 g/cm³, which was additionally scanned before and after each scan. A high-resolution mode was set, and a scan time of 4 min was used.

The caprine samples were scanned with the same settings except for 36 mm FOV, 72 µm isotropic voxel size. Image processing included modest Gauss filtering (sigma = 0.8 voxel, width = 1 voxel) and segmentation using a single threshold. A cylindrical region (4 mm diameter and 5 mm height) within the original defect (6 mm diameter and 6 mm height) was selected as a volume of interest (VOI) for the caprine samples. In this VOI, the following morphometric parameters were measured: bone volume per total volume

(BV/TV), trabecular thickness (Tb.Th), trabecular number (Tb.N), and trabecular separation (Tb.Sp). Morphological analyses were performed using IPL (Scanco Medical AG, Bruettisellen, Switzerland).

2.8. Histology and immunohistochemistry

The bovine osteochondral plugs cultured *ex vivo* were decalcified for 2 weeks using 10% formic acid (Sigma, Saint Louis, MI, USA). After micro-CT scanning, the bovine osteochondral plugs harvested from mice were decalcified using 10% ethylenediaminetetraacetic acid (EDTA, Sigma, Saint Louis, MI, USA) for 4 weeks. The caprine samples were decalcified for 3 weeks using 10% formic acid. Subsequently, all samples were embedded in paraffin and sectioned at 6 μm . Following dewaxing, H&E staining was performed with Hematoxylin (Sigma, Saint Louis, MI, USA) and Eosin Y (Merck, Kenilworth, NJ, USA) to study general cell and tissue morphology. To visualise glycosaminoglycans in the extracellular matrix (ECM), dewaxed sections were stained with Safranin O (Fluka, Buchs, Switzerland) and Light green (Fluka, Buchs, Switzerland). To study the regenerated tissue type in the osteochondral defects, RGB staining was performed (Proteoglycans/hyaline cartilage appears blue, mineralised cartilage matrix appears pink/greenish, collagen fibres/uncalcified bone appears red, and mineralised bone appears green) using Alcian Blue (Sigma, Saint Louis, MI, USA), Fast Green (Sigma, Saint Louis, MI, USA), and Picrosirius Red (Sigma, Saint Louis, MI, USA) [39]. The cell number in the scaffolds was counted under microscopy. NDP View2 software (version 2.8.24, 2020 Hamamatsu Photonics K.K.) was used to measure the tissue volume in the defect at three sections that were taken at the middle, 0.5 mm, and 1 mm further away for bovine samples or at the middle for caprine samples (Supplementary Figure S2). The percentage of the defect covered with newly formed osteochondral tissue (100% indicated that the defect was fully filled with newly formed tissue) was calculated (Supplementary Figure S3). All slides were independently scored by two investigators blinded to the experimental condition. The measurements of the two investigators were averaged for each section.

To investigate the presentation of neutrophils in the defect, immunohistochemistry for myeloperoxidase (MPO) was performed on retrieved bovine osteochondral samples from the mouse study. After dewaxing, antigen retrieval was performed by placing the slides with Tris/EDTA (pH9) in a water bath at 95 °C for 20 min. Then, the slides were pre-incubated with 10% normal rabbit serum (NRS, Invitrogen, Waltham, MA, USA) in PBS containing 1% bovine serum albumin (BSA, Sigma, Saint Louis, MI, USA) and 1% milk powder (ELK, Campina, Amersfoort, The Netherlands). The slides were incubated by the first antibody against MPO (Thermo Scientific, Waltham, MA, USA, 1:200 dilution) or rabbit IgG antibody (DakoCytomation, California, USA, 1:10,000 dilution) as the negative control in PBS containing 1% BSA for 1 h. Next, the slides were incubated by biotinylated goat α -rabbit (Biogenex, Fremont, CA, USA, 1:50 dilution in PBS containing 1% BSA and 5% mouse serum of total volume) for 30 min. Then, the reaction was amplified by streptavidin-labelled alkaline phosphatase (Biogenex, Fremont, CA, USA) diluted 1:50 in PBS containing 1% BSA and visualized by subsequent incubation of Neu Fuchsin substrate. Slides were counterstained with Hematoxylin.

To evaluate the infiltration of macrophages in the defect, immunohistochemistry for F4/80 was performed on the bovine osteochondral plugs retrieved from the *in vivo* mouse study.

For antigen retrieval, each dewaxed slide was treated with 300 μ L proteinase K (20 μ g/mL, Thermo Scientific, Waltham, MA, USA) solution and incubated at 37 °C for 30 min. Then, the slides were pre-incubated with 10% NRS in PBS containing 1% BSA and 1% milk powder. The following steps were similar to the immunohistochemistry for F4/80, with the first antibody against F4/80 (eBioscience, San Diego, CA, USA, 1 μ g/mL) or rat IgG2a (eBioscience, San Diego, CA, USA, 1 μ g/mL) as the negative control in PBS containing 1% BSA; the second antibody: biotinylated rabbit anti-rat IgG (6 μ g/mL in PBS containing 1% BSA and 5% mouse serum of total volume), and third antibody: streptavidin-labelled alkaline phosphatase (Biogenex, Fremont, CA, USA) diluted 1:50 in PBS containing 1% BSA. To distinguish between pro-inflammatory (M1) and anti-inflammatory/tissue-repair (M2) macrophages, immunohistochemistry for inducible Nitric Oxide Synthase (iNOS, as an indicator for pro-inflammatory M1 macrophages) was performed. The steps were similar to the immunohistochemistry for MPO, with the first antibody against iNOS (2 μ g/mL, Abcam, Cambridge, UK).

The slides were ranked according to the positive degree of immunohistochemical staining, and all negatively stained sections were ranked 0. Only areas that were also stained for F4/80 were taken into account when the iNOS staining was ranked.

2.9. Statistical analysis

All statistical tests were performed using SPSS software 28.0 (SPSS Inc., Chicago, IL, USA). The repair tissue volume was expressed as mean \pm standard deviation (SD). The rankings of immunohistochemical MPO, F4/80, and iNOS staining were presented as column plots in graphs. Multiple comparisons between scaffold-only, BMP-2, and PDGF groups in bovine osteochondral plug samples were analysed by a Kruskal-Wallis test. Statistically significant differences between scaffold-only and scaffold + BMP-2 groups or between trochlear groove and femoral condyle groups in caprine samples were determined by a Mann-Whitney U test. A p value \leq 0.05 was considered statistically significant.

3. RESULTS

3.1. Scaffold characterization

SEM images show the detailed morphology of the cartilaginous layer (collagen, Figure 1A) and the bone layer (60% collagen and 40% magnesium-hydroxyapatite, Figure 1B) of the

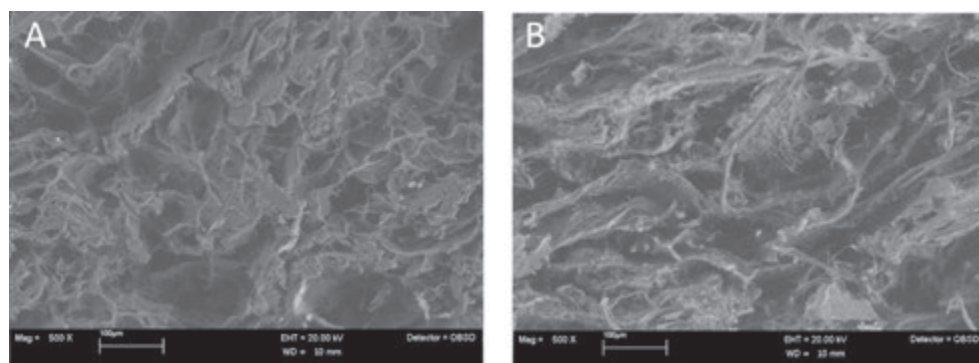


Figure 1. SEM images of (A) the cartilaginous layer (collagen) and (B) the bone layer (60% collagen and 40% magnesium-hydroxyapatite).

scaffolds. The ratio between collagen and magnesium-hydroxyapatite is 69/31 w/w%. The mineral phase is composed of non-stoichiometric, calcium deficient, magnesium-substituted hydroxyapatite. The total porosity of the osteochondral scaffold was $83 \pm 1\%$.

3.2. The release profiles of BMP-2 and PDGF-BB *in vitro*

Of the added BMP-2, 0.6% was detected in the medium after adsorption for the collagen-only layer and 3.0% for the Col-Mg-HAP layer, indicating that most of the BMP-2 was indeed adsorbed and that both layers had a similar adsorption capacity at the tested volume. Over 14 days, only 48.8 ± 14.8 ng and 22.1 ± 3.4 ng of the adsorbed BMP-2 was released from the collagen-only layers or Col-Mg-HAP layers, respectively (Figure 2A). BMP-2 was largely retained within the scaffolds. A similar release pattern was observed for both layers, although the collagen-only layer released (2-fold) more over the 14-day period (Figure 2A).

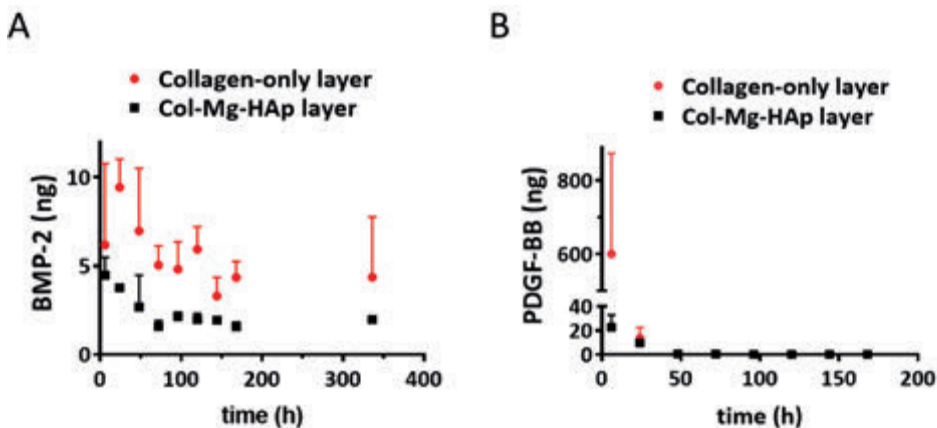


Figure 2. Bone morphogenetic protein 2 (BMP-2) and platelet-derived growth factor-BB (PDGF-BB) released from the different layers of the Col/Col-Mg-HAP scaffold. (A) In vitro release of BMP-2 from the different layers of Col/Col-Mg-HAP scaffold over a 14-day period. (B) In vitro release of PDGF-BB from the different layers of the Col/Col-Mg-HAP scaffold over a 7-day period. The release of BMP-2 and PDGF-BB is presented as the released dose at each time point. Data points indicate the mean \pm SD of 3 samples per time point.

Of the added PDGF-BB, 3.9% was detected in the medium after adsorption for the collagen-only layer and 5.9% for the Col-Mg-HAP layer, indicating that most of the PDGF-BB was adsorbed and that both layers had a similar adsorption capacity. In contrast to BMP-2, a rapid release of PDGF-BB from the collagen-only layer was observed, and 600.4 ± 273.6 ng was released within 6 h (Figure 2B). Interestingly, almost no release was observed from the Col-Mg-HAP layer; only 33.8 ± 11.8 ng PDGF-BB was cumulatively released from the Col-Mg-HAP layer over seven days.

3.3. Effect of BMP-2 and PDGF-BB on cell ingrowth in an *ex vivo* culture model

To evaluate the effect of BMP-2 or PDGF-BB addition onto the scaffold on cell recruitment from adjacent osteochondral tissues, an *ex vivo* model was used. After three weeks, the scaffolds filled the osteochondral defects, and cells infiltrated the scaffolds. In the scaffold without growth factors, cells were mostly located at the periphery of the scaffold (Figure 3A). Interestingly, when BMP-2 or PDGF-BB was added, cell infiltration was also observed in the centre, particularly in the collagen-only layer (Figure 3A). Almost no cells were found in the Col-Mg-HAp layer. Overall, the addition of growth factors significantly increased cell infiltration into the scaffolds (Figure 3B).

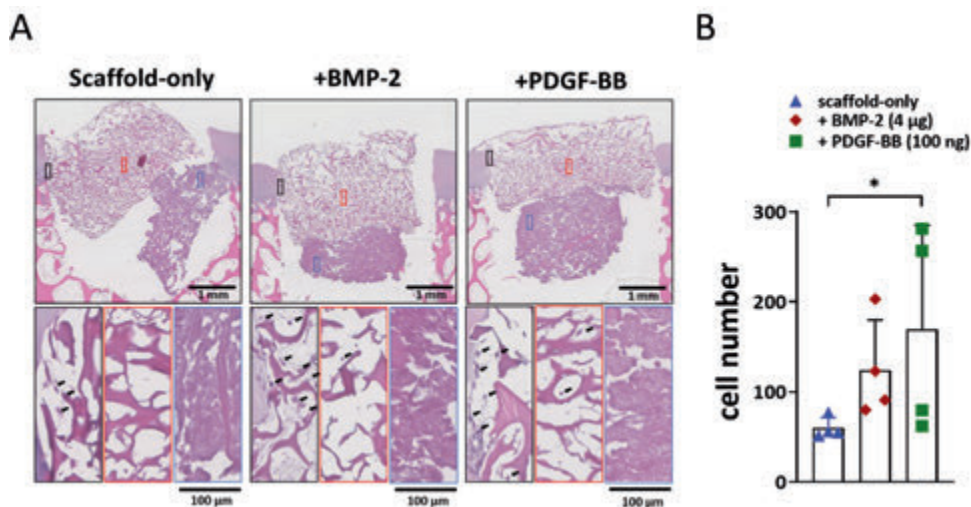


Figure 3. Adsorption of BMP-2 or PDGF-BB might improve the cell recruitment property *ex vivo*. (A) Representative images of the 3-week constructs stained with H&E. Scale bars indicate 1 mm and 100 μm, respectively. Magnified images showed cell infiltration at the periphery (black square), in the centre (red square) of the collagen-only layer, and in the Col-Mg-HAp layer (blue square) of the scaffold. Black arrows indicate infiltrated cells. (B) The number of cells infiltrated into the scaffolds. Each bar indicates the mean \pm SD of 4 samples per condition. * $p < 0.05$ analysed by a Kruskal-Wallis test.

3.4. Effect of BMP-2 and PDGF-BB at the early phases of bone repair in an *in vivo* semi-orthotopic osteochondral defect model in mice

One dose of BMP-2 (4 μg) and two doses of PDGF-BB (100 ng and 2 μg) were tested in order to investigate their potential effect on the early stages of bone repair. After four weeks, neither cartilage nor bone formation were observed in any of the samples with scaffold-only (Figure 4A). When BMP-2 or PDGF-BB was adsorbed into the scaffold, cartilage-like tissue was found in 1 out of 4 samples with 100 ng PDGF-BB, 2 out of 4 samples with 2 μg PDGF-BB and 2 out of 4 samples with 4 μg BMP-2 (Figure 4B). Interestingly, the scaffolds adsorbed with either 4 μg BMP-2 or 2 μg PDGF-BB showed less MPO (as an indicator for neutrophils) and iNOS (as an indicator for pro-inflammatory macrophages) staining; albeit, this did not reach statistical significance due to the relatively low sample size (Supplementary Figure S4).

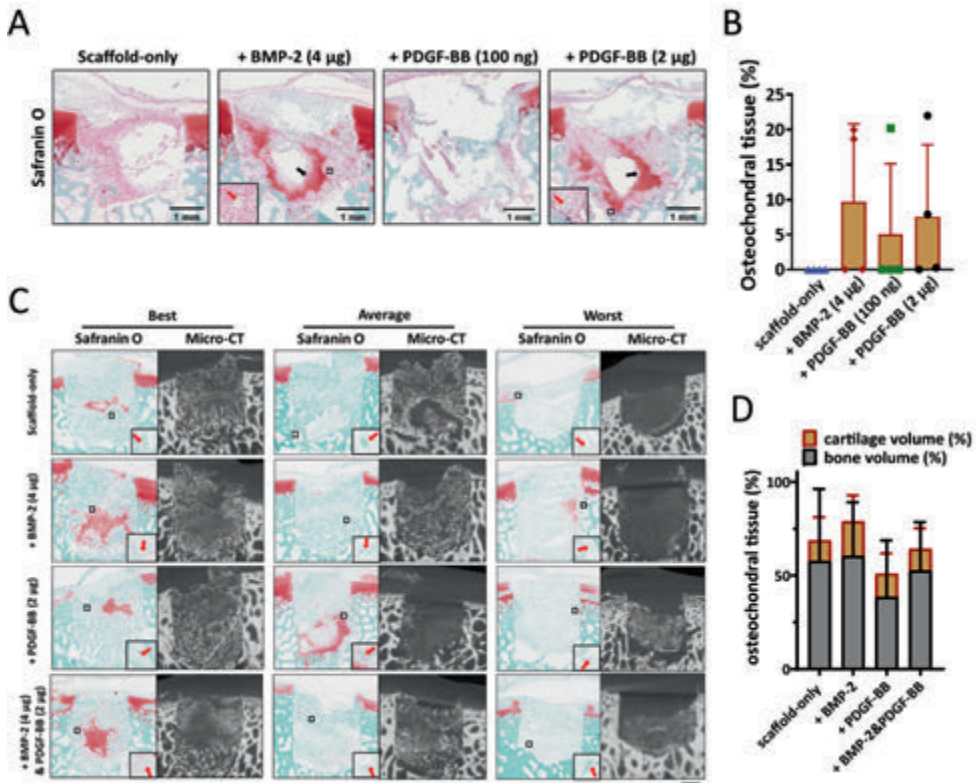


Figure 4. The effect of BMP-2 or PDGF-BB adsorption onto Col/Col-Mg-HAP scaffolds on osteochondral defect repair in a semi-orthotopic model in vivo. (A) Representative images of the 4-week repair constructs stained with Safranin O. Scale bars indicate 1 mm. Black arrows indicate cartilage-like tissue. Red arrows indicate blood vessels. (B) The percentage of the defect filled with osteochondral tissue (%) in the osteochondral defects at 4 weeks. (C) Representative images of the 8-week repair constructs stained with Safranin O, and the 8-week CT images. The best, average, and worst repaired samples are presented based on osteochondral tissue volume (%). Scale bars indicate 1 mm. Red arrows indicate blood vessels. (D) The percentage of the defect filled with osteochondral tissue (%) in the osteochondral defects at 8 weeks. Scale bars indicate 1 mm.

The effect of 4 µg BMP-2, 2 µg PDGF-BB, or the combination of the two were further investigated in the semi-orthotopic mouse model after eight weeks. Inflammation was largely resolved in all samples. Immunohistochemical staining for MPO and iNOS was negative in all but one defect that was from the scaffold-only group. No difference was found between the different groups. All defects were filled with bone tissue, and blood vessels were observed, independent of the presence of growth factors (Figure 4C). Overall, there was slightly more tissue repair in BMP-2-adsorbed scaffolds (78.9 ± 23.1% of the defect filled) compared with PDGF-BB-adsorbed scaffolds (50.9 ± 28.0%) or scaffold-only (68.8 ± 36.2%) (Figure 4D). Partially repaired bone defects were found in 5 out of 7 defects fitted with PDGF-BB-adsorbed scaffolds, while only in 3 out of 7 in the scaffold-only group and 2 out of 7 in the group of BMP-2-adsorbed scaffolds.

3.5. Effect of BMP-2 on bone repair in an *in vivo* caprine model

3.5.1. Scaffold implantation and clinical observations

Most of the osteochondral tissue was regenerated in the osteochondral defects when 4 μg BMP-2 was adsorbed to the Col/Col-Mg-HAp scaffold in the mouse model. Therefore, BMP-2 was selected to be further investigated in an established bilateral preclinical caprine osteochondral defect model. Two differently loaded locations were selected in this caprine model: a weight-bearing region of the medial femoral condyle and a non-weight-bearing area in the trochlear groove. During surgery, scaffolds were successfully press fit into osteochondral defects flush with the surrounding cartilage. All defects bled after drilling, and scaffolds became saturated with fresh blood upon implantation, as observed by a change in colour of the implanted scaffold.

Recovery was uneventful and no postoperative complications occurred except for the unforeseen death of one animal three days post-surgery due to ruminal acidosis caused by overeating of concentrates, unrelated to the experimental procedure. Macroscopic appearance after three days in the unforeseen dead animal showed that scaffolds were stable in the osteochondral defects (Supplementary Figure S5A). The two layers of the scaffold were clearly visible in the defects (Supplementary Figure S5B).

Clinical examination of animals daily for 14 days post-surgery and weekly until the endpoint at six months demonstrated excellent recovery from surgery and a normal pain-free range of movement and normal locomotion from 3-10 days post-surgery. After six months, there were no signs of inflammation or cartilage abnormalities found during a post-mortem evaluation of the joints. No signs of joint swelling, effusion, abnormal mobility, synovial adhesions, synovial fluid and membrane abnormalities, abnormal wound healing, patellar luxation, or erosions or lesions on the opposite cartilage surface were found in any of the animals.

3.5.2. Tissue repair in the non-weight-bearing trochlear groove osteochondral defects

To quantify the subchondral bone formation within the bone defect, micro-CT analysis was performed. Well-repaired subchondral bone was observed in the images of the trochlear groove treated with both the scaffold-only and BMP-2-adsorbed scaffold at six months (Figure 5A). A slightly higher Tb.N was found in the defects with BMP-2-adsorbed scaffolds. No significant differences in the BV/TV, Tb.Th, Tb.N, or Tb.Sp were found between the groups (Figure 5B).

Macroscopical and histological evaluation of the cross sections of the defect supported the micro-CT quantification (Figure 5C). Overall, the scaffolds were completely degraded, and a well-structured subchondral trabecular bone was observed in most bone defects after six months (Figure 5C). Slightly more bone tissue ($93.9 \pm 4.4\%$ vs. $90.1 \pm 8.4\%$) and less fibrous tissue ($4.0 \pm 4.5\%$ vs. $7.8 \pm 8.4\%$) was found in the bone defects when the scaffolds were adsorbed with BMP-2 compared with the scaffold-only, although no significant difference was reached (Figure 5D). Notably, a structure without trabecular bone but with only bone marrow was observed underneath some defects, independent of the condition.

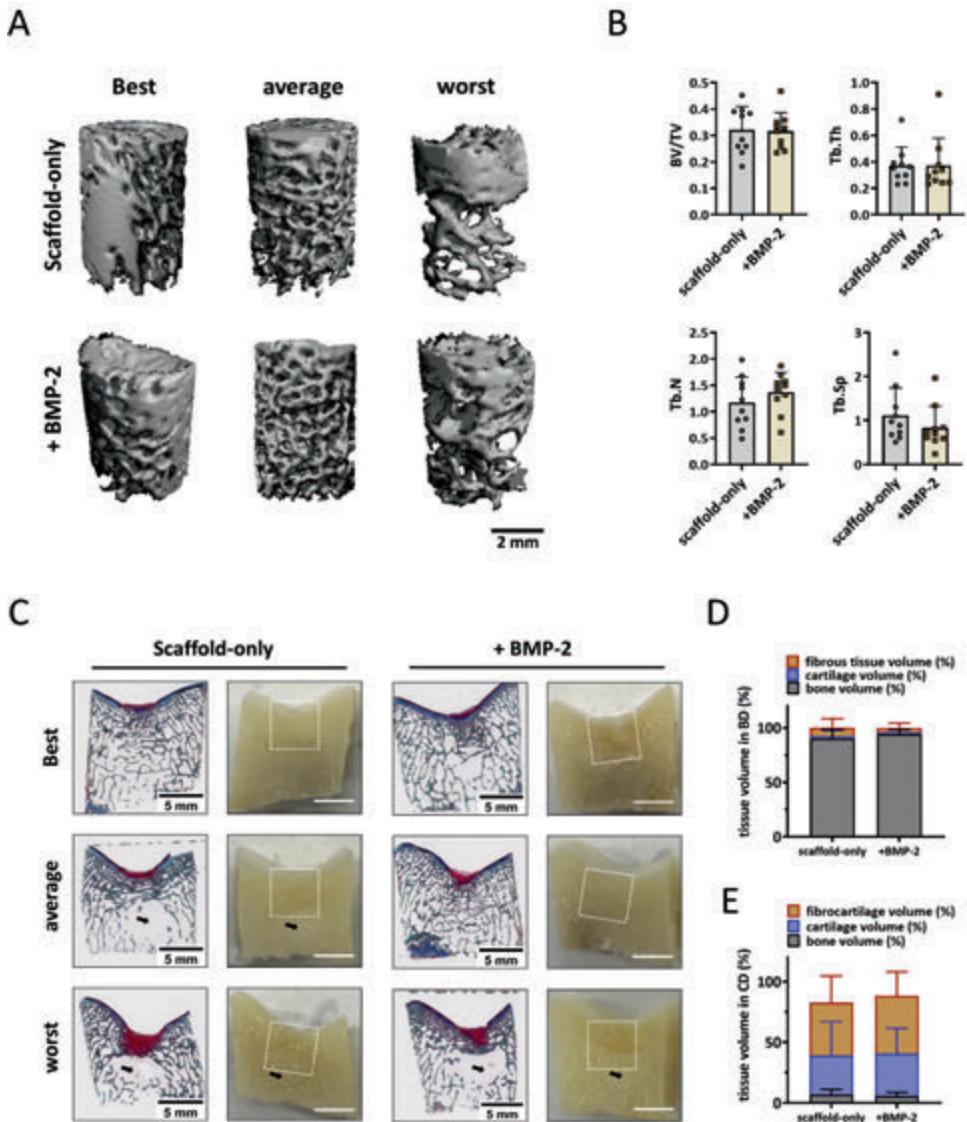


Figure 5. Tissue repair in non-weight-bearing trochlear groove defects. (A) Representative micro-CT reconstructions treated with either scaffold-only or scaffold adsorbed with BMP-2. The best, average, and worst repaired samples are presented based on BV/TV. The scale bar indicates 2 mm. (B) BV/TV, trabecular thickness (Tb.Th [mm]), trabecular number (Tb.N [1/mm]), and trabecular separation (Tb.Sp [mm]) in the bone defects after 6 months. (C) RGB (Alcian Blue, Fast Green, and Picosirius Red) staining and macroscopic cross-sectional view of osteochondral defects treated with either scaffold-only or scaffold adsorbed with BMP-2. The best, average, and worst repaired samples are presented. White squares indicate 6 * 6 mm osteochondral defects. Black arrows indicate the structure with only bone marrow. The scale bar indicates 5 mm. (D) The percentage of tissue volume calculated in the bone defects (BD). (E) The percentage of tissue volume calculated in the cartilage defects (CD).

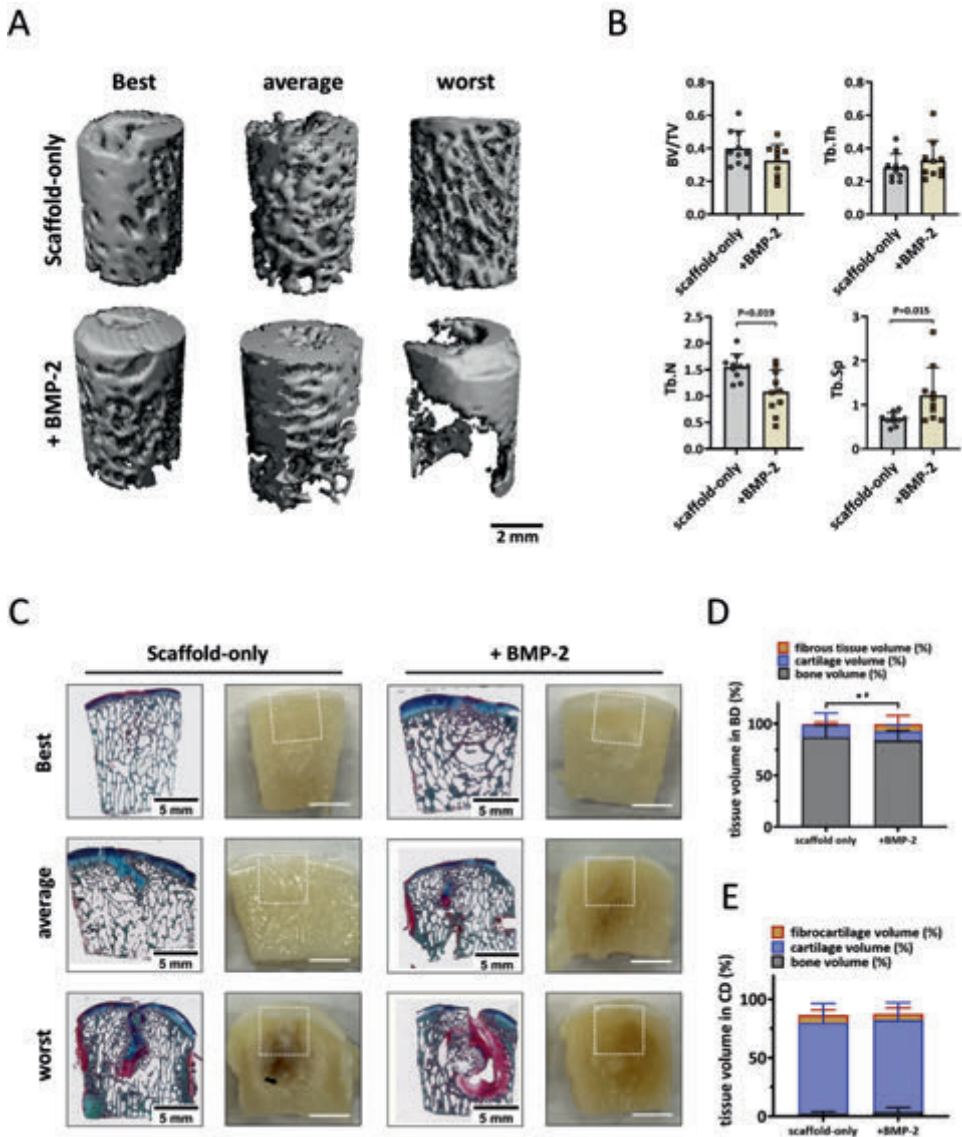


Figure 6. Bone repair in the weight-bearing femoral condyle defects deteriorated with the adsorption of BMP-2 onto the scaffold. (A) Representative micro-CT reconstructions treated with either scaffold-only or scaffold adsorbed with BMP-2. The best, average, and worst repaired samples are presented based on BV/TV. The scale bar indicates 2 mm. (B) BV/TV, trabecular thickness (Tb.Th [mm]), trabecular number (Tb.N [1/mm]), and trabecular separation (Tb.Sp [mm]) in the bone defects after 6 months. Tissue repair in the femoral condyle defects. (C) RGB (Alcian Blue, Fast Green, and Picrosirius Red) staining and macroscopic images of osteochondral defects treated with either scaffold-only or scaffold adsorbed with BMP-2. The best, average, and worst repaired samples are presented. White squares indicate 6 * 6 mm osteochondral defects. The scale bar indicates 5 mm. (D) The percentage of tissue volume calculated in the bone defects (BD). * $p < 0.05$ in fibrous tissue, # $p < 0.05$ in osteochondral (cartilage-like and bone-like) tissue. (E) The percentage of tissue volume calculated in the cartilage defects (CD).

Macroscopically, defects were covered with newly formed cartilage with good integration into the surrounding native tissue. Small, scattered fissures or cracks were observed on the surfaces of some defects, and no noticeable depressions were observed (Supplementary Figure S6A). The ICRS and Goebel scores for the scaffold-only group had a median score of 11.3 ± 0.5 and 19.0 ± 0.7 , respectively (Supplementary Figure S6B). For the scaffold + BMP-2 group, the macroscopic ICRS and Goebel scores were 11.6 ± 0.6 and 19.3 ± 0.5 , respectively (Supplementary Figure S6B). All the trochlear groove samples were classified as normal (grade I) or nearly normal (grade II) cartilage. Overall, no significant difference was observed in cartilage repair between scaffold-only and BMP-2-adsorbed scaffold. On histology, $43.2 \pm 22.1\%$ (scaffold-only) and $47.4 \pm 19.8\%$ (scaffold + BMP-2) of the newly formed tissue generated in the cartilage defects was fibrous tissue after six months as indicated by predominantly Picrosirius Red instead of Alcian Blue staining in RGB staining (Figure 4E). Moreover, only $32.4 \pm 27.6\%$ (scaffold-only) and $35.2 \pm 20.6\%$ (scaffold + BMP-2) of the repaired tissue in the cartilage region was Alcian Blue-positive, indicating hyaline cartilage (Figure 5E).

3.5.3. Tissue repair in the weight-bearing femoral condyle osteochondral defects

For the femoral condyle, micro-CT analysis was performed in the same manner as for the trochlear groove. In the weight-bearing femoral condyle, well-structured subchondral bone was formed after six months in defects treated with the scaffold-only or the BMP-2-adsorbed scaffold (Figure 6A), no significant difference was found in the BV/TV and Tb.Th parameters (Figure 6B). Surprisingly, a slightly lower BV/TV was found in defects with BMP-2-adsorbed scaffolds, indicating relatively worse bone repair when BMP-2 was adsorbed. A significantly smaller Tb.N (1.1 ± 0.4 vs. 1.5 ± 0.2 , $P = 0.019$, Figure 6B) and a greater Tb.Sp (1.2 ± 0.6 vs. 0.7 ± 0.1 , $P = 0.015$, Figure 5B) were observed in the femoral condyle bone defects fitted with BMP-2-adsorbed scaffolds, suggesting a relatively courser bone structure when BMP-2 was adsorbed.

Macroscopic and histological evaluation of the cross sections through the defect supported the micro-CT quantification (Figure 6C). Newly formed hyaline cartilage-like tissues were mostly supported by a well-structured subchondral trabecular bone that was well integrated in the surrounding native bone (Figure 6C). Surprisingly, significantly less cartilage and bone tissue were observed in the bone defects fitted with BMP-2-adsorbed scaffolds compared with the bone defects treated with scaffold-only ($92.7 \pm 9.5\%$ vs. $99.1\% \pm 1.7\%$, $P = 0.043$, Figure 6D). In addition, significantly more fibrous tissue was found in the bone defects when BMP-2 was adsorbed onto the Col/Col-Mg-HAp scaffolds ($6.9 \pm 8.4\%$ vs. $1.0 \pm 1.6\%$, $P = 0.035$, Figure 6D). Some defects demonstrated cyst-like areas without trabecular bone below some of the defects. However, marrow-like tissue was found in these areas.

The defects were mostly covered with hyaline cartilage-like tissue with macroscopically good integration with the surrounding native tissue (Supplementary Figure S6C). Small, scattered fissures or cracks were observed on surfaces of some defects, and no noticeable depressions were observed except for one sample treated with Col/Col-Mg-HAp scaffold-only. The median ICRS score was 10.8 ± 0.5 out of 12, and the median Goebel score was 18.9 ± 0.5 out of 20 (Supplementary Figure S6D) when scaffold-only was placed in the defects. The defects with the scaffold + BMP-2 received median ICRS scores of 10.3 ± 1.8

out of 12 and median Goebel scores of 18.5 ± 1.8 out of 20 (Supplementary Figure S6D). All the samples were classified as normal (grade I) or nearly normal (grade II) cartilage except for one sample treated with BMP-2 (grade III). By histological examination, the scaffolds were completely degraded after six months, and round cells residing within lacunae were present in the cartilage region. GAG and collagen were present in the repair tissue in the defects demonstrated by RGB staining (Figure 6C), indicating cartilaginous tissue formation. In fact, $77.8 \pm 16.5\%$ (scaffold-only) and $78.8 \pm 14.7\%$ (scaffold + BMP-2) of the newly formed tissue was Alcian Blue-positive, indicating hyaline-like cartilage (Figure 6E).

3.5.4. Different tissue repair in the non-weight-bearing trochlear groove and the weight-bearing femoral condyle osteochondral defects

In trochlear groove bone defects, the trabecular number was smaller (1.2 ± 0.5 vs. 1.5 ± 0.2 , $P = 0.063$) and the trabecular separation was greater (1.1 ± 0.6 vs. 0.7 ± 0.1 , $P = 0.052$) compared with the femoral condyle defects when scaffold-only was implanted, although no significant difference was found. Interestingly, when BMP-2 was adsorbed onto the scaffold, an opposite trend was found in the Tb.N (1.4 ± 0.4 in trochlear groove and 1.1 ± 0.4 in femoral condyle, $P = 0.143$) and the Tb.Sp (0.8 ± 0.5 in trochlear groove and 1.2 ± 0.6 in femoral condyle $P = 0.105$). In other words, there was a 0.2 ± 0.6 greater Tb.N and a 0.3 ± 0.9 smaller Tb.Sp in the trochlear groove defect versus a 0.47 ± 0.6 smaller Tb.N ($P = 0.029$, compared with trochlear groove) and a 0.5 ± 0.7 greater Tb.Sp ($P = 0.063$, compared with trochlear groove) in the femoral condyle defect when BMP-2 was adsorbed onto the scaffold, indicating that bone repair was improved in trochlear groove defects and reduced in femoral condyle defects when BMP-2 was added. Histological results further confirmed that significantly more bone-like tissue was regenerated in the trochlear groove defects compared with the femoral condyle defects when BMP-2 was added ($93.9 \pm 4.4\%$ vs. $83.5 \pm 9.8\%$, $P = 0.011$), while no difference between weight-bearing and non-weight-bearing sites was observed when scaffold-only was implanted ($90.1 \pm 8.4\%$ vs. $86.7 \pm 11.5\%$, $P = 0.579$). For cartilage repair, however, significantly less hyaline cartilage-like tissue was observed in the non-weight-bearing trochlear groove compared with the weight-bearing femoral condyle defects with either scaffold-only ($32.4 \pm 27.6\%$ vs. $77.8 \pm 16.5\%$, $P = 0.003$) or BMP-2-adsorbed scaffold ($35.2 \pm 20.6\%$ vs. $78.8 \pm 14.7\%$, $p < 0.001$).

4. DISCUSSION

In this study, we evaluated the effectiveness of growth factor adsorption onto a bi-layered Col/Col-Mg-HAp scaffold in osteochondral defect repair. *In vitro* release results showed that the Col-Mg-HAp (bone) layer retained more growth factor than the collagen-only (cartilage) layer and that BMP-2 was retained much better than PDGF-BB. In an *ex vivo* osteochondral defect model, cell ingrowth into the scaffold was enhanced by BMP-2 and by PDFG-BB. In a semi-orthotopic non-weight-bearing osteochondral defect mouse model representing the early phase (four weeks) of defect repair *in vivo*, the addition of growth factors resulted in fewer pro-inflammatory cells and better tissue repair, with BMP-2 showing the most favourable results. Therefore, BMP-2 addition was taken forward for testing in an established preclinical large animal osteochondral defect model to study scaffold enhancement by BMP-2 in a physiological environment with different loading conditions. After six months in goats, both the scaffold-only and the BMP-2-adsorbed

scaffold induced good osteochondral defect healing. Surprisingly, the addition of BMP-2 led to worse bone repair in the weight-bearing femoral condyle osteochondral defects, whereas this negative effect of BMP-2 was not seen in the non-weight-bearing trochlear groove osteochondral defect location.

Our approach was based on the sequential use of osteochondral defect models: the first experiments were performed in an *ex vivo* bovine osteochondral explant model, followed by a semi-orthotopic non-weight-bearing model where we implanted bovine osteochondral explants subcutaneously in mice. This took into account the effects of the innate immune system and blood vessel invasion. We then selected the most promising condition to be further evaluated in a preclinical caprine osteochondral defect model, where we tested both weight-bearing and non-weight-bearing repair conditions simultaneously. All models were developed and used previously to evaluate new osteochondral repair approaches [34,40]. *In vivo* animal models can closely resemble the human osteochondral microenvironment in the context of the presence of immune cells and tissue repair factors. The mouse model allows the screening of four conditions in one animal, whereas the caprine bilateral osteochondral defect model is a fully immune-competent model using outbred animals. That model also allows within-animal controls (comparing left and right knees), and provides the opportunity to assess tissue regeneration in both weight-bearing and non-weight-bearing locations within the same joint. These animal models offered the opportunity to investigate the possible effect of incorporating growth factors into a Col/Col-Mg-HAp scaffold for osteochondral repair towards translation into the human patient.

Loading can have a significant effect on tissue repair [41,42]. Not much is known about the interaction between mechanical loading and growth factors and their effect upon osteochondral tissue repair [43,44]. To study the effect of mechanical stimuli on osteochondral repair during normal ambulation, we used both a non-weight-bearing location (a distal region in the trochlear groove) and a weight-bearing location (a central region on the medial femoral condyle) in the bilateral stifle caprine osteochondral defect model [45,46]. Better subchondral bone repair was observed in the non-weight-bearing trochlear groove defects than in the weight-bearing femoral condyle defects when BMP-2 was adsorbed onto the scaffold, while no significant difference in repair was found between locations when the scaffold without additions was evaluated. In the non-weight-bearing trochlear groove defects, there was a trend towards more bone-like tissue being generated in the BMP-2-adsorbed scaffolds compared with the scaffold-only. However, this difference did not reach statistical significance, which might be due to the excellent repair capacity of the scaffold-only. The weight-bearing femoral condyle defects implanted with BMP-2-adsorbed scaffolds appeared to have less bone repair and more fibrous tissues in the bone defect compared with the scaffold-only.

Notably, there was no mechanical loading in the semi-orthotopic mouse model and at the four-week time point, the addition of BMP-2 to the scaffolds seemed beneficial. Our results reveal the interesting hypothesis that, with a specific dose of BMP-2, the beneficial effect of BMP-2 on bone repair is apparent in non-weight-bearing conditions, whilst BMP-2 addition can be detrimental to bone repair in weight-bearing conditions. Although the effect of BMP-2 on osteochondral defect repair in different loading environments is still unknown, the action of BMP-2 on tibia fractures or femoral bone defect healing was

demonstrated to be dependent on the mechanical environment *in vivo* [47,48]. This might be due to an interaction between BMP-2 and mechanical loading [49] and related to the dosage used. Compression and loading affect BMP signalling both immediately and in a long-term manner [50]. Mechanical loading was shown to increase BMP-2 expression [51], and the effect of BMP-2 can be strongly potentiated by mechanical forces [49]. It is possible that the combination of added and locally produced BMP-2 might lead to an overstimulation of BMP-2 signalling, which is shown to cause inflammation, bone resorption, and fibrotic tissue formation [52,53,54]. No previous study has reported this potential side effect nor the relationship with mechanical loading. However, the mechanical loading patterns in long bone defects with fixation and osteochondral defects with scaffolds in the femoral condyle (especially with the presence of synovial fluid) are quite distinct from one another. Therefore, further studies are needed to elucidate if and at which step of the BMP signalling cascade the pathway is modulated and by which type of mechanical stimuli.

BMP-2 is, to date, the only FDA-approved and commercially available osteoinductive growth factor used in clinics. The function and application of BMP-2 in promoting bone regeneration and bone remodelling has been widely investigated preclinically and clinically [55,56,57]. Mg²⁺ was incorporated in this scaffold, which might upregulate the bioactivity of BMP-2 upon calcium phosphate cement via enhanced BMP receptor recognition [58]. Previous studies have demonstrated that BMP-2 accelerated the migration of bone marrow mesenchymal stromal cells (MSCs) *in vitro* and *in vivo* [59,60]. In the presented study, we also observe the promotion of cell ingrowth by BMP-2 addition in our *ex vivo* culture model. Although the primary expected functions of BMP-2 in promoting bone repair are to enhance MSC migration to the sites and differentiation into osteoblasts and to enhance the osteogenic capacity of osteoblasts, BMP-2-induced osteogenesis may also involve an immunoregulatory role [61,62]. Macrophages act as immune cells and osteoclast precursors and are involved in multiple stages of bone healing [63]. BMP-2 might diminish the expression of pro-inflammatory phenotypic markers and promote the macrophage transition towards a more tissue repair-like phenotype [62]. Neutrophils and M1 macrophages participate in tissue repair as effector cells in inducing inflammation, and M2 macrophages are involved in the resolution of inflammation, promoting angiogenesis, and matrix remodelling [64]. In our semi-orthotopic model, fewer M1 macrophages, as well as neutrophils, were found in the BMP-2 condition than in the scaffold-only condition after four weeks. Therefore, the regulatory effect of BMP-2 in a local osteoimmune environment might be one of the potential mechanisms for promoting bone healing in the early phase.

Although BMP-2 has been clinically applied because of its osteogenic effect, it is still not widely used due to the adverse events associated with implanted supraphysiological high doses [57]. The most documented side effect is ectopic ossification. Aulin et al. demonstrated that intra-articular injection of a hyaluronan hydrogel containing BMP-2 (150 µg/mL) resulted in excessive ectopic bone formation on the knee joint surface of rabbits (6-7-month-old females) [65]. In our study, we used 57.1 µg/mL BMP-2 for both 4 mm × 4 mm and 6 mm × 6 mm cylindrical osteochondral defects according to our previous *in vivo* results [30]. HAp was reported to have a high affinity for BMP-2 due to the large surface area and functional groups [29,66]. Three types of functional groups, -OH, -NH₂,

and $-COO$, allow BMP-2 to adsorb on the HAp surface [66]. This is not the case for all growth factors, where, for example, no functional groups or only one might be present. *In vitro*, we demonstrated that BMP-2 was bound and largely retained in both layers, especially in the Col-Mg-HAp layer. In this way, a sustained release was expected, thereby reducing the adverse effects of BMP-2. Over longer periods, however, correlations between the *in vitro* and *in vivo* settings become ever more unreliable since the release *in vivo* will be determined by the degradation of the scaffold as well. In fact, no BMP-2-related ectopic ossification or abnormal inflammation was observed in the knee joints of our experimental goats macroscopically or on micro-CT. Similarly, no ectopic ossification was reported in a publication that investigated the addition of 625 $\mu\text{g}/\text{mL}$ of BMP-2 (adsorbed onto Col/HAp scaffolds) in skeletally mature male rabbits [29].

Consistent with other studies, we found that PDGF-BB is an effective chemoattractant of cells *ex vivo* [31,67]. PDGF-BB was rapidly released from the collagen-only layers within six hours; most of the PDGF-BB was retained in the Col-Mg-HAp layers *in vitro*. This might be due to the capacity of HAp in adsorbing a large quantity of proteins and drugs. At the early repair phase in the *in vivo* mouse model, both dosages (1 μg and 100 ng) of PDGF-BB slightly improved tissue formation. Most of the regenerated tissue was in the bone defect area, which might be related to the sustained release from the Col-Mg-HAp layers, which is aimed at the repair of the bone defect specifically. Lee et al. reported that labelled cells migrated towards the osteochondral defect when defects were treated with PDGF-AA or PDGF-BB-loaded heparin-conjugated fibrin [67]. Overall, the chemotactic ability of PDGF-BB might be one of the mechanisms in inducing tissue repair in the early phase. However, after eight weeks, the defects loaded with PDGF-BB generated slightly less osteochondral tissue compared with scaffold-only. A previous study on osteochondral repair also showed that the addition of 1 $\mu\text{g}/\text{mL}$ PDGF-BB worsened the cartilage repair in an *in vivo* subcutaneous mouse model, although cell recruitment was enhanced *in vitro*. The short half-life of PDGF might be one of the reasons for the different results between *in vitro* and *in vivo* studies. Zhang et al. demonstrated that PDGF-BB overexpression improved the osteogenic and angiogenic abilities of MSCs in a critical-sized rat calvaria defect model [68].

We also expected the combination of BMP-2 and PDGF-BB to further improve bone repair, since PDGF was reported to modulate BMP-2-induced osteogenesis in periosteal progenitor cells [69]. However, no significant improvement was found after eight weeks in the semi-orthotopic mouse model *in vivo*. Therefore, PDGF-BB and the combination of BMP-2 and PDGF-BB were not further evaluated in our large animal osteochondral defect model.

Suboptimal subchondral bone repair of osteochondral defects might lead to damage of the renewed overlying cartilage in the long term [16,17,18]. In our caprine large animal model, a blinded macroscopic evaluation of repaired cartilage tissue indicated the presence of a smooth white cartilaginous layer that was continuous with surrounding naive cartilage, both with control scaffolds and BMP-2-enhanced scaffolds. Histology further confirmed the presence of hyaline cartilage in the superficial layer, with no significant improvement or deterioration observed when BMP-2 was added. This might be due to the fact that tissue repair was assessed at only one, relatively early, six-month time point in the caprine model. A longer 12- or 24-month study might be useful to confirm the

potential effectiveness of enhanced bone repair on the long-term survival of the neo-cartilage.

5. CONCLUSION

Adsorption of BMP-2 onto a Col/Col-Mg-HAp scaffold reduced bone formation in weight-bearing osteochondral defects but not in non-weight-bearing osteochondral defects. Since the application of BMP-2 adsorbed to a Col/Col-Mg-HAp scaffold in osteochondral defects did not lead to adverse effects in the joint of goats, and human patients are not allowed full weight-bearing in the first weeks after the osteochondral repair, further investigation is warranted, taking into consideration the dose of BMP-2, timing, and location of application for osteochondral defect repair.

SUPPLEMENTARY MATERIALS

Table S1: Clinical Orthopedic Assessment. This tool is to evaluate the clinical health of goat joints.

Parameter	Variables	Score
Lameness	Walks normally	5
	Slightly lame when walking	4
	Moderately lame when walking	3
	Severely lame when walking	2
	Reluctant to rise and will not walk more than five paces	1
Joint mobility	Full range of motion	5
	Mild limitation (10-20%) in ROM; no crepitus	4
	Mild limitation (10-20%) in ROM; with crepitus	3
	Moderate limitation (20-50%) in ROM; \pm crepitus	2
	Severe limitation (>50%) in ROM; \pm crepitus	1
Pain on knee palpation and movement	None	5
	Mild signs; Goat turns head in recognition	4
	Moderate signs; Goat pulls limb away	3
	Severe signs; Goat vocalises or becomes aggressive	2
	Goat will not allow palpation	1
Weight-bearing	Equal on all limbs standing and walking	5
	Normal standing; favours affected limb when walking	4
	Partial weight-bearing standing and walking	3
	Part. weight-bearing standing; non-weight-bearing walk	2
	Non-weight-bearing standing and walking	1
Overall score of clinical condition	Not affected	5
	Mildly affected	4
	Moderately affected	3
	Severely affected	2
	Very severely affected	1
Total score		25

Table S2: Macroscopic joint Assessment. This tool is to evaluate the macroscopic normalization of goat joints when the joints were opened.

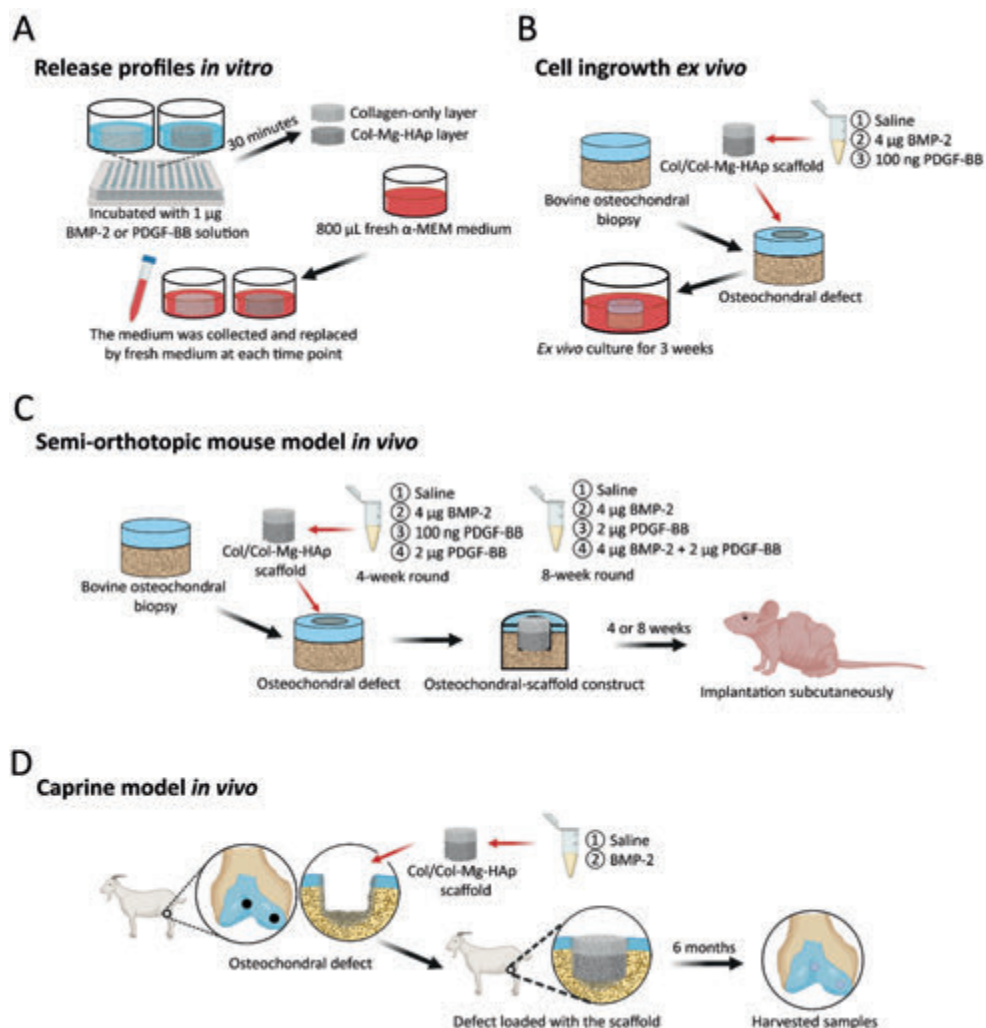
Parameter	Variables	Score
Wound healing abnormal	Yes	0
	No	1
Swelling of soft tissues surrounding joints	Yes	0
	No	1
Effusion of the joints	Yes	0
	No	1
Patellar luxation	Yes	0
	No	1
Joint mobility abnormal	Yes	0
	No	1
Adhesions in the joint	Yes	0
	No	1
Erosions of the joint	Yes	0
	No	1
Synovial fluid abnormal	Yes	0
	No	1
Synovial membrane abnormal	Yes	0
	No	1
Lesion on the opposite cartilage surface (trochlear groove vs patella)	Yes	0
	No	1
Lesion on the opposite cartilage surface (medial femoral condyle vs meniscus/tibia plateau)	Yes	0
	No	1
	Total	0-11

Table S3: International Cartilage Repair Society (ICRS) cartilage repair scoring system. This tool is to evaluate the macroscopic appearance of cartilage repair tissue.

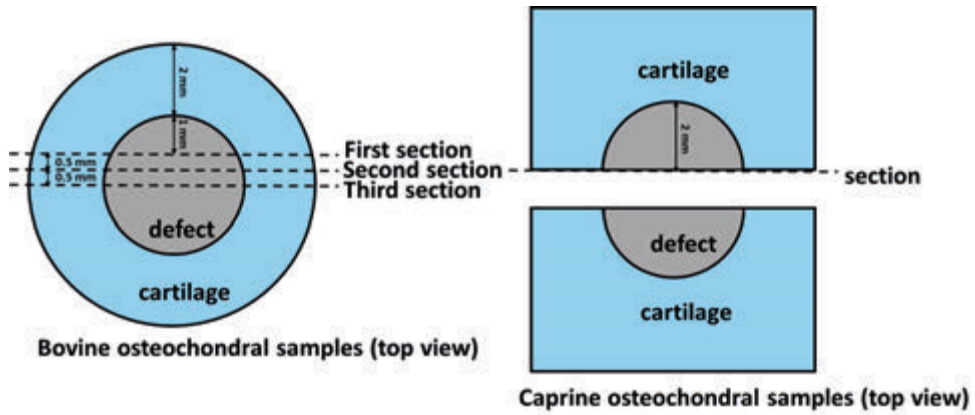
Parameter	Variables	Scores
Degree of defect repair	In level with surrounding cartilage	4
	75% repair of defect depth	3
	50% repair of defect depth	2
	25% repair of defect depth	1
	0% repair of defect depth	0
Integration to border zone	Complete integration with surrounding cartilage	4
	Demarcating border < 1 mm	3
	¾ of graft integrated, ¼ with a notable border > 1 mm	2
	1/2 of graft integrated with surrounding cartilage, 1/2 with a notable border > 1 mm	1
	From no contact to ¼ of graft integrated with surrounding cartilage	0
Macroscopic appearance	Intact smooth surface	4
	Fibrillated surface	3
	Small, scattered fissures or cracks	2
	Several, small or few but large fissures	1
	Total degeneration of grafted area	0
Overall	Grade I normal	12
	Grade II nearly normal	11-8
	Grade III abnormal	7-4
	Grade IV severely abnormal	3-1

Table S4: A semi-quantitative macroscopic scoring system developed by Goebel et al. for the macroscopic description of articular cartilage repair.

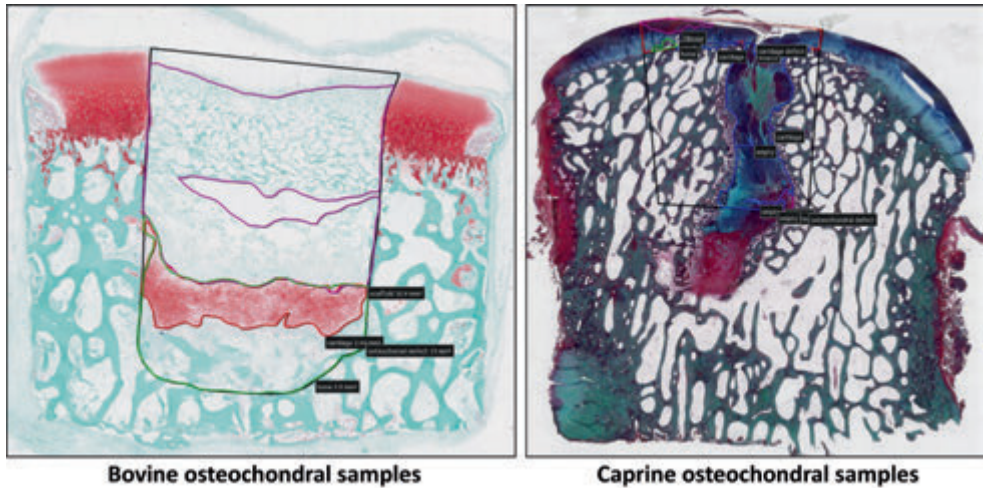
Parameter	Variables	Scores
Color of the repair tissue	Hyaline or white	4
	Predominantly white (>50%)	3
	Predominantly translucent (>50%)	2
	Translucent	1
	No repair tissue	0
Presence of blood vessels in the repair tissue	No	4
	Less than 25% of the repair tissue	3
	25-50% of the repair tissue	2
	50-75% of the repair tissue	1
	More than 75% of the repair tissue	0
Degeneration of adjacent articular cartilage	Normal	4
	Cracks and/or fibrillations in integration zone	3
	Diffuse osteoarthritic changes	2
	Extension of defect into the adjacent cartilage	1
	Subchondral bone damage	0
Surface of the repair tissue	Smooth, homogeneous	4
	Smooth, heterogeneous	3
	Fibrillated	2
	Incomplete new repair tissue (rough)	1
	No repair tissue	0
Percentage defect filling	80-100 %	4
	60-80 %	3
	40-60 %	2
	20-40%	1
	0-20 %	0
Total Scores		20



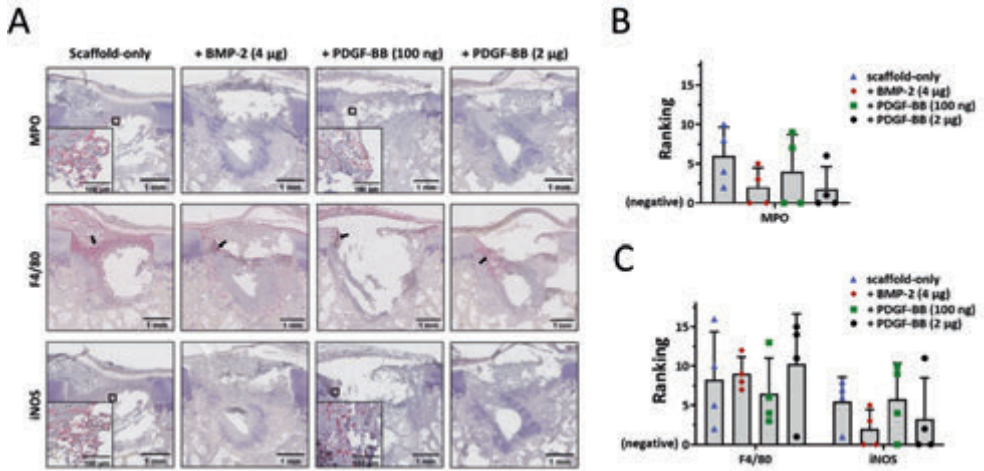
Supplementary Figure S1. Experiment setup of both *in vitro* and *in vivo* studies. (A) Scheme of the *in vitro* release of BMP-2 and PDGF-BB from the different layers of the Col/Col-Mg-HAp scaffold. (B) Scheme of the *ex vivo* osteochondral defect culture model. (C) Scheme of the *in vivo* osteochondral defect mouse model. (D) Scheme of the *in vivo* osteochondral defect in medial femoral condyle and trochlear groove defects in caprine model.



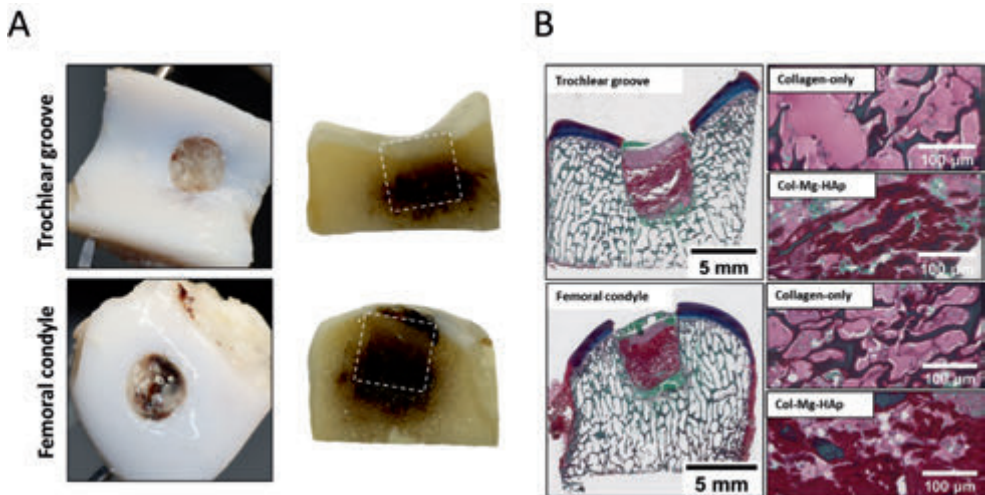
Supplementary Figure S2. Collection of sections from bovine or caprine samples for histology.



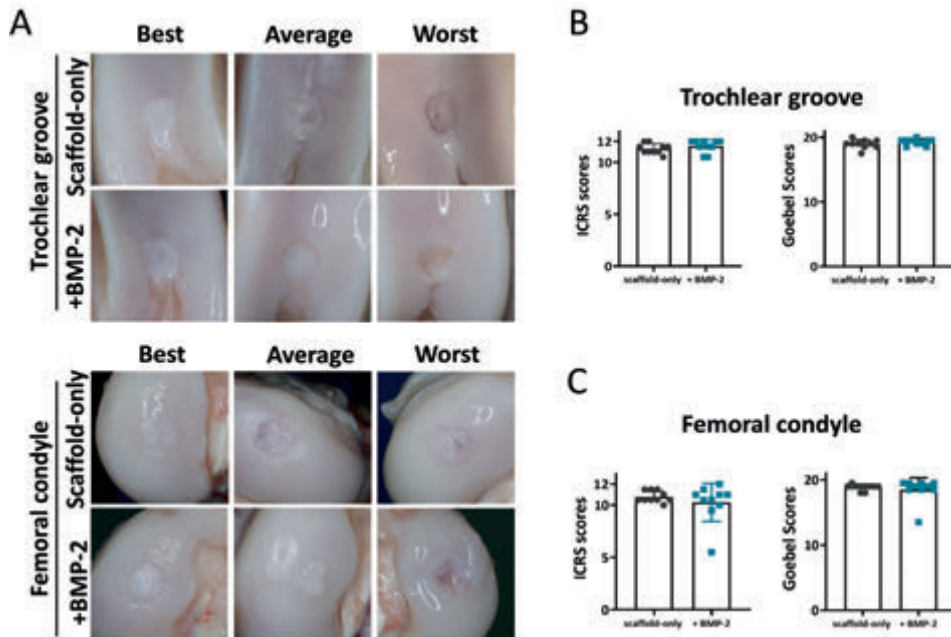
Supplementary Figure S3. Example on defining the defect region, newly formed cartilage-like tissue formation, bone-like tissue formation, fibrous-like tissue formation, remnants of the scaffold for quantification.



Supplementary Figure S4. Association between inflammation and tissue repair at the early phase. (A) Representative images of the 4-week repair constructs stained with immunohistochemistry for MPO and iNOS. Scale bars indicate 1 mm and 100 μ m respectively. Black arrows indicated positive areas. Ranking of MPO (B), F4/80 and iNOS (C) staining in the 4-week osteochondral defects.



Supplementary Figure S5. Osteochondral defects 3 days after implantation. (A) The macroscopic appearance of osteochondral defects 3 days after implantation. The white squares indicated 6*6 mm osteochondral defects. (B) two layers of the scaffold implanted in the femoral condyle defect and trochlear groove defect (stained with Alcian Blue, Fast Green, and Picrosirius Red). The scale bar indicated 5 mm and 100 μ m.



Supplementary Figure S6. Macroscopic assessment of femoral condyle and trochlear groove defect repair. (A) representative examples of trochlear groove defect sites treated with scaffold-only or BMP-2-adsorbed scaffold after 6 months. Best, average, and worst samples determined according to the ICRS scores, are presented. (B) macroscopic scores (according to ICRS Score and Goebel Score) of repair tissue in the trochlear groove defects. (C) representative examples of femoral condyle defect sites treated with scaffold-only or BMP-2-adsorbed scaffold after 6 months. Best, average, and worst samples determined according to the ICRS scores, are presented. (D) macroscopic scores of repair tissue in the femoral condyle defects (according to ICRS score and Goebel Score). The maximum score for ICRS is 12 (indicating the best), and the maximum score for Goebel score is 20 (indicating the best).

References

- [1] van den Borne MP, Raijmakers NJ. International Cartilage Repair Society (ICRS) and Oswestry macroscopic cartilage evaluation scores validated for use in Autologous Chondrocyte Implantation (ACI) and microfracture. *Osteoarthr. Cartil.* 2007, 15, 1397-1402.
- [2] Goebel L, Orth P. Experimental scoring systems for macroscopic articular cartilage repair correlate with the MOCART score assessed by a high-field MRI at 9.4 T—comparative evaluation of five macroscopic scoring systems in a large animal cartilage defect model. *Osteoarthr. Cartil.* 2012, 20, 1046-1055.

REFERENCES

- [1] Hu Y, Chen X. Subchondral bone microenvironment in osteoarthritis and pain. *Bone Res.* 2021;9:20.
- [2] Temenoff JS, Mikos AG. Review: tissue engineering for regeneration of articular cartilage. *Biomaterials.* 2000;21:431-440.
- [3] Mano JF, Reis RL. Osteochondral defects: present situation and tissue engineering approaches. *Journal of Tissue Engineering and Regenerative Medicine.* 2007;1:261-273.
- [4] Tamaddon M, Gilja H. Osteochondral scaffolds for early treatment of cartilage defects in osteoarthritic joints: from bench to clinic. *Biomater Transl.* 2020;1:3-17.
- [5] Donate R, Tamaddon M. Translation through collaboration: practice applied in BAMOS project in *in vivo* testing of innovative osteochondral scaffolds. *Biomater Transl.* 2022;3:102-104.
- [6] Rutgers M, Saris DB. Effect of collagen type I or type II on chondrogenesis by cultured human articular chondrocytes. *Tissue Engineering. Part A.* 2013;19:59-65.
- [7] Ragetly G, Griffon DJ. The effect of type II collagen coating of chitosan fibrous scaffolds on mesenchymal stem cell adhesion and chondrogenesis. *Acta Biomaterialia.* 2010;6:3988-3997.
- [8] Xue X, Hu Y. Recent Advances in Design of Functional Biocompatible Hydrogels for Bone Tissue Engineering. *Advanced Functional Materials.* 2021;31:2009432.
- [9] Zhou H, Liang B. Magnesium-based biomaterials as emerging agents for bone repair and regeneration: from mechanism to application. *Journal of Magnesium and Alloys.* 2021;9:779-804.
- [10] Tampieri A, Sandri M. Design of graded biomimetic osteochondral composite scaffolds. *Biomaterials.* 2008;29:3539-3546.
- [11] Sosio C, Di Giancamillo A. Osteochondral repair by a novel interconnecting collagen-hydroxyapatite substitute: a large-animal study. *Tissue Engineering. Part A.* 2015;21:704-715.
- [12] Levingstone TJ, Thompson E. Multi-layered collagen-based scaffolds for osteochondral defect repair in rabbits. *Acta Biomaterialia.* 2016;32:149-160.
- [13] Kon E, Delcogliano M. A novel nano-composite multi-layered biomaterial for treatment of osteochondral lesions: technique note and an early stability pilot clinical trial. *Injury.* 2010;41:693-701.
- [14] Perdisa F, Filardo G. One-Step Treatment for Patellar Cartilage Defects With a Cell-Free Osteochondral Scaffold: A Prospective Clinical and MRI Evaluation. *The American Journal of Sports Medicine.* 2017;45:1581-1588.
- [15] Di Martino A, Perdisa F. Cell-Free Biomimetic Osteochondral Scaffold for the Treatment of Knee Lesions: Clinical and Imaging Results at 10-Year Follow-up. *The American Journal of Sports Medicine.* 2021;49:2645-2650.
- [16] Dhollander AA, Huyse WC. MRI evaluation of a new scaffold-based allogenic chondrocyte implantation for cartilage repair. *European Journal of Radiology.* 2010;75:72-81.
- [17] Brown TD, Pope DF. Effects of osteochondral defect size on cartilage contact stress. *Journal of Orthopaedic Research: Official Publication of the Orthopaedic Research Society.* 1991;9:559-567.

- [18] Christensen BB, Foldager CB. Poor osteochondral repair by a biomimetic collagen scaffold: 1- to 3-year clinical and radiological follow-up. *Knee Surgery, Sports Traumatology, Arthroscopy: Official Journal of the ESSKA*. 2016;24:2380-2387.
- [19] Xue X, Zhang H. Rational Design of Multifunctional CuS Nanoparticle-PEG Composite Soft Hydrogel-Coated 3D Hard Polycaprolactone Scaffolds for Efficient Bone Regeneration. *Advanced Functional Materials*. 2022;32:2202470.
- [20] Burkus JK, Transfeldt EE. Clinical and radiographic outcomes of anterior lumbar interbody fusion using recombinant human bone morphogenetic protein-2. *Spine (Phila Pa 1976)*. 2002;27:2396-2408.
- [21] Burkus JK, Gornet MF. Anterior lumbar interbody fusion using rhBMP-2 with tapered interbody cages. *J Spinal Disord Tech*. 2002;15:337-349.
- [22] Zhang W, Zhu C. VEGF and BMP-2 promote bone regeneration by facilitating bone marrow stem cell homing and differentiation. *European Cells & Materials*. 2014;27:1-11; discussion 11-12.
- [23] Nash TJ, Howlett CR. Effect of platelet-derived growth factor on tibial osteotomies in rabbits. *Bone*. 1994;15:203-208.
- [24] Heldin CH, Westermark B. Mechanism of action and *in vivo* role of platelet-derived growth factor. *Physiological Reviews*. 1999;79:1283-1316.
- [25] Phipps MC, Xu Y. Delivery of platelet-derived growth factor as a chemotactic factor for mesenchymal stem cells by bone-mimetic electrospun scaffolds. *PLoS One*. 2012;7.
- [26] Hankenson KD, Dishowitz M. Angiogenesis in bone regeneration. *Injury*. 2011;42:556-561.
- [27] Kim SE, Yun YP. Co-delivery of platelet-derived growth factor (PDGF-BB) and bone morphogenetic protein (BMP-2) coated onto heparinized titanium for improving osteoblast function and osteointegration. *Journal of Tissue Engineering and Regenerative Medicine*. 2015;9.
- [28] Keceli HG, Bayram C. Dual delivery of platelet-derived growth factor and bone morphogenetic factor-6 on titanium surface to enhance the early period of implant osseointegration. *Journal of Periodontal Research*. 2020;55:694-704.
- [29] Taniyama T, Masaoka T. Repair of Osteochondral Defects in a Rabbit Model Using a Porous Hydroxyapatite Collagen Composite Impregnated With Bone Morphogenetic Protein-2. *Artificial Organs*. 2015;39:529-535.
- [30] Mumcuoglu D, Fahmy-Garcia S. Injectable BMP-2 delivery system based on collagen-derived microspheres and alginate induced bone formation in a time- and dose-dependent manner. *European Cells & Materials*. 2018;35:242-254.
- [31] Vainieri ML, Lolli A. Evaluation of biomimetic hyaluronic-based hydrogels with enhanced endogenous cell recruitment and cartilage matrix formation. *Acta Biomaterialia*. 2020;101:293-303.
- [32] de Vries-van Melle ML, Narcisi R. Chondrogenesis of mesenchymal stem cells in an osteochondral environment is mediated by the subchondral bone. *Tissue Engineering. Part A*. 2014;20:23-33.
- [33] de Vries-van Melle ML, Tihaya MS. Chondrogenic differentiation of human bone marrow-derived mesenchymal stem cells in a simulated osteochondral environment is hydrogel dependent. *European Cells & Materials*. 2014;27:112-123; discussion 123.

- [34] Levingstone TJ, Ramesh A. Cell-free multi-layered collagen-based scaffolds demonstrate layer specific regeneration of functional osteochondral tissue in caprine joints. *Biomaterials*. 2016;87:69-81.
- [35] Browe DC, Burdis R. Promoting endogenous articular cartilage regeneration using extracellular matrix scaffolds. *Materials Today Bio*. 2022;16:100343.
- [36] Burdis R, Chariyev-Prinz F. Spatial patterning of phenotypically distinct microtissues to engineer osteochondral grafts for biological joint resurfacing. *Biomaterials*. 2022;289:121750.
- [37] van den Borne MP, Raijmakers NJ. International Cartilage Repair Society (ICRS) and Oswestry macroscopic cartilage evaluation scores validated for use in Autologous Chondrocyte Implantation (ACI) and microfracture. *Osteoarthritis and Cartilage*. 2007;15:1397-1402.
- [38] Goebel L, Orth P. Experimental scoring systems for macroscopic articular cartilage repair correlate with the MOCART score assessed by a high-field MRI at 9.4 T--comparative evaluation of five macroscopic scoring systems in a large animal cartilage defect model. *Osteoarthritis and Cartilage*. 2012;20:1046-1055.
- [39] Gaytan F, Morales C. A novel RGB-trichrome staining method for routine histological analysis of musculoskeletal tissues. *Scientific Reports*. 2020;10:16659.
- [40] de Vries-van Melle ML, Mandl EW. An osteochondral culture model to study mechanisms involved in articular cartilage repair. *Tissue Engineering. Part C, Methods*. 2012;18:45-53.
- [41] Rath B, Nam J. Compressive forces induce osteogenic gene expression in calvarial osteoblasts. *J Biomech*. 2008;41:1095-1103.
- [42] Bergmann P, Body JJ. Loading and skeletal development and maintenance. *J Osteoporos*. 2010;2011:786752.
- [43] Jeppsson C, Aspenberg P. BMP-2 can inhibit bone healing. Bone-chamber study in rabbits. *Acta Orthop Scand*. 1996;67:589-592.
- [44] Wescott DC, Pinkerton MN. Osteogenic gene expression by human periodontal ligament cells under cyclic tension. *J Dent Res*. 2007;86:1212-1216.
- [45] Egli PS, Hunzinker EB. Quantitation of structural features characterizing weight-and less-weight-bearing regions in articular cartilage: A stereological analysis of medial femoral condyles in young adult rabbits. *The Anatomical Record*. 1988;222:217-227.
- [46] Athanasiou KA, Rosenwasser M. Interspecies comparisons of *in situ* intrinsic mechanical properties of distal femoral cartilage. *Journal of Orthopaedic Research*. 1991;9:330-340.
- [47] Cuenca-López MD, Peris JL. Action of recombinant human BMP-2 on fracture healing in rabbits is dependent on the mechanical environment. *Journal of Tissue Engineering and Regenerative Medicine*. 2010;4:543-552.
- [48] Boerckel JD, Kolambkar YM. Effects of *in vivo* mechanical loading on large bone defect regeneration. *Journal of Orthopaedic Research*. 2012;30:1067-1075.
- [49] Kopf J, Petersen A. BMP2 and mechanical loading cooperatively regulate immediate early signalling events in the BMP pathway. *BMC Biol*. 2012;10:37.
- [50] da Silva Madaleno C, Jatzlau J. BMP signalling in a mechanical context - Implications for bone biology. *Bone*. 2020;137:115416.

- [51] Rui YF, Lui PP. Mechanical loading increased BMP-2 expression which promoted osteogenic differentiation of tendon-derived stem cells. *Journal of Orthopaedic Research: Official Publication of the Orthopaedic Research Society*. 2011;29:390-396.
- [52] Kanatani M, Sugimoto T. Stimulatory effect of bone morphogenetic protein-2 on osteoclast-like cell formation and bone-resorbing activity. *J Bone Miner Res*. 1995;10:1681-1690.
- [53] Kaneko H, Arakawa T. Direct stimulation of osteoclastic bone resorption by bone morphogenetic protein (BMP)-2 and expression of BMP receptors in mature osteoclasts. *Bone*. 2000;27:479-486.
- [54] Zara JN, Siu RK. High doses of bone morphogenetic protein 2 induce structurally abnormal bone and inflammation *in vivo*. *Tissue Engineering. Part A*. 2011;17:1389-1399.
- [55] Halloran D, Durbano HW. Bone Morphogenetic Protein-2 in Development and Bone Homeostasis. *J Dev Biol*. 2020;8:19.
- [56] Lo KW, Ulerly BD. Studies of bone morphogenetic protein-based surgical repair. *Adv Drug Deliv Rev*. 2012;64:1277-1291.
- [57] James AW, LaChaud G. A Review of the Clinical Side Effects of Bone Morphogenetic Protein-2. *Tissue Engineering Part B Rev*. 2016;22:284-297.
- [58] Ding S, Zhang J. Magnesium modification up-regulates the bioactivity of bone morphogenetic protein-2 upon calcium phosphate cement via enhanced BMP receptor recognition and Smad signaling pathway. *Colloids Surf B Biointerfaces*. 2016;145:140-151.
- [59] Zwingenberger S, Yao Z. Enhancement of BMP-2 Induced Bone Regeneration by SDF-1 α Mediated Stem Cell Recruitment. *Tissue Engineering Part A*. 2014;20:810-818.
- [60] Liu S, Liu Y. Recombinant human BMP-2 accelerates the migration of bone marrow mesenchymal stem cells via the CDC42/PAK1/LIMK1 pathway *in vitro* and *in vivo*. *Biomater Sci*. 2018;7:362-372.
- [61] Wei F, Zhou Y. The Immunomodulatory Role of BMP-2 on Macrophages to Accelerate Osteogenesis. *Tissue Engineering Part A*. 2018;24:584-594.
- [62] Wu DH, Hatzopoulos AK. Bone morphogenetic protein signaling in inflammation. *Exp Biol Med (Maywood)*. 2019;244:147-156.
- [63] Sinder BP, Pettit AR. Macrophages: Their Emerging Roles in Bone. *J Bone Miner Res*. 2015;30:2140-2149.
- [64] Ode Boni B, Lamboni L. Immunomodulation and Cellular Response to Biomaterials: The Overriding Role of Neutrophils in Healing. *Materials Horizons*. 2019;6:1122-1137.
- [65] Aulin C, Jensen-Waern M. Cartilage repair of experimentally induced osteochondral defects in New Zealand White rabbits. *Laboratory Animals*. 2013;47:58-65.
- [66] Dong X, Wang Q. Understanding Adsorption-Desorption Dynamics of BMP-2 on Hydroxyapatite (001) Surface. *Biophysical Journal*. 2007;93:750-759.
- [67] Lee JM, Kim BS. *In vivo* tracking of mesenchymal stem cells using fluorescent nanoparticles in an osteochondral repair model. *Molecular Therapy*. 2012;20:1434-1442.
- [68] Zhang M, Yu W. The Effects of Platelet-Derived Growth Factor-BB on Bone Marrow Stromal Cell-Mediated Vascularized Bone Regeneration. *Stem Cells Int*. 2018;2018:3272098.
- [69] Wang X, Matthews BG. PDGF Modulates BMP2-Induced Osteogenesis in Periosteal Progenitor Cells. *JBMR Plus*. 2019;3:e10127.

6

Effect of sex on scaffold-enhanced subchondral bone repair in experimentally induced osteochondral defects in female and castrated male goats

Jietao Xu, Manuela Salerno, Giuseppe Filardo, Margot C. Labberté, Joeri Kok, Bert van Rietbergen, Eric Farrell, Gerjo J.V.M. van Osch, Pieter A.J. Brama

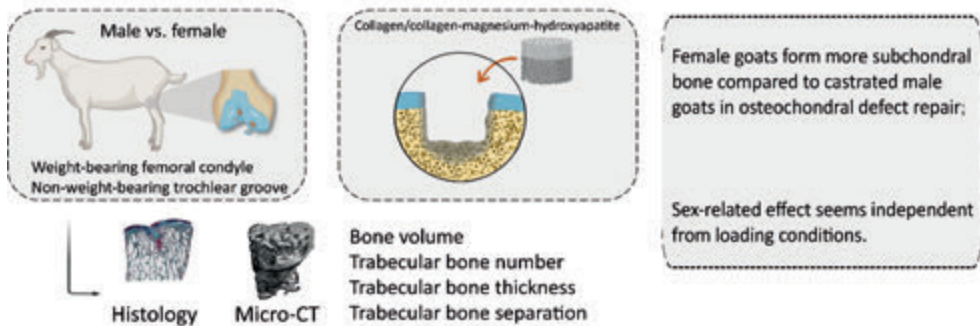
Unpublished

ABSTRACT

The knee osteochondral defect model in the goat is extensively utilized because of its translational advantages regarding cartilage thickness, joint size, loading conditions, anatomy and limited intrinsic healing capacity. However, despite the fact that sex has been suggested to influence bone regeneration, goat studies often lack sex-balancing because of financial, welfare and husbandry constraints. In order to assess the effect of sex on scaffold-enhanced subchondral bone repair in experimentally induced osteochondral defects, we pooled and re-used positive control data of previous studies on the subchondral bone repair capacity of a clinically used collagen/collagen-magnesium-hydroxyapatite scaffold in castrated male and female goats. Significantly higher bone volume, trabecular bone number, trabecular thickness, and lower trabecular separation were observed in subchondral bone defects in female goats compared to castrated male goats. The same trend was found in both the weight-bearing femoral condyle and the non-weight-bearing trochlear groove defects in micro-CT and histological quantification. In conclusion, female goats form more subchondral bone compared to castrated male goats in scaffold enhanced osteochondral defect repair and this effect seems independent of mechanical loading conditions. Future studies evaluating osteochondral defect repair therefore ideally should consider the option of sex balancing.

Keywords: sex; osteochondral defect; goat; weight-bearing; regenerative medicine; tissue engineering

Effect of sex on scaffold enhanced subchondral bone repair



1. INTRODUCTION

Traumatic injuries and chronic diseases within the joint can result in primary or secondary pathologic osteochondral lesions. These have been recognized to contribute to the development and progression of osteoarthritis [1,2]. Biomaterial-based scaffolds have shown promise in regenerating damaged osteochondral tissues [3,4]. However, long-term subchondral bone repair remained suboptimal [5]. Functionally, subchondral bone provides mechanical support for overlying articular cartilage [6,7]. Unrepaired subchondral bone submits the regenerated overlying neocartilage to increased loads, leading to secondary damage of the neocartilage [8]. This subsequently leads to renewed osteochondral damage and joint disease [9]. Meanwhile, since healthy hyaline cartilage does not contain nociceptors (pain receptors), the highly innervated subchondral bone may be an important source of joint pain in osteochondral defects [10]. Therefore, repaired subchondral bone is essential for supporting the long-term survival of the overlying neocartilage and for a stable clinical improvement of the treated osteochondral defect [11].

The clinical literature supports overall good results when addressing lesions of the articular surface with biomaterials, but the clinical outcome is not satisfactory in all patients [4]. Many prognostic factors have been identified and, among these, sex is a key factor that has been explored in clinical studies with controversial results [12,13]. Some preclinical studies report faster bone regeneration in male mice and rats compared to females [14-16], which might be related to differences in sex hormones [17]. On the other hand, there are also studies showing no sex-specific differences in fracture healing in mice [18,19]. Both androgens and estrogens seem to be independently able to maintain cancellous bone mass and integrity [20]. In this context, no studies so far have investigated the effect of sex on subchondral bone repair in osteochondral defects. Preclinical studies may help to shed some light on the differences in terms of sex-related tissue regeneration when treating the osteochondral unit. This is an important research focus, as sex can influence the results through biological but also biomechanical features, which are also key when addressing a structure that is mechanically loaded. In fact, loading can also affect bone regeneration. Bone uniquely adapts and remodels its architecture in response to the mechanical environment. Mechanical loading is also important for the maintenance of normal bone structure and function [21]. In the knee joint, different locations, such as femoral condyle and trochlear ridge or groove, are exposed to different loading patterns, which can potentially influence subchondral bone repair. Therefore, sex-related biological features, as well as other parameters like body weight (indirectly also influenced by sex) and local loading patterns in osteochondral defects may be all critically involved and interplay in determining the results when implanting a scaffold to treat the subchondral unit [22].

The translational goat model is widely applied in biomaterial-based osteochondral repair. Notably, the inclusion of sex-balance in experimental animal studies has become more critical and often specific requirements must be met for funding providers and regulatory bodies. The aim of this study was to investigate the effect of sex on scaffold-enhanced subchondral bone repair in experimentally induced osteochondral defects. To this aim, we re-evaluated the subchondral bone repair capacity of a clinically used collagen/collagen-magnesium-hydroxyapatite (Col/Col-Mg-HAp) scaffold (that was used as a positive control

in previous studies) in both weight-bearing and non-weight-bearing locations of the knee joint of castrated male and female goats.

2. MATERIALS AND METHODDS

2.1. *In vivo* osteochondral defect model

A well validated translational bilateral osteochondral defect model in goats was used to investigate the effect of sex on subchondral bone repair in 18 skeletally mature (2-3 years old) Saanen goats (13 female and 5 castrated male subjects) [23-25]. For this use we obtained and reused positive control data from two similar experimental studies in which we either added growth factors or strontium-enriched amorphous calcium phosphate into the collagen/collagen-magnesium-hydroxyapatite (Col/Col-Mg-HAp) osteochondral scaffold (experimental groups) to improve the subchondral bone repair compared to a scaffold-only positive control group in which we implanted a clinically used Col/Col-Mg-Hap scaffold [26,27]. Both weight-bearing (femoral condyle) and non-weight-bearing (femoral trochlea) osteochondral defect locations were implanted with the Col/Col-Mg-HAp scaffold acting as a positive control towards enhancements of the same scaffold in the other limb. In short: After withholding roughage for 24h animals received profylactic antibiotics (amoxycillin clavulanic acid 8.75 mg/kg intramuscular; Noroclav, Norbrook, Ireland) and sedation was performed with butorphanol (0.2 mg/kg, Butador, Chanelle Pharma, Ireland) and diazepam (0.2 mg/kg, Diazemuls; Accord Healthcare, UK) intravenously. While in sternal recumbancy a lumbosacral epidural block was placed with lidocaine (2 mg/kg, Lidocaine HCl 2%, B.Braun Medical Inc., EU) and morphine (0.2 mg/kg, Morphine Sulphate 10mg/ml, Kalceks, Latvia). Anaesthesia was induced with propofol IV to effect (max. 6 mg/kg, Propofol-Lipuro 1%, B. Braun Medical Inc., EU) and was maintained with isoflurane (Vetflurane, Virbac Animal Health, UK). Ninety minutes after the epidural block animals received analgesia with meloxicam IV (0.5 mg/kg, Rheumocam, Chanelle, Ireland) and morphine IV (0.2 mg/kg, Morphine sulphate, Mercury Pharmaceuticals, Ireland).

In dorsal recumbency, an arthrotomy using the lateral parapatellar approach was performed in both knees. Under constant irrigation with saline, a pointed 6 mm drill bit was used to drill an approximate 3-4 mm deep defect in the transition of the distal 1/3 to the middle 1/3 of the trochlear groove and in the medial femoral condyle. Subsequently, a custom-made flattened drill bit and a depth guide were used to create an exact flat circular critical-sized osteochondral defect (6 mm deep by 6 mm wide) in both locations. The joint was flushed with saline to remove any debris, and the positive control defects were press fitted with a similar-sized Col/Col-Mg-HAp scaffold (6 mm diameter, 6 mm height, osteochondral scaffold, Finceramica, Italy) before surgical closure. Either left or right knee joints were randomly assigned to the positive control treatment.

During the postoperative period analgesia was provided for 5 days (meloxicam) and animals were housed in indoor pens for daily welfare monitoring and scoring. .Fourteen days after the procedure, following removal of skin sutures, animals were moved to pasture or loose housing (weather dependent) until the 6-month endpoint of the study with daily health checks. All the joints were dissected, and photographed (Body Canon EOS

R5, lens: Canon EF 100mm f/2.8L Macro IS USM, flash: Macro Ring lite MR-14EX II). Biopsies 1 cm by 1 cm square containing the entire defects were harvested with an oscillating saw.

This animal experiment complied with the ARRIVE guidelines. Ethical evaluation and approval were provided by the Health Products Regulatory Authority of Ireland (AE1898217/P142), The Animal Research Ethics Committee of University College Dublin (AREC-18-17-Brama) and the Lyons Animal Welfare Board (Health, Husbandry and Monitoring plans; 201907).

2.2. Macroscopic assessment of the osteochondral defect repair

Cartilage repair quality was scored using two macroscopic evaluation systems: (1) the International Cartilage Repair Society (ICRS) system (Table S1) [28], which grades the macroscopic appearance of repaired cartilage tissue as Grade I (normal), Grade II (nearly normal), Grade III (abnormal), or Grade IV (severely abnormal); (2) the Goebel macroscopic scoring system (Table S2) [29], which evaluates macroscopic repaired articular cartilage with five major evaluation categories. The quality of cartilage repair was independently and blindly scored by two investigators on fresh samples. The scores were averaged for further analysis. Subsequently, fixation of all samples were conducted using 4% formalin for 10 days.

2.3. Micro-computed tomography of the osteochondral defect repair

Samples were scanned under micro-CT (Quantum GX, Perkin Elmer, USA) with the following settings: energy 90 KV, intensity 88 μ A, 36 mm FOV, 72 μ m isotropic voxel size. All scans were performed under an X-ray filter of Cu (thickness = 0.06 mm) and Al (thickness = 0.5 mm) and calibrated with a phantom (density 0.75 g/cm³). A high-resolution mode was set with a scan time of 4 minutes.

Image processing included modest Gauss filtering (sigma = 0.8 voxel, width = 1 voxel) and segmentation using a single threshold. A cylindrical region (4 mm diameter and 5 mm height) within the original defect (6 mm diameter and 6 mm height) was selected as a volume of interest (VOI). In this VOI the following morphometric parameters were measured: bone volume per total volume (BV/TV), trabecular bone number (Tb.N), trabecular thickness (Tb.Th), and trabecular separation (Tb.Sp). Morphological analyses were performed using IPL (Scanco Medical AG, Bruettisellen, Switzerland).

2.4. Histology and immunohistochemistry of osteochondral defect repair

All samples were decalcified for 3 weeks using 10% formic acid (Sigma, Saint Louis, USA), subsequently embedded in paraffin and sectioned at 6 μ m sections. Following dewaxing, RGB staining was performed using Alcian Blue (Sigma, Saint Louis, USA), Fast Green (Sigma, Saint Louis, USA), and Picrosirius Red (Sigma, Saint Louis, USA) [30] to study the regenerated tissue type in the osteochondral defects. Red staining indicates collagen fibers or uncalcified bone tissue. Green staining indicates mineralized bone tissue. Pink/greenish staining indicates mineralised cartilage matrix. Blue staining indicates proteoglycans/hyaline cartilage tissue. NDP View2 software (version 2.8.24, 2020 Hamamatsu Photonics K.K.) was used to quantify tissue volume in the osteochondral defect at three sections that were taken in the centre. The percentage of the defect filled

with newly formed osteochondral tissue was calculated. All slides were independently and blindly scored by two investigators, and averaged for each section.

2.5. Statistical analysis

All statistical tests were performed using SPSS software 28.0 (SPSS inc., Chicago, USA). The repair tissue volume was expressed as mean \pm standard deviation (SD). Equality of variances was tested by Levene's test. Statistically significant differences between two groups were determined by a Student's T test or a Mann-Whitney U test (depending on normality tested by a Shapiro-Wilk test). A p value \leq 0.05 was considered statistically significant.

3. RESULTS

3.1. Clinical observations and scaffold implantation

To reduce the use of animals in line with the 3Rs, 5 castrated male and 13 female skeletally mature goats (2-3 years old) that were used as positive controls in previous studies performed by the authors were included in this study [26,27]. These goats showed no difference in weights between male and female animals (38.0 ± 2.8 vs. 37.2 ± 8.0 kg, $P = 0.839$). Therefore, the effect of weight as a confounding factor in evaluating sex effects was excluded. During surgery, scaffolds were successfully press-fitted into defects created on the weight-bearing (femoral condyle) and non-weight-bearing (trochlear groove) locations. Intra-operatively scaffolds were filled instantly with blood from healthy surrounding subchondral bone (Figure 1). Postoperatively all animals recovered without complications. Within 5 days all goats moved freely without signs of distress or significant lameness for the duration of the study up to the endpoint of 6 months.



Figure 1. Location of osteochondral defects in the femoral condyle (weight-bearing) and the trochlear groove (non-weight-bearing). Note the fresh bleeding from the defect before press fit implantation of the scaffold and the soaking of the scaffold with blood (turning white scaffold red) after implantation.

3.2. Female goats formed more subchondral bone compared to male goats and this was independent from loading conditions

Micro-CT reconstruction was performed for the quantification of the subchondral bone formation in the osteochondral defect. Well-healed subchondral bone was found in the osteochondral defect at 6 months (Figure 2A,B). Since female controls originated from two different studies (10 female goats from study 1 [26] and 3 females from study 2 [27]), the difference in subchondral bone repair between females of the two groups was first evaluated to exclude the effect of different studies as a confounding factor in evaluating

sex effects. No significant difference was found in subchondral bone repair between females of the two groups and data were pooled for further comparison (Supplementary Figure S1).

Two differently loaded defect locations, weight-bearing (femoral condyle) and non-weight-bearing (trochlear groove), were evaluated in this study. To investigate the influence of local mechanical loading patterns on subchondral bone repair the two differently loaded locations in both male and female subjects were initially investigated separately (Figure 2A,B). A trend was found in both weight-bearing and non-weight-bearing defects with more subchondral bone repair in female goats (Figure 2C). Specifically, in the weight-bearing femoral condyle bone defects, higher bone volume per total volume (BV/TV, $P = 0.043$), trabecular bone number (Tb.N, $P = 0.084$), trabecular thickness (Tb.Th, $P = 0.208$), and lower trabecular separation (Tb.Sp, $P = 0.059$) was observed in female goats compared to male goats (Figure 2C). Similarly, higher BV/TV ($P = 0.051$), Tb.N ($P = 0.326$), Tb.Th ($P = 0.173$), and lower Tb.Sp ($P = 0.513$) in the non-weight-bearing trochlear groove bone defects were observed in female goats (Figure 2C).

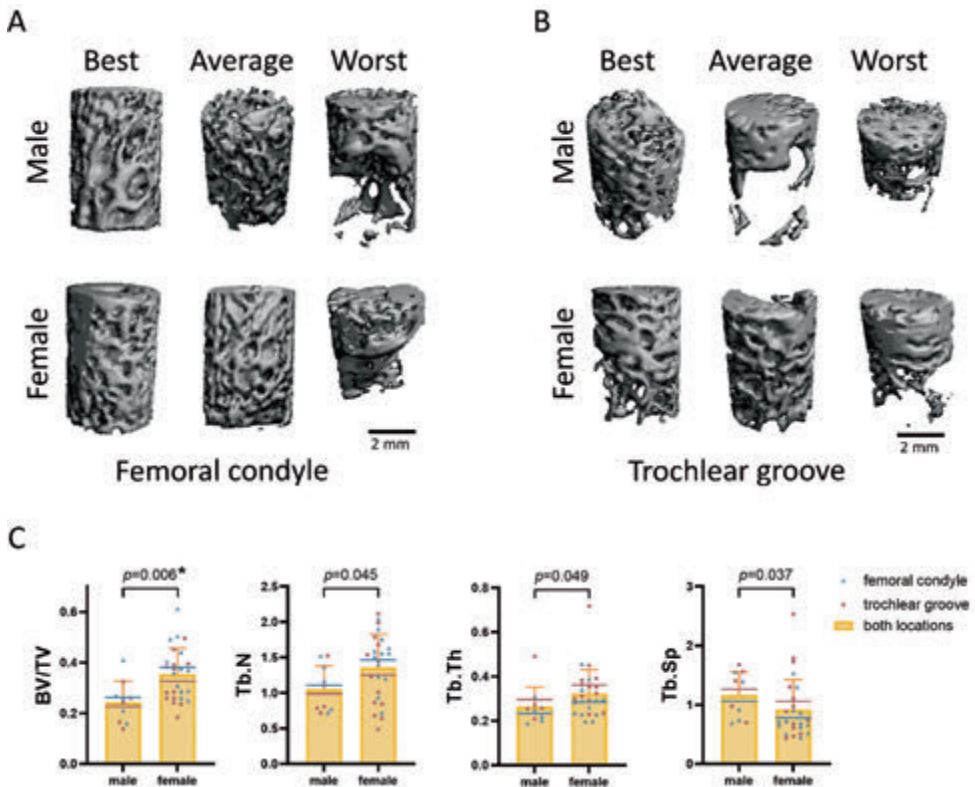


Figure 2 More bone repair was observed in female goats after 6 months. (A) Representative micro-CT reconstructions in the femoral condyle bone defects. Best, Average and Worst samples were presented according to bone volume. The scale bar indicates 2 mm. (B) Representative micro-CT reconstructions in the trochlear groove bone defects. Best, Average and Worst samples were presented according to bone volume. The scale bar indicates 2 mm. (C) bone volume per total volume (BV/TV), trabecular number (Tb.N [1/mm]), trabecular thickness (Tb.Th [mm]), and trabecular separation (Tb.Sp [mm]) in the subchondral bone defects.

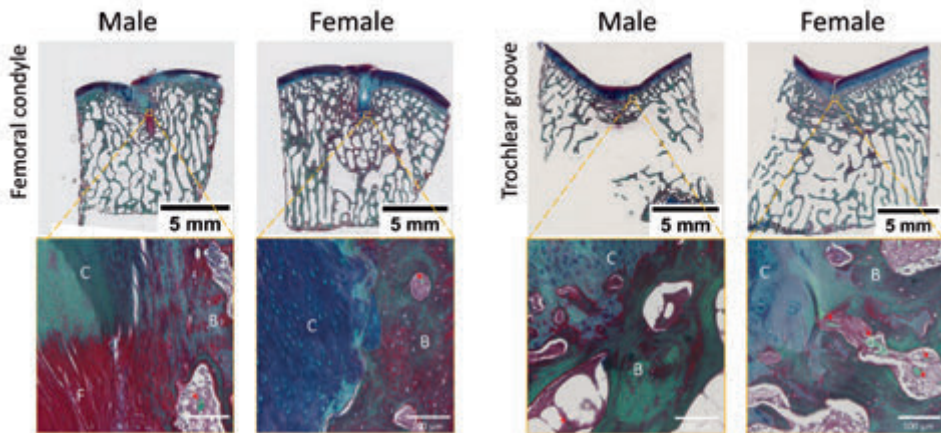
The blue (femoral condyle) and red (trochlear groove) lines in the bar graphs indicate the mean value. The blue (femoral condyle) and red (trochlear groove) dots in the bar graphs indicate the value of each sample. The *p* value above the bars in the graphs indicate the significant difference between male and female goats when femoral condyle and trochlear groove bone defects were combined in the analyses. * *p* < 0.05 indicates the difference between male and female goats in only the femoral condyle.

Between femoral condyle bone defects and trochlear groove bone defects in male goats, no significant difference was observed in BV/TV (*P* = 0.545), Tb.N (*P* = 0.841), Tb.Th (*P* = 0.222), or Tb.Sp (*P* = 0.443). Similarly, in female goats, no significant difference was found in BV/TV (*P* = 0.183), Tb.N (*P* = 0.259), or Tb.Sp (*P* = 0.336) between femoral condyle bone defects and trochlear groove bone defects, although higher Tb.Th (*P* = 0.034) was observed in trochlear groove bone defects (Figure 2C). When both locations were combined to investigate the difference in bone repair between male and female goats, significantly higher BV/TV, Tb.N, Tb.Th, and Tb.Sp were observed in the subchondral bone defects in female goats compared to male goats (Figure 2C).

3.3. Female goats formed more subchondral bone on histology compared to male goats in both femoral condyle and trochlear groove defects

Histological evaluation supported the micro-CT quantification results (Figure 3A,B). In the femoral condyle, the same trend as with CT quantification with slightly more bone-like tissue was observed in female compared to male goats (85.7 ± 10.5 vs. 73.8 ± 13.3%,

A



B

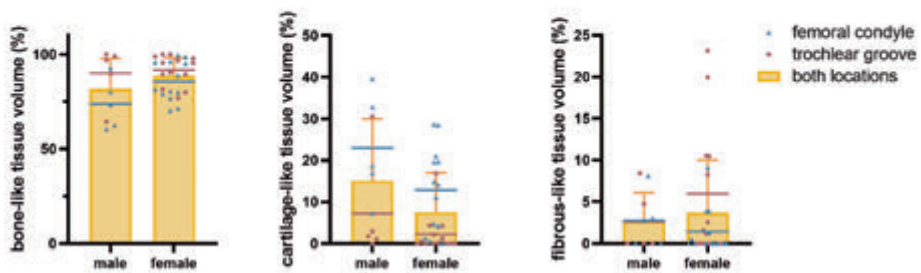


Figure 3. Slightly more bone repair in female goats in both femoral condyle and trochlear groove osteochondral defects. (A) Representative RGB (Picosirius Red, Fast Green, and Alcian Blue) staining of femoral condyle and trochlear groove osteochondral defects. The scale bar indicates 5 mm and 100 μ m. B: bone-like tissue; C: cartilage-like tissue; F: fibrous-like tissue; Red arrows indicate blood vessels. (B) Percentage of tissue volume calculated in the femoral condyle and trochlear groove subchondral bone defects. The blue (femoral condyle) and red (trochlear groove) lines in the bar graphs indicate the mean value. The blue (femoral condyle) and red (trochlear groove) dots in the bar graphs indicate the value of each sample.

$P = 0.063$). This might be related to a slightly decreased cartilage-like tissue ($12.9 \pm 10.2\%$ vs. $23.0 \pm 13.0\%$, $P = 0.099$) and fibrous-like tissue ($1.4 \pm 2.7\%$ vs. $2.8 \pm 3.3\%$, $P = 0.503$) volume in female femoral condyle subchondral bone defects (Figure 3B). No difference in bone-like tissue volume was found in trochlear groove bone defects between male and female goats ($90.1 \pm 14.9\%$ vs. $91.7 \pm 7.9\%$, $P = 0.703$), but decreased cartilage-like tissue volume ($2.3 \pm 4.7\%$ vs. $7.2 \pm 13.1\%$, $P = 0.336$) was also observed in female trochlear groove bone defects (Figure 3B). Interestingly, in both male and female, slightly less bone-like tissue ($P = 0.106$ for male, $P = 0.113$ for female) and more cartilage-like tissue ($P = 0.092$ for male, $P = 0.002$ for female) were generated in the femoral condyle subchondral bone defects compared to the trochlear groove bone defects (Figure 3B).

3.4. Well-healed cartilage was observed in both male and female goats

Macroscopically, hyaline cartilage like tissue was observed on the surface of the defects with good integration into surrounding native cartilage tissue. No noticeable depressions were observed, although small, scattered fissures or cracks were observed in some defects (Figure 4A). The cartilage was classified as normal (grade I) or nearly normal (grade II) in all samples except for one female sample that graded III. No difference in both macroscopic scores in cartilage repair between male and female goats was found (Figure 4B). On histology, the scaffolds had been degraded completely after 6 months and round cells residing within lacunae were present in the cartilage region. Glycosaminoglycan (GAGs) and collagen were present in the repair tissue in the defect as demonstrated by RGB staining (Figure 3A), indicating cartilaginous tissue formation.

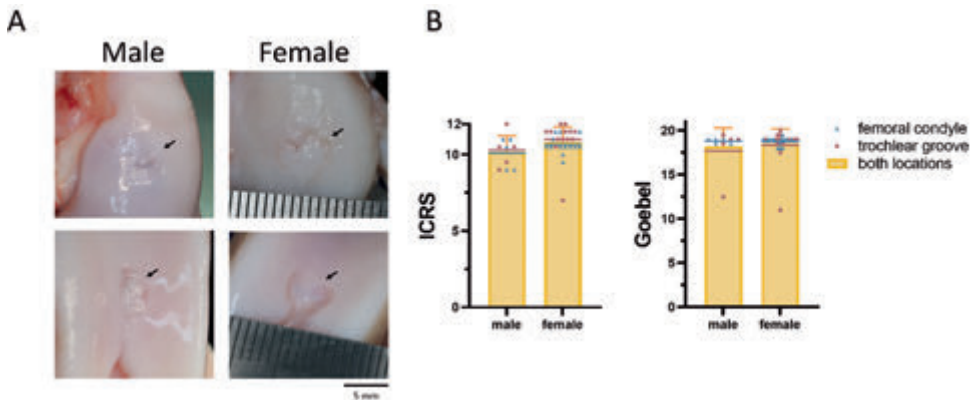


Figure 4. Macroscopic assessment of femoral condyle and trochlear groove osteochondral defect repair. (A) Representative examples of defect sites after 6 months. Arrows indicate the defects. (B) Macroscopic scores of repair tissue in the trochlear groove osteochondral defects. 12 and 20 (indicating the best) are the

maximum scores for the ICRS score and the Goebel score, respectively. The blue (femoral condyle) and red (trochlear groove) lines in the bar graphs indicate the mean value. The blue (femoral condyle) and red (trochlear groove) dots in the bar graphs indicate the value of each sample.

4. DISCUSSION

In this study, we evaluated the effect of sex on scaffold-enhanced subchondral bone repair in experimentally induced weight-bearing and non-weight-bearing osteochondral defects in a large animal model. Although some studies have investigated the role of sex in bone fracture or large bone defect healing, no preclinical large animal studies have investigated the effect of sex on biomaterial enhanced subchondral bone repair in osteochondral defects previously. Our analyses indicate that female goats generated more subchondral bone repair compared to castrated male goats, and the improved subchondral bone healing was independent from loading conditions.

The goat model is a fully immune competent model using outbred animals, and offers advantages regarding joint size, cartilage thickness, loading, comparative anatomy and limited intrinsic healing capacity [31]. In goats, the ratio of cartilage to subchondral bone is closer to humans than in small animals. Also, the goat model provides the opportunity to assess tissue regeneration in critical size osteochondral defects in two different mechanical loading environments within the same joint. Specifically, the scaffolds were successfully implanted in the trochlear groove, with no/low direct mechanical loading, and in the medial femoral condyle, with direct mainly compressional mechanical loading [32]. In our study there was no difference in weights between male and female animals investigated. So, a potential bias caused by the direct effect of weight-related mechanical loading was excluded, thus avoiding a potential bias when studying sex differences and strengthening the study results.

Recently the inclusion of sex-balance in experimental animal studies has become more critical and often specific requirements have to be met for funding providers, ethical approval and regulatory bodies. To study the effect of sex on subchondral bone repair in preclinical large animal models, and to make the translation from bench to bed, the chosen model should clearly demonstrate close physiological and pathophysiological analogies with the osteochondral environment in humans, where sex is considered an important factor in determining treatment results [13]. Although no previous preclinical studies investigated the effect of sex on subchondral bone repair, some studies reported the effect of sex on bone healing after fracture. Estrogen and testosterone both have receptors on osteoclasts, osteoblasts, and osteocytes [33], and the effects of sex hormones on bone formation have been shown by several experiments on animals as well as clinical case reports [34]. In males, testosterone has a key role in development and maintenance of cortical and trabecular bone mass [34]. In mice, androgen deficiency accounts for cancellous bone loss due to higher resorption, this effect being more pronounced in males compared to females [35,36] and the treatment with testosterone is able to rescue orchidectomy-induced bone loss [36]. In female animals, as well as in humans, estrogens have important effects on bone turnover, with optimal levels required to achieve a normal bone growth. Estrogen is required to control bone metabolism and trabecular bone mineral density [37]. At cellular level 17β -estradiol, a biologically active form of estrogen, promotes osteogenic activity and exerts anti-apoptotic effects on osteoblasts and pro-

apoptotic effect on osteoclasts [38,39]. In mouse models, estrogen-induced osteogenesis in long bones [40] as well as beneficial effects on bone healing, especially in the late phase, have been reported [41]. On the other hand, estrogen deficiency is responsible for bone destruction through several mechanisms [42].

Considering the potential influence of all the aforementioned aspects on the repair processes, the inclusion of both sexes can provide important information on the potential of the implanted biomaterials, although this requires larger studies with some practical limitations which impaired the inclusion of both sexes in a large part of the previous literature.

The husbandry situation in large animal studies, however, limits the possibilities to include non-castrated males unless extensive separation of groups is implemented. This in itself induces new issues such as variation in environment during the study and potential physiological hormonal and stress effects due to fighting that might occur in one sex male groups [43,44]. Castration of male animals would allow sex-balanced groups but changes male reproduction hormone levels with potential consequences for bone metabolism [44]. These difficulties in study design, welfare issues and additional costs have impeded researchers from implementing sex-balance in well validated and widely applied translational preclinical osteochondral defect models in goats. In our study, the male goats were castrated after reaching sexual maturity, at the age of one year, for husbandry purposes. This led to decreased testosterone [36,45], which may have potentially influenced subchondral bone repair. In fact, orchietomized animals might be subjected to a reduction in bone mineral content, as shown in rats [46]. However, although the difference in osteogenesis might be due to the function of estrogens and androgens in skeletal physiology and pathophysiology [47], as well as the changes induced by castration in this model, other sex-related effects can also play an important role. Other hormones may further contribute to the development of the skeletal sexual dimorphism. For example, the GH-IGF1 axis, even more than sex-steroid action, is likely to be a primary determinant of sex differences which develop during pubertal bone growth [34]. VEGF has also been explored as a potential key mediator of sex-based differences in bone healing, with findings in the mice model showing how VEGF conditional deletion produced sexually dimorphic effects on bone mineralization and vascularization [48]. Bone healing was also reported to be related with the number of stem cells [49]. Stem cells isolated from male donors were reported to have better osteogenic capacity compared to female donors *in vitro* and *in vivo* [50], while other findings suggest that the intrinsic osteogenic capacity of male and female stem cells seems to be independent of sex [49]. Interestingly, a study evaluated the cranial defect repair in intact males, castrated males, intact females, and ovariectomized females. The results demonstrated that sex of the host, but not sex hormones, affects bone formation [51] with intact or castrated males forming more bone than females at the defect site [51]. The complexity of hormonal, genetic, and cellular differences is further increased by another factor, since not all bone locations seem to respond the same. In subchondral bone some clinical studies indicated an opposite trend, deterioration in osteochondral repair was seen in male subjects in long-term follow up compared to female patients [52,53]. Our study indicates that female goats form more subchondral bone with higher bone volume, trabecular number and thickness compared to castrated male goats. Some studies also reported that female mice achieved better

bone remodeling. This might be attributed to elevated BMP-9 expression levels and increased osteoclast numbers that promote faster remodeling of the fracture calluses. On the other hand, male mice formed larger bone calluses than females which might be attributed to higher IGF-1 expression, and increased osteoblast numbers during callus formation [54]. Overall, all these components accounting for sex differences are likely to play an important role in subchondral bone repair of osteochondral defect experimental models. The results are of high relevance as they provide new insight on the importance of looking into sex-related differences when investigating osteochondral regeneration, even when specific male hormonal influences are removed.

The results also indicated that the effect of sex on subchondral bone is not directly dependent on mechanical loading, since in both weight-bearing and non-weight-bearing osteochondral defects, female goats achieved more subchondral bone repair. However, in both male and female goats, higher bone volume and trabecular numbers were observed in the weight-bearing osteochondral defect location compared to the non-weight-bearing location. The crosstalk between mechanical loading and sex hormones was already reported [55]. Changes in estrogen (for example during puberty and menopause) influence the adaptive response of bone to mechanical loading. The response to strain of osteoblastic cell proliferation *in vitro* requires estrogen receptor- α (ER α), which is associated with stimulation of IGF-1 and Wnt signaling [56-59]. Some studies have explored the potential role of androgens in modulating bone's adaptive response to mechanical loading [47]. In adult male mice androgens were shown to inhibit the osteogenic response to mechanical loading [60]. Cyclic loading was demonstrated to prevent the increase in trabecular separation and substantially increased trabecular thickness to preserve cancellous bone mass after orchidectomy [61]. Therefore, sex and mechanical loading can both independently and interactively affect subchondral bone repair.

The presented study re-used data by using positive control data from previous studies published by our group. Data reuse is an essential component of open science, but scientific etiquette and research integrity require fair reuse of data such as for instance novel purpose [62]. We strongly believe that our study created a novel purpose by investigating sex differences in the translational goat osteochondral defect model. Subchondral bone regeneration is crucial in osteochondral defect repair and to investigate biomaterial-based osteochondral repair, the utility of an optimal animal model is crucial. The translational goat model is widely applied in osteochondral repair. Notably, sex has been suggested to influence bone regeneration, and the inclusion of sex-balance in experimental animal studies has become more critical and is often required by funding providers and regulatory bodies. In addition, our study contributes significantly to Reduction in the use of experimental animals as is recommended when adhering to ARRIVE compliance and the 3Rs [63].

However, our study also has limitations. The presented study makes use of positive controls from historical studies in which we did not assess bone status or hormone levels before implantation of the positive control scaffold. However, animals were selected randomly out of a larger animal cohort available to the research group and therefore we do not expect any significant differences in bone status nor hormone levels between animals within the castrated male or female groups respectively. In addition, all animals

were assessed by the veterinary team (using SOPs for the pre-anaesthetic exam, clinical exam, and a bilateral orthopaedic knee exam) before inclusion in the study. We also assessed the macroscopic health status of the joint during surgery and concluded that all animals had normal joints. Androgen hormone levels are expected to be significantly reduced in castrated male goats compared to non-castrated animals. But other significant hormonal differences between randomly chosen animals of the same age and weight within each sex group are unlikely to occur when husbandry and environment conditions are identical.

Finally, we have an unequal distribution of female and male subjects due to unexpected but experimentally unrelated animal deaths caused by a *Clostridium* outbreak in our original sex balanced study. Therefore, we had only 5 castrated males and 3 females left and we were required to add female subjects to our analyses from another study to obtain sufficient power for our experiment to analyse a sex effect. Although females were technically obtained from two different studies both studies ran in parallel, and all animals were kept together in one herd under similar husbandry conditions. All animals underwent the same surgery and received the same positive control scaffold in one of their knee joints. All surgeries, aftercare and analyses of samples was performed by the same team. In addition, statistical testing was performed to exclude differences between females from different experiments before data were pooled.

Overall, this study provides indications that sex can affect subchondral bone repair and this effect in itself seems to be independent from mechanical loading. Even if husbandry requirements may require castration, future studies evaluating subchondral bone repair should therefore consider the option of sex balancing.

5. CONCLUSION

Female goats form more subchondral bone compared to castrated male goats in osteochondral defect repair with a Col/Col-Mg-HAp scaffold, and this sex-related effect seems independent from loading conditions, with similar findings observed when treating both weight-bearing femoral condyle and non-weight-bearing femoral trochlea groove osteochondral defects.

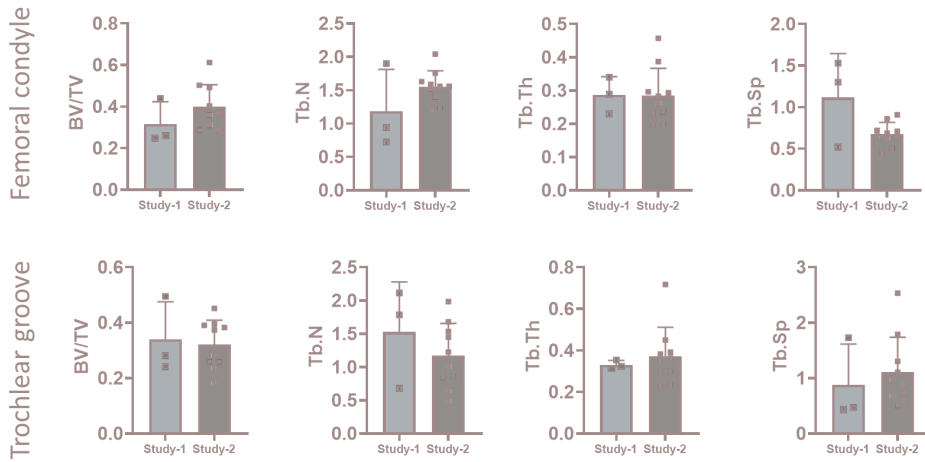
SUPPLEMENTARY MATERIALS

Table S1: International Cartilage Repair Society (ICRS) cartilage repair scoring system. This tool is to evaluate the macroscopic appearance of cartilage repair tissue.

Parameter	Variables	Scores
Degree of defect repair	In level with surrounding cartilage	4
	75% repair of defect depth	3
	50% repair of defect depth	2
	25% repair of defect depth	1
	0% repair of defect depth	0
Integration to border zone	Complete integration with surrounding cartilage	4
	Demarcating border < 1 mm	3
	¾ of graft integrated, ¼ with a notable border > 1 mm	2
	1/2 of graft integrated with surrounding cartilage, 1/2 with a notable border > 1 mm	1
	From no contact to ¼ of graft integrated with surrounding cartilage	0
Macroscopic appearance	Intact smooth surface	4
	Fibrillated surface	3
	Small, scattered fissures or cracks	2
	Several, small or few but large fissures	1
	Total degeneration of grafted area	0
Overall	Grade I normal	12
	Grade II nearly normal	11-8
	Grade III abnormal	7-4
	Grade IV severely abnormal	3-1

Table S2: A semi-quantitative macroscopic scoring system developed by Goebel et al. for the macroscopic description of articular cartilage repair.

Parameter	Variables	Scores
Color of the repair tissue	Hyaline or white	4
	Predominantly white (>50%)	3
	Predominantly translucent (>50%)	2
	Translucent	1
	No repair tissue	0
Presence of blood vessels in the repair tissue	No	4
	Less than 25% of the repair tissue	3
	25-50% of the repair tissue	2
	50-75% of the repair tissue	1
	More than 75% of the repair tissue	0
Degeneration of adjacent articular cartilage	Normal	4
	Cracks and/or fibrillations in integration zone	3
	Diffuse osteoarthritic changes	2
	Extension of defect into the adjacent cartilage	1
	Subchondral bone damage	0
Surface of the repair tissue	Smooth, homogeneous	4
	Smooth, heterogeneous	3
	Fibrillated	2
	Incomplete new repair tissue (rough)	1
	No repair tissue	0
Percentage defect filling	80-100 %	4
	60-80 %	3
	40-60 %	2
	20-40%	1
	0-20 %	0
Total Scores		20



Supplementary Figure S1. No significant difference in bone repair between females of two groups. Bone volume per total volume (BV/TV), trabecular thickness (Tb.Th [mm]), trabecular number (Tb.N [1/mm]), and trabecular separation (Tb.Sp [mm]) in the bone defects.

References

[1] van den Borne MP, Raijmakers NJ. International Cartilage Repair Society (ICRS) and Oswestry macroscopic cartilage evaluation scores validated for use in Autologous Chondrocyte Implantation (ACI) and microfracture. *Osteoarthr. Cartil.* 2007, 15, 1397-1402.

[2] Goebel L, Orth P. Experimental scoring systems for macroscopic articular cartilage repair correlate with the MOCART score assessed by a high-field MRI at 9.4 T--comparative evaluation of five macroscopic scoring systems in a large animal cartilage defect model. *Osteoarthr. Cartil.* 2012, 20, 1046-1055.

REFERENCES

- [1] Mano JF, Reis RL. Osteochondral defects: present situation and tissue engineering approaches. *J Tissue Eng Regen Med.* 2007;1:261-273.
- [2] Suri S, Walsh DA. Osteochondral alterations in osteoarthritis. *Bone.* 2012;51:204-211.
- [3] Sessa A, Romandini I. Treatment of Juvenile Knee Osteochondritis Dissecans with a Cell-Free Biomimetic Osteochondral Scaffold: Clinical and MRI Results at Mid-Term Follow-up. *Cartilage.* 2021;13:1137s-1147s.
- [4] Filardo G, Andriolo L. Scaffolds for Knee Chondral and Osteochondral Defects: Indications for Different Clinical Scenarios. A Consensus Statement. *Cartilage.* 2021;13:1036s-1046s.
- [5] Di Martino A, Perdisa F. Cell-Free Biomimetic Osteochondral Scaffold for the Treatment of Knee Lesions: Clinical and Imaging Results at 10-Year Follow-up. *The American Journal of Sports Medicine.* 2021;49:2645-2650.
- [6] Madry H, van Dijk CN. The basic science of the subchondral bone. *Knee Surgery, Sports Traumatology, Arthroscopy.* 2010;18:419-433.
- [7] Hu Y, Chen X. Subchondral bone microenvironment in osteoarthritis and pain. *Bone Res.* 2021;9:20.
- [8] Li G, Yin J. Subchondral bone in osteoarthritis: insight into risk factors and microstructural changes. *Arthritis Res Ther.* 2013;15:223.
- [9] Brown TD, Pope DF. Effects of osteochondral defect size on cartilage contact stress. *J Orthop Res.* 1991;9:559-567.
- [10] van Dijk CN, Reilingh ML. Osteochondral defects in the ankle: why painful? *Knee Surg Sports Traumatol Arthrosc.* 2010;18:570-580.
- [11] Dhollander AA, Huysse WC. MRI evaluation of a new scaffold-based allogenic chondrocyte implantation for cartilage repair. *European Journal of Radiology.* 2010;75:72-81.
- [12] Filardo G, Kon E. Does patient sex influence cartilage surgery outcome? Analysis of results at 5-year follow-up in a large cohort of patients treated with Matrix-assisted autologous chondrocyte transplantation. *Am J Sports Med.* 2013;41:1827-1834.
- [13] Filardo G, Kon E. Clinical profiling in cartilage regeneration: prognostic factors for midterm results of matrix-assisted autologous chondrocyte transplantation. *Am J Sports Med.* 2014;42:898-905.
- [14] Mehta M, Schell H. A 5-mm femoral defect in female but not in male rats leads to a reproducible atrophic non-union. *Arch Orthop Trauma Surg.* 2011;131:121-129.
- [15] Deng Z, Gao X. Gender differences in tibial fractures healing in normal and muscular dystrophic mice. *American Journal of Translational Research.* 2020;12:2640-2651.
- [16] Mehta M, Duda GN. Influence of gender and fixation stability on bone defect healing in middle-aged rats: a pilot study. *Clin Orthop Relat Res.* 2011;469:3102-3110.
- [17] Callewaert F, Venken K. Differential regulation of bone and body composition in male mice with combined inactivation of androgen and estrogen receptor-alpha. *Faseb J.* 2009;23:232-240.
- [18] Collier CD, Hausman BS. Characterization of a reproducible model of fracture healing in mice using an open femoral osteotomy. *Bone Rep.* 2020;12:100250.
- [19] Working ZM, Morris ER. A quantitative serum biomarker of circulating collagen X effectively correlates with endochondral fracture healing. *J Orthop Res.* 2021;39:53-62.

- [20] Callewaert F, Venken K. Differential regulation of bone and body composition in male mice with combined inactivation of androgen and estrogen receptor- α . *The FASEB Journal*. 2009;23:232-240.
- [21] Bergmann P, Body JJ. Loading and skeletal development and maintenance. *J Osteoporos*. 2011;786752.
- [22] Haffner-Luntzer M, Fischer V. Differences in Fracture Healing Between Female and Male C57BL/6J Mice. *Front Physiol*. 2021;12:712494.
- [23] Levingstone TJ, Ramesh A. Cell-free multi-layered collagen-based scaffolds demonstrate layer specific regeneration of functional osteochondral tissue in caprine joints. *Biomaterials*. 2016;87:69-81.
- [24] Browe DC, Burdis R. Promoting endogenous articular cartilage regeneration using extracellular matrix scaffolds. *Materials Today Bio*. 2022;16:100343.
- [25] Burdis R, Chariyev-Prinz F. Spatial patterning of phenotypically distinct microtissues to engineer osteochondral grafts for biological joint resurfacing. *Biomaterials*. 2022;289:121750.
- [26] Xu J, Fahmy-Garcia S. Effectiveness of BMP-2 and PDGF-BB Adsorption onto a Collagen/Collagen-Magnesium-Hydroxyapatite Scaffold in Weight-Bearing and Non-Weight-Bearing Osteochondral Defect Bone Repair: *In Vitro*, *Ex Vivo* and *In Vivo* Evaluation. *J Funct Biomater*. 2023;14:111.
- [27] Xu J, Vecstaudza J. Incorporating strontium enriched amorphous calcium phosphate granules in collagen/collagen-magnesium-hydroxyapatite osteochondral scaffold improves subchondral bone repair. *Mater Today Bio*. 2024;25:100959.
- [28] van den Borne MP, Raijmakers NJ. International Cartilage Repair Society (ICRS) and Oswestry macroscopic cartilage evaluation scores validated for use in Autologous Chondrocyte Implantation (ACI) and microfracture. *Osteoarthritis and Cartilage*. 2007;15:1397-1402.
- [29] Goebel L, Orth P. Experimental scoring systems for macroscopic articular cartilage repair correlate with the MOCART score assessed by a high-field MRI at 9.4 T--comparative evaluation of five macroscopic scoring systems in a large animal cartilage defect model. *Osteoarthritis and Cartilage*. 2012;20:1046-1055.
- [30] Gaytan F, Morales C. A novel RGB-trichrome staining method for routine histological analysis of musculoskeletal tissues. *Scientific Reports*. 2020;10:16659.
- [31] van Bergen CJ, Kerkhoffs GM. Osteochondral defects of the talus: a novel animal model in the goat. *Tissue Eng Part C Methods*. 2013;19:449-457.
- [32] Maglio M, Brogini S. Current Trends in the Evaluation of Osteochondral Lesion Treatments: Histology, Histomorphometry, and Biomechanics in Preclinical Models. *Biomed Res Int*. 2019;2019:4040236.
- [33] Notelovitz M. Androgen effects on bone and muscle. *Fertil Steril*. 2002;77 Suppl 4.
- [34] Callewaert F, Sinnesael M. Skeletal sexual dimorphism: relative contribution of sex steroids, GH-IGF1, and mechanical loading. *J Endocrinol*. 2010;207:127-134.
- [35] Chen JF, Lin PW. Androgens and Androgen Receptor Actions on Bone Health and Disease: From Androgen Deficiency to Androgen Therapy. *Cells*. 2019;8:8111318.
- [36] Ucer S, Iyer S. The Effects of Androgens on Murine Cortical Bone Do Not Require AR or ER α Signaling in Osteoblasts and Osteoclasts. *J Bone Miner Res*. 2015;30:1138-1149.
- [37] Lindberg MK, Alatalo SL. Estrogen receptor specificity in the regulation of the skeleton in female mice. *J Endocrinol*. 2001;171:229-236.

- [38] Parikka V, Peng Z. Estrogen responsiveness of bone formation in vitro and altered bone phenotype in aged estrogen receptor- α -deficient male and female mice. *Eur J Endocrinol*. 2005;152:301-314.
- [39] Siddiqui JA, Partridge NC. Physiological Bone Remodeling: Systemic Regulation and Growth Factor Involvement. *Physiology (Bethesda)*. 2016;31:233-245.
- [40] Bain SD, Bailey MC. High-dose estrogen inhibits bone resorption and stimulates bone formation in the ovariectomized mouse. *J Bone Miner Res*. 1993;8:435-442.
- [41] Beil FT, Barvencik F. Effects of estrogen on fracture healing in mice. *J Trauma*. 2010;69:1259-1265.
- [42] Weitzmann MN, Pacifici R. Estrogen deficiency and bone loss: an inflammatory tale. *J Clin Invest*. 2006;116:1186-1194.
- [43] McDonnell SM, Murray SC. Bachelor and Harem Stallion Behavior and Endocrinology. *Biology of Reproduction*. 2018;52:577-590.
- [44] Kannan G, Estrada-Reyes ZM. Social isolation of goats: significance of visual contact with conspecifics on behavioral and physiological responses. *J Anim Sci*. 2021;99.
- [45] Määttä JA, Büki KG. Inactivation of the androgen receptor in bone-forming cells leads to trabecular bone loss in adult female mice. *Bonekey Rep*. 2013;2:440.
- [46] Straub B, Müller M. Osteoporosis and mild metabolic acidosis in the rat after orchietomy and their prevention: should prophylactic therapy be administered to patients with androgen deprivation? *J Urol*. 2001;165:1783-1789.
- [47] Almeida M, Laurent MR. Estrogens and Androgens in Skeletal Physiology and Pathophysiology. *Physiol Rev*. 2017;97:135-187.
- [48] Goring A, Sharma A. Regulation of the Bone Vascular Network is Sexually Dimorphic. *J Bone Miner Res*. 2019;34:2117-2132.
- [49] Strube P, Mehta M. Sex-specific compromised bone healing in female rats might be associated with a decrease in mesenchymal stem cell quantity. *Bone*. 2009;45:1065-1072.
- [50] Scibetta AC, Morris ER. Characterization of the chondrogenic and osteogenic potential of male and female human muscle-derived stem cells: Implication for stem cell therapy. *Journal of Orthopaedic Research*. 2019;37:1339-1349.
- [51] Meszaros LB, Usas A. Effect of host sex and sex hormones on muscle-derived stem cell-mediated bone formation and defect healing. *Tissue Eng Part A*. 2012;18:1751-1759.
- [52] Gianakos AL, Okedele O. Autologous Osteochondral Transplantation for Osteochondral Lesions of the Talus-Does Sex Play a Role? *J Foot Ankle Surg*. 2023;62:96-101.
- [53] Gianakos AL, Williamson ERC. Gender Differences May Exist in the Presentation, Mechanism of Injury and Outcomes Following Bone Marrow Stimulation for Osteochondral Lesions of the Talus. *J Foot Ankle Surg*. 2023;62:75-79.
- [54] Deng Z, Gao X. Gender differences in tibial fractures healing in normal and muscular dystrophic mice. *Am J Transl Res*. 2020;12:2640-2651.
- [55] Frost HM. On the estrogen-bone relationship and postmenopausal bone loss: A new model. *J Bone Miner Res*. 1999;14:1473-1477.
- [56] Damien E, Price JS. Mechanical strain stimulates osteoblast proliferation through the estrogen receptor in males as well as females. *J Bone Miner Res*. 2000;15:2169-2177.
- [57] Armstrong VJ, Muzylak M. Wnt/ β -catenin signaling is a component of osteoblastic bone cell early responses to load-bearing and requires estrogen receptor α . *J Biol Chem*. 2007;282:20715-20727.

- [58] Almeida M, Iyer S. Estrogen receptor- α signaling in osteoblast progenitors stimulates cortical bone accrual. *J Clin Invest*. 2013;123:394-404.
- [59] Galea GL, Meakin LB. Estrogen receptor α mediates proliferation of osteoblastic cells stimulated by estrogen and mechanical strain, but their acute down-regulation of the Wnt antagonist Sost is mediated by estrogen receptor β . *J Biol Chem*. 2013;288:9035-9048.
- [60] Sinnesael M, Laurent MR. Androgens inhibit the osteogenic response to mechanical loading in adult male mice. *Endocrinology*. 2015;156:1343-1353.
- [61] Fritton JC, Myers ER. Bone mass is preserved and cancellous architecture altered due to cyclic loading of the mouse tibia after orchidectomy. *J Bone Miner Res*. 2008;23:663-671.
- [62] Sielemann K, Hafner A. The reuse of public datasets in the life sciences: potential risks and rewards. *PeerJ*. 2020;8.
- [63] eBioMedicine. The 3Rs of Animal Research. *EBioMedicine*. 2022;76:103900.

7

An articular cartilage culture model to study mechanisms of cartilage calcification *ex vivo*: the role of different zones

Jietao Xu, Eric Farrell, Nicole Kops, Pieter A.J. Brama, Gerjo J.V.M. van Osch

Unpublished

ABSTRACT

The zone of calcified cartilage (ZCC) acts as a transitional layer that anchors articular cartilage to the subchondral bone. Without the ZCC, the transition from non-calcified articular cartilage to the subchondral bone plate would be quite an abrupt mechanical transition. Regenerating the ZCC during osteochondral defect repair remains a major challenge. In this study, we aimed to study mechanisms of formation of the ZCC with an *ex vivo* zonal cartilage culture model. Briefly, full-thickness cartilage explants were harvested from bovine metacarpophalangeal joints before skeletal maturity. Explants were cultured as one complete full-thickness structure or were divided into two layers (top and bottom layers) and subsequently cultured in the presence of 10 mM β -glycerophosphate for 3 weeks to allow calcification to occur. No calcification was observed in the top layers, as confirmed by micro-CT and von Kossa/thionine staining. Conversely, the deep zone of the bottom layer alone calcified *ex vivo*, and formed more calcification compared to full-thickness cartilage. Less calcification was observed when the bottom layers were directly and indirectly co-cultured with the top layers, suggesting that the top layer has the potential to inhibit deep layer calcification. To investigate the role of zonal chondrocytes in cartilage calcification, cartilage explants were devitalised. Viable full-thickness cartilage or top layers formed less calcification compared to devitalised explants, while more calcification was observed in viable bottom layers compared to devitalised bottom layers. With this model, we demonstrated an inherent zone-specific calcification pattern within the cartilage explants. The viable top layers exhibited the capacity to inhibit cartilage calcification via releasing bioactive factors. The viable chondrocytes residing in the bottom layers have a role in stimulating calcification but are also capable of responding to bioactive factors that inhibit calcification. The model allows future studies investigating the mechanism of ZCC formation, to provide clues how to regenerate calcified cartilage in osteochondral defect repair as well as investigating potential treatments for pathological cartilage calcification.

Keywords: cartilage; calcification; zonal structure; *ex vivo* model; tissue engineering

1. INTRODUCTION

Osteochondral defects might lead to joint pain, limited range of movements and even dysfunction [1]. The limited regenerative capacity of articular cartilage has stimulated the investigation of tissue engineering approaches to regenerate the cartilage-bone unit. However, regenerating the zonal structure of the cartilage-bone unit, especially the zone of calcified cartilage (ZCC), appears to remain a major challenge [2]. The ZCC is the interface between articular cartilage and subchondral bone [3]. It consists of dispersed chondrocytes within lacunae in the calcified matrix, which is composed of collagen, sodium hyaluronate and hydroxyapatite in varying proportions [4]. As a transition layer from non-calcified cartilage to the subchondral bone plate, the ZCC prevents a mechanically discontinuous transition, and minimises the shear stress on the interface of cartilage and bone [5-7]. Additionally, the ZCC functions as a barrier that prevents vascular invasion from the subchondral bone to non-calcified cartilage with a lower diffusion coefficient [8]. Therefore, regenerating the ZCC in full-thickness cartilage or osteochondral defects is critical for restoring physiological functions.

Understanding the mechanism underlying cartilage calcification is essential for the successful regeneration of the ZCC in (osteo)chondral tissue engineering. *In vitro*, cell lines are commonly used to study cartilage matrix calcification [9-11]. Formation of this zone involves a multifactorial process resulting from a balance between pro-calcification factors and calcification inhibitors [12]. The physiological or pathological imbalances might be attributed to various factors, including chondrocyte phenotype (e.g. altered responses to bioactive factors and secreted matrix vesicles), dysregulated inorganic pyrophosphate and inorganic phosphate metabolism in the extracellular matrix and extracellular Ca^{2+} levels [13]. Conventional *in vitro* models with cell lines do not include the extracellular matrix nor zone-specific differences that are important for the complex interplay between the different zones in articular cartilage. For instance, the presence of bioactive factors in the superficial zone, such as parathyroid hormone-related protein (PTHrP), can affect cartilage calcification [14], while Indian hedgehog (Ihh) signalling from prehypertrophic chondrocytes residing in the deep zone has been implicated in the control of chondrocyte maturation by way of feedback control of PTHrP. Alkaline phosphatase activity, that is important for tissue calcification, is predominately localized to the deep zone [15]. Moreover, although tissue engineering techniques have led to the generation of 3D culture models, the extracellular matrix produced in these models is immature and lacks the architecture of articular cartilage [16-18].

Investigating cartilage calcification *in vitro* requires more sophisticated models that can better emulate the native cartilage tissue environment with the specific biochemical gradients and chondrocyte phenotypes present within each cartilage zone. Mammalian tissues in *ex vivo* settings provide a more realistic environment that closely mimics the *in vivo* situation for studying cartilage physiology and responses to stimuli. Their utilisation has the potential to reduce the need for animal experiments in future research endeavours, aligning with ethical considerations. Therefore, we developed a new culture model to investigate the mechanism of ZCC formation. To do this, we first hypothesised that an explant of immature bovine cartilage (with the ZCC not yet formed) would retain the ability to form the ZCC *ex vivo*. Then, we investigated the role of chondrocytes residing

in the different zones of articular cartilage in calcified cartilage formation with this *ex vivo* zonal cartilage culture model.

2. MATERIALS AND METHODDS

2.1. Cartilage explant preparation and culture

Full-thickness cartilage explants were harvested from metacarpophalangeal joints of 6- to 8-month-old calves (LifeTec, Eindhoven, The Netherlands) using a 4 mm diameter biopsy punch and a scalpel (15, Swann Morton, Sheffield, UK), and osteochondral explants (8 mm diameter and 5 mm height) were harvested using a drill. In the metacarpophalangeal joints at this age, the ZCC was not yet formed. Full-thickness cartilage explants were divided into two layers (referred to as top layer and bottom layer) with a scalpel. Explants were kept overnight in Dulbecco's Modified Eagle Medium (DMEM, 1 g/L glucose, Gibco, Waltham, MA, USA) supplemented with 10% fetal bovine serum (FBS, Gibco, Waltham, MA, USA), 25 µg/ml ascorbic acid (Sigma Aldrich, Saint Louis, MI, USA), 50 µg/mL gentamycin (Gibco, Waltham, MA, USA), and 1.5 µg/mL fungizone (Gibco, Waltham, MA, USA) at 37 °C and 5% CO₂. The next day, the cartilage explants were scanned with Micro-Computed Tomography (micro-CT) and around half of explants with underlying subchondral bone tissue were excluded from culture.

To allow tissue calcification, β-glycerophosphate (β-GP, Sigma Aldrich, Saint Louis, MI, USA) was added to the culture medium. A concentration of 10 mM was used based on an experiment using 0, 2.5, 5, 10 and 50 mM β-GP (Supplementary Figure 1) and previous publications. Osteochondral explants were cultured in a specialised well plate (LifeTec, Eindhoven, The Netherlands) designed to separate the medium for cartilage and subchondral bone (Supplementary Figure 2A). Experiments for direct co-culture of four top layers with a bottom layer utilised a transwell system (PET membrane; 8 µm pore size, Life Sciences, Arizona, United States). For in-direct co-culture, the culture medium collected from the top layer-only was used to culture the bottom layer. Specifically, the top layer-only was cultured without β-GP. Every two days, the culture medium collected from top layer-only samples was mixed with the same amount of fresh medium and β-GP (at final concentration of 10 mM). This mixture was then used to culture the bottom layer-only explants. To evaluate the effect of bioactive proteins in the medium conditioned by top layers, the mixed medium was first heated up to 56 degrees for half an hour. To further study the interaction between the top and the bottom layer, a single top layer and a bottom layer were brought into close contact by either making an incomplete cut or embedding them together in agarose.

To study the role of chondrocytes, cartilage explants were devitalised either by fixing in 4% formalin or subjected to two freeze-thaw cycles. To study the response of cartilage to a known inhibitor of cartilage calcification, 0, 10, 50 and 100 nM PTHrP (Phoenix Pharmaceuticals, Burlingame, United States) were added to the medium.

For all experiments, the medium was refreshed every 2 days and the amount of calcium taken up from the medium was measured with a calcium assay. After 3 weeks, the explants were harvested and scanned under micro-CT, followed by fixation in 4% formalin for 3 days for histological analyses.

2.2. Calcium assay of medium

Ca²⁺ concentration in the medium was measured and cumulative Ca²⁺ uptake was calculated. Briefly, 100 µl fresh reagent (0.5 M Ethanolamine, 0.175 mM o-cresolphthalein complexone, 9.9 mM 8-hydroxyquinoline, 0.3 M hydrochloric acid, Sigma Aldrich, Saint Louis, MI, USA) was added to 10 µl collected medium in a 96 well plate. The control medium without explants was incubated and refreshed every two days to eliminate the effect of evaporation. The range of calcium concentration (calcium chloride) for the standard curve is 0-3 mM. Optical density was measured at 570 nm on the versamax.

2.3. Micro-Computed Tomography and quantification

The explants were scanned in a micro-CT scanner (Quantum GX, Perkin Elmer, Akron, OH, USA) in medium in 48 well plates with the following settings: energy 90 KV, intensity 88 µA, 172 mm FOV, 86 µm isotropic voxel size. All the scans were under an X-ray filter of Cu (thickness = 0.06 mm) and Al (thickness = 0.5 mm). A high-resolution mode was set, and a scan time of 4 min was used. To quantify the volume of calcified tissue, a single threshold was set to exclude the signalling of the medium and the well plate. Each 3D reconstructed explant was selected manually as the volume of interest, and the calcification volumes (mm³) of each explant were measured.

2.4. Histology

The formalin fixed cartilage explants were embedded in paraffin and sectioned at 6 µm. The formalin fixed osteochondral explants were embedded in methyl methacrylate (MMA) and sectioned at 10 µm. Following dewaxing or MMA-removal, von Kossa/thionine staining was performed with 5% silver nitrate solution (Sigma, Saint Louis, MI, USA) and 0.4% thionine (Sigma, Saint Louis, MI, USA) to visualise calcium deposition in the extracellular matrix and general cell/tissue morphology.

To validate the devitalisation of cartilage explants, live/dead staining was performed. Viable or devitalised cartilage explants were cut into a thin piece cross-sectionally by a scalpel. After rinsing in phosphate buffered saline (PBS, Sigma Aldrich, Saint Louis, MI, USA), the tissues were incubated in the staining solution (consisting of 10 µM calcein AM and 20 µM Ethidium homodimer-1, Molecular Probes, Eugene, OR) for half an hour. Fluorescent images of tissues were obtained by using a fluorescence microscopy (ECHO, San Diego, US).

2.5. Statistical Analysis

All statistical tests were performed using SPSS software 28.0 (SPSS Inc., Chicago, IL, USA). The calcium concentration and volume of calcified tissue were expressed as mean ± standard deviation (SD). Normality was tested by a Shapiro-Wilk test. Depending on the normality, statistically significant differences between two groups were determined by a Student's T test or a Mann-Whitney U test. One-way ANOVA test or the Kruskal-Wallis H test with Bonferroni-correction were used to determine the statistically significant differences among three groups. The homogeneity of variances was tested using Levene's test. A p-value ≤ 0.05 was considered statistically significant.

3. RESULTS

3.1. Inherent zone-specific calcification observed within the cartilage explants cultured *ex vivo*

3.1.1. Calcification was observed only in the deep zone of cartilage explants

After a 3-week incubation period, calcification was observed only in the deep zone of full-thickness cartilage explants, as confirmed by von Kossa/thionine staining (Figure 1A, B). To further verify the region of calcification within the articular cartilage and mitigate any influence from medium accessibility, full-thickness cartilage explants were divided into two layers (top layers and bottom layers) and cultured separately for 3 weeks (Figure 1C). The bottom layers took up significantly more calcium compared to the top layers after 3 weeks ($P < 0.001$, Figure 1D). In fact, the top layers took up very low amounts of calcium from the medium. Micro-CT analysis validated these findings, revealing no cartilage calcification in any of the top layers; while all the bottom layers exhibited calcification ($P < 0.001$, figure 1E). von Kossa/thionine staining further supported these results observed by micro-CT quantification, demonstrating calcification formation exclusively in the deep zone of bottom layers, consistent with observations in full-thickness cartilage (Figure 1B, F).

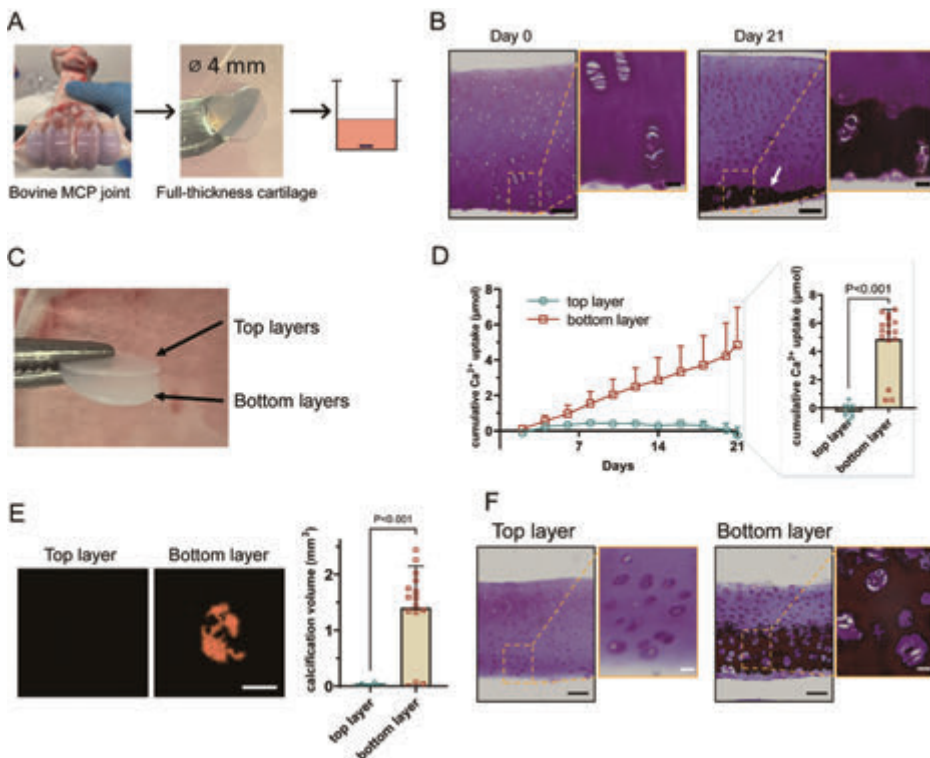


Figure 1. The deep zone of cartilage exhibited the capability of calcification *ex vivo*. (A) Experimental scheme for full-thickness cartilage explants harvesting and culturing. 0.5 ml medium was used to culture the cartilage explants. (B) Representative von Kossa/thionine staining of full-thickness cartilage at day 0 and after

3 weeks in culture. The arrow indicates calcification indicated by von Kossa positive staining. Scale bars indicates 100 μm and 20 μm (magnified images), respectively. (C) Experimental scheme for separating the top layers and the bottom layers from full-thickness cartilage explants. (D) The cumulative Ca^{2+} taken up from the medium by top layers ($n = 8$) or bottom layers ($n = 16$) of cartilage at each time point of medium refreshing during culture. The bar graph expresses the cumulative Ca^{2+} uptake at 3 weeks. (E) Representative 3D reconstructed micro-CT images and volume of calcified tissue (mm^3) after 3 weeks. Scale bar indicates 2 mm. (F) Representative von Kossa/thionine staining of a top layer and a bottom layer after 3 weeks of culture. Scale bars indicates 100 μm and 20 μm (magnified images), respectively. The Mann-Whitney U test was used to test statistical significance.

3.1.2. A distinct layer of calcification was formed in the deep zone of the cartilage in osteochondral explants

To further evaluate the location of the layer of calcification found in relation to the architecture of the entire cartilage-unit, osteochondral tissue explants were cultured *ex vivo* (Figure 2A). A layer of calcification was again observed in the deep zone of articular cartilage (Figure 2B, C). Interestingly, a non-calcified cartilage layer was observed between the newly formed calcification and the native subchondral bone plate (Figure 2B, C), which is hypothesized to be a remnant of the secondary ossification centre.

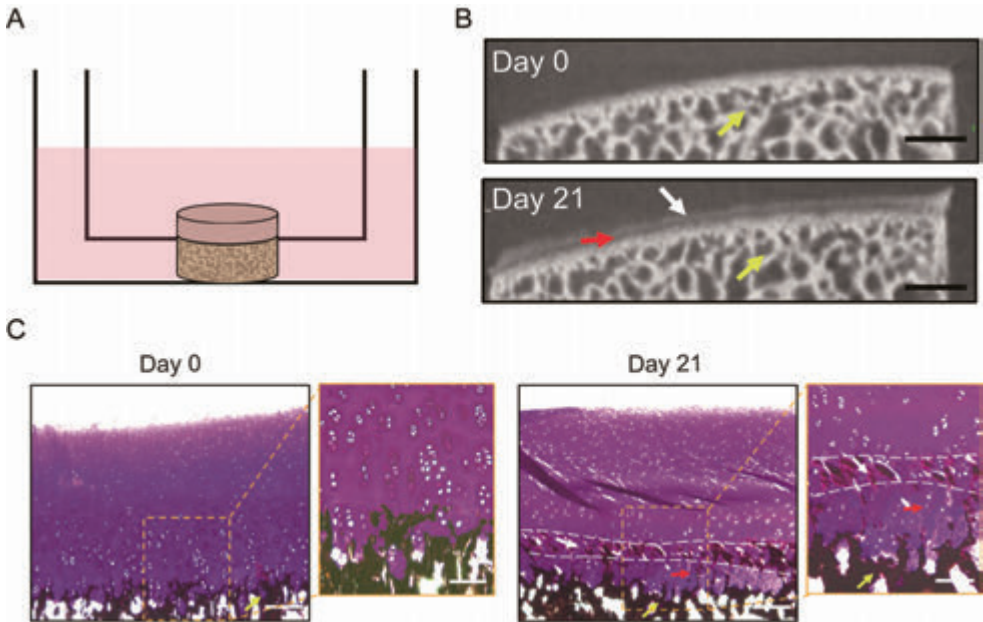


Figure 2. A distinct calcification layer was formed in the deep layer of the articular cartilage in immature osteochondral explants *ex vivo*. (A) Experimental scheme for osteochondral explants culturing. 3 ml medium was used to culture the cartilage explants, 4 ml medium was used to culture the subchondral bone. (B) Representative micro-CT images. Scale bar indicates 1 mm. (C) Representative von Kossa/thionine staining at day 0 and after 3 weeks in culture. Scale bars indicates 200 μm and 100 μm (magnified images), respectively. The red arrows indicate the non-calcified layer in between. The white arrows and white lines indicate the new calcification layer. The yellow arrows indicate the subchondral bone.

3.2. Top layers inhibited cartilage calcification in the bottom layer

3.2.1. The presence of top layers in full-thickness cartilage reduced calcification

In the full thickness cultures, only five out of twelve full-thickness cartilage explants were calcified, whereas all sixteen bottom layers that were cultured separately, exhibited calcification (Figure 1). Drawing from this observation, we hypothesised that the presence of top layers within the full-thickness cartilage explants might potentially inhibit cartilage calcification. To investigate the interplay between top layers and bottom layers, we cultured cartilage explants as follows: (1) one bottom layer-only; (2) one bottom layer directly co-cultured with one top layer in the same well; (3) divided full-thickness cartilage (with top and bottom layers connected at one edge); and (4) full-thickness cartilage. Results showed that two connected layers ($P = 0.018$) and full-thickness cartilage ($P < 0.001$) took up significantly less calcium compared to the bottom layer-only (Figure 3A). This trend was consistently observed in micro-CT and histological analyses ($P < 0.01$, Figure 3B-D), where the calcification was formed in the bottom layer-only explants.

3.2.2. Top layers inhibited cartilage calcification via releasing bioactive factors in a dose-dependent manner

Notably, co-culturing a separated top and bottom layer in the same well did not significantly reduce the calcification of the bottom layer (Figure 3A-D). We hypothesized that the inhibition might be via the release of factors and that a certain concentration is required. To investigate this, the bottom layer was co-cultured with four top layers in a transwell system (Figure 3E). Over the 3-week culture period, the bottom layer co-cultured with four top layers took up significantly less calcium than the bottom-only explants ($P = 0.002$, Figure 3F). Micro-CT analysis and von Kossa/thionine staining further confirmed less calcification in bottom layer co-cultured with four top layers ($P = 0.043$, Figure 3G-I).

These results indicate that the top layer secretes factors that can inhibit calcification of cartilage. The indirect co-culture experiments with conditioned medium of top layers on the bottom layer suggested that the secreted factors are heat-sensitive (Supplementary Figure 2), indicating that the secreted factors might be proteins.

3.3. Cartilage calcification can be modulated by viable chondrocytes in the top and the bottom layer

To further investigate the role of viable chondrocytes in the cartilage calcification process, full-thickness cartilage explants were devitalised by fixation in 4% formalin for 3 hours, or two freeze-thaw cycles. Live/dead staining confirmed the devitalisation of chondrocytes in cartilage explants (Figure 4A). During a 3-week culture period, devitalised full-thickness cartilage explants calcified more than viable explants, as determined by significantly more calcium uptake from the medium ($P < 0.001$, Figure 4B), and a significantly higher volume of calcified tissue on micro-CT and von Kossa/thionine staining ($P = 0.019$, Figure 4C-E). This consistent trend was observed across various concentrations of β -GP (2.5, 5, 10 and 50 mM) added during the culture (Supplementary Figure 3). Interestingly, the inherent zone-specific calcification present in the deep zone, was also exhibited within the devitalised cartilage explants. The calcification was, however, more scattered in the devitalised explants compared to the calcification in viable explants that was denser in a restricted region (Figure 4E).

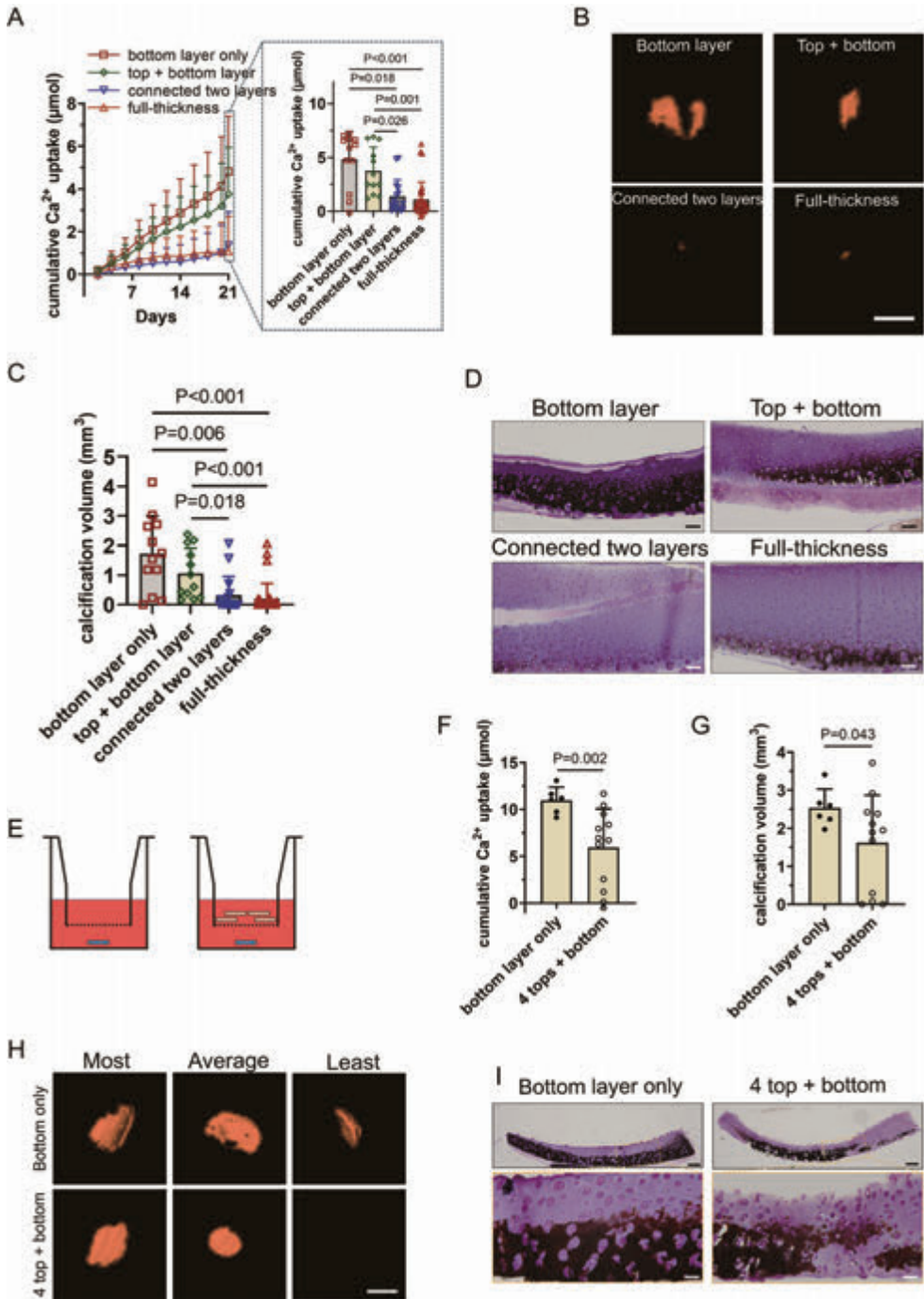


Figure 3. Factors secreted from the top layers inhibited the calcification of the extracellular matrix in the bottom layers. (A) Cumulative Ca^{2+} taken up from the medium by different cartilage explants (bottom layer-only, $n = 12$; top + bottom layer, $n = 12$; connected two layers, $n = 16$, full-thickness cartilage, $n = 32$) at each timepoint of medium refreshing. The bar graph showed the cumulative Ca^{2+} uptake over 3 weeks. 0.5 ml

medium was used to culture the cartilage explants. The Kruskal-Wallis H test was used to test statistical significance. (B) Representative 3D reconstructed micro-CT images at 3 weeks. The scale bar indicated 2 mm. (C) Volume of calcified tissue (mm^3) on micro-CT after 3 weeks of culture. The Kruskal-Wallis H test was used to test statistical significance. (D) Representative von Kossa/thionine staining of cartilage explants cultured for 3 weeks. Scale bars indicates 100 μm . (E) Experimental scheme for co-culture of four top layers with a bottom layer in a transwell system (PET membrane; 8 μm pore size). 1 ml medium was used to culture the cartilage explants. (F) Cumulative Ca^{2+} taken up from the medium by cartilage explants (bottom layer-only, $n = 6$; 4 top layers + bottom layer, $n = 12$) over 3 weeks. The independent t-test was used to test statistical significance. (G) The volume of calcified tissue (mm^3) at 3 weeks. The independent t-test was used to test statistical significance. (H) Representative 3D reconstructed micro-CT images at 3 weeks. The scale bar indicated 2 mm. (I) Representative von Kossa/thionine staining of cartilage explants cultured for 3 weeks. Scale bars indicates 200 μm and 50 μm (magnified images), respectively.

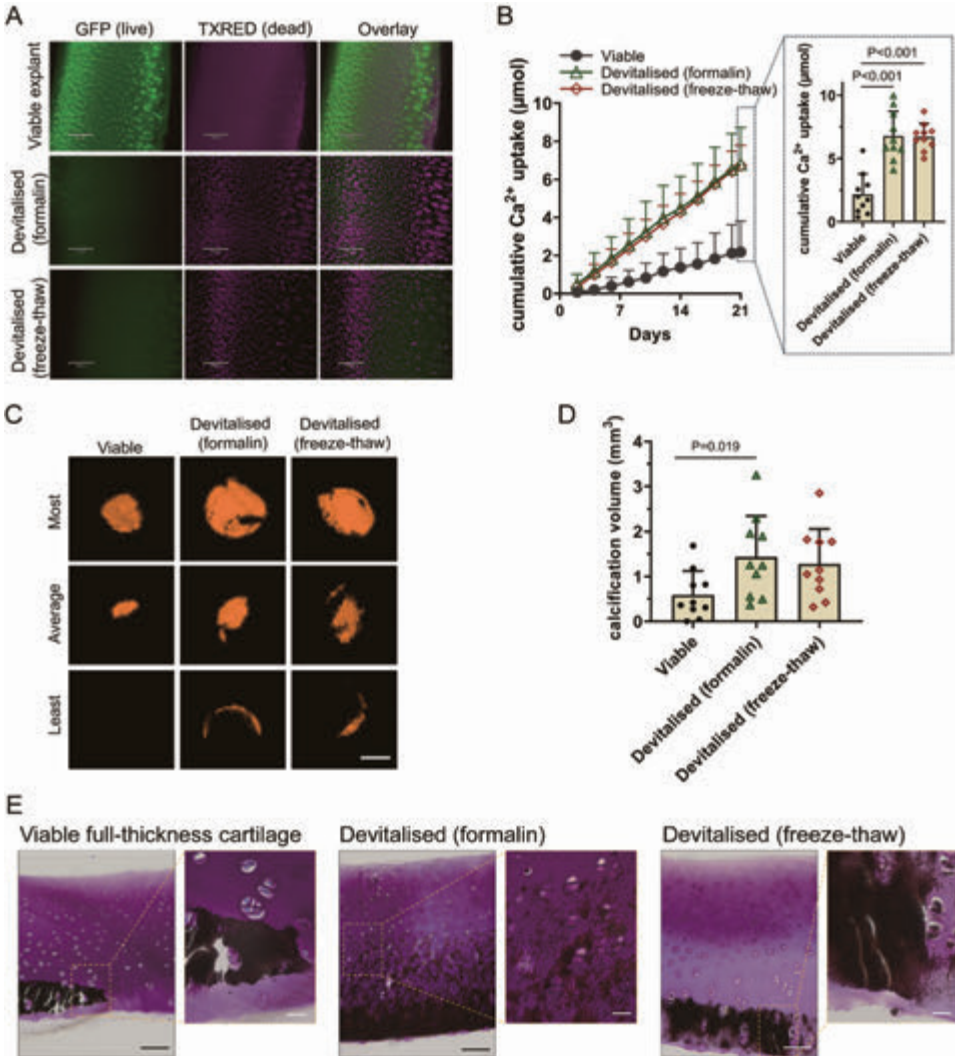


Figure 4. Viable chondrocytes in full-thickness cartilage reduced cartilage calcification. (A) Live/dead staining on the cartilage explants showed that massive chondrocytes were devitalised in both formalin-fixed

or freeze-thaw explants. (B) Cumulative Ca^{2+} taken up from the medium by different cartilage explants ($n = 10$) at each time point of medium refreshing. The bar graph showed the cumulative Ca^{2+} taken up by viable and devitalised full-thickness cartilage explants at 3 weeks. (C) Representative 3D reconstructed micro-CT images at 3 weeks. The scale bar indicated 2 mm. (D) The bar graph showed the volume of calcified tissue (mm^3) at 3 weeks. (E) Representative von Kossa/thionine staining of cartilage explants cultured for 3 weeks. Scale bars indicates 100 μm and 20 μm (magnified images), respectively. 1 ml medium was used to culture the cartilage explants. One-way ANOVA test was used to test statistical significance.

We then continued investigating the role of viable cells in the top layers and bottom layers separately. Top-only layers devitalised with formalin took up more calcium from the medium compared to viable top-only layers ($P < 0.001$, Figure 5A), and demonstrated more calcified tissue on micro-CT and histology (Figure 5B, C), whereas there was no calcified tissue visible in viable top-only layers after 3 weeks (Figure 5B, C). Notably, the calcification in devitalised top layers was scattered around devitalised chondrocytes predominantly in the lower region of the top layer (Figure 5C).

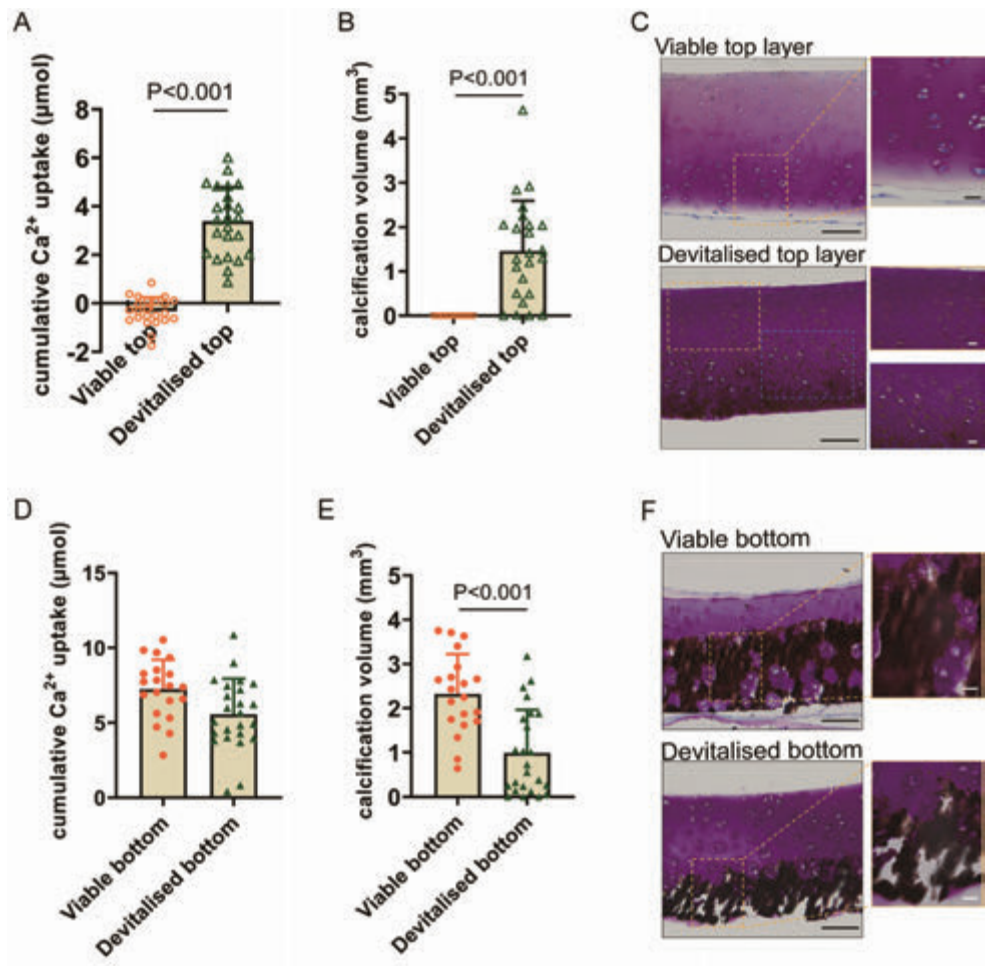


Figure 5. Viable chondrocytes in the top layers inhibited calcification whereas viable chondrocytes in the bottom layers actively induced calcification. (A) Cumulative Ca^{2+} taken up from the medium by viable ($n =$

23) and devitalised top layers ($n = 24$) after 3 weeks. (B) The volume of calcified tissue (mm^3) at 3 weeks. A low threshold was set to quantify the calcification volume in top layers. (C) Representative von Kossa/thionine staining of cartilage explants cultured for 3 weeks. Scale bars indicates $100 \mu\text{m}$ and $20 \mu\text{m}$ (magnified). (D) Cumulative Ca^{2+} taken up by viable ($n = 20$) and devitalised bottom layers ($n = 24$) after 3 weeks. (E) The volume of calcified tissue (mm^3) at 3 weeks. (F) Representative von Kossa/thionine staining of cartilage explants cultured for 3 weeks. Scale bars indicates $100 \mu\text{m}$ and $20 \mu\text{m}$ (magnified images), respectively. 1 ml medium was used to culture the cartilage explants. Two independent experiments with two different donors were performed. The Kruskal-Wallis H test or one-way ANOVA test (based on normality) was used to test statistical significance.

Interestingly, devitalised bottom-only layers took up less calcium from the medium than viable bottom-only layers (Figure 5D, $P = 0.083$). The volume of calcified tissue visible on micro-CT and histology was less in the devitalised bottom layers compared to viable bottom layers ($P < 0.001$, Figure 5E). The calcification in both viable and devitalised bottom layers was densely located in the lower zone of the bottom layer (Figure 5F).

These results indicated the distinct roles of viable chondrocytes in the top layers and the bottom layers. Viable chondrocytes residing in the top layers inhibit cartilage calcification, whereas viable chondrocytes in the bottom layers might actively induce cartilage calcification.

3.4. Some bioactive factors secreted by top layers that inhibit cartilage calcification do not require the response of viable chondrocytes

We have demonstrated that chondrocytes in top and bottom layers have an effect on calcification in their own layer. Since we have demonstrated that factors secreted from the top layer can actively inhibit calcification in the bottom layer, we investigated the role of viable bottom layers in response to calcification-inhibiting factors that might come from the top layers. Adding PTHrP to the culture of bottom layers significantly reduced the calcium taken up ($P < 0.001$, Figure 6A) and the volume of calcified tissue formation ($P < 0.001$, Figure 6B, C), exhibiting a dose-dependent response. Meanwhile, 100 nM PTHrP only inhibited calcification in viable bottom layers (Figure 6D-F). Thus, the chondrocytes in the bottom layers can actively induce calcification as well as be modulated to inhibit calcification.

We then investigated the role of viable chondrocytes in the interplay between the two layers. Surprisingly, viable top layers might still be able to inhibit calcification of devitalised bottom layers (Figure 7A-D). This indicated that the viable top layers modulate cartilage calcification partly via releasing bioactive factors that do not require the response of viable chondrocytes in the bottom layer. Moreover, devitalised top layers were also able to inhibit calcification of viable bottom layers, as confirmed by higher calcification volume on micro-CT (Figure 7E-G), indicating that the inhibitory factors might have pre-existed in the top layers. Data of cumulative Ca^{2+} taken up by viable bottom layer and devitalised top + viable bottom was not shown since devitalised top took up Ca^{2+} as well.

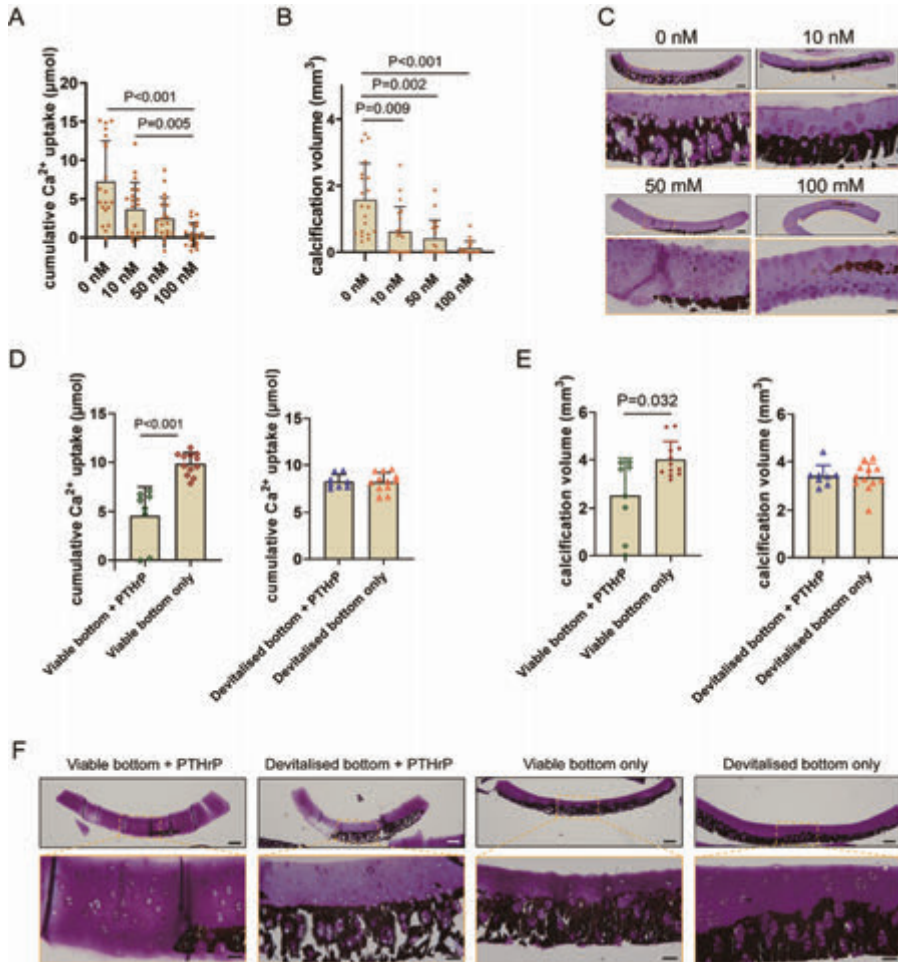


Figure 6. Viable chondrocytes in the bottom layers responded to calcification-inhibiting factors. (A) Cumulative Ca²⁺ uptake by different cartilage explants (n=20) over 3 weeks. The Kruskal-Wallis H test was used to test statistical significance. (B) The volume of calcified tissue (mm³) at 3 weeks. The Kruskal-Wallis H test was used to test statistical significance. (C) Representative von Kossa/thionine staining of cartilage explants cultured for 3 weeks ex vivo. The yellow squares indicate the magnified images. The scale bar indicated 200 µm and 50 µm (magnified images), respectively. (D) The cumulative Ca²⁺ uptake by different cartilage explants over 3 weeks. The independent t-test (devitalised bottom layer conditions) or the Mann-Whitney U test (viable bottom layer conditions) was used to test statistical significance. (E) The volume of calcified tissue (mm³) at 3 weeks. The independent t-test (viable bottom layer conditions) or the Mann-Whitney U test (devitalised bottom layer conditions) was used to test statistical significance. (F) Representative von Kossa/thionine staining of cartilage explants cultured for 3 weeks ex vivo. The yellow squares indicate the magnified images. The scale bar indicated 200 µm and 50 µm (magnified images), respectively. 1 ml medium was used to culture the cartilage explants. Two independent experiments with two different donors were performed.

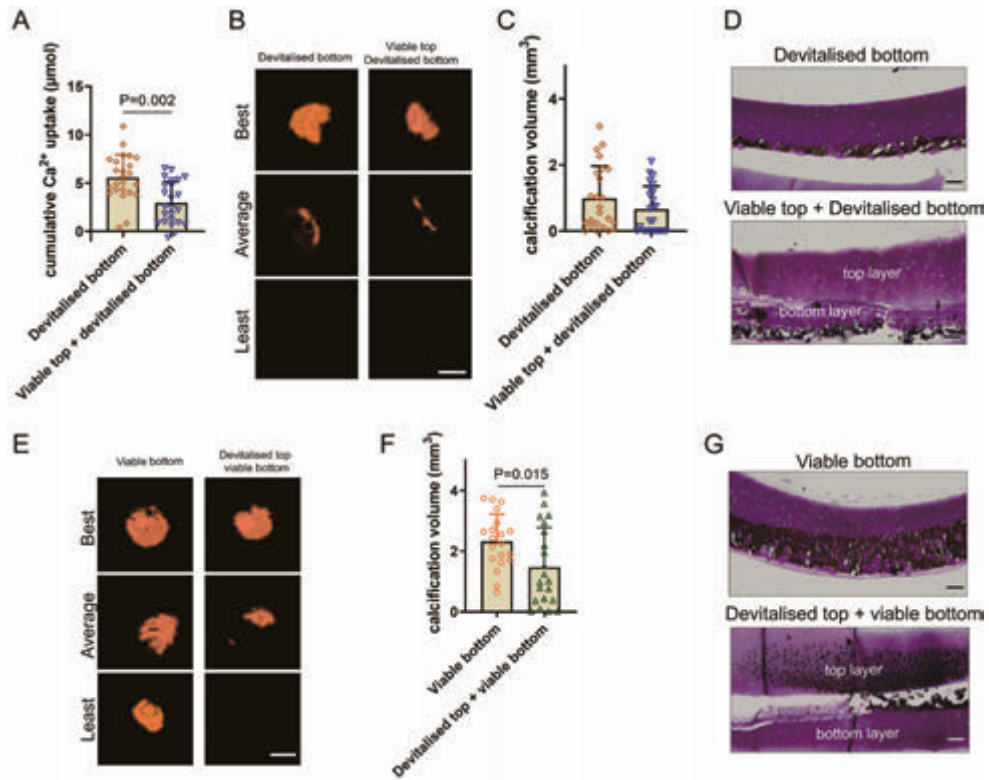


Figure 7. The role of viable chondrocytes in the interplay between the two layers. (A) Cumulative Ca^{2+} uptake by devitalised bottom layer-only ($n = 24$, same group as in Figure 5) and viable top + devitalised bottom ($n = 24$) over 3 weeks. (B) Representative 3D reconstructed micro-CT images. The scale bar indicated 2 mm. (C) The volume of calcified tissue (mm^3) at 3 weeks. (D) Representative von Kossa/thionine staining of cartilage explants cultured for 3 weeks. Scale bars indicates 100 μm . (E) Representative 3D reconstructed micro-CT images. The scale bar indicated 2 mm. (F) The volume of calcified tissue (mm^3) in viable bottom layer-only ($n=20$, same group as in Figure 5) and devitalised top + viable bottom ($n = 21$) at 3 weeks. (G) Representative von Kossa/thionine staining of cartilage explants cultured for 3 weeks. Scale bars indicates 100 μm . 1 ml medium was used to culture the cartilage explants. The Kruskal-Wallis H test or one-way ANOVA test (based on normality) was used to test statistical significance. Two independent experiments with two different donors were performed.

4. DISCUSSION

In this study, we developed an *ex vivo* cartilage culture model to investigate the formation of the ZCC in articular cartilage. Our findings revealed the inherent zone-specific calcification processes exhibited within the cartilage explants. The top layer expressed the capacity to inhibit cartilage calcification via releasing bioactive factors. The viable chondrocytes in the bottom layer can actively stimulate cartilage calcification as well as respond to bioactive factors that inhibit cartilage calcification. These results indicate the critical role of the different layers of articular cartilage in the formation of a ZCC.

Ex vivo explant culture models represent powerful tools in cartilage research, bridging the gap between *in vitro* models and pre-clinical studies and reducing the need for animal

experiments in our research endeavours [19-21]. With the complex physico-chemical properties of cartilage, the *ex vivo* culture preserves crucial cell-cell and cell-matrix interactions, essential for better understanding cell behaviour within their natural three-dimensional environment. Our explant culture model includes the different layers of articular cartilage that contain chondrocytes of different phenotypes and matrix of different structures/compositions [22]. The presence of an extracellular matrix prevents the de-differentiation that often occurs in monolayer cultures. By retaining the zonal organisation and 3D structure, the specific biochemical gradients and chondrocyte phenotypes present within each cartilage zone can be preserved. Moreover, we used immature articular cartilage where the ZCC has not yet been formed. In this study, the calcification layer formed in osteochondral explants was not connected to the secondary ossification centre, indicating that the calcification zone might be the future ZCC. With this culture model, we explored the interplay between top and bottom zones of articular cartilage in the formation of the ZCC. We revealed that the regulation of formation of this ZCC involves the complex interplay between viable chondrocytes from different zones. Such a model could provide useful insights into mechanisms of cartilage calcification and the effects of involved factors.

The coordinated expression of inhibitory and stimulatory factors of calcification by chondrocytes in different zones may be involved in calcified cartilage formation. In our study, the top layers released bioactive factors that inhibited calcification of the deep zone of cartilage. Delve et al. suggested that FGF-18 might be one of the bioactive factors secreted by the chondrocytes from the superficial zone of articular cartilage that inhibit cartilage calcification by up-regulating polyphosphate [23]. PTHrP secreted by the superficial chondrocytes [14], is another factor that has been shown to regulate cartilage calcification by suppressing ALP activity [24]. Most knowledge about cartilage calcification, however, comes from research on the growth plate where the PTHrP-IHH loop is known to play an important role [25]. In our study, PTHrP significantly reduced the calcification of viable bottom layer cartilage, but not of devitalised bottom layers, indicating that viable chondrocytes are needed to respond to the regulators of cartilage calcification. Indian hedgehog (Ihh) signalling from prehypertrophic chondrocytes has been implicated in the control of chondrocyte maturation by way of feedback control of a second secreted factor, PTHrP, and PTHrP also inhibits Ihh secretion via a negative feedback loop [24, 26, 27]. On the other hand, the deep zone of immature articular cartilage readily calcifies during culture. In fact, our results showed that less calcification was formed in devitalised bottom layer-only explants than in viable bottom layer-only explants, indicating that chondrocytes in the bottom layers might actively stimulate cartilage calcification. Chondrocytes that undergo hypertrophy-like changes produce a number of proteins that are involved in calcification, such as alkaline phosphatase [28]. These findings indicated that the presence of viable chondrocytes in both layers is essential for the regulation of formation of the ZCC. Chondrocytes in the different zones play critical and distinct roles in modulating cartilage calcification via expression of inhibitory and stimulatory factors.

On the other hand, although viable chondrocytes are required to respond to PTHrP, our results showed that viable top layers were still able to inhibit calcification of devitalised bottom layers, and devitalised top layers were also capable to inhibit calcification of viable bottom layers. This indicates that the inhibitory effect of top layers on calcification does

not entirely rely on the presence of viable chondrocytes. Fetuin is a liver-derived protein that acts as a potent inhibitor of ectopic mineralization via binding small clusters of calcium and phosphate [29]. Therefore, the function of fetuin in inhibiting mineralisation does not require the presence of viable cells. Moreover, fetuin has been found to be present in human articular cartilage and chondrocytes are capable of fetuin uptake [30]. In fact, the fetuin-matrix Gla protein complex is assembled in matrix vesicles in healthy articular cartilage, but not in osteoarthritic cartilage [30]. This might explain the mineralisation observed in osteoarthritic cartilage, since fetuin-A levels are inversely associated with clinical severity in osteoarthritis patients [31]. Overall, there might be multiple factors released by top layers for inhibiting cartilage calcification, such as FGF18 or PTHrP that requires the presence of viable chondrocytes in both layers, or fetuin that is able to function without viable chondrocytes.

In our cultures, the calcified zone that was formed represents approximately 20-30% of the tissue thickness. Interestingly, only the deep zone of the viable articular cartilage calcified. Moreover, the calcification layer formed in osteochondral explants was not connected to the secondary ossification centre, indicating that the calcification in the deep zone might be the future ZCC. This zone-specific mineralisation indicates the role of the zonal layering of cartilage, including the chondrocytes and matrix. A similar situation is the calcification in growth plate cartilage, that occurs only in the zone of terminally differentiated growth plate chondrocytes close to the chondro-osseous border. Several theories have been proposed to elucidate the process of calcification [32]. One theory suggests that matrix vesicles might be the initiator of physiological and pathological calcification [33]. These membrane-enclosed particles are released from the plasma membrane of mineralisation-competent cells (hypertrophic chondrocytes). These vesicles contain calcium-inorganic phosphate-phospholipid complexes that serve as a nucleus for the formation of the first crystal phase [33]. Non-collagenous proteins in the extracellular matrix, such as glycoproteins, were also reported to play a critical role in the initiation and growth of the calcium phosphate mineral phase [33]. This role of proteins or vesicles in the matrix, aligns with our findings that calcification of the matrix still happened in devitalised cartilage, and was still located predominately in the deep zone. These matrix vesicles and proteins might already have been present in the deep zone of the matrix before the devitalisation.

Various parameters for the explant culture model presented in this study were based on previous investigations, including the concentration of 10% fetal calf serum and 10mM β -GP [34-36]. 10% fetal calf serum and 25 μ g/ml ascorbic acid were reported to be optimal [37]. 20% fetal calf serum was demonstrated to inhibit cartilage calcification [37], possibly due to the presence of serum proteins, including transforming growth factor β [38]. β -GP is commonly used to achieve the formation of phosphate-calcium crystals. In serum or plasma, the level of inorganic phosphate (Pi) is 1.0-1.5 mM, whereas the organic phosphate level is about 3 mM [39]. The hydrolysis of 10 mM β -GP by alkaline phosphatase results in medium Pi levels that are suprphysiological. The calcification in the presence of this suprphysiological concentration of Pi *in vitro* can, however, lead to the formation of large crystals in the matrix [37], which was confirmed to be hydroxyapatite [40]. Kandel et al. compared this calcification present in the cartilage explants formed *ex vivo* to the calcification present in the zone of calcified cartilage of bovine articular cartilage and

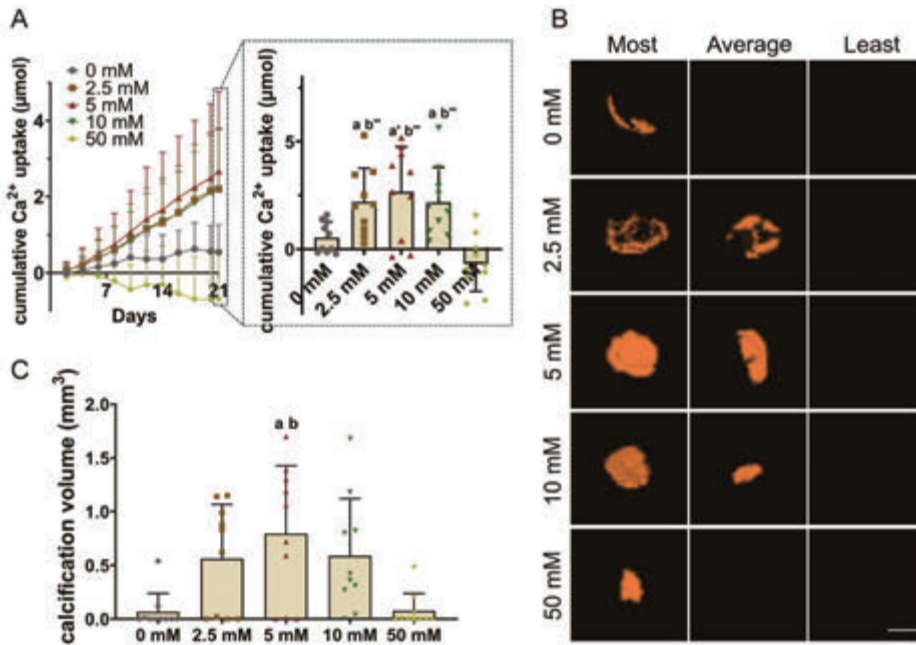
demonstrated that the crystals that formed in the presence of 10 mM β -GP were found to be similar in organisation, structure, and size to those present in the *in vivo* calcified articular cartilage [35]. Since we have not characterised the crystals in our study, we cannot exclude formation of pathological crystals. Furthermore, the explants were devitalised by either formalin fixation or freeze-thaw cycles, potentially damaging the cartilage matrix, which could influence cartilage calcification. Another limitation of our study is that while FGF18, PTHrP or fetuin could be the bioactive factors released by the top layers for inhibiting cartilage calcification, we did not provide evidence for the specific release mechanisms involved. Future studies should focus on elucidating the exact mechanisms of these factors in the interplays between zonal cartilage.

Overall, the formation of calcified cartilage might be a result of the intricate interaction between the chondrocytes and the extracellular matrix. The insights obtained in this study are useful for the regeneration of a biomimetic calcified cartilage to integrate cartilaginous tissue to bone, ultimately forming a mechanically functional osteochondral unit. The clear differences in behaviour between top and bottom chondrocytes might also explain the challenge to successfully regenerate this unit. Using zonal chondrocytes to regenerate a mature, stratified articular cartilage with a zone of calcified cartilage might be promising [41]. However, this has yet to be realised and might be challenged by the lack of an efficient zonal chondrocyte isolation method and an expansion platform that would allow both cell propagation and phenotype maintenance [41]. This model can also be a valuable tool for investigating pathological cartilage calcification. Cartilage calcification is a crucial hallmark of osteoarthritis [42]. With this model, the role of different processes involved in cartilage calcification, such as the role of inflammation and matrix degradation, can be investigated [43]. Moreover, this *ex vivo* model offers a platform for testing novel compounds targeting anti-calcification as a potential therapeutic approach.

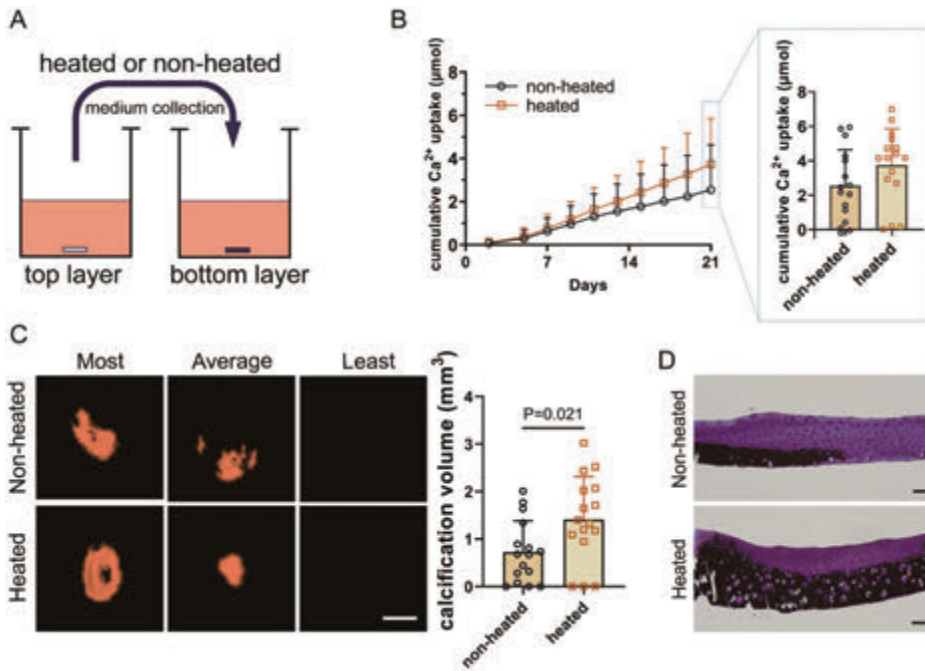
5. CONCLUSION

Immature articular cartilage that has not yet formed calcified cartilage retains the inherent zone-specific capacity to calcify when cultured *ex vivo* and thus can be used as a model to study the mechanism of ZCC formation. Our studies demonstrated that top layers of articular cartilage exhibited the capacity to inhibit cartilage calcification via secreting bioactive factors, while viable chondrocytes in bottom layers can actively induce cartilage calcification as well as respond to inhibitory factors secreted from top layers. Understanding the processes of calcified cartilage formation can help to improve osteochondral tissue engineering as well as to find treatments for pathological cartilage calcifications.

SUPPLEMENTARY MATERIALS

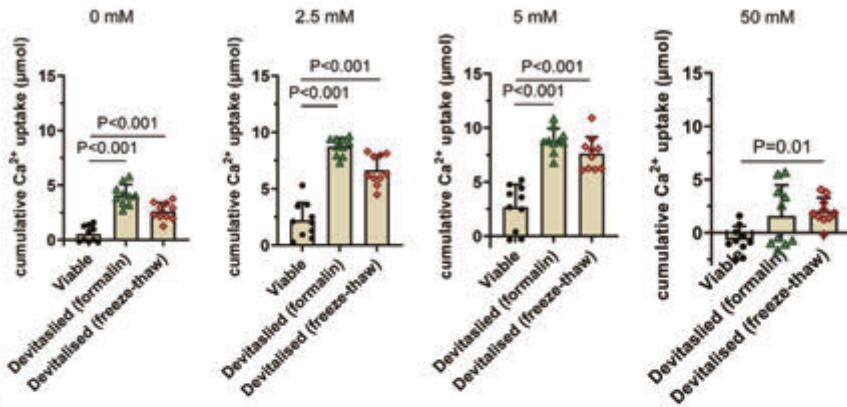


Supplementary Figure 1. 2.5-10 mM β -glycerophosphate allowed calcification in full-thickness cartilage ex vivo. Full-thickness cartilage explants were cultured with the addition of 0, 2.5, 5, 10 and 50 mM β -glycerophosphate in 1 ml culture medium for a duration of 3 weeks ($n = 10$ per condition). (A) The line graph depicted the cumulative Ca^{2+} taken up from the medium at each time point. The bar graph showed the cumulative Ca^{2+} uptake at 3 weeks. $a: P < 0.05$ compared to 0 mM, $a': P < 0.01$ compared to 0 mM, $b'': P < 0.001$ compared to 50 mM. One-way ANOVA test was used to test statistical significance. (B) Representative 3D reconstructed micro-CT images of calcification after 3 weeks, scale bar indicated 2 mm. (C) The volume of calcified tissue (mm^3) in cartilage explants. $a: P < 0.05$ compared to 0 mM, $b: P < 0.05$ compared to 50 mM. The Kruskal-Wallis H test was used to test statistical significance.

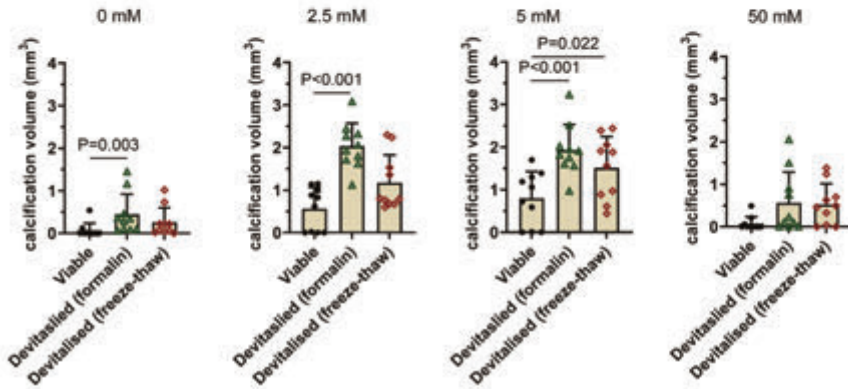


Supplementary Figure 2. The top layers secreted bioactive factors to inhibit cartilage calcification. (A) Experimental scheme for in-direct co-culture of top layers and bottom layers. The medium collected from the top layers was mixed with fresh medium, and then was heated or not heated to culture the bottom layers (0.5 ml). (B) The line graph depicted the cumulative Ca^{2+} taken up from the medium by different cartilage explants ($n=16$) at each time point of medium refreshing. The bar graph showed the cumulative Ca^{2+} uptake over 3 weeks. (C) Representative 3D reconstructed micro-CT images and volume of calcified tissue (mm^3) at 3 weeks. The scale bar indicated 2 mm. (D) Representative von Kossa/thionine staining of cartilage explants cultured for 3 weeks ex vivo. 0.5 ml medium was used to culture the cartilage explants. Scale bars indicates 100 μm . The independent t-test was used to test statistical significance.

A



B



Supplementary Figure 3. Viable chondrocytes in full-thickness cartilage inhibited extracellular matrix calcification with 0 mM, 2.5 mM, 5 mM and 50 mM 8-glycerophosphate concentrations. (A) Cumulative Ca^{2+} taken up by viable and devitalised full-thickness cartilage explants ($n = 10$) at 3 weeks. (B) Volume of calcified tissue (mm^3) at 3 weeks. 1 ml medium was used to culture the cartilage explants. The Kruskal-Wallis H test or one-way ANOVA test (based on normality) was used to test statistical significance.

REFERENCES

- [1] Deng C, Chang J, Wu C. Bioactive scaffolds for osteochondral regeneration. *J Orthop Translat.* 2019;17:15-25.
- [2] Zhou L, Gjym VO, Malda J, Stoddart MJ, Lai Y, Richards RG, Ki-wai Ho K, Qin L. Innovative Tissue-Engineered Strategies for Osteochondral Defect Repair and Regeneration: Current Progress and Challenges. *Advanced Healthcare Materials.* 2020;9(23):2001008.
- [3] Bhosale AM, Richardson JB. Articular cartilage: structure, injuries and review of management. *British Medical Bulletin.* 2008;87(1):77-95.
- [4] Zhou H, Yuan L, Xu Z, Yi X, Wu X, Mu C, Ge L, Li D. Mimicking the composition and structure of the osteochondral tissue to fabricate a heterogeneous three-layer scaffold for the repair of osteochondral defects. *ACS Applied Bio Materials.* 2022;5(2):734-746.
- [5] Broom ND, Poole CA. A functional-morphological study of the tidemark region of articular cartilage maintained in a non-viable physiological condition. *J Anat.* 1982;135(Pt 1):65-82.
- [6] Radin EL, Rose RM. Role of Subchondral Bone in the Initiation and Progression of Cartilage Damage. *Clinical Orthopaedics and Related Research.* 1986;213.
- [7] Mente PL, Lewis JL. Elastic modulus of calcified cartilage is an order of magnitude less than that of subchondral bone. *Journal of Orthopaedic Research.* 1994;12(5):637-647.
- [8] Wang W, Ye R, Xie W, Zhang Y, An S, Li Y, Zhou Y. Roles of the calcified cartilage layer and its tissue engineering reconstruction in osteoarthritis treatment. *Front Bioeng Biotechnol.* 2022;10:911281.
- [9] Hinek A, Reiner A, Poole AR. The calcification of cartilage matrix in chondrocyte culture: studies of the C-propeptide of type II collagen (chondrocalcin). *J Cell Biol.* 1987;104(5):1435-1441.
- [10] Kandel R, Boyle J, Gibson G, Cruz T, Speagle M. *In Vitro* formation of mineralized cartilagenous tissue by articular chondrocytes. *In Vitro Cellular & Developmental Biology-Animal.* 1997;33:174-181.
- [11] Yan J, Shen M, Sui B, Lu W, Han X, Wan Q, Liu Y, Kang J, Qin W, Zhang Z, Chen D, Cao Y, Ying S, Tay FR, Niu LN, Jiao K. Autophagic LC3(+) calcified extracellular vesicles initiate cartilage calcification in osteoarthritis. *Sci Adv.* 2022;8(19).
- [12] Ea HK, Nguyen C, Bazin D, Bianchi A, Guicheux J, Reboul P, Daudon M, Lioté F. Articular cartilage calcification in osteoarthritis: Insights into crystal-induced stress. *Arthritis & Rheumatism.* 2011;63(1):10-18.
- [13] Hamade T, Bianchi A, Sebillaud S, Netter P, Jouzeau JY, Cailotto F. Inorganic phosphate (Pi) modulates the expression of key regulatory proteins of the inorganic pyrophosphate (PPi) metabolism in TGF- β 1-stimulated chondrocytes. *Biomed Mater Eng.* 2010;20(3):209-215.
- [14] Tsukazaki T, Ohtsuru A, Enomoto H, Yano H, Motomura K, Ito M, Namba H, Iwasaki K, Yamashita S. Expression of parathyroid hormone-related protein in rat articular cartilage. *Calcified Tissue International.* 1995;57:196-200.
- [15] Miao D, Scutt A. Histochemical localization of alkaline phosphatase activity in decalcified bone and cartilage. *J Histochem Cytochem.* 2002;50(3):333-340.
- [16] Wang Y, Kim UJ, Blasioli DJ, Kim HJ, Kaplan DL. *In Vitro* cartilage tissue engineering with 3D porous aqueous-derived silk scaffolds and mesenchymal stem cells. *Biomaterials.* 2005;26(34):7082-7094.

- [17] Little CJ, Bawolin NK, Chen X. Mechanical properties of natural cartilage and tissue-engineered constructs. *Tissue Eng Part B Rev.* 2011;17(4):213-227.
- [18] Chen J, Yuan Z, Liu Y, Zheng R, Dai Y, Tao R, Xia H, Liu H, Zhang Z, Zhang W, Liu W, Cao Y, Zhou G. Improvement of *In Vitro* Three-Dimensional Cartilage Regeneration by a Novel Hydrostatic Pressure Bioreactor. *Stem Cells Transl Med.* 2017;6(3):982-991.
- [19] Anderson JR, Phelan MM, Foddy L, Clegg PD, Peffers MJ. *Ex Vivo* Equine Cartilage Explant Osteoarthritis Model: A Metabolomics and Proteomics Study. *Journal of Proteome Research.* 2020;19(9):3652-3667.
- [20] Monaco G, El Haj AJ, Alini M, Stoddart MJ. *Ex Vivo* Systems to Study Chondrogenic Differentiation and Cartilage Integration. *Journal of Functional Morphology and Kinesiology.* 2021;6(1):6.
- [21] Trengove A, Duchi S, Onofrillo C, Sooriyaaratchi D, Di Bella C, O'Connor AJ. Bridging bench to body: *Ex Vivo* models to understand articular cartilage repair. *Current Opinion in Biotechnology.* 2024;86:103065.
- [22] Jeon J, Malda J, Schrobback K, Irawan D, Masuda K, Sah RL, Hutmacher DW, Klein T. Engineering cartilage tissue with zonal properties. *Methods in Bioengineering: 3D Tissue Engineering.* 2010;205-224.
- [23] Delve E, Bromand S, St-Pierre JP, Grynepas M, Kandel R. Superficial zone chondrocytes secrete a factor that regulates deep zone cartilage mineralization by modulating polyphosphate levels. *Osteoarthritis and Cartilage.* 2015;23.
- [24] Jiang J, Leong NL, Mung JC, Hidaka C, Lu HH. Interaction between zonal populations of articular chondrocytes suppresses chondrocyte mineralization and this process is mediated by PTHrP. *Osteoarthritis and Cartilage.* 2008;16(1):70-82.
- [25] Kronenberg HM, Chung U. The parathyroid hormone-related protein and Indian hedgehog feedback loop in the growth plate. *Novartis Found Symp.* 2001;232:144-152; discussion 152-157.
- [26] van Donkelaar CC, Huiskes R. The PTHrP–Ihh Feedback Loop in the Embryonic Growth Plate Allows PTHrP to Control Hypertrophy and Ihh to Regulate Proliferation. *Biomechanics and Modeling in Mechanobiology.* 2007;6(1):55-62.
- [27] Chow WA. Chondrosarcoma: biology, genetics, and epigenetics. *F1000Res.* 2018;7.
- [28] van der Kraan PM, van den Berg WB. Chondrocyte hypertrophy and osteoarthritis: role in initiation and progression of cartilage degeneration? *Osteoarthritis and Cartilage.* 2012;20(3):223-232.
- [29] Jahnen-Dechent W, Heiss A, Schäfer C, Ketteler M, Towler DA. Fetuin-A Regulation of Calcified Matrix Metabolism. *Circulation Research.* 2011;108(12):1494-1509.
- [30] Wallin R, Schurgers LJ, Loeser RF. Biosynthesis of the vitamin K-dependent matrix Gla protein (MGP) in chondrocytes: a fetuin–MGP protein complex is assembled in vesicles shed from normal but not from osteoarthritic chondrocytes. *Osteoarthritis and Cartilage.* 2010;18(8):1096-1103.
- [31] Xiao J, Wang XR, Hu KZ, Li MQ, Chen JW, Ma T, Li ZC. Serum fetuin-A levels are inversely associated with clinical severity in patients with primary knee osteoarthritis. *Biomarkers.* 2013;18(1):51-54.
- [32] Huitema LF, Vaandrager AB. What triggers cell-mediated mineralization? *Front Biosci.* 2007;12:2631-2645.
- [33] Kirsch T. Determinants of pathological mineralization. *Curr Opin Rheumatol.* 2006;18(2):174-180.

- [34] Hwang J, Kyubwa EM, Bae WC, Bugbee WD, Masuda K, Sah RL. *In Vitro* Calcification of Immature Bovine Articular Cartilage: Formation of a Functional Zone of Calcified Cartilage. *Cartilage*. 2010;1(4):287-297.
- [35] Kandel R, Hurtig M, Grynblas M. Characterization of the mineral in calcified articular cartilagenous tissue formed *In Vitro*. *Tissue Eng*. 1999;5(1):25-34.
- [36] Jiang J, Leong NL, Mung JC, Hidaka C, Lu HH. Interaction between zonal populations of articular chondrocytes suppresses chondrocyte mineralization and this process is mediated by PTHrP. *Osteoarthritis Cartilage*. 2008;16(1):70-82.
- [37] Boskey AL, Stiner D, Doty SB, Binderman I, Leboy P. Studies of mineralization in tissue culture: optimal conditions for cartilage calcification. *Bone Miner*. 1992;16(1):11-36.
- [38] Kato Y, Iwamoto M, Koike T, Suzuki F, Takano Y. Terminal differentiation and calcification in rabbit chondrocyte cultures grown in centrifuge tubes: regulation by transforming growth factor beta and serum factors. *Proc Natl Acad Sci U S A*. 1988;85(24):9552-9556.
- [39] Chung CH, Golub EE, Forbes E, Tokuoka T, Shapiro IM. Mechanism of action of beta-glycerophosphate on bone cell mineralization. *Calcif Tissue Int*. 1992;51(4):305-311.
- [40] Kandel RA, Boyle J, Gibson G, Cruz T, Speagle M. *In Vitro* formation of mineralized cartilagenous tissue by articular chondrocytes. *In Vitro Cell Dev Biol Anim*. 1997;33(3):174-181.
- [41] Tee CA, Han J, Hui JHP, Lee EH, Yang Z. Perspective in Achieving Stratified Articular Cartilage Repair Using Zonal Chondrocytes. *Tissue Eng Part B Rev*. 2023;29(3):310-330.
- [42] Fuerst M, Bertrand J, Lammers L, Dreier R, Echtermeyer F, Nitschke Y, Rutsch F, Schäfer FKW, Niggemeyer O, Steinhagen J. Calcification of articular cartilage in human osteoarthritis. *Arthritis & Rheumatism*. 2009;60(9):2694-2703.
- [43] Faure E, Wegrzyn J, Bernabei I, Falgayrac G, Bertheaume N, Pascart T, Hugle T, Busso N, Nasi S. A new *ex vivo* human model of osteoarthritis cartilage calcification. *Rheumatology*. 2024;keae064.

8

Discussion

DISCUSSION

This thesis investigated the endogenous repair of osteochondral tissue defects, with a special focus on biochemical and biophysical cues of exogenous implants to stimulate osteochondral repair. In addition, we investigated the mechanism of calcified cartilage formation, since it plays a pivotal role in successful osteochondral repair. Throughout this thesis, various *in vitro*, *ex vivo* and *in vivo* models were employed to comprehensively study the process of osteochondral tissue repair. We have demonstrated that manipulating the biophysical and biochemical cues of biomaterials is an effective and feasible strategy for enhancing regeneration of osteochondral tissue, but the interaction between exogenous and endogenous cues needs to be considered when designing biomaterial-based implants.

Biophysical and biochemical modification of biomaterials to improve osteochondral repair

Biomaterials are vital elements of tissue engineering strategies, offering structural support and delivering biophysical and biochemical cues for the cells involved in tissue repair. Particularly, acellular strategies heavily rely on the biophysical and biochemical cues provided by implants in osteochondral repair [1]. In fact, in the patient, a limited quantity of bioactive factors, such as chemokines and growth factors, is released within a short period after osteochondral injury [2]. Consequently, only minimal endogenous stem/progenitor cells are recruited for osteochondral repair [2]. A meta-analysis demonstrated that implanting acellular regenerative biomaterials, such as collagen, hyaluronic acid, hydroxyapatite and/or polycaprolactone, substantially enhanced articular cartilage repair by 15.6% compared to non-treated defects [3]. The addition of biologics, such as bone morphogenetic protein (BMP) and platelet-rich plasma, to biomaterials, have demonstrated to significantly improve cartilage regeneration by 7.6% compared to control biomaterials [3]. Therefore, the further development of regenerative hydrogels or scaffolds with appropriate biophysico-chemical properties seems logical to further enhance acellular osteochondral repair strategies.

Biochemical modification of biomaterials to improve osteochondral repair

Biochemical modification of biomaterials involves tailoring biochemical cues via incorporating chondrogenic/osteogenic components or bioactive factors into biomaterials. In **Chapter 2**, we highlighted the presence of resident endogenous stem/progenitor cells in joints, and discussed the significant role of endogenous stem/progenitor cells and bioactive factors during the repair process. We reviewed the biochemical cues, including bioactive factors, such as chemokines, cytokines, and growth factors, along with various spatiotemporal delivery/release modalities to achieve controlled release of bioactive factors to the defect site, such as liposomes and nano-carriers. Many methodologies have been employed to design and fabricate osteochondral defect implants with biochemical cues that can interact with adjacent tissues and cells. These approaches showed promising applications to achieve robust repair by manipulating biochemical cues of exogenous implants.

Integrating additional biochemical components into biomaterials is one of the options to modify biochemical cues of biomaterials. In **Chapter 3** and **Chapter 4**, we investigated the

effect of integrating additional chondrogenic or osteogenic components in implants to enhance osteochondral repair. Hydrogels have emerged as a promising material in cartilage repair due to their good biocompatibility, reproducibility and cartilage-like characteristics, such as three-dimensional hydrophilic polymer networks [4]. The combination of multiple natural and synthetic polymers enables the manipulation of biochemical cues of hydrogels [5]. For instance, hyaluronic acid, a natural polysaccharide present in articular cartilage with good biocompatibility, can be modified with polyethylene glycol [6] or norbornene hyaluronic acid [7] to manipulate cell behaviours. The initial step of osteochondral repair with cell-free therapeutic approaches is to recruit tissue-forming cells to defect sites, and then induce their participation in the repair process. The main limitation of hyaluronic acid-based materials is the limited cell adhesion [8, 9], making them less optimal for cells to infiltrate that material, a process that is necessary for endogenous repair procedures. The effect of adding collagen to tyramine functionalised hyaluronic acid on endogenous cell infiltration into osteochondral defects is one of the biomaterials we investigated in **Chapter 3**. The addition of collagen enhanced the migration of surrounding mesenchymal stromal cells and chondrocytes *in vitro*, *ex vivo* and *in vivo*. In native cartilage, the core fibrillar network is a crosslinked copolymer of collagens [10], which imparts bio-instructive properties that are perceived by the cells. The chondrocytes express receptors capable of directly binding to the triple helical domains in collagens [11]. Therefore, the addition of collagen into the tyramine-functionalised hyaluronic acid hydrogel might offer an additional advantage for cell adhesion and migration. This concept of incorporating collagen to improve cell adhesion has been applied to other materials that encounter challenges with cell adhesion, such as polyethylene glycol (PEG) and hydroxyapatite [12-18].

In **Chapter 4**, we modified the bone layer of a clinically used scaffold and developed a novel synthesis method for the production of amorphous calcium phosphate (ACP) granules. ACP is a hydrated calcium phosphate characterised by an amorphous structure. This amorphous nature enables it to closely resemble the low crystalline nanoparticles of the biological apatite with a higher solubility and reactivity due to its high specific surface area [19]. The presence of an amorphous phase, high specific surface area and hydrated structure of ACP ensures its solubility, excellent adsorption properties and bioactivity of biologically relevant ions and molecules [19-24]. To enhance the amorphous phase stability of ACP, we modified its structure with strontium ions (Sr^{2+}). Sr^{2+} was reported to stabilise the amorphous state of ACP [25]. As expected, the modification of the ACP structure with Sr^{2+} ensured prolonged amorphous phase stability of Sr-ACP in the dry state for at least 3.5 years. This Sr-ACP was integrated into a collagen-magnesium-hydroxyapatite (Col-Mg-HAp) scaffold to manipulate biochemical cues. With the addition of Sr-ACP into the collagen-magnesium-hydroxyapatite (Col-Mg-HAp) scaffold, the presence of Sr^{2+} can further enhance the stabilisation effect of Mg^{2+} on ACP due to the exclusion of Mg during HAp nucleation from ACP [26]. Moreover, Sr^{2+} , Ca^{2+} , Mg^{2+} , and PO_4^{3-} were expected to be released from the enhanced scaffold to favour chemotaxis, scaffold colonisation, and the cell mineralisation process. This was supported by the porous nano-structure of the scaffold to provide efficient ion delivery. In a caprine pre-clinical osteochondral defect model the addition of Sr-ACP was shown to significantly improve subchondral bone repair capacity of this scaffold. Overall, we demonstrated the

potential of integrating additional biochemical components to improve the subchondral bone repair capacity of biomaterials.

Another way to modify biochemical cues of implants is by delivering bioactive factors. The migration of endogenous cells is a fundamental stage for endogenous osteochondral repair. The limited release of bioactive factors following an osteochondral injury may not recruit a sufficient number of endogenous cells from adjacent niches, leading to failed osteochondral healing. Given that no exogenous cells will be seeded in the biomaterials in acellular strategies, incorporating exogenous bioactive factors presents a favourable approach to enhance cell infiltration and promote tissue repair. Numerous bioactive factors are involved in the process of osteochondral repair. Many of them, such as platelet-derived growth factor (PDGF), BMP-2, and insulin-like growth factor (IGF), have been intensively investigated for their physiological effects on osteochondral repair. However, the retention capacity and release profiles of bioactive factors vary across different biomaterials. Although complex bioactive factor delivery systems have been developed, simplicity and reproducibility are crucial criteria in clinical applications. In **Chapter 5**, BMP-2 and PDGF-BB were conveniently adsorbed onto a Col/Col-Mg-HAp scaffold. *In vitro* release kinetics demonstrated that PDGF-BB was burst released from the collagen-only layer, whereas BMP-2 was largely retained in both layers. The adsorption of BMP-2 or PDGF-BB led to enhanced cell ingrowth in a bovine osteochondral defect model cultured *ex vivo*. In an *in vivo* semi-orthotopic athymic mouse model, the addition of BMP-2 or PDGF-BB resulted in increased tissue repair. This finding aligns with previous studies that showed BMP-2 and PDGF-BB can function as effective bioactive factors for cell recruitment and tissue repair [27-30]. Unexpectedly, in our study, BMP-2 reduced bone regeneration in weight-bearing femoral condyle locations in the goat osteochondral defect model, while it slightly improved the subchondral bone repair in non-weight-bearing trochlear groove osteochondral defects. This is possibly due to local dosage and its interaction with mechanical loading. Mechanical loading has been demonstrated to enhance BMP-2 expression [31]. Consequently, the combination of exogenous and locally produced BMP-2 could potentially result in an overstimulation of BMP-2 signalling, leading to inflammation, bone resorption, and fibrotic tissue formation [32-34]. Therefore, the incorporation of bioactive factors requires thorough investigations of their release profile, stability *in vivo*, and effects in the specific biophysical and biochemical environments present in joints in large animal translational models.

Biophysical modification of biomaterials to improve osteochondral repair

Biophysical cues, encompassing factors such as pore size and interconnectivity, exert significant influence over a wide range of cellular behaviours, including adhesion, migration, proliferation, and differentiation [35-40]. Biophysical cues, including mechanical properties, pore size, and biodegradability of hydrogels, are tunable to suit various biomedical applications [41, 42]. In **Chapter 3**, we investigated the effect of the degradability of the crosslinker in hyaluronic acid hydrogel, and the degree of functionalisation in Gelatin methacryloyl (GelMA) hydrogel, on cell migration and tissue formation *in vitro*, *ex vivo* and *in vivo*. Hyaluronic acid, one of the most commonly utilised proteoglycan hydrogels, is frequently functionalised with biophysical cues, including adjustments to mechanical properties, porosity and pore size to stimulate cell ingrowth and promote matrix deposition [7, 43, 44]. Thiol-norbornene has been introduced to

enhance the rheological properties, tunability of mechanical properties, printability and interaction with the host tissue of hyaluronic acid [7]. A degradable and cleavable crosslinker, matrix metalloproteinase (MMP), leads to a larger mesh size in the norbornene hyaluronic acid (norHA) hydrogel compared to a non-degradable 1,4-Dithiothreitol (DTT) crosslinker. We found that using MMP resulted in significantly more cell migration and tissue formation than using DTT *in vivo*. Similarly, an increased degree of functionalisation (DoF) in GelMA hydrogels resulted in a higher crosslinking density and, thus smaller pore size [45]; and we found that lower DoF of GelMA led to a higher migration score *ex vivo* and more tissue formation *in vivo*. Another phenomenon, MSCs spreading in the hydrogels might be caused by a larger mesh size in the hydrogel. Appropriate pore size and interconnectivity of the network are critical parameters in cell migration, nutrient diffusion and removal of metabolic substances [36, 38]. Chondrocytes prefer pore sizes between 250 to 500 μm for better cell proliferation and extracellular matrix production [36]. Notably, the optimal pore size for cartilage falls within the range of 100-200 μm , and chondrocytes tend to differentiate to an osteogenic pathway with the larger pore size (300-500 μm) [38]. Therefore, hydrogels applied in osteochondral repair need a multiple-layer structure design for regenerating cartilage and subchondral bone simultaneously.

Cartilage-bone interface regeneration

Calcified cartilage in mature joints is located between non-calcified articular cartilage and the subchondral bone plate. It comprises hypertrophic chondrocytes within lacunae in a calcified cartilage matrix, which consists of sodium hyaluronate, collagen, and hydroxyapatite [46]. The presence of calcified cartilage minimises the shear stress and prevents a mechanically discontinuous transition from non-calcified cartilage to the subchondral bone plate. As a transition layer, calcified cartilage bears both compressive and shear forces [47-49]. Additionally, calcified cartilage serves as a barrier that prevents vascular invasion from subchondral bone to non-calcified cartilage with a lower diffusion coefficient compared to non-calcified cartilage [50]. Therefore, regenerating the calcified cartilage in osteochondral repair is critical for restoring physiological functions.

In **Chapter 4** and **Chapter 5**, a bilayered Col/Col-Mg-HAp scaffold was employed to repair osteochondral defects in a large animal translational osteochondral defect model. While this scaffold was successful in promoting the formation of robust articular cartilage and subchondral bone, a structured calcified cartilage layer was notably absent, even six months after implantation in the goat. The bony layer of this bilayered scaffold comprises 60% collagen and 40% Mg-HAp. Notably, in clinical practice for treating osteochondral defects, this Col/Col-Mg-HAp scaffold is applied in the trilayered configuration. The calcified layer is composed of 60% collagen and 40% Mg-HAp, and the bony layer consists of 30% collagen and 70% Mg-HAp [13-18]. However, the formation of a stable calcified cartilage layer between the articular cartilage and subchondral bone has not yet been achieved in horses after 6 months [51]. Similarly, many attempts to regenerate this critical cartilage-bone interface with trilayered scaffolds have been reported [52-55]. Huang et al. developed a trilayered scaffold containing acellular subchondral bone with a natural calcified cartilage zone from healthy pigs to mimic the calcified cartilage and the subchondral bone layer [53]. Although the presence of a transitional layer in the scaffold achieved better regeneration of hyaline cartilage compared to the bi-layered scaffold, they

still did not fully regenerate the intricate hierarchical structure inherent in the native osteochondral unit [53].

Understanding the mechanisms underlying calcified cartilage formation would be beneficial in developing effective regeneration strategies for osteochondral defect repair. In **Chapter 7**, we developed an *ex vivo* articular cartilage culture model to study cartilage calcification. Our findings demonstrated the inherent zone-specific calcification process within articular cartilage. We observed that the calcified zone developed only in the deep zone of the cartilage explants. This zone-specific calcification might be attributed to the zonal structure of articular cartilage, including the chondrocyte phenotypes, various matrix vesicles and non-collagenous proteins present in the different zones [56, 57]. The chondrocytes residing in the top layers and the bottom layers of full-thickness cartilage demonstrated distinct roles in the process of cartilage calcification. Specifically, viable chondrocytes present in the top layers exhibited the capacity to inhibit cartilage calcification via secreting bioactive factors. This suppression might be partly regulated by the parathyroid hormone-related peptide (PTHrP) secreted by chondrocytes residing in the superficial zone of articular cartilage [58]. In situ hybridisation of rodent cartilage revealed that chondrocytes in the superficial zone of articular cartilage expressed PTHrP [59], while its receptor, PTH1R, is mainly expressed in pre-hypertrophic chondrocytes [60]. Although cartilage is avascular, physical cell-cell communication between zonal sub-populations via voltage-gated gap junctions has been demonstrated [61]. On the other hand, viable chondrocytes residing in the bottom layers would actively induce cartilage calcification. More calcification was formed with the presence of viable chondrocytes in the bottom layers compared to devitalised bottom layers. Moreover, viable chondrocytes residing in the bottom layers are capable of responding to bioactive factors, such as PTHrP, and thereby influencing cartilage calcification. Hence, the formation of calcified cartilage might be a result of the intricate interaction between the zonal chondrocytes and the extracellular matrix. Previous designs for calcified cartilage formation in multi-layered scaffolds usually aimed to replicate the structural composition of the calcified cartilage matrix, and paid less attention to inducing endogenous cell differentiation towards particular chondrocyte phenotypes. Our findings are insightful for the design of an optimal layered implant to mimic both non-calcified and calcified cartilage. Specifically, an ideal multi-layered scaffold should incorporate distinct biochemical and biophysical cues within different layers. These cues should be able to direct chondrocyte phenotypes towards superficial or deep chondrocytes, respectively, to prevent calcification in upper hyaline cartilage, and allow calcification in lower calcified cartilage. Future efforts in calcified cartilage formation should prioritise elucidating the mechanisms of interplay between the chondrocytes and biochemical/biophysical cues of biomaterials. In this way, precise cues for manipulating particular tissue formation, such as hyaline articular cartilage, calcified cartilage and subchondral bone, can be designed.

The importance of model selection for precise and reliable osteochondral repair research

Any novel treatment strategy must undergo thorough testing in various models to ensure its safety, feasibility, and effectiveness before advancing to clinical trials. The selection of appropriate models is crucial, as variations in biochemical and biophysical environments

provided by various models can yield different outcomes. Our research has elucidated several examples where these variations across different models significantly influenced the outcomes. In **Chapter 3**, for example, several models from *in vitro*, to *ex vivo* and *in vivo* were employed to investigate the tissue repair capacity of the hydrogels. *In vitro* human mesenchymal stem cell migration within the hydrogels was investigated using a 3D spheroid migration model. Chondrocyte infiltration into the defects filled with the hydrogels *ex vivo* was studied using bovine cartilage explants. Cell ingrowth into the defects and tissue repair capacity of the hydrogels *in vivo* was evaluated in a semi-orthotopic mouse model. No improvement was observed *in vitro* and *ex vivo* when norbornene hyaluronic acid was crosslinked with a degradable crosslinker. However, significantly increased tissue formation *in vivo* was found with the degradable crosslinker compared to the non-degradable crosslinker. MMPs produced *in vivo* might explain the difference among these models. In **Chapter 4**, enhanced cell ingrowth in a bovine osteochondral defect *ex vivo* and increased tissue repair were observed when BMP-2 was adsorbed onto the scaffolds in the semi-orthotopic mouse model. However, the adsorption of BMP-2 led to reduced bone formation in weight-bearing osteochondral defects in the stifle joint of goats. And in **Chapter 5**, while we observed no significant improvement in the semi-orthotopic mouse model when Sr-ACP granules were incorporated into the scaffolds, a significant improvement was noted when Sr-ACP enriched scaffolds were implanted in weight-bearing osteochondral defects in the goat model.

The findings regarding the same biomaterials described in **Chapters 3-5** did not always consistently align across different experimental models. The differences in the biochemical and biophysical environments provided by the *in vitro*, *ex vivo*, and *in vivo* models may have attributed to these inconsistent outcomes. Compared to the *in vitro* and *ex vivo* models, there is a more complex biochemical environment in the mouse model with the secretion of various bioactive factors, such as matrix metalloproteinase [62]. *In vivo* models aim to provide a more complex environment that mimics the native osteochondral unit [63]. Notably, our semi-orthotopic mouse model lacks mechanical loading, whereas the osteochondral defects in the femoral condyle of the goat are constantly loaded. This might explain the inconsistent outcomes observed between the mouse and goat model when BMP-2 or Sr-ACP were incorporated into the scaffolds. Corroboratively, the osteochondral repair in the non-weight-bearing trochlear groove aligns with the outcomes observed in the mouse model when BMP-2 or Sr-ACP were incorporated into the scaffolds.

Overall, these findings highlight the importance of employing a diverse range of models from *in vitro* to *in vivo*, and considering their respective advantages and limitations when evaluating novel treatment strategies for osteochondral defect repair. *In vitro* models serve well for probing specific aspects, such as studying migration within hydrogels or assessing the biocompatibility of biomaterials with cell cultures [64, 65]. *Ex vivo* models offer a more intricate microenvironment that mimics the native osteochondral unit, making them suitable for preliminary screening before advancing to *in vivo* animal models [66]. However, *ex vivo* models have limited capability for the regeneration of cartilage and bone tissue, necessitating investigation in an *in vivo* environment to assess the repair capacity of biomaterials [64, 67]. Despite the absence of mechanical loading in our mouse models, they provide a platform to explore the local responses of osteochondral tissue

when biomaterials are implanted, involving not only chondrocytes and osteoblasts but also immune cells, such as neutrophils and macrophages [68], which play crucial roles in tissue repair. Moreover, our mouse model offers four defect sites per mouse, serving as an efficient tool for screening before transitioning to larger animal models and minimising the use of animals. The caprine model represents a fully immune-competent model and provides the opportunity to evaluate osteochondral defect repair in two locations with different mechanical loading within the same joint that more closely resembles that of humans [67].

Sex is another key factor to consider when selecting animal models for studying osteochondral repair [69-71]. To test the effectiveness of a novel treatment strategy for osteochondral repair, the selected animal model should exhibit similar physiological and pathophysiological environments with the osteochondral unit in humans, where sex is considered an important factor in determining treatment results [72]. In **Chapter 3-5**, only female mice were involved in the investigations due to husbandry constraints. In **Chapter 4** and **Chapter 5**, we have used female and castrated male goats. Castration of male animals would allow sex-balanced groups but changes male reproduction hormone levels with potential consequences for bone metabolism [73]. To evaluate the effect of sex on scaffold-enhanced subchondral bone repair, in **Chapter 6**, we pooled and re-used control data from **Chapter 4** and **Chapter 5**. Female goats formed more subchondral bone compared to castrated male goats and this effect seems independent of mechanical loading conditions. In contrast, some preclinical studies reported more rapid bone regeneration in male rats and mice compared to females [69-71], which might be related to sex hormones and weight-related mechanical loading [74, 75]. Both estrogen and testosterone have receptors on osteoclasts, osteoblasts, and osteocytes [76]. Notably, in our study, the male goats were castrated after reaching sexual maturity, at the age of one year, for husbandry purposes. This led to decreased testosterone [77, 78], which may have potentially influenced subchondral bone repair [73]. These difficulties in study design, welfare issues and additional costs have impeded researchers from implementing sex balance in well-validated and widely applied translational preclinical osteochondral defect models in goats. Recently, the inclusion of sex balance in experimental animal studies has become more critical with most grant providers and ethics committees requesting sex balancing. On the basis of our findings, even if husbandry requirements may require castration, future studies evaluating subchondral bone repair should consider the option of sex balancing.

Future directions and perspectives

Further studies should focus on regenerating the intricate and hierarchical structure of the osteochondral unit. The key point of the acellular strategy for osteochondral repair is to recruit endogenous stem/progenitor cells, and accurately guide their fate and functionalisation specifically towards hyaline cartilage, calcified cartilage and subchondral bone at the injury site. However, once endogenous stem/progenitor cells leave their niches, their phenotype, functionality, and viability can easily be distorted. Therefore, creating a situation that closely mimicks the native environment with biomaterials for tissue-forming cells to maintain their properties and exhibit therapeutic effects is crucial. Manipulating biophysical and biochemical cues of biomaterials is an effective and feasible strategy. Recent advances in the design and manufacture of biomaterials with tunable

parameters, such as 3D printing technology, provide feasible and efficient approaches for manipulating biophysical and biochemical cues. Extrusion-based printing enables the modulation of pore size, pore shape and porosity that can direct cell alignment and spatial distribution [79]. The novel design of innovative biomaterial-based drug delivery systems presents new opportunities for precise control over the release kinetics of various bioactive factors, including growth factors, chemokines, peptides and mineral ions, among others. These biophysical and biochemical cues need to be precisely integrated and adjusted according to the needs of the repair area of the osteochondral unit.

In this thesis, we modulated various biochemical and biophysical cues of implants to manipulate endogenous cell behaviours and tissue regeneration. Notably, the effect of these biochemical and biophysical cues was not always consistent across various models. This might be due to the interplay between the biochemical and biophysical cues of exogenous implants and the native osteochondral units. Many cues *in vivo*, such as released bioactive factors and mechanical loading, will interact with the cues of exogenous implants. These findings highlighted the necessity of considering the interaction between exogenous and endogenous cues when designing biomaterial-based implants. This necessitates understanding the fundamental processes of osteochondral tissue formation during development and growth, and mechanisms of interplay between cells, bioactive factors and matrix/biomaterials. As an example, we confirmed the different roles of chondrocytes residing in the top and bottom layers, their interplay and their reaction to bioactive factors during the process of cartilage calcification. Future research focusing on biomaterial-driven osteochondral defect repair should aim to further elucidate these interactions and the fundamental processes of tissue formation. This knowledge can guide the design of biomaterials and drug delivery systems that effectively mimic the environment during native tissue formation, thereby promoting cell recruitment, differentiation, and extracellular matrix remodelling. Additionally, this knowledge can serve personalized medicine approaches, such as tailoring biomaterial properties to the specific biological environments of different defects sites and individuals, ultimately enhancing the efficacy of osteochondral repair strategies. It is hoped that with continued advancements in this field and multidisciplinary research advancement, the next-generation biomaterials with accurately integrated induction cues for endogenous stem/progenitor cells will pave the way for a more successful and long-lasting osteochondral repair.

REFERENCES

- [1] Li J, Liu Y, Zhang Y, Yao B, Enhejirigala, Li Z, Song W, Wang Y, Duan X, Yuan X, Fu X, Huang S. Biophysical and Biochemical Cues of Biomaterials Guide Mesenchymal Stem Cell Behaviors. *Front Cell Dev Biol.* 2021;9:640388.
- [2] Im GI. Endogenous Cartilage Repair by Recruitment of Stem Cells. *Tissue Eng Part B Rev.* 2016;22(2):160-171.
- [3] Pot MW, Gonzales VK, Buma P, Int'Hout J, van Kuppevelt TH, de Vries RBM, Daamen WF. Improved cartilage regeneration by implantation of acellular biomaterials after bone marrow stimulation: a systematic review and meta-analysis of animal studies. *PeerJ.* 2016;4.
- [4] Wei W, Ma Y, Yao X, Zhou W, Wang X, Li C, Lin J, He Q, Leptihn S, Ouyang H. Advanced hydrogels for the repair of cartilage defects and regeneration. *Bioact Mater.* 2021;6(4):998-1011.
- [5] Ansari M, Darvishi A, Sabzevari A. A review of advanced hydrogels for cartilage tissue engineering. *Front Bioeng Biotechnol.* 2024;12:1340893.
- [6] Kwartta CP, Widiyanti P, Siswanto. Hyaluronic Acid (HA)-Polyethylene glycol (PEG) as injectable hydrogel for intervertebral disc degeneration patients therapy. *Journal of Physics: Conference Series.* 2017;853(1):012036.
- [7] Galarraga JH, Kwon MY, Burdick JA. 3D bioprinting via an in situ crosslinking technique towards engineering cartilage tissue. *Sci Rep.* 2019;9(1):19987.
- [8] Shu XZ, Ghosh K, Liu Y, Palumbo FS, Luo Y, Clark RA, Prestwich GD. Attachment and spreading of fibroblasts on an RGD peptide-modified injectable hyaluronan hydrogel. *J Biomed Mater Res A.* 2004;68(2):365-375.
- [9] Lam J, Truong NF, Segura T. Design of cell-matrix interactions in hyaluronic acid hydrogel scaffolds. *Acta Biomater.* 2014;10(4):1571-1580.
- [10] Eyre D. Articular cartilage and changes in Arthritis: Collagen of articular cartilage. *Arthritis Research & Therapy.* 2001;4(1):30.
- [11] Heino J. The collagen family members as cell adhesion proteins. *Bioessays.* 2007;29(10):1001-1010.
- [12] Zhang N, Lock J, Sallee A, Liu H. Magnetic Nanocomposite Hydrogel for Potential Cartilage Tissue Engineering: Synthesis, Characterization, and Cytocompatibility with Bone Marrow Derived Mesenchymal Stem Cells. *ACS Appl Mater Interfaces.* 2015;7(37):20987-20998.
- [13] Tampieri A, Sandri M, Landi E, Pressato D, Francioli S, Quarto R, Martin I. Design of graded biomimetic osteochondral composite scaffolds. *Biomaterials.* 2008;29(26):3539-3546.
- [14] Sosio C, Di Giancamillo A, Deponti D, Gervaso F, Scalera F, Melato M, Campagnol M, Boschetti F, Nonis A, Domeneghini C, Sannino A, Peretti GM. Osteochondral repair by a novel interconnecting collagen-hydroxyapatite substitute: a large-animal study. *Tissue Eng Part A.* 2015;21(3-4):704-715.
- [15] Levingstone TJ, Thompson E, Matsiko A, Schepens A, Gleeson JP, O'Brien FJ. Multi-layered collagen-based scaffolds for osteochondral defect repair in rabbits. *Acta Biomater.* 2016;32:149-160.
- [16] Kon E, Delcogliano M, Filardo G, Pressato D, Busacca M, Grigolo B, Desando G, Marcacci M. A novel nano-composite multi-layered biomaterial for treatment of

osteochondral lesions: technique note and an early stability pilot clinical trial. *Injury*. 2010;41(7):693-701.

[17] Perdisa F, Filardo G, Sessa A, Busacca M, Zaffagnini S, Marcacci M, Kon E. One-Step Treatment for Patellar Cartilage Defects With a Cell-Free Osteochondral Scaffold: A Prospective Clinical and MRI Evaluation. *Am J Sports Med*. 2017;45(7):1581-1588.

[18] Di Martino A, Perdisa F, Filardo G, Busacca M, Kon E, Marcacci M, Zaffagnini S. Cell-Free Biomimetic Osteochondral Scaffold for the Treatment of Knee Lesions: Clinical and Imaging Results at 10-Year Follow-up. *Am J Sports Med*. 2021;49(10):2645-2650.

[19] Combes C, Rey C. Amorphous calcium phosphates: Synthesis, properties and uses in biomaterials. *Acta Biomater*. 2010;6(9):3362-3378.

[20] Vecstaudza J, Locs J. Effect of synthesis temperature and Ca/P ratios on specific surface area of amorphous calcium phosphate. *Key Engineering Materials*. 2017;700:172-176.

[21] Vecstaudza J, Locs J. Novel preparation route of stable amorphous calcium phosphate nanoparticles with high specific surface area. *Journal of Alloys and Compounds*. 2017;700:215-222.

[22] Vecstaudza J, Gasik M, Locs J. Amorphous calcium phosphate materials: Formation, structure and thermal behaviour. *Journal of the European Ceramic Society*. 2019;39(4):1642-1649.

[23] Rubenis K, Zemjane S, Vecstaudza J, Biteniekis J, Locs J. Densification of amorphous calcium phosphate using principles of the cold sintering process. *Journal of the European Ceramic Society*. 2021;41(1):912-919.

[24] Fulmer MT, Ison IC, Hankermayer CR, Constantz BR, Ross J. Measurements of the solubilities and dissolution rates of several hydroxyapatites. *Biomaterials*. 2002;23(3):751-755.

[25] Root MJ. Inhibition of the amorphous calcium phosphate phase transformation reaction by polyphosphates and metal ions. *Calcified Tissue International*. 1990;47(2):112-116.

[26] Jin W, Liu Z, Wu Y, Jin B, Shao C, Xu X, Tang R, Pan H. Synergic Effect of Sr²⁺ and Mg²⁺ on the Stabilization of Amorphous Calcium Phosphate. *Crystal Growth & Design*. 2018;18(10):6054-6060.

[27] Zwingenberger S, Yao Z. Enhancement of BMP-2 Induced Bone Regeneration by SDF-1 α Mediated Stem Cell Recruitment. *Tissue Engineering Part A*. 2014;20(3-4):810-818.

[28] Liu S, Liu Y, Jiang L, Li Z, Lee S, Liu C, Wang J, Zhang J. Recombinant human BMP-2 accelerates the migration of bone marrow mesenchymal stem cells via the CDC42/PAK1/LIMK1 pathway *in vitro* and *in vivo*. *Biomater Sci*. 2018;7(1):362-372.

[29] Lee JM, Kim BS, Lee H, Im GI. *In Vivo* tracking of mesenchymal stem cells using fluorescent nanoparticles in an osteochondral repair model. *Molecular Therapy*. 2012;20(7):1434-1442.

[30] Vainieri ML, Lolli A, Kops N, D'atri D, Eglin D, Yayon A, Alini M, Grad S, Sivasubramanian K, van Osch G. Evaluation of biomimetic hyaluronic-based hydrogels with enhanced endogenous cell recruitment and cartilage matrix formation. *Acta Biomater*. 2020;101:293-303.

[31] Rui YF, Lui PPY, Ni M, Chan LS, Lee YW, Chan KM. Mechanical loading increased BMP-2 expression which promoted osteogenic differentiation of tendon-derived stem cells. *Journal of Orthopaedic Research*. 2011;29(3):390-396.

- [32] Zara JN, Siu RK, Zhang X, Shen J, Ngo R, Lee M, Li W, Chiang M, Chung J, Kwak J. High doses of bone morphogenetic protein 2 induce structurally abnormal bone and inflammation *in vivo*. *Tissue Engineering Part A*. 2011;17(9-10):1389-1399.
- [33] Kanatani M, Sugimoto T, Kaji H, Kobayashi T, Nishiyama K, Fukase M, Kumegawa M, Chihara K. Stimulatory effect of bone morphogenetic protein-2 on osteoclast-like cell formation and bone-resorbing activity. *Journal of Bone and Mineral Research*. 2020;10(11):1681-1690.
- [34] Kaneko H, Arakawa T, Mano H, Kaneda T, Ogasawara A, Nakagawa M, Toyama Y, Yabe Y, Kumegawa M, Hakeda Y. Direct stimulation of osteoclastic bone resorption by bone morphogenetic protein (BMP)-2 and expression of BMP receptors in mature osteoclasts. *Bone*. 2000;27(4):479-486.
- [35] Griffon DJ, Sedighi MR, Schaeffer DV, Eurell JA, Johnson AL. Chitosan scaffolds: Interconnective pore size and cartilage engineering. *Acta Biomater*. 2006;2(3):313-320.
- [36] Lien SM, Ko LY, Huang TJ. Effect of pore size on ECM secretion and cell growth in gelatin scaffold for articular cartilage tissue engineering. *Acta Biomater*. 2009;5(2):670-679.
- [37] Nuernberger S, Cyran N, Albrecht C, Redl H, Vécsei V, Marlovits S. The influence of scaffold architecture on chondrocyte distribution and behavior in matrix-associated chondrocyte transplantation grafts. *Biomaterials*. 2011;32(4):1032-1040.
- [38] Stenhamre H, Nannmark U, Lindahl A, Gatenholm P, Brittberg M. Influence of pore size on the redifferentiation potential of human articular chondrocytes in poly(urethane urea) scaffolds. *Journal of Tissue Engineering and Regenerative Medicine*. 2011;5(7):578-588.
- [39] Kawakami M, Tomita N, Shimada Y, Yamamoto K, Tamada Y, Kachi N, Suguro T. Chondrocyte distribution and cartilage regeneration in silk fibroin sponge. *Bio-Medical Materials and Engineering*. 2011;21(1):53-61.
- [40] Zhang Q, Lu H, Kawazoe N, Chen G. Pore size effect of collagen scaffolds on cartilage regeneration. *Acta Biomater*. 2014;10(5):2005-2013.
- [41] Vainieri ML, Lolli A, Kops N, D'Atri D, Eglin D, Yayon A, Alini M, Grad S, Sivasubramanian K, van Osch G. Evaluation of biomimetic hyaluronic-based hydrogels with enhanced endogenous cell recruitment and cartilage matrix formation. *Acta Biomater*. 2020;101:293-303.
- [42] Yamane S, Iwasaki N, Kasahara Y, Harada K, Majima T, Monde K, Nishimura SI, Minami A. Effect of pore size on *in vitro* cartilage formation using chitosan-based hyaluronic acid hybrid polymer fibers. *Journal of Biomedical Materials Research - Part A*. 2007;81(3):586-593.
- [43] Xia H, Li X, Gao W, Fu X, Fang RH, Zhang L, Zhang K. Tissue repair and regeneration with endogenous stem cells. *Nature Reviews Materials*. 2018;3(7):174-193.
- [44] Nicolas J, Magli S, Rabbachin L, Sampaolesi S, Nicotra F, Russo L. 3D Extracellular Matrix Mimics: Fundamental Concepts and Role of Materials Chemistry to Influence Stem Cell Fate. *Biomacromolecules*. 2020;21(6):1968-1994.
- [45] Nguyen AH, McKinney J, Miller T, Bongiorno T, McDevitt TC. Gelatin methacrylate microspheres for controlled growth factor release. *Acta Biomater*. 2015;13:101-110.
- [46] Zhou H, Yuan L, Xu Z, Yi X, Wu X, Mu C, Ge L, Li D. Mimicking the composition and structure of the osteochondral tissue to fabricate a heterogeneous three-layer scaffold for the repair of osteochondral defects. *ACS Applied Bio Materials*. 2022;5(2):734-746.

- [47] Broom ND, Poole CA. A functional-morphological study of the tidemark region of articular cartilage maintained in a non-viable physiological condition. *J Anat.* 1982;135(Pt 1):65-82.
- [48] Radin EL, Rose RM. Role of Subchondral Bone in the Initiation and Progression of Cartilage Damage. *Clinical Orthopaedics and Related Research*®. 1986;213.
- [49] Mente PL, Lewis JL. Elastic modulus of calcified cartilage is an order of magnitude less than that of subchondral bone. *Journal of Orthopaedic Research.* 1994;12(5):637-647.
- [50] Wang W, Ye R, Xie W, Zhang Y, An S, Li Y, Zhou Y. Roles of the calcified cartilage layer and its tissue engineering reconstruction in osteoarthritis treatment. *Front Bioeng Biotechnol.* 2022;10:911281.
- [51] Kon E, Mutini A, Arcangeli E, Delcogliano M, Filardo G, Nicoli Aldini N, Pressato D, Quarto R, Zaffagnini S, Marcacci M. Novel nanostructured scaffold for osteochondral regeneration: pilot study in horses. *Journal of Tissue Engineering and Regenerative Medicine.* 2010;4(4):300-308.
- [52] Cao R, Xu Y, Xu Y, Brand DD, Zhou G, Xiao K, Xia H, Czernuszka JT. Development of Tri-Layered Biomimetic Atelocollagen Scaffolds with Interfaces for Osteochondral Tissue Engineering. *Advanced Healthcare Materials.* 2022;11(11):2101643.
- [53] Huang Y, Fan H, Gong X, Yang L, Wang F. Scaffold With Natural Calcified Cartilage Zone for Osteochondral Defect Repair in Minipigs. *The American Journal of Sports Medicine.* 2021;49(7):1883-1891.
- [54] Zhai C, Fei H, Hu J, Wang Z, Xu S, Zuo Q, Li Z, Wang Z, Liang W, Fan W. Repair of Articular Osteochondral Defects Using an Integrated and Biomimetic Trilayered Scaffold. *Tissue Eng Part A.* 2018;24(21-22):1680-1692.
- [55] Wu D, Zheng K, Yin W, Hu B, Yu M, Yu Q, Wei X, Deng J, Zhang C. Enhanced osteochondral regeneration with a 3D-Printed biomimetic scaffold featuring a calcified interfacial layer. *Bioactive Materials.* 2024;36:317-329.
- [56] Huitema LF, Vaandrager AB. What triggers cell-mediated mineralization?. *Front Biosci.* 2007;12:2631-2645.
- [57] Kirsch T. Determinants of pathological mineralization. *Curr Opin Rheumatol.* 2006;18(2):174-180.
- [58] Jiang J, Leong NL, Mung JC, Hidaka C, Lu HH. Interaction between zonal populations of articular chondrocytes suppresses chondrocyte mineralization and this process is mediated by PTHrP. *Osteoarthritis Cartilage.* 2008;16(1):70-82.
- [59] Tsukazaki T, Ohtsuru A, Enomoto H, Yano H, Motomura K, Ito M, Namba H, Iwasaki K, Yamashita S. Expression of parathyroid hormone-related protein in rat articular cartilage. *Calcified Tissue International.* 1995;57:196-200.
- [60] Lee K, Deeds JD, Segre GV. Expression of parathyroid hormone-related peptide and its receptor messenger ribonucleic acids during fetal development of rats. *Endocrinology.* 1995;136(2):453-463.
- [61] Mayan MD, Gago-Fuentes R, Carpintero-Fernandez P, Fernandez-Puente P, Filgueira-Fernandez P, Goyanes N, Valiunas V, Brink PR, Goldberg GS, Blanco FJ. Articular chondrocyte network mediated by gap junctions: role in metabolic cartilage homeostasis. *Annals of the Rheumatic Diseases.* 2015;74(1):275-284.
- [62] Kevorkian L, Young DA, Darrach C, Donell ST, Shepstone L, Porter S, Brockbank SMV, Edwards DR, Parker AE, Clark IM. Expression profiling of metalloproteinases and their inhibitors in cartilage. *Arthritis & Rheumatism.* 2004;50(1):131-141.

- [63] Maglio M, Tschon M, Sicuro L, Lolli R, Fini M. Osteochondral tissue cultures: Between limits and sparks, the next step for advanced *in vitro* models. *Journal of Cellular Physiology*. 2019;234(5):5420-5435.
- [64] Saleh LS, Bryant SJ. *In vitro* and *in vivo* models for assessing the host response to biomaterials. *Drug Discovery Today: Disease Models*. 2017;24:13-21.
- [65] Ahmed U, Ahmed R, Masoud MS, Tariq M, Ashfaq UA, Augustine R, Hasan A. Stem cells based *in vitro* models: trends and prospects in biomaterials cytotoxicity studies. *Biomed Mater*. 2021;16(4):042003.
- [66] Trengove A, Duchi S, Onofrillo C, Sooriyaaratchi D, Di Bella C, O'Connor AJ. Bridging bench to body: *ex vivo* models to understand articular cartilage repair. *Current Opinion in Biotechnology*. 2024;86:103065.
- [67] Meng X, Ziadlou R, Grad S, Alini M, Wen C, Lai Y, Qin L, Zhao Y, Wang X. Animal Models of Osteochondral Defect for Testing Biomaterials. *Biochemistry Research International*. 2020;2020:9659412.
- [68] Ode Boni B, Lamboni L, Souho T, Gauthier M, Yang G. Immunomodulation and Cellular Response to Biomaterials: The Overriding Role of Neutrophils in Healing. *Materials Horizons*. 2019;6.
- [69] Mehta M, Schell H, Schwarz C, Peters A, Schmidt-Bleek K, Ellinghaus A, Bail HJ, Duda GN, Lienau J. A 5-mm femoral defect in female but not in male rats leads to a reproducible atrophic non-union. *Arch Orthop Trauma Surg*. 2011;131(1):121-129.
- [70] Deng Z, Gao X, Sun X, Cui Y, Amra S, Huard J. Gender differences in tibial fractures healing in normal and muscular dystrophic mice. *American Journal of Translational Research*. 2020;12(6):2640-2651.
- [71] Mehta M, Duda GN, Perka C, Strube P. Influence of gender and fixation stability on bone defect healing in middle-aged rats: a pilot study. *Clin Orthop Relat Res*. 2011;469(11):3102-3110.
- [72] Filardo G, Kon E, Andriolo L, Di Matteo B, Balboni F, Marcacci M. Clinical profiling in cartilage regeneration: prognostic factors for midterm results of matrix-assisted autologous chondrocyte transplantation. *Am J Sports Med*. 2014;42(4):898-905.
- [73] Callewaert F, Sinnesael M, Gielen E, Boonen S, Vanderschueren D. Skeletal sexual dimorphism: relative contribution of sex steroids, GH-IGF1, and mechanical loading. *J Endocrinol*. 2010;207(2):127-134.
- [74] Callewaert F, Venken K, Ophoff J, De Gendt K, Torcasio A, van Lenthe GH, Van Oosterwyck H, Boonen S, Bouillon R, Verhoeven G, Vanderschueren D. Differential regulation of bone and body composition in male mice with combined inactivation of androgen and estrogen receptor-alpha. *Faseb j*. 2009;23(1):232-240.
- [75] Haffner-Luntzer M, Fischer V, Ignatius A. Differences in Fracture Healing Between Female and Male C57BL/6J Mice. *Front Physiol*. 2021;12:712494.
- [76] Notelovitz M. Androgen effects on bone and muscle. *Fertil Steril*. 2002;77 Suppl 4.
- [77] Määttä JA, Büki KG, Ivaska KK, Nieminen-Pihala V, Elo TD, Kähkönen T, Poutanen M, Härkönen P, Väänänen K. Inactivation of the androgen receptor in bone-forming cells leads to trabecular bone loss in adult female mice. *Bonekey Rep*. 2013;2:440.
- [78] Ucer S, Iyer S, Bartell SM, Martin-Millan M, Han L, Kim HN, Weinstein RS, Jilka RL, O'Brien CA, Almeida M, Manolagas SC. The Effects of Androgens on Murine Cortical Bone Do Not Require AR or ER α Signaling in Osteoblasts and Osteoclasts. *J Bone Miner Res*. 2015;30(7):1138-1149.

[79] Zieliński PS, Gudeti PKR, Rikmanspoel T, Włodarczyk-Biegun MK. 3D printing of bio-instructive materials: Toward directing the cell. *Bioactive Materials*. 2023;19:292-327.

9

Summary

SUMMARY

Osteochondral defect repair involves the intricate process of regenerating articular cartilage, calcified cartilage and underlying subchondral bone. Biomaterial-based scaffolds are commonly used to regenerate a hierarchical osteochondral unit. When choosing a biomaterial-based acellular strategy, recruiting endogenous joint-resident stem/progenitor cells to the defects and inducing the formation of various tissue types are crucial steps. In **Chapter 2**, we reviewed the current knowledge on the presence of endogenous stem/progenitor cells in joints, such as bone marrow-derived, synovium-derived and Intra-articular fat pad-derived stem cells. To modulate their behaviours during the healing process, manipulating the biophysical and biochemical properties of biomaterials is feasible and promising. In this review, we summarised the recent advances in novel design and application of regenerative biomaterials with favourable biochemical properties to establish an instructive microenvironment. Such a microenvironment should guide endogenous cell migration, proliferation and differentiation during tissue repair.

Hydrogels have emerged as a promising class of biomaterials in cartilage repair due to their good biocompatibility, reproducibility and cartilage-like characteristics. However, the specific properties that allow or even improve the behaviour of cells are not yet clear. In **Chapter 3**, we investigated the effects of biophysical and biochemical properties of different hydrogels on cell migration and tissue repair. We used an *in vitro* model for cell migration of human bone marrow derived mesenchymal stromal cells, an *ex vivo* bovine cartilage explant model and a semi-orthotopic *in vivo* model where a defect was made in an explant of bovine cartilage with subchondral bone that was implanted subcutaneously in mice. Specifically, three hydrogels were modified: to a tyramine functionalised hyaluronic acid hydrogel, collagen was added to modify the biochemical cues; A norbornene hyaluronic acid (norHA) hydrogel was crosslinked by either a degradable crosslinker (matrix metalloproteinase cleavable), or a non-degradable 1,4-Dithiothreitol (DTT) crosslinker; A gelatin methacryloyl (GelMA) hydrogel was modified by adapting the degree of functionalisation. Results showed that the addition of collagen resulted in greater cell migration *in vitro* and more tissue formation *in vivo*. The introduction of a degradable crosslinker in norHA hydrogels did not improve cell infiltration *in vitro* or *ex vivo*, but resulted in more tissue formation *in vivo*. A lower degree of functionalisation of GelMA did not affect cell migration *in vitro* but led to a higher migration score *ex vivo* and more tissue formation *in vivo*. Overall, our study shows that cell migration is dependent on multiple material characteristics, including tunable physicochemical and bio-instructive properties.

Next to hydrogels, scaffolds are often used for the repair of osteochondral defects. In **Chapter 4**, we manipulated the properties of a clinically used bi-layered collagen/collagen-magnesium-hydroxyapatite (Col/Col-Mg-HAp) scaffold, that has demonstrated good cartilage repair clinically but less optimal subchondral bone repair. We aimed to improve the bone repair capacity of this scaffold by integrating an additional component with the bony layer. To do this, a novel synthesis method was developed to produce amorphous calcium phosphate (ACP) granules with a large specific surface area and strontium was added. The strontium-ACP granules were well embedded and distributed in the collagen matrix of the Col-Mg-HAp layer. Incorporation of strontium-enriched ACP granules into the

Col/Col-Mg-HAp osteochondral scaffolds showed good biocompatibility and an overall promising early tissue repair in a semi-orthotopic mouse model. In a goat osteochondral defect model, addition of strontium-ACP led to significantly more bone, in particular in the weight-bearing femoral condyle subchondral bone defect. Overall, the incorporation of osteogenic strontium-ACP granules in Col/Col-Mg-HAp scaffolds was shown to be a feasible and promising biochemical modification to improve subchondral bone repair.

Another approach to modify the biochemical properties of a scaffold is to load it with bioactive factors that will be delivered into the osteochondral defect. Numerous complex bioactive factor delivery systems have been developed; yet in clinical practice, simplicity and reproducibility are essential criteria. In **Chapter 5**, to improve the bone repair capacity of the Col/Col-Mg-HAp scaffold, the growth factors BMP-2 and PDGF-BB were adsorbed onto the scaffold through soaking. The *in vitro* release kinetics of BMP-2/PDGF-BB demonstrated that PDGF-BB was released in a burst from the collagen-only layer, whereas BMP-2 was largely retained in both layers of the scaffolds. Cell ingrowth into the scaffold was enhanced by BMP-2 and PDGF-BB in an *ex vivo* osteochondral defect model. In the semi-orthotopic non-weight-bearing osteochondral defect mouse model, the addition of growth factors resulted in better tissue repair, with BMP-2 showing the most favourable results. Surprisingly, in a translational goat osteochondral defect model the adsorption of BMP-2 resulted in significantly less bone repair compared with scaffold-only in the weight-bearing (femoral condyle) defects and a trend to more bone repair in the non-weight-bearing (trochlear groove) defects. This could be attributed to an interaction between BMP-2 and mechanical loading, and potentially influenced by the dose administered. Therefore, the incorporation of bioactive factors necessitates studying their release profile, stability *in vivo*, and effects in specific biophysical and biochemical environments in the joints. Moreover, these results highlighted the need for screening biomaterials in different models and different defect locations with various biomechanical environments, since the selection of models might determine the result.

Sex is another key factor to consider when selecting animal models for studying osteochondral repair. In **Chapter 6**, we pooled and re-used control data from **Chapters 4** and **5** on the subchondral bone repair in female and castrated male goats to evaluate the effect of sex on scaffold-enhanced subchondral bone repair in experimentally induced osteochondral defects. Overall, female goats form more subchondral bone compared to castrated male goats in scaffold-enhanced osteochondral defect repair and this effect seems independent of mechanical loading conditions. For future studies evaluating subchondral bone repair, the option of sex balancing should be considered when using an animal model.

In **Chapter 4** and **Chapter 5**, the modified Col/Col-Mg-HAp scaffolds yielded a well-integrated osteochondral unit with articular cartilage and subchondral bone. However, even after 6 months, calcified cartilage was not formed between articular cartilage and subchondral bone. To study the formation of calcified cartilage, we developed an *ex vivo* culture model using immature bovine cartilage explants in **Chapter 7**. Specifically, cartilage explants were harvested from metacarpophalangeal joints of 6- to 8-month-old calves, and β -glycerophosphate was introduced to allow cartilage calcification. A layer of calcified cartilage was generated only in the deep zone of the cartilage explants, indicating an inherent zone-specific calcification process within articular cartilage. Next, explants were

carefully separated into the top layers and the bottom layers to explore the interplay between zonal structures. The viable chondrocytes residing in the top layers expressed the capacity to inhibit cartilage calcification via the secretion of bioactive factors. The viable bottom layer can actively stimulate cartilage calcification and respond to bioactive factors that inhibit cartilage calcification. Conclusively, the formation of calcified cartilage is under the precise control of zonal chondrocytes within articular cartilage via intricate interaction.

To conclude, manipulating the biophysical and biochemical properties of biomaterials is an effective and feasible strategy for regenerating the hierarchical structure of the osteochondral unit. A multiple-layered scaffold solely mimicking the components of native osteochondral tissue might not be sufficient. Better understanding of the fundamental developmental processes of osteochondral tissue formation, and mechanisms of interplay between cells, bioactive factors and matrix/biomaterials is crucial. With this knowledge, osteochondral implants can be designed that manipulate endogenous cell behaviour to achieve full regeneration or osteochondral tissue. Additionally, investigating novel therapeutic approaches for osteochondral repair should involve utilising multiple models ranging from *in vitro* to *in vivo*, with careful consideration given to sex balance and the choice of defect sites in joints when employing animal models. By continuous research advancements, regenerative medicine will achieve a more successful and long-lasting osteochondral repair in the future.

NEDERLANDSE SAMENVATTING

Het herstel van beschadigingen van kraakbeen en bot in het gewricht omvat het ingewikkelde proces van regeneratie van gewrichtskraakbeen, verkalkt kraakbeen en onderliggend subchondraal bot. Biomaterialen worden vaak gebruikt om de weefselstructuur te regenereren. Bij het kiezen van een op biomaterialen gebaseerde acellulaire strategie zijn het rekruteren van endogene stamcellen/progenitorcellen naar de lesie en het induceren van hun differentiatie naar verschillende celtypen die kraakbeen en bot kunnen vormen, cruciale stappen. In **Hoofdstuk 2** hebben we de huidige kennis over de aanwezigheid van endogene stam/progenitorcellen in gewrichten besproken, zoals stamcellen uit beenmerg, synovium en intra-articulaire vetkussentjes. Om hun gedrag tijdens het herstelproces te moduleren, is het manipuleren van de biofysische en biochemische eigenschappen van de biomaterialen haalbaar en veelbelovend. In dit hoofdstuk geven we een samenvatting van de recente vooruitgang in ontwerp en de toepassing van nieuwe regeneratieve biomaterialen met gunstige biochemische eigenschappen om een instructieve micro-omgeving te creëren voor de cellen om te migreren, prolifereren en differentieren tijdens weefselherstel.

Hydrogelen zijn veelbelovende biomaterialen voor kraakbeenherstel vanwege hun goede biocompatibiliteit, reproduceerbaarheid en kraakbeenachtige eigenschappen. De specifieke eigenschappen die het gedrag van cellen beïnvloeden of zelfs verbeteren zijn echter nog niet duidelijk. In **Hoofdstuk 3** onderzochten we de effecten van biofysische en biochemische eigenschappen van verschillende hydrogels op celmigratie en weefselherstel. We gebruikten een *in vitro* model voor celmigratie van mesenchymale stromale cellen afkomstig van beenmerg van patiënten, een *ex vivo* runderkraakbeenexplantaat model en een semi-orthotopisch *in vivo* model waarbij een defect werd gemaakt in een explantaat van runderkraakbeen met subchondraal bot dat subcutaan werd geïmplanterd bij muizen. Er werden drie hydrogels gemodificeerd: aan een hyaluronzuur-hydrogel met tyraminefunctionaliteit werd collageen toegevoegd om de biochemische signalen te modifieren; een norbornene hyaluronzuur-hydrogel (norHA) werd gecrosslinked met een afbreekbare crosslinker (matrixmetalloproteïnase splitsbaar) of een niet-afbreekbare 1,4-dithiothreitol (DTT)-crosslinker; een gelatine-methacryloyl (GelMA)-hydrogel werd gemodificeerd door de mate van de functionalisatie aan te passen. De resultaten toonden aan dat de toevoeging van collageen resulteerde in meer celmigratie *in vitro* en meer weefselvorming *in vivo*. De introductie van een afbreekbare crosslinker in norHA hydrogels verbeterde de celinfiltratie *in vitro* maar niet in een *ex vivo* model. Ook vond meer weefselvorming *in vivo* plaats door introductie van de afbreekbare crosslinker. Een lagere mate van functionalisatie van GelMA had geen invloed op celmigratie *in vitro*, maar leidde tot meer celmigratie *ex vivo* en meer weefselvorming *in vivo*. Over het geheel genomen toont onze studie aan dat celmigratie afhankelijk is van meerdere materiaaleigenschappen, waaronder modificeerbare fysisch-chemische en bio-instructieve eigenschappen.

Naast hydrogels worden ook andere biomaterialen vaak gebruikt voor het herstel van kraakbeen en bot defecten in het gewricht. In **Hoofdstuk 4** hebben we de eigenschappen gemanipuleerd van een klinisch gebruikt dubbellaagse collageen/collageen-magnesium-hydroxyapatiet (Col/Col-Mg-HAp) biomateriaal, dat klinisch goed kraakbeenherstel heeft

laten zien, maar minder optimaal subchondraal botherstel. We wilden het botherstellend vermogen van dit biomateriaal verbeteren door een extra component te integreren in de botlaag. Hiervoor werd een nieuwe synthesemethode ontwikkeld om amorfe calciumfosfaat (ACP) korrels met een groot specifiek oppervlak te produceren en daaraan strontium toe te voegen. Dit zorgde voor langdurige stabiliteit van de amorfe fase en de strontium-ACP korrels waren goed ingebed en verdeeld in de collageen matrix van de Col-Mg-HAp laag. De integratie van strontium-verrijkte ACP-korrels in de Col/Col-Mg-HAp biomaterialen vertoonde een goede biocompatibiliteit en veelbelovende resultaten voor vroeg weefselherstel in een semi-orthotopisch muismodel. In een kraakbeen-bot defectmodel bij geiten gaf toevoeging van strontium-ACP significant meer botherstel, met name in defecten in de gewichtdragende femur condyle. Over het geheel genomen bleek de incorporatie van strontium-ACP korrels in Col/Col-Mg-HAp biomaterialen een haalbare en veelbelovende biochemische modificatie om subchondraal botherstel te verbeteren.

Een andere benadering om de biochemische eigenschappen van een biomateriaal aan te passen is deze te laden met bioactieve factoren die in het kraakbeen-botdefect worden afgegeven. Er zijn talloze complexe systemen ontwikkeld voor het toedienen van bioactieve factoren, maar in de klinische praktijk zijn eenvoud en reproduceerbaarheid essentiële criteria. Om het botherstellend vermogen van het Col/Col-Mg-HAp-biomateriaal te verbeteren, werden in **Hoofdstuk 5** de groeifactoren BMP-2 en PDGF-BB in het biomateriaal geadsorbeerd. De *in vitro* kinetiek van het vrijkomen van BMP-2/PDGF-BB toonde aan dat PDGF-BB snel vrijkwam uit de collageenlaag, terwijl BMP-2 grotendeels in de beide lagen van het biomateriaal werd vastgehouden. De ingroei van cellen in het biomateriaal in een *ex vivo* kraakbeen-botdefect model werd bevorderd door BMP-2 en PDGF-BB. In het semi-orthotope, niet-gewichtdragende, kraakbeen-botdefectmodel in de muis resulteerde de toevoeging van groeifactoren in beter weefselherstel, waarbij BMP-2 de gunstigste resultaten liet zien. Verrassend genoeg resulteerde adsorptie van BMP-2 in een translationeel gewrichtsdefectmodel bij geiten in significant minder botherstel in de gewichtdragende defecten (femur condyle) en een trend naar meer botherstel in de niet-gewichtdragende defecten (trochleaire groeve). Dit kan worden toegeschreven aan een interactie tussen BMP-2 en mechanische belasting, en wordt mogelijk beïnvloed door de toegediende dosis. Daarom is het voor de incorporatie van bioactieve factoren nodig om hun afgifteprofiel, stabiliteit *in vivo* en effecten in specifieke biofysische en biochemische omgevingen in gewrichten te bestuderen. Bovendien benadrukten deze resultaten de noodzaak van het screenen van biomaterialen in verschillende modellen en verschillende defectlocaties met verschillende biomechanische omgevingen, aangezien de selectie van modellen bepalend kan zijn voor het resultaat.

Geslacht is een andere belangrijke factor om te overwegen bij het selecteren van diersmodellen voor het bestuderen van gewrichtsdefect herstel. In **Hoofdstuk 6** hebben we controlegegevens uit de **Hoofdstukken 4** en **5** bij vrouwelijke en gecasteerde mannelijke geiten samengevoegd en hergebruikt om het effect van sekse op het subchondrale botherstel met biomateriaal te evalueren. De resultaten toonden aan dat significant meer botweefsel werd waargenomen in subchondrale botdefecten bij vrouwelijke dan bij gecasteerde mannelijke geiten en dit effect lijkt onafhankelijk van mechanische belastingscondities. Voor toekomstige studies naar subchondraal botherstel, moet de optie van seksebalancerings overwogen worden bij het gebruik van een diersmodel.

In **Hoofdstuk 4** en **Hoofdstuk 5** leverden de gemodificeerde Col/Col-Mg-HAP biomaterialen een goed geïntegreerd herstel van gewrichtskraakbeen en subchondraal bot. Echter, zelfs na 6 maanden werd er geen verkalkt kraakbeen gevormd tussen het gewrichtskraakbeen en het subchondrale bot. Om de vorming van verkalkt kraakbeen te bestuderen, ontwikkelden we in **Hoofdstuk 7** een *ex vivo* kweekmodel met kalfskraakbeenexplanten. Kraakbeenexplanten werden geogst uit metacarpophalangeale gewrichten van 6 tot 8 maanden oude kalveren en β -glycerofosfaat werd toegevoegd aan het kweekmedium om verkalking van het kraakbeen mogelijk te maken. De resultaten toonden dat er alleen in de diepe zone van de kraakbeenexplantaten een laag verkalkt kraakbeen werd gevormd, wat wijst op een inherent zonespecifiek verkalkingsproces binnen het gewrichtskraakbeen. Vervolgens werden de explantaten zorgvuldig gescheiden in een bovenste en een onderste laag om de wisselwerking tussen de zonale structuren te onderzoeken. De levende chondrocyten in de bovenste laag hadden de capaciteit om verkalking van het kraakbeen te remmen via de uitscheiding van bioactieve factoren. De levende onderste laag stimuleerde actief kraakbeenverkalking en reageerde op bioactieve factoren die kraakbeenverkalking remmen. Conclusie is dat de vorming van verkalkt kraakbeen via interacties onder nauwkeurige controle staat van zonale chondrocyten binnen articulaire kraakbeen.

Concluderend is het manipuleren van de biofysische en biochemische eigenschappen van biomaterialen een effectieve en haalbare strategie voor het regenereren van de hiërarchische structuur van gewrichtskraakbeen en onderliggend bot. Een meerlagig biomateriaal dat alleen de componenten van natief kraakbeen en bot weefsel nabootst is mogelijk niet voldoende. Het beter begrijpen van de processen van de vorming van gewrichtskraakbeen en bot en de mechanismen van de interactie tussen cellen, bioactieve factoren en matrix/biomaterialen is van fundamenteel belang. Met deze kennis kunnen nauwkeurig ontworpen kraakbeen-bot implantaten worden ontwikkeld, die het endogene celgedrag manipuleren en zo volledig herstel van de kraakbeen en bot structuur kunnen bewerkstelligen. Bovendien moet bij het onderzoek naar nieuwe therapeutische benaderingen voor het herstel van kraakbeen en botdefecten gebruik worden gemaakt van meerdere modellen, variërend van *in vitro* tot *in vivo*, waar bij het gebruik van diermodellen zorgvuldig rekening moet worden gehouden met de keuze van geslacht en lokatie van het defect. Met voortdurend onderzoek streeft de regeneratieve geneeskunde naar een succesvoller en langduriger herstel van defecten in het gewricht in de toekomst.

总结

骨软骨缺损修复涉及关节软骨、钙化软骨层和软骨下骨再生的复杂过程。基于生物材料的支架通常用于再生分层骨软骨单元。将内源性关节驻留干/祖细胞募集到缺损处、并诱导多种组织类型的形成，是基于生物材料的无细胞策略的关键步骤。在**第二章**中，我们对当前关于内源性关节内驻留干/祖细胞的研究进展进行了综述，例如骨髓来源、滑膜来源和关节内脂肪垫来源的干细胞。通过调节生物材料的生物物理和生化特性，以在修复过程中调控内源性干细胞的行为，是可行且有前景的。在这篇综述中，我们对再生生物材料的新颖设计和应用的最新进展进行了总结。这些具有良好生化特性的材料设计致力于建立指导性微环境，从而在组织修复过程中指导内源性细胞迁移、增殖和分化。

水凝胶由于其良好的生物相容性、可重复性和类软骨特性，已成为软骨修复领域一类有前景的生物材料。然而，能够改善细胞行为的具体特性尚不明确。在**第三章**中，我们研究了不同水凝胶的生物物理和生化特性对细胞迁移和组织修复的影响。我们使用了基于人骨髓来源的间充质基质细胞的体外细胞迁移模型、牛软骨外植体离体模型和小鼠半原位体内模型。在该小鼠半原位体内模型中，具有骨软骨缺损的牛骨软骨外植体被植入小鼠皮下。具体来说，对三种水凝胶进行了修饰：在酪胺功能化透明质酸水凝胶中添加胶原蛋白以改变生化线索；降冰片烯透明质酸（norbornene hyaluronic acid, norHA）水凝胶通过可降解交联剂（基质金属蛋白酶可裂解的）或不可降解的 1,4-二巯苏糖醇（1,4-Dithiothreitol, DTT）交联剂进行交联；通过调整功能化程度对明胶甲基丙烯酸酯（gelatin methacryloyl, GelMA）水凝胶进行改性。结果表明，在体外模型中，添加胶原蛋白有利于更多的细胞迁移；在体内模型中，添加胶原蛋白促进更多的组织形成。在 norHA 水凝胶中引入可降解的交联剂并没有改善体外或离体模型中的细胞浸润，但其促进体内模型中更多的组织形成。GelMA 较低的功能化程度不会影响体外模型中的细胞迁移，但会导致离体模型中更高的迁移分数和体内模型中更多的组织形成。总体而言，我们的研究表明细胞迁移取决于多种材料特性，包括可调节的物理化学和生物指导特性。

除水凝胶外，固体支架也常用于骨软骨缺损修复。在**第四章**中，我们对已临床使用的双层胶原蛋白/胶原蛋白-镁-羟基磷灰石（collagen/collagen-magnesium-hydroxyapatite, Col/Col-Mg-HAp）支架的特性进行调节。该支架在临床上表现出良好的软骨修复能力，但软骨下骨修复效果尚不理想。我们致力于通过将额外成分与骨层集成来提高该支架的骨修复能力。为此，我们开发了一种新的合成方法来生产具有大比表面积的无定形磷酸钙（amorphous calcium phosphate, ACP）颗粒，并在其中添加了锶（strontium, Sr）元素。Sr-ACP 颗粒很好地嵌入并分布在 Col-Mg-HAp 层的胶原基质中。在小鼠半原位模型中，将 Sr-ACP 颗粒掺入 Col/Col-Mg-HAp 骨软骨支架中表现出良好的生物相容性和良好的早期组织修复能力。在山羊骨软骨缺损模型中，添加 Sr-ACP 导致新生骨量显著增加，特别是在负重的股骨髁骨软骨缺损中。总

体而言，在 Col/Col-Mg-HAp 支架中掺入成骨性 Sr-ACP 颗粒是一种可行且有前景的生化修饰，用以改善软骨下骨修复。

改变支架生化特性的另一种方法是在支架上加载生物活性因子，并将其输送到骨软骨缺损处。目前已开发了诸多复杂的生物活性因子输送系统。然而在临床实践中，简单性和可重复性是基本标准。在**第五章**中，我们将生长因子 BMP-2 (bone morphogenetic protein-2) 和 PDGF-BB (platelet-derived growth factor-BB) 通过浸泡的方式吸附到 Col/Col-Mg-HAp 支架上，以提高该支架的骨修复能力。BMP-2/PDGF-BB 的体外释放动力学表明，PDGF-BB 会从胶原蛋白层中突然释放，而 BMP-2 则大部分被保留在支架的两层中。在离体骨软骨缺损模型中，BMP-2 和 PDGF-BB 增强了细胞向支架内的浸润。在半原位非负重骨软骨缺损小鼠模型中，添加生长因子改善了组织修复，其中 BMP-2 显示出最佳结果。令人惊讶的是，在山羊骨软骨缺损模型中，与原支架相比，在负重（股骨髁）缺损中，BMP-2 的吸附导致骨修复明显减少，而在非负重（滑车沟）缺损中，骨修复呈增加趋势。这可能归因于 BMP-2 和机械负荷之间的相互作用，并可能受到给药剂量的影响。因此，生物活性因子的纳入需要研究它们的释放曲线、体内稳定性以及在关节特定生物物理和生化环境中的影响。此外，这些结果强调需要在不同的模型和不同的缺损位置以及各种生物力学环境中筛选生物材料，因为模型的选择可能导致结果不一。

在选择研究骨软骨修复的动物模型时，性别是另一个需要考虑的关键因素。在**第六章**中，我们整合并重复使用了**第四章**和**第五章**中关于雌性和去势雄性山羊软骨下骨修复的对照组数据，以评估性别对实验诱导的骨软骨缺损中支架修复软骨下骨的影响。总体而言，在支架修复骨软骨缺损中，较之于去势雄性山羊，雌性山羊形成更多的软骨下骨，并且这种效应似乎与机械负荷无关。未来对于评估软骨下骨修复的研究应在使用动物模型时考虑性别平衡。

在**第四章**和**第五章**中，改进的 Col/Col-Mg-HAp 支架产生了具有关节软骨和软骨下骨的良好整合的骨软骨单元。然而，即使在术后 6 个月，关节软骨和软骨下骨之间未形成钙化软骨层。为了研究钙化软骨层的形成，我们在**第七章**中利用未成熟的牛软骨外植体开发了离体培养模型。具体来说，从 6 至 8 个月大的小牛的掌指关节中收获软骨外植体，并以 β -甘油磷酸盐诱导软骨钙化。结果显示，软骨钙化仅于软骨外植体的深部区域形成，表明关节软骨内存在固有的区域特异性钙化过程。随后，我们将全层软骨外植体分为顶层和底层，以探索软骨带状结构之间的相互作用。位于顶层的活性软骨细胞表现出通过分泌生物活性因子以抑制软骨钙化的能力。而活性底层可以主动刺激软骨钙化，并对抑制软骨钙化的生物活性因子做出反应。总之，关节软骨钙化软骨层的形成是由区域性软骨细胞通过复杂的相互作用精确控制形成。

总而言之，操纵生物材料的生物物理和生化特性是再生骨软骨单元层次结构有效且可行的策略。仅模仿天然骨软骨组织成分的多层支架可能还不足以完整修复骨软骨缺损。更好地了解骨软骨组织形成的基本发育过程，以及细胞、生物活性因子和基质/生物材料之间相互作用的机制至关重要。有了这些基础，就可以设计骨软骨植

入物来操纵内源性细胞行为，以实现骨软骨组织的完全再生。此外，研究骨软骨修复的新疗法应涉及利用从体外到体内的多种模型，并在使用动物模型时仔细考虑性别平衡和关节缺损部位的选择。通过不断的研究和进展，再生医学未来将实现更成功、更持久的骨软骨缺损修复。

A

Appendices

A

List of publications

LIST OF PUBLICATIONS

Xu J[#], Vecstaudza J[#], Wesdorp MA, Labberté M, Kops N, Salerno M, Kok J, Simon M, Harmand MF, Vancíková K, van Rietbergen B, Misciagna MM, Dolcini L, Filardo G, Farrell E, van Osch GJVM, Locs J, Brama PAJ. Incorporating strontium enriched amorphous calcium phosphate granules in collagen/collagen-magnesium-hydroxyapatite osteochondral scaffolds improves subchondral bone repair. *Material Today Bio*. 2024;20(25):100959.

Xu J, Fahmy-Garcia S, Wesdorp MA, Kops N, Forte L, De Luca C, Misciagna MM, Dolcini L, Filardo G, Labberté M, Vancíková K, Kok J, van Rietbergen B, Nickel J, Farrell E, Brama PAJ, van Osch GJVM. Effectiveness of BMP-2 and PDGF-BB Adsorption onto a Collagen/Collagen-Magnesium-Hydroxyapatite Scaffold in Weight-Bearing and Non-Weight-Bearing Osteochondral Defect Bone Repair: *In Vitro*, *Ex Vivo* and *In Vivo* Evaluation. *Journal of Functional Biomaterials*. 2023;14(2):111.

Zhou L[#], **Xu J[#]**, Schwab A, Tong W, Xu J, Zheng L, Li Y, Li Z, Xu S, Chen Z, Zou L, Zhao X, van Osch GJVM, Wen C, Qin L. Engineered biochemical cues of regenerative biomaterials to enhance endogenous stem/progenitor cells (ESPCs)-mediated articular cartilage repair. *Bioactive Materials*. 2023;2(26):490-512.

Schwab A[#], Wesdorp MA[#], **Xu J**, Abinzano F, Loebel C, Falandt M, Levato R, Eglin D, Narcisi R, Stoddart MJ, Malda J, Burdick JA, D'Este M, van Osch GJVM. Modulating design parameters to drive cell invasion into hydrogels for osteochondral tissue formation. *Journal of Orthopaedic Translation*. 2023;41:42-53.

Xu J, Li Y, Wang B, Lv GH, Wu P, Dai Y, Jiang B, Zheng Z, Xiao S. Percutaneous Endoscopic Lumbar Discectomy for Lumbar Disc Herniation with Modic Changes via a Transforaminal Approach: A Retrospective Study. *Pain Physician*. 2019;22(6):E601-E608.

Xu J, Li Y, Wang B, Lv G, Li L, Dai Y, Jiang B, Zheng Z. Minimum 2-Year Efficacy of Percutaneous Endoscopic Lumbar Discectomy versus Microendoscopic Discectomy: A Meta-Analysis. *World Neurosurgery*. 2020;138:19-26.

Xu J[#], He Y[#], Li Y, Lv GH, Dai YL, Jiang B, Zheng Z, Wang B. Incidence of Subsidence of Seven Intervertebral Devices in Anterior Cervical Discectomy and Fusion: A Network Meta-Analysis. *World Neurosurgery*. 2020;141:479-489.

Wang B, Jiang B, Li Y, Dai Y, Li P, Li L, **Xu J**, Li L, Wu P. AKAP2 overexpression modulates growth plate chondrocyte functions through ERK1/2 signaling. *Bone*. 2021; 146:115875.

Li P, Li Y, Dai Y, Wang B, Li L, Jiang B, Wu P, Xu J. The LncRNA H19/miR-1-3p/CCL2 axis modulates lipopolysaccharide (LPS) stimulation-induced normal human astrocyte proliferation and activation. *Cytokine*. 2020;131:155106.

Zheng ZZ, Tu Z, Li Y, Dai Y, Wu PF, Jiang B, Xu J, Xiao S, Li L, Lv GH, Wang B. Full-Endoscopic Lumbar Discectomy for Lumbar Disc Herniation with Posterior Ring Apophysis Fracture: A Retrospective Study. *World Neurosurgery*. 2018;24:S1878-8750(18)32877-8.

Li Y, Dai Y, Wang B, Li L, Li P, Xu J, Jiang B, Lü G. Full-Endoscopic Posterior Lumbar Interbody Fusion Via an Interlaminar Approach Versus Minimally Invasive Transforaminal Lumbar Interbody Fusion: A Preliminary Retrospective Study. *World Neurosurgery*. 2020 Dec;144:e475-e482.

A

PhD Portfolio

PHD PORTFOLIO

Personal details

Name	Jietao Xu
Department	Orthopaedics and Sports Medicine, Erasmus MC University Medical Center, Rotterdam, The Netherlands
Research school	Erasmus MC Graduate school
PhD period	September 2020 – August 2024
Promotors	Prof. Gerjo J.V.M. van Osch, PhD, Prof. Pieter A.J. Brama, PhD and Prof. Eric Farrell, PhD

		Workload (ECTS)
Courses		
Nov 2020	Laboratory Animal Science	3.00
Jul 2021	Indesign CC	0.15
Jul 2021	Leica Confocal Introduction	0.20
Nov 2021	Stem Cells, Organoids and Regenerative Medicine (SCORE)	1.00
Feb 2022	Biomedical English Writing	2.00
May 2022	Scientific Integrity	0.30
Nov 2023	Translational Imaging Workshop by AMIE "From Mouse to Man"	1.00
(Inter)national Conferences		
Nov 2020	29 th annual meeting of the Netherlands Society for Biomaterials and Tissue Engineering	0.60
Nov 2021	6 th world congress of the Tissue Engineering and Regenerative Medicine International Society	1.50
Apr 2022	30 th annual meeting of the Netherlands Society for Biomaterials and Tissue Engineering	1.60
Apr 2022	16 th World Congress of International Cartilage Regeneration & Joint Preservation Society	1.70
Mar 2023	Tissue Engineering and Regenerative Medicine International Society (TERMIS) European Chapter	1.70
Department/consortium presentations and meetings		
2020-2022	NANOScores consortium meetings	1.00

Appendices

2020-2024	Orthopaedics and Sports Medicine Science Day	0.50
2020-2024	Research meetings depts. Of Internal Medicine and Orthopedics	2.00
2020-2024	Journal Club	1.00
2020-2024	Meeting depts. Of Orthopaedics and Oral Maxillofacial Surgery	2.00
2021-2021	Lab-clinical meeting	0.50
2021-2022	ACE Bone & Joint Meeting	1.00
2022-2023	3D bioprint cluster meeting	0.50
2022-2024	Soup and Science Meeting	1.00
2022-2024	TEAM understanding and modulating chondrocyte hypertrophy and calcified cartilage	2.00
2022-2024	PhD day	1.90
Student supervision		
2022-2023	Spervision of bachelor and Master students	2.0
Miscellaneous		
Jan 2023	Organize Lab Day Orthopaedics, Oral Maxillofacial Surgery	0.50

Total 30.65

A

Acknowledgements

ACKNOWLEDGEMENTS

These past four years have been like a dream. I often doubted if I could ever reach this point. Completing this journey seemed beyond my grasp. Yet, here I am, standing at the end of this incredible journey, realizing that I've authored a book like this thesis after four years. Fortunately and thankfully, I've had the support of incredible people who guided me through this challenging yet amazing journey. Each step forward and every small victory was made with the help of my supervisors, colleagues, family, and friends. This journey has been more than an academic endeavour, it has been an incredible experience that has shaped me in various ways. Thank you to everyone who has been a part of this incredible journey.

Professor. dr. Gerjo J.V.M. van Osch, you are the guide who supported me in reaching this point. Thank you so much for the opportunity you provided me to pursue my dreams. I already sensed that you are such a nice and remarkable person from our very first interview, and these four years have only proven it further. Despite your busy schedule, you've remained approachable, consistently offering valuable feedback and insights that eased my PhD journey. I know that supervising a student from a country with a completely different language and culture is no easy feat, yet your thoughtfulness shined through in our every talk. You have always been considerate of both my life and my future career in every small detail. I will forever cherish these memories. Thank you for everything!

Professor. dr. Pieter A.J. Brama, half of my thesis involves the caprine models, and it was you who helped me complete this incredible work. Although we haven't met in person often, your presence was always felt. You have always been there on the other side of the screen, providing me with valuable suggestions and assistance. You are always able to provide unexpected yet profound insights that often help me see my work from new and beneficial perspectives. Your insights have greatly improved the quality of my work. Sincerely thank you!

Professor. dr. Eric Farrell, I still remember the warm welcome you gave me. Although you couldn't be in the lab often, you were always on the other side of the screen, providing me with excellent advice and guidance that made my project progress more smoothly. You speak quickly, but your thinking is even faster! I have learned a lot from our meetings, and they have made me realize how reassuring it is to have the support of teammates when working in a team. Thank you!

Professor. dr. Harold Brommer, dr. Nathalie Bravenboer, and dr. Bram van der Eerden, thank you for taking the time to review and comment on this thesis!

Thank you to all the **NANOScores members**, especially to **Professor. dr. Giuseppe Filardo, Professor. dr. Janis Locs, Professor. dr. Claudio De Luca, dr. Jana Vecstaudža and dr. Manuela Salerno**. Thanks to **dr. Bert van Rietbergen, dr. Shorouk Fahmy-Garcia, dr. Joeri Kok, Ms. Margot Labberté, Ms. Karin Vancíková**. Also thanks to **Medical Delta Program Regenerative Medicine 4D**. Thank you all so much for your help and inputs in my projects!

Dr. Marinus A. (Tim) Wesdorp, your guidance and help in my first year eased my four-year journey. I was lost in my first month, but your patience and support made all the difference.

I feel that I can turn to you for help with any problem I encounter. I have learned a lot from you, not only scientific skills but also life attitudes. Thank you!

Dr. Roberto Narcisi, your enthusiasm for life is truly inspiring, especially your passion for marathons! I enjoyed all the talks we had in the lab! **Dr. Andrea Lolli**, you are always approachable whenever doubts arose! And you always solved my problem with smile and patience! Thank you!

Sandra, without you, I might have spent much more time dealing with those forms, documents, and other things that I couldn't figure out. Thank you for handling so many things for me, allowing me to focus entirely on my scientific work!

To our dedicated lab technicians, **Nicole, Wendy, Janneke**, thank you so much for organising everything in our lab! I had limited lab skills as a medical doctor, but your support over the past four years has ensured the smooth progress of my lab work. **Nicole**, I met you on my first day in the lab, and I learned sectioning from you on the same day! Over the past four years, most of my days in the lab began with hearing your laughter! **Wendy**, learning cell culture and qPCR from you has been a pleasure, and our chatting in the lab is always enjoyable! **Janneke**, your patience and reminders really make my lab work go more smoothly! **Yanto**, thank you so much for introducing micro-CT, which greatly enriched my thesis!

To all my colleagues, **Amaia, Andrea Schwab, Anna, Anne, Elias, Encheng, Imke, Ivy, Judith, Marta, Mauricio, Michele, Mike, Pedro, Tess**, thank you for everything! Our meetings, talks, and lab days make this journey truly memorable! Coming from different countries with different languages and cultures, we can gather in one lab, talking about everything with fun!

To **Hong (张弘), Jialong (朱佳龙), Yuhan (吴侯舍), Peifen (张培芬), Tingyue (李廷跃), Danlu (杨丹璐), Weicheng (徐伟宸), Xiaoming (程凯昕), Hairong (陆海蓉), Ziyun (程子芸), Jing Yu (郁静), Jixing (王继新), Zewei (韩泽围), Jing Ye (叶静)**, and all my friends, you're the reason I eagerly look forward to the weekends! Our time together is filled with laughter, delicious food, and silly but fun games!

To **my parents, parents-in-law, my sister (徐洁) and brother-in-law (梁惠)**, and **my nephews, Zisheng (梁梓晟) and Zichen (梁梓晨)**, I feel regretful that I haven't been there with you during these past four years, but you know that I miss you! Now I'm here, I cannot wait to see you all!

Dear **Yi (何懿)**, you have been my greatest fortune. Thank you for your support, comfort, and love over the past ten years. Thank you for encouraging me to come to the Netherlands and for your decision to move to Rotterdam. Over the past four years, we have created many wonderful memories in various European cities, now I am looking forward to reuniting with you back home! I love you!

A

Curriculum Vitae

CURRICULUM VITAE

Jietao Xu (徐洁涛) was born on 24th January 1993 in Zhejiang, China. Driven by a keen interest in healthcare, he set his sights on pursuing a career in medicine. After completing his high school education in 2012, he began his medical studies at Central South University in Changsha, China. In 2017, he obtained a Bachelor's degree in Clinical Medicine. In the same year, he started his orthopaedic training in the Second Xiangya Hospital of Central South University. In 2020, he completed his specialised training in the Department of Orthopaedics and obtained his Master's degree in Surgery. Due to his keen interest in academic medicine, he began his PhD project at the Department of Orthopedics and Sports Medicine at Erasmus MC, University Medical Center in Rotterdam, the Netherlands in November 2020. This opportunity allowed him to engage in research and collaborate with international experts. He mainly worked on the project entitled "NANOstructured oSteoChOndral scaffold: novel biomimetic tRiggErS for enhanced bone regeneration" under the supervision of professor. dr. Gerjo J.V.M. van Osch, professor. dr. Pieter A.J. Brama and professor. dr. Eric Farrell. In 2024, upon completing his PhD, he was enrolled as a spine surgeon in the Department of Orthopaedics at Zhejiang Provincial People's Hospital, and will start his spine surgery career in December 2024. He will continue his research to advance the field of connective tissue repair.



A

